2009

Subject Specific Computational Models of the Knee to Predict Anterior Cruciate Ligament Injury

Bhushan S. Borotikar
Cleveland State University

SUBJECT SPECIFIC COMPUTATIONAL MODELS OF THE KNEE TO PREDICT ANTERIOR CRUCIATE LIGAMENT INJURY

BHUSHAN S. BOROTIKAR

Master of Science in Biomedical Engineering

University of Texas at Arlington

December, 2003

submitted in partial fulfillment of requirement for the degree

DOCTOR OF ENGINEERING IN APPLIED BIOMEDICAL ENGINEERING

at the

CLEVELAND STATE UNIVERSITY

DECEMBER, 2009

This dissertation has been approved
for the Department of CHEMICAL AND BIOMEDICAL ENGINEERING
and the College of Graduate Studies by

____

Dissertation Committee Chairperson, **Antonie J. van den Bogert, Ph.D.**
Department of Chemical and Biomedical Engineering

____

Date

____

Kathleen Derwin, Ph.D.
Department of Chemical and Biomedical Engineering

____

Date

____

Ahmet Erdemir, Ph.D.
Department of Chemical and Biomedical Engineering

____

Date

____

Jorge E. Gatica, Ph.D.
Department of Chemical and Biomedical Engineering

____

Date

____

Scott G. McLean, Ph.D.
Department of Chemical and Biomedical Engineering

____

Date

____

Kathleen J. Pantano, Ph.D.
Department of Health Sciences

____

Date

To my grandparents

Pushpakar and Kusum

ACKNOWLEDGEMENT

I sincerely express my gratitude to my research advisor and mentor Dr. van den Bogert for providing me the opportunity to pursue this research in his laboratory. He has instilled in me his pursuit of excellence and sense of achievement which I will keep with me throughout my career. Throughout my stay in Cleveland, Dr. van den Bogert has supplied me with all the support I needed to conduct my research and has been instrumental in developing me as a researcher. His strong applied mathematical skills and profound knowledge of the human musculoskeletal system has been invaluable to me as I learned many skills in the biomechanics research. I am deeply indebted to him for his guidance, suggestions and encouragement throughout the course of this work.

I would like to thank Dr. Leendert Blankevoort and Dr. Scott McLean for their constant help, advice and guidance in this research. The modeling part of this thesis was based on the previous work done by Dr. Blankevoort and he tremendously helped and guided me whenever needed. Dr. McLean exposed me to the world of motion analysis and movement science and together we conducted many studies that helped me understand the joint biomechanics in a better way. I would like to express my gratitude towards Dr. Ahmet Erdemir for his constructive guidance time to time no matter whatever small my problem was. I thank Dr. Pantano for giving me the opportunity to work with her and enhancing my physical therapy knowledge and skills. I also would like to thank Dr. Marko Ackermann for his invaluable guidance on optimization theory and its applications. I specifically thank Robb Colbrunn for his support and help during experimental protocols and Dr. Jason Halloran for his timely help at various occasions. I am indebted to all these people and many others who have advised, helped and encouraged me during my five years of study at the Cleveland Clinic.

I would like to thank my wife Archana whose unconditional support, especially during the trying time of writing this dissertation, has helped me achieve my goal. Her enormous sacrifices have helped me concentrate on my studies that otherwise would not have been possible. I would like to express my utmost gratitude to my parents Sou. Shobhana and Shree. Sonyabapu, and brother Ashish for all their sacrifice while I pursued my dreams in this country. Without their moral support, I would not have survived this endeavor. Finally, I thank my friend Amit for convincing and helping me to pursue doctoral studies and maintaining his support throughout my life.

I would like to thank my other committee members Dr. Jorge Gatica and Dr. Kathleen Derwin for their helpful criticism. This study was supported in parts by grants from NIH (R01- AR049735) and ISB (dissertation grant, 2008).

SUBJECT SPECIFIC COMPUTATIONAL MODELS OF THE KNEE TO PREDICT ANTERIOR CRUCIATE LIGAMENT INJURY

BHUSHAN S. BOROTIKAR

ABSTRACT

Knee joint is a complex joint involving multiple interactions between cartilage, bone, muscles, ligaments, tendons and neural control. Anterior Cruciate Ligament (ACL) is one ligament in the knee joint that frequently gets injured during various sports or recreational activities. ACL injuries are common in college level and professional athletes especially in females and the injury rate is growing in epidemic proportions despite significant increase in the research focusing on neuromuscular and proprioceptive training programs. Most ACL injuries lead to surgical reconstruction followed by a lengthy rehabilitation program impacting the health and performance of the athlete. Furthermore, the athlete is still at the risk of early onset of osteoarthritis. Regardless of the gender disparity in the ACL injury rates, a clear understanding of the underlying injury mechanisms is required in order to reduce the incidence of these injuries.

Computational modeling is a resourceful and cost effective tool to investigate the biomechanics of the knee. The aim of this study was twofold. The first aim was to develop subject specific computational models of the knee joint and the second aim to gain an improved understanding of the ACL injury mechanisms using the subject specific models. We used a quasi-static, multi-body modeling approach and developed MRI based tibio-femoral computational knee joint models. Experimental joint laxity and combined loading data was obtained using five cadaveric knee specimens and a state-of-the-art

robotic system. Ligament zero strain lengths and insertion points were optimized using joint laxity data. Combined loading and ACL strain data were used for model validations. ACL injury simulations were performed using factorial design approach comprising of multiple factors and levels to replicate a large and rich set of loading states. This thesis is an extensive work covering all the details of the ACL injury project explained above and highlighting the importance of 1) computational modeling in injury biomechanics, 2) incorporating subject specificity in the models, and 3) validating the models to establish credibility. Techniques used in this study can be employed in developing subject specific injury prevention strategies. These models can be further used to identify gender specific risk factors associated with the ACL injury.

TABLE OF CONTENTS

LIST OF TABLES

LIST OF FIGURES

CHAPTER I

INTRODUCTION

1.1 INTRODUCTION TO THE ANTERIOR CRUCIATE LIGAMENT INJURY

Injuries to the knee joint are common in any organized or recreational sports regardless of age, gender or playing level. Knee joint injuries are especially a concern among the college level or professional athletes from different organized sports such as soccer, basketball, team handball, volleyball, football, lacrosse, softball to name a few. Of all types of knee injuries, injury to Anterior Cruciate Ligament (ACL) is a frequently occurring event in these organized sports. National Collegiate Athletic Association's (NCAA) Injury Surveillance System (ISS) for example, reported that 8% of all the game injuries were ACL injuries among the NCAA female basketball athletes from 1988 to 2004 [Agel, et al. 2007]. ACL injury is a growing concern in recreational athletes as well. The outbreak of ACL injuries has a compounding impact on the athlete and the society. Early onset of osteoarthritis [Maletius, et al. 1999, Messner, et al. 1999, Lohmander, et al. 2004] and lengthy rehabilitation programs are the areas of concern for the athlete undergoing ACL reconstruction surgery. Higher rate of ACL injuries in female athletes

[Griffin, et al. 2000] and overall surgery and rehabilitation cost surmounting 2 billion dollars are the areas of concern for researchers, health professionals and government alike. Center for Disease Control and Prevention (CDC) revealed that (http://www.cdc.gov/datastatistics) in year 2006 alone, 46,000 female athletes, age 19 and younger, experienced the ACL injury with 30,000 requiring ACL reconstruction surgery. Both NCAA and CDC have expressed concerns over growing ACL injury rate and directed their efforts and support to injury prevention programs.

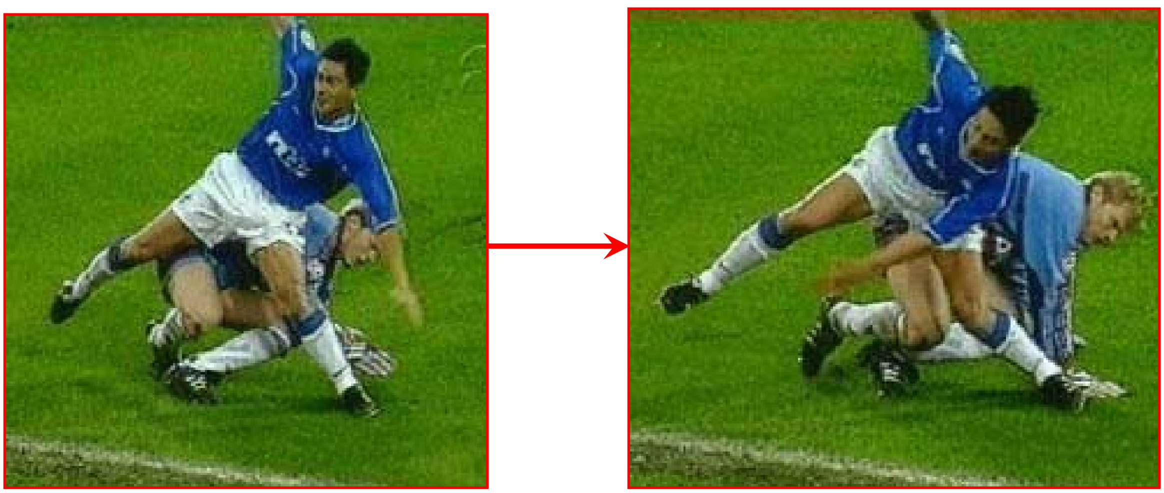

Figure 1.1: Most of the non-contact ACL injuries occur during landing phase.

70% of the ACL injuries are non-contact injuries [Boden, et al. 2000] involving early ground contact and its effect on the knee during landing or cutting tasks (Figure 1.1). A simple PubMed search (http://www.ncbi.nlm.nih.gov/pubmed) using the keyword "ACL injuries" produced 2773 results in past 31 years. Out of these, almost 98% of the articles were focused on surgical treatment and diagnosis, post-surgical rehabilitation programs, procedures to facilitate speedy recovery, and post-injury knee biomechanics of these injuries. Only 2% of articles were dedicated to actual injury mechanisms and prevention strategies with researchers typically focusing on modifying neuromuscular control and developing core strength training programs to prevent ACL injuries. In this 2% category, abundance of research was conducted on examining the effects of isolated and/or combined knee load motion states on ACL loading [Kanamori, et al. 2000, Pflum, et al. 2004, Shelburne, et al. 2004, Kanamori, et al. 2002, Li, et al. 2004, Bach, et al. 1995, Bach, et al. 1997, Blankevoort, et al. 1988, Blankevoort, et al. 1991, Darcy, et al. 2006, Woo, et al. 1998]. There were numerous studies pertaining to knee joint biomechanics and its relationship to neuromuscular control and joint anatomy [Withrow, et al. 2006, Pandy, et al. 1997, Pandy, et al. 1998a, Pandy, et al. 1998b, Steele, et al. 1999, Cowling, et al. 2003]. Through these studies, researchers have provided great insights to ACL injury and risk factors involved [Griffin, et al. 2000, Uhorchak, et al. 2003, Lephart, et al. 2002, Huston, et al. 2000, Borotikar, et al. 2008]. These studies have found that not only knee kinematics, but hip and ankle kinematics should also be studied in light of the ACL injuries. Using statistical design approach, these studies have identified certain key risk factors to ACL injury such as body mass index, joint laxity, femoral inter-condylar notch width, initial contact knee and hip flexion and valgus, initial contact hip internal rotation and neuromuscular fatigue. Using the key findings in these studies, there has been a subsequent development of neuromuscular training programs designed to prevent ACL injury [Mandelbaum, et al. 2005, Beynnon, et al. 2005, Hewett, et al. 2001, Cerulli, et al. 2001, Myer, et al. 2004]. These neuromuscular and proprioceptive training programs continue to grow [Mandelbaum, et al. 2005, Hewett, et al. 2005] with researchers elucidating risk factors involved. With higher rate of injuries in female athletes and their increased participation in sports, major research is now focused on finding gender specific risk factors and prevention strategies. Female athletes exhibit altered neuromuscular control during movements incorporating rapid changes in speed or direction, typically manifesting in lower limb joint biomechanics [Griffin, et al. 2000, Lephart, et al. 2002, Hewett, et al. 1996]. These gender differences are suggested to increase their risk of ACL injury compared to males. Recently, similar features, specifically less knee flexion and more valgus were found to be associated with ACL injury in a prospective study by Hewett and associates [Hewett, et al. 2005].

Despite increases in prevention and strength training programs over past 10 years, a decreasing trend in ACL injuries and injury rates can not be identified (Figure 1.2). It is specifically true for young female athletes that the presumable increase in the fitness and core strength of these athletes over the years has not made any significant impact on

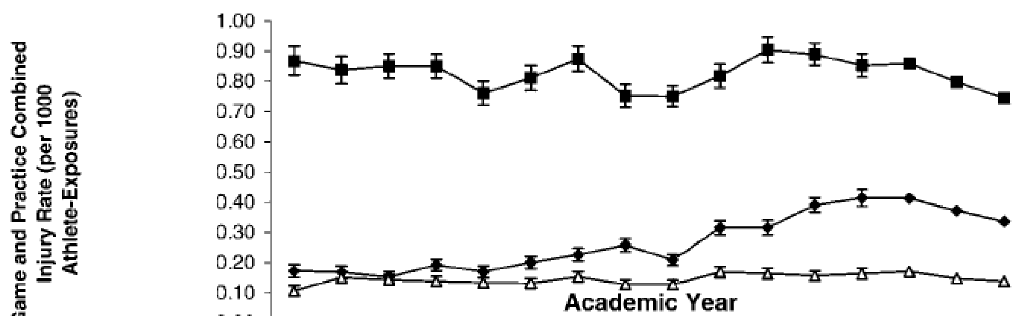

	88-89	89-90	90-91	91-92	92-93	93-94	94-95	95-96	96-97	97-98	98-99	99-00	00-01	01-02	02-03	03-04
Concussions	0.17	0.17	0.15	0.19	0.17	0.20	0.23	0.26	0.21	0.32	0.32	0.39	0.41	0.41	0.37	0.34
Ankle ligament sprains	0.87	0.84	0.85	0.85	0.76	0.81	0.87	0.75	0.75	0.82	0.90	0.89	0.85	0.86	0.80	0.75
Anterior cruciate ligament injuries	0.11	0.15	0.14	0.14	0.13	0.13	0.15	0.13	0.13	0.17	0.16	0.16	0.16	0.17	0.15	0.14

Figure 1.2: Injury rates for select conditions (concussions, ankle ligament sprains, and anterior cruciate ligament injuries) for games and practices combined for 15 sports, National Collegiate Athletic Association, 1988–1989 through 2003–2004 (Hootman et. al., 2007)

reducing the risk of injury. ACL injuries are still growing in epidemic proportions indicating that these studies are missing key factors in addressing the ACL injury problem. One such key factor lies in understanding the actual ACL injury mechanisms and related joint loading and the second factor is the incorporation of subject specificity in the neuromuscular training programs. There are very few studies that incorporate complex joint loading conditions that may put hazardous strains on the ACL. Furthermore, there are currently no methods to determine whether an individual's knee joint has a higher than normal risk of injury in such loading conditions.

Few cadaveric injury models [DeMorat, et al. 2004, Hashemi, et al. 2007, Meyer, et al. 2008] studied specific known injury mechanisms confirming the ACL injury; nevertheless the actual ACL injury mechanism remains unknown. Evidently, cadaveric experiments to study ACL injury mechanisms are not feasible since ACL failure can only be done once in each specimen. This limitation can be overcome by developing computational joint models. These models can be repeatedly simulated for injuries to understand the mechanisms. Modeling attempts in this area are limited to either normal joint mechanics or joint geometry that is not subject specific [Shelburne, et al. 2004, Blankevoort, et al. 1996]. Large variability in anatomical shapes of knee structures [Biscevic, et al. 2005], anthropometric data, and tissue mechanical properties [Woo, et al. 1991] between individuals restrict the use of the generic models developed so far and calls for the subject specificity with regards to these factors while evaluating the injury mechanisms. Importance of understanding ACL injury mechanisms has been previously discussed by researchers [Borotikar, et al. 2008, Van den Bogert, et al. 2007] stating the need for developing robust computational models that can evolve as a tool for studying the underlying mechanisms of injury.

Computational methods to estimate or simulate the muscle forces and external knee joint loading during real or simulated in vivo activities have been developed by researchers. These studies used different modeling domains and applied mechanics techniques to estimate knee joint loading. Inverse dynamics approach was used by many researchers [van den Bogert, et al. 1994, Erdemir, et al. 2007, Winter. 2005] to calculate the joint forces and moments from joint kinematic data and ground reaction forces. Lloyd and Besier [Lloyd, et al. 2003] used EMG driven inverse dynamic muscle models to predict joint moments and muscle forces and these models were further evaluated by Buchanan and associates [Buchanan, et al. 2005]. Forward dynamic musculoskeletal models were developed and validated by McLean and associates [McLean, et al. 2003] to estimate the resultant knee joint forces and moments and were further used to evaluate ACL injuries during simulated side-step cutting movements [McLean, et al. 2004]. Output of the models used in these studies were the 3D forces and moments acting on the passive tibiofemoral joint in a specific subject. So, methods to determine external knee joint loading have already been developed, but there were no studies that analyzed the distribution of these forces among the internal structures of the knee joint and whether any combination of these loads could cause injury to the joint structures, especially the ACL. Based on the difference between the injury rates in male and female athletes [Griffin, et al. 2000] and the observations made during the studies that were focused on ACL injuries [Boden, et al., 2000], it can be suspected that the mechanical response of the joint varies between the individuals. Thus, there is a need to develop subject specific joint mechanics models that estimate the distribution of external joint loading to internal structures and can be used together with the existing subject specific analysis or simulation methods for whole body movement.

Insights in ACL injury mechanisms would give us specific directions on prevention strategies rather than using generalized neuromuscular and proprioceptive training programs. Understanding these mechanisms would help us separate abnormal movement patterns from desirable neuromuscular adaptation [Van den Bogert, et al. 2007], the knowledge of which is important while developing prevention strategies on individual basis. Non-contact ACL injuries usually occur during the landing and/or stance phase of movements (Figure 1.1) incorporating rapid changes in speed and/or direction, often accompanied by sudden tibial rotations [Boden, et al. 2000, Arendt, et al. 1995]. Simultaneous valgus and internal rotation torques on tibia, for example, are generated in cutting movements that may place ACL at risk [Besier, et al. 2001a, Besier, et al. 2001b]. Due to complex 3D force and moment combinations acting at the knee joint during execution of such movements, it is not clear which of such combinations are responsible for increased ACL loading and how it is affected by anatomical and soft tissue parameters as a subsequent risk of injury. Much less attention is given to study and analyze actual injury mechanisms in the knee joint mechanics studies even though knee ligament biomechanics has been a subject of interest for many researchers for years.

1.2 AIMS AND SCOPE OF THIS THESIS

Keeping the above facts in mind, this dissertation is set to achieve three specific aims.

Aim 1: To develop computational knee joint models having subject specific geometry and tissue properties.

Aim 2: To validate these models through cadaveric testing, with respect to (1) prediction of knee kinematics for combined loading conditions, and (2) prediction of force in the ACL.

Aim 3: To demonstrate the ability of these models to determine which loading conditions are likely to injure the ACL in a specific joint.

This dissertation describes in detail the methodology of building subject specific knee joint models, optimizing and validating these models with experimental data and subsequently using these models to simulate ACL injury mechanisms.

In any case whether gender specific or not, knee anatomy plays an important role in deciding the joint mechanics and consequent neuromuscular control. It is therefore utmost important to understand knee joint anatomy and ligament function before endeavoring the causes that injure this complex structure. First part of Chapter 2 thus briefly introduces the anatomy of the knee joint and the ACL structure followed by a brief description of the role of ACL in the knee biomechanics. While studying this well known area of research, the contribution from other researchers must be acknowledged and minutely analyzed in the wake of the current study. The second part of Chapter 2 covers a systematic literature review of cadaveric and computational methods and models that measure or predict ACL force or strain.

Chapter 3 describes the detailed methods used to collect experimental data from cadaveric specimens. In its first part, the experimental setup is explained, followed by detailed discussion of the robotics testing system its control interface that is used to maneuver it in either force or motion control. Second part describes the specimen preparation, strain gauge mounting on the ACL and ultimately mounting the specimen on the robot. Third part describes different loading scenarios applied to the specimen and some interesting results from each specimen.

In our preliminary studies, we have demonstrated our ability to develop computational knee joint models based on the Magnetic Resonance Imaging (MRI). Due to its accessibility and high computational performance, multi-body quasi-static modeling approach used in these models makes it a right candidate to be used in our studies. Chapter 4 is devoted to methods that describe joint model development.

In order to build subject specific joint models, it is important that model parameters reflect the subject specific properties. Not all properties can be obtained non-invasively from live humans or cadaveric specimens. Thus, optimizing the model parameters to match a subset of model mechanics to the experimental data becomes an inevitable task. Tibio-femoral knee joint models were used in our analysis while proposing two optimization methods to fit the model to joint laxity data. Chapter 5 illustrates these optimization methods and analyzes the optimization results obtained using a favorable optimization method.

Chapter 6 provides detailed information on the validation of each specimen while discussing the validation results. Kinematic data pertaining to combined loading conditions on the cadaveric specimen is used for validation purposes. Data collected from a strain gauge placed on the ACL are also used for validation. Therefore validation confirms the quality of overall knee joint model response and the accuracy to predict ACL strain data.

It is obvious that ACL loading is the ultimate effect of loads imposed on knee joint as a result of landing, sudden stopping or cutting maneuvers during any sports or activity. ACL injury mechanisms during these types of activities could be highly diverse involving many complex loading conditions. Using the validated models from above, it is possible to apply large combination of loading conditions and find out hazardous combinations that give high ACL loads. Chapter 7 provides detailed description of how this is achieved using factorial analysis of different combinational loads. Finally, Chapter 8 concludes the results of this dissertation in a short summary followed by an extensive list of references.

Readers are requested to keep in mind that Chapters 5, 6 and 7 are originally written for journal publications, so some part of the methods and discussion in these three chapters are similar and the introductions may be overlapping. Attempt is being made to make a smooth transition from one chapter to another by including transition paragraphs at the start or end of each of these chapters.

The techniques developed in this study can be used to understand the ACL injury mechanisms on individual basis and develop prevention strategies based on these findings. These models can also be used further to identify gender specific risk factors associated with ACL injury.

CHAPTER II

STRUCTURE AND FUNCTION OF THE KNEE JOINT AND ACL

Knee joint, ACL anatomy and their function go hand in hand and it is impossible to start any discussion on ligament injuries without understanding the anatomical structure. This is specifically true in this study since we will be developing subject specific knee joint models. Subject specificity comes from creating anatomically accurate models and developing structurally accurate mathematical models of the ligaments and articular cartilage. ACL anatomy has been studied in great detail by many researchers focusing on each vital component of its structure (macro or micro) and function. The first part of this Chapter gives a brief overview of the knee anatomy followed by a detailed description of the ACL anatomy and function.

2.1 BRIEF ANATOMY OF THE KNEE JOINT

The knee-joint was formerly described as a ginglymus or hinge-joint, but is really of a much more complex character. It is one of the multiaxial synovial joints in the body and characterized by seven basic structures of synovial joints viz. Joint Capsule, Synovial membrane, Articular Cartilage, Joint Cavity, Menisci, Ligaments and Bursae. It must be regarded as a joint consisting of three articulations in one: two condyloid joints, and a third between the patella and the femur. The condyles of the femur articulate with the flat upper surface of the tibia. Although this arrangement is precariously unstable, counter acting forces are supplied by joint capsule, cartilages and numerous ligaments and muscle

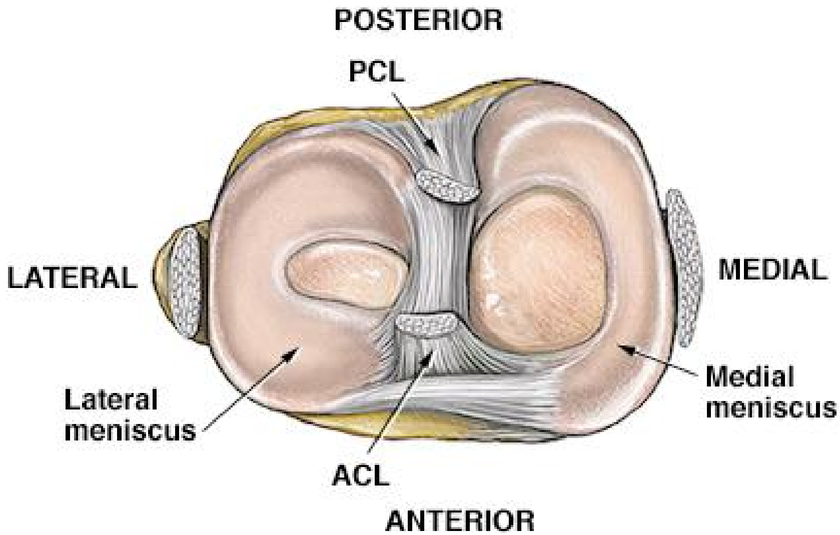

Figure 2.1: Top view of the tibial plateau showing knee ligament attachments and menisci. (www.nucleusinc.com)

tendons. The medial and lateral meniscus attach to the flat top of tibia and, because of their concavity, form a kind of shallow socket for the condyles of the femur (Figure 2.1).

Out of many ligaments that hold the knee joint together, four are of major importance. These are the Medial Collateral ligament (MCL), Lateral Collateral ligament (LCL), Anterior Cruciate ligament (ACL) and Posterior Cruciate ligament (PCL) (Figure 2.2). The superior attachments of collateral ligaments start just beneath the medial and lateral epicondyles of femur. The LCL extends distally and posteriorly and gets attached to superior head of the fibula. The MCL extends distally and anteriorly and gets attached to tibia. The cruciate ligaments are of considerable strength, situated in the middle of the joint, nearer to its posterior than to its anterior surface. They are called cruciate because they cross each other somewhat like the lines of the letter X; and have received the names anterior and posterior, from the position of their attachments to the tibia. These four ligaments guide the normal asymmetric medial and lateral contact of femur on tibia throughout the range of knee motion [Dye, et al. 1988, Fu, et al. 1994]. The ACL and PCL (the cruciates) do not heal when they get injured whereas the MCL and LCL (the collaterals) heal themselves after the injury or damage.

2.2 THE ACL ANATOMY

Understanding the anatomy of the ACL is crucial for understanding its function. The anatomy of the ACL and PCL is directly related to the function of these structures in constraining joint motion [Girgis, et al. 1975]. Knowing this anatomy is a prerequisite for

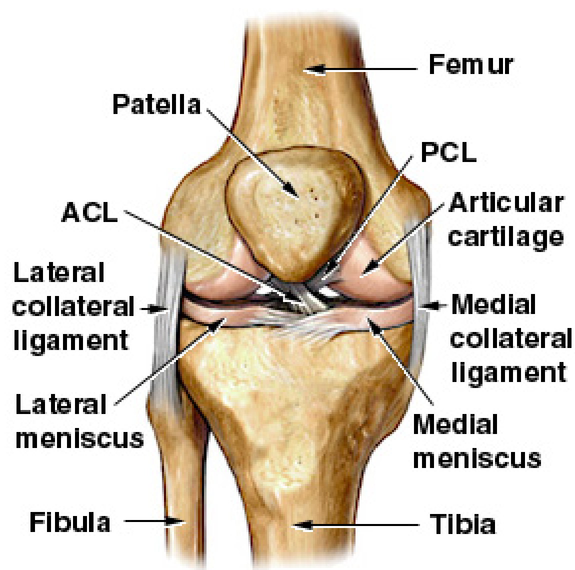

Figure 2.2: Knee joint anatomy showing bone and ligament terminology. (www.nucleusinc.com)

any discussion of the cruciate ligament function, injury or repair. The ACL anatomy can be described using different terminologies, each having its own importance in the functionality of this ligament. These are discussed in brief in the following paragraphs.

2.2.1 Macroscopic (Gross) Anatomy:

2.2.1.1 Size and Orientation

The cruciate ligaments ACL and PCL are bands of regularly oriented, dense connective tissue that connect the femur and tibia. ACL is attached to a fossa on the posterior aspect of the medial surface of the lateral femoral condyle (Figure 2.3). On the tibia, ACL is attached to fossa in front, and lateral to the anterior tibial spine. At this attachment, the ACL passes beneath the transverse meniscal ligament, and few fibres of the ACL may blend with the anterior attachment of the lateral meniscus (Figure 2.3). Both the tibial and

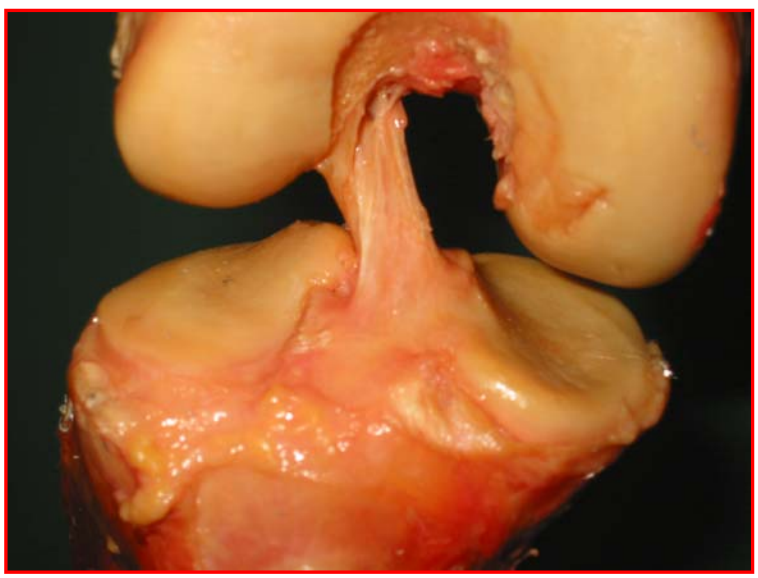

Figure 2.3: Gross image of the ACL

femoral attachments are planar with the tibial attachment area larger (136 $\pm$33 mm^2) and oval shaped compared to relatively smaller (113 $\pm$27 mm^2) and circular femoral attachment [Harner, et al. 1999]. The mean length of the ACL is 32 mm ($\pm$10 mm), mid-substance thickness 5mm ($\pm$1 mm) and mid-substance width ranges from 7 to 12 mm [Odensten, et al. 1985, Amis, et al. 1991, Smith, et al. 1993].

2.2.1.2 Structure and Fiber Bundle Classification

The ACL is primarily composed of water and densely packed collagen fibers. 70% of the collagen fibers are type I, with small amounts of type III and small traces of types V, X, XII and VIV [Dye, et al. 1988, Fu, et al. 1994, Woo, et al. 1999]. This fibrous structure along with water and small number of proteoglycans forms a non-parallel interlacing fascicular network that ultimately forms the ACL. The fascicles of this structure are

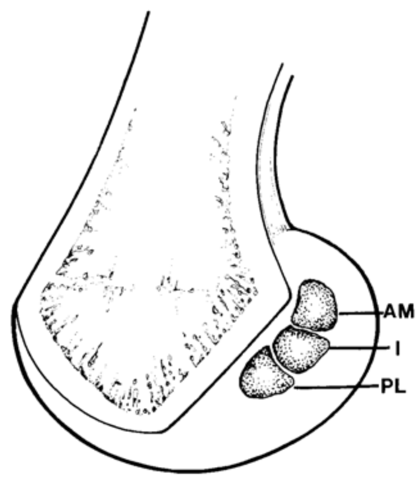

Figure 2.4: Femoral insertion areas of the ACL (Norwood and Cross, 1979)

shown to have a characteristic crimp that allows the ligament to lengthen (or shorten) in accordion like fashion [Fu, et al. 1994] and provides motion restraints to the joint [Woo, et al. 1999].

The complex fan shaped and spiraling nature of the ACL makes different fibers of the ligament functionally active throughout the entire range of motion [Bach, et al. 1997, Girgis, et al. 1975, Kennedy, et al. 1974]. Based on the tension in the portion of the ligament, it is divided into two functional parts or bundles: longer Anteromedial bundle (AMB) and smaller Posterolateral bundle (PLB) [Girgis, et al. 1975, Harner, et al. 1999]. Even though some studies distinctly divided the ACL in three bundles (Figure 2.4) [Norwood, et al. 1979, Hollis, et al. 1991], medial bundle (MB) being the third, it is now largely accepted that ACL has two definite bundles namely AMB and PLB.

2.2.2 Microscopic Anatomy

The smallest component of the ligament is known as a fibril. Fibrils are collectively grouped into subfascicular units which in turn form the fascicles. Fascicles form the ligament which is superficially surrounded by a synovial sheath. It is interesting to report the micro level structure of the ACL just before entering into bone. In this so called transition zone, the two outer layers are formed of fibro-cartilage and mineralized fibro-cartilage [Arnoczky. 1983] changing the ligament from soft tissue to rigid bone. The ACL is also reported to have vascular supply via synovial sheath covering the ligament [Arnoczky. 1983]. The synovial sheath possesses large number of blood vessels networking the entire ligament. These vessels then branch out penetrating and covering the entire substance of the ligament [Arnoczky. 1983]. The posterior articular nerve supplies rich neural network to the ligament consisting of a variety of mechanoreceptors [Kennedy, et al. 1982]. Even though the exact role and functioning of these mechanoreceptors are not yet identified, majority of the mechanoreceptors are located near the attachment sites of the ligament [Raunest, et al. 1996].

2.3 THE ACL BIOMECHANICS

2.3.1 Structural and Mechanical Properties of the ACL

The ACL material response is highly viscoelastic in nature [Smith, et al. 1993, Pioletti, et al. 1995, Kwan, et al. 1993, Woo, et al. 1993] showing time and history dependent creep, stress-relaxation and hysteresis. This behavior may help protect the ligament when subjected to rapid deformation cycles [Kwan, et al. 1993]. It is specifically important to

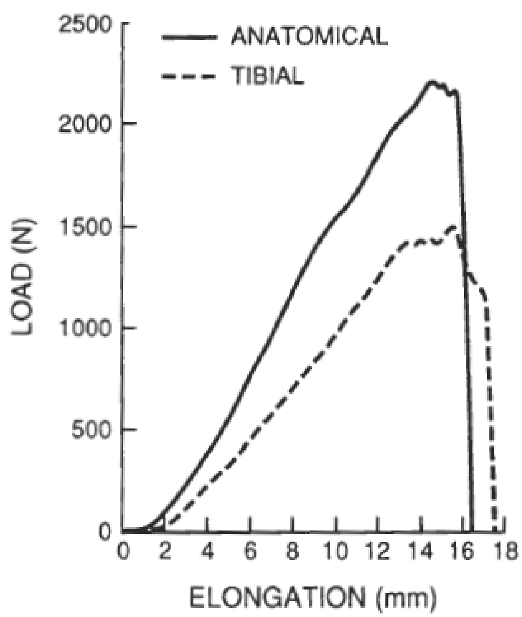

Figure 2.5: Load-elongation relationship from a paired young specimen (Woo et. al., 1991)

mention and consider the stress-relaxation behavior of the ligament. Due to this property, cadaveric joint specimens should be preconditioned prior to the mechanical testing. Studies focusing on determining the effect of gender differences and age related changes in these time dependent properties are warranted.

ACL acts as a primary restraint to the anterior displacement of tibia [Butler, et al. 1990], suggesting that ACL resists tensile loading while keeping the femoral condyle subluxating from the tibial plateau. Since the ligament tissue is too short to clamp and test for tension failure, it is generally tested as a bone-ligament-bone functional unit. Using this methodology of testing functional units, various tensile loading tests had been conducted on the ACL [Woo, et al. 1991, Woo, et al. 1983, Noyes, et al. 1984a, Noyes, et al. 1984b]. Noyes and group [Noyes, et al. 1984a] determined that young adult human ACL can withstand 1730 N of tensile load before failure. Woo and colleagues used 27 specimens of Femur-ACL-Tibia Complex (FATC) to determine tensile properties of ACL [Woo, et al. 1991]. They tested the FATC tensile properties in two orientation scenarios. In the first case, the tensile load was applied along the axis of anatomical orientation of the ACL and in the second case; load was along the axis of the tibia. Interestingly, ACL failure load was higher when loaded in its anatomical orientation. A Typical load-elongation curve is shown in Figure 2.5 [Woo, et al. 1991]. The ultimate failure load along the anatomical orientation for young specimen (age 22-35 years) was 2160 N ($\pm$157 N) and for old specimen (age 60-97 years) it was 658 N ($\pm$129 N). Theoretical models have also been developed [Frankel, et al. 1980] dividing the ACL load-elongation curve into three functional zones viz. clinical testing zone, normal physiologic loading zone and injury zone. Even though the curve was predicted to be non linear in the physiological loading zone, the actual testing from Woo's study [Woo, et al. 1991] revealed that it was mostly a linear relationship (Figure 2.5) in this zone having a stiffness value of 242 N/mm ($\pm$28 N/mm). They also observed higher strain of approximately 10% at failure load for young adult specimen as compared to 3% observed for older adult specimens.

We will consider the pioneering work done by Woo and associates [Woo, et al. 1991] throughout this thesis while referring to the ACL failure strains or loads. Table 2.1 below is adapted from this study as a ready reference to the reader. This clearly indicates that the properties of the ACL are affected by the age of the person as well as the orientation

Table 2.1: Structural properties of Femur-ACL-Tibia Complex – Effect of specimen age and orientation (Woo et. al., 1991)

Age Group	Specimen orientation	Stiffness (N/mm)	Ultimate load (N)	Energy absorbed (N-m)
Young (22-35)	Anatomical	242±28	2160±157	11.6±1.7
	Tibial	218±27	1602±167	8.3±2.0
Middle (40-50)	Anatomical	220±24	1503±83	6.1±0.5
	Tibial	192±17	1160±104	4.3±0.5
Older (60-97)	Anatomical	180±25	658±129	1.8±0.5
	Tibial	124±16	495±85	1.4±0.3

of the load application. The ACL structure fails at lower loading conditions if the loads are not acting in the line of its longitudinal axis. Furthermore, being viscoelastic in nature suggests that structural properties of the ACL will depend on the rate of loading as well.

Chandrashekhar and colleagues [Chandrashekar, et al. 2006] showed that for loading at the speed of 100% /s strain rate, the same FATC failed at significantly lower load (1818±699 N) as compared to Woo and associates' study [Woo, et al. 1991] which was designed at 200 mm/min strain rate. They also showed that there was a significant difference due to gender in the tensile properties of the ACL. The failure loads for female specimens in this study were 1266±527 N whereas for male specimens, failure loads were 1818±699 N.

2.3.2 Functional Biomechanics of the ACL

As previously mentioned, the human knee joint is hold together by four major ligaments namely the ACL, PCL, MCL and LCL. The quadriceps and hamstrings muscle groups are responsible for normal flexion extension motion of the knee joint. During any activity, sufficient ground reaction and muscle forces are transferred to the knee joint and the four major ligaments play the important role of stabilizing the knee joint throughout its range of motion. The complex structure of the knee joint gives rise to complex functionality of each of the ligaments in stabilizing every DOF of the knee joint motion.

From the knee joint motion perspective, ACL acts as a primary restraint to anterior tibial translation when anterior drawer force is applied on the tibia [Woo, et al. 1999, Butler, et al. 1990]. ACL is not a primary stabilizer to restrain medial-lateral loads on tibia however, at higher medial loads; ACL gets significantly high strains [Piziali, et al. 1980]. Each bundle of the ACL plays a unique role in flexion extension motion of the knee joint. The AMB is tight in flexion and PLB is tight in extension [Amis, et al. 1991]. However, ACL loading is different in active and passive knee joint motion. In case of the passive knee flexion-extension, ACL strain increases with extension while femur is kept horizontal [Woo, et al. 1998]. ACL appears loaded maximally at or near full extension, with minimum loading occurring at approximately 30° of knee flexion [Bach, et al. 1997, Kennedy, et al. 1977, Kurosawa, et al. 1991a, Kurosawa, et al. 1991b]. For active flexion-extension, the ACL is again maximally loaded at or near full extension, with the strained-unstrained transition occurring at a slightly larger (approximately 40° - 50°) knee flexion angle [Beynnon, et al. 1992, Beynnon, et al. 1995, Beynnon, et al. 1997]. Tension in the ACL is least at 40^0 to 50^0 of knee flexion [Beynnon, et al. 1992, Beynnon, et al. 1995, Beynnon, et al. 1997]. When returning to extension from flexion, the lateral femoral condyle rolls on the tibial surface, whereas the medial femoral condyle, being less convex, translates backward on the tibia continuing its forward roll. This mechanism rotates the tibia laterally and referred as screw home mechanism of the knee in clinical terminology.

ACL plays secondary role in restraining internal-external rotation of the tibia [Norwood, et al. 1979, Seering, et al. 1980, Markolf, et al. 1981]. Differences exist while depicting ACL's role in controlling internal external rotation of the tibia. Ahmed and associates [Ahmed, et al. 1987] found that ACL has very little restraining role to play in external rotation, but plays certain restraining role at 40^0 flexion. But, it is worth to note here that Ahmed's study used strain gauges mounted on certain fiber bundles (typically AMB) of the ACL and may not represent the entire ACL strain. Role of the ACL in varus-valgus knee rotation has been carefully studied by researchers [Hollis, et al. 1991, Markolf, et al. 1976, Grood, et al. 1988, Wroble, et al. 1993]. Grood and Markolf studies concluded that ACL plays secondary role to MCL while restraining the varus-valgus motion at full extension. Wroble and colleagues [Wroble, et al. 1993] reported increase in knee valgus in the ACL deficient knees, whereas, Hollis and colleagues [Hollis, et al. 1991] observed increases in the ACL length during valgus loading.

2.4 METHODS TO ESTIMATE ACL LOADING

Understanding the ACL injury mechanisms is utmost important as it is a key component in developing subject specific neuromuscular training programs that will prevent athletes from ACL injuries. These mechanisms will not only elucidate the subject specific structural risk factors involved but also help determine alterations in the modifiable neuromuscular factors to promote prevention. Researchers developed different techniques through cadaveric and computational modeling to elucidate knee biomechanics and ACL loading, yet none of them reported on various injury mechanisms. Normal ACL biomechanics can not be simply extrapolated to represent high loads due to complex loading conditions and anatomical and neuromuscular factors involved during normal or sports movements. The second part of this Chapter provides a detailed literature review of the methods and models used to predict ACL forces and determine injury. The format of this part of the Chapter is kept as publication format so that it can be easily modified into a review publication in future.

2.4.1 Introduction

The Anterior cruciate ligament (ACL) injury is one of the most upsetting injuries to an athlete for his/her career. Besides losing significant playing time, the athlete is also at the risk of early onset of osteoarthritis [Lohmander, et al. 2004]. Almost 70% of the ACL injuries are of non-contact nature [Boden, et al. 2000] and involve ground contact that produces complex loading conditions on the knee joint injuring the ACL. It is now well known fact that young and physically active female athletes injure their ACL 2 to 6 times more frequently than their male counterparts when normalized to number of game exposures [Griffin, et al. 2000], making the female athletes more vulnerable to this injury. The overwhelming participation of the female athletes in different organized sports calls for immediate scientific attention to solving the ACL injury mechanism enigma to help understand and develop preventive measures based on the findings.

There is an abundance of research conducted on examining effects of isolated and/or combined knee load motion states on the ACL loading [Kanamori, et al. 2000, Pflum, et al. 2004, Shelburne, et al. 2004, Kanamori, et al. 2002, Li, et al. 2004, Bach, et al. 1995, Bach, et al. 1997, Blankevoort, et al. 1988, Blankevoort, et al. 1991a, Blankevoort, et al. 1991b]. There are numerous studies pertaining to the knee joint biomechanics and its relationship to neuromuscular control and joint anatomy [Pandy, et al. 1997, Pandy, et al. 1998a, Pandy, et al. 1998b, Steele, et al. 1999, Cowling, et al. 2003, Withrow, et al. 2006]. Through these studies, researchers have provided great insights to ACL injury and risk factors involved [Griffin, et al. 2000, Uhorchak, et al. 2003, Lephart, et al. 2002, Huston, et al. 2000]. Using the key findings in these studies, there is a subsequent development of neuromuscular training programs that are designed to prevent the ACL injury [Mandelbaum, et al. 2005, Beynnon, et al. 2005, Hewett, et al. 2001, Cerulli, et al. 2001, Myer, et al. 2004]. Despite these facts, ACL injury rates remain epidemic, suggesting that current training programs are excluding some key components of underlying ACL injury mechanisms. One of the key components is to understand the actual ACL load during different loading conditions and relating it to the injury.

ACL loading or strain has been quantified using a variety of research techniques, including in vivo models, cadaveric research, and computational models. Strain is a quantity with no units and it is determined by dividing the change in length of the ACL by its initial length and is reported in percentage. Many of these studies focus more on the methods involved and very few relate the findings to the ACL injury mechanisms. The objective of this part of the Chapter is to conduct a systematic review of the literature for each of the methods used to measure the ACL loading or strain by summarizing the highest level of scientific evidence available. The impact of each method is further examined in determining the ACL injury mechanisms.

2.4.2 Methods

2.4.2.1 Study Selection

We searched MEDLINE from 1950 through 2009 using a combination of following keywords: *anterior cruciate ligament + loading; anterior cruciate ligament + strain; anterior cruciate ligament + strain + model; anterior cruciate ligament +load + in vivo*. After carefully reading the abstracts, we included the studies in this review if the authors (1) described methods to measure the ACL loading or strain, (2) used the methods to study ACL load or strain during certain activities or tasks, and (3) assessed non-contact ACL injuries using these techniques. Additional studies were obtained via references from the identified articles and recommendations from the experts.

2.4.2.2 Study Classification

All the included studies were then classified into three major groups: (1) studies conducted in vitro on cadaveric specimens, (2) studies conducted in vivo on live subjects, and (3) studies involving computational methods. Each of these classifications was further divided into sub-groups based on the techniques used. In vitro study deals with a research conducted using specific tissue, joint structure (e.g., knee joint), organ or cell preparations, whereas in vivo studies indicate a research conducted with a living organism. The cadaveric methods gave insights to the ACL loading during passive knee biomechanics whereas the in vivo methods gave active ACL loading. The computational methods, on the other hand, were used to determine the ACL loading in complex loading conditions on the knee joint that could not be mimicked in cadaveric experiments without injuring the ACL.

2.4.3 Results

The initial search retrieved 1254 articles through MEDLINE. We scrutinized these articles for the subject relevance and found total 48 articles meeting our inclusion criteria. There are 22 article that use cadaveric specimens in understanding the ACL loading, 12 use in vivo techniques and the remaining use computational modeling approaches for the same purpose. Cadaveric studies were dated as back as 1982 whereas computational modeling studies did not start until 1991.

2.4.3.1 ACL Loading In Vitro (Cadaveric Studies)

Tissue loading can be quantified by measuring stress, strain, or force. Researchers have used either contact or non-contact methods to quantify the ACL loading. In contact methods, direct physical contact is made with the ligament mid-substance by a force measuring device. Ahmed and associates used buckle transducers as shown in Figure 2.6 to understand tension in the ligaments [Ahmed, et al. 1987, Ahmed, et al. 1992]. Lewis and colleagues [Lew, et al. 1978, Lewis, et al. 1989] also used buckle transducers to

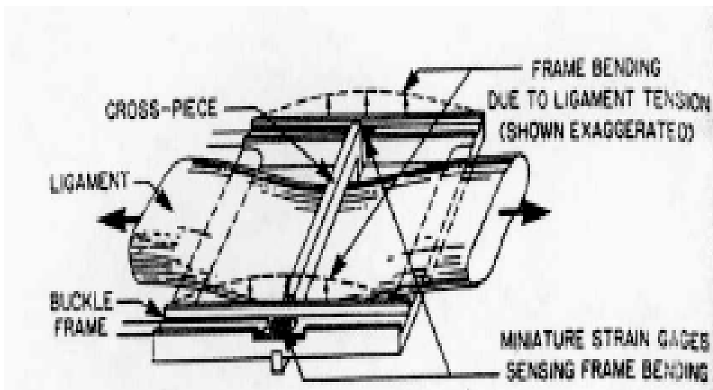

Figure 2.6: Schematic representation of a buckle transducer (Ahmed et al., 1987)

measure ligament forces. However, the instrumentation used required direct contact with the ACL causing the ACL length to alter and thus introducing the error in the force measured. Force was measured within a small section of the ligament, having few bundles from the ligament, and not on the entire length. Due to these limitations, many researchers developed non-contact approaches to determine the ACL loading. France and colleagues placed strain gauges near the ligament insertion sites [France, et al. 1983]; Vahey and associates used X-rays to make the kinematic calculations [Vahey, et al. 1991]. Markolf and associates [Markolf, et al. 1990, Markolf, et al. 1995] used external force transducers (load cell), attached in-line to ACL, to measure the forces produced in ACL in vitro. These methods avoided the contact problems, but are limited either by complexity of the technique or its ability to easily vary flexion angle and applied loads. Woo et al [Woo, et al. 1983] and Butler et al [Butler, et al. 1986] used optical techniques to determine the surface strains in the soft tissue. These techniques were ideal for monitoring the surface strains, but not useful for the out-of-plane movements. Another non contact method was proposed by Woo and associates [Woo, et al. 1998]. They applied various loads to the cadaver knees using a robotic arm with 6 degrees of freedom force transducer attached to it. The computer interface recorded the knee kinematics during these loads. Then the ACL was cut and the kinematic path of the ACL intact knee was repeated by robotic arm while the corresponding forces on the load cell were recorded. Load in the ACL was determined by calculating the difference between the applied forces and recorded forces. The primary advantage using this method was the ease in controlling the knee joint kinematics and kinetics.

2.4.3.2 ACL Loading In Vivo

In vitro studies quantified the ACL loading during passive knee loading, where the

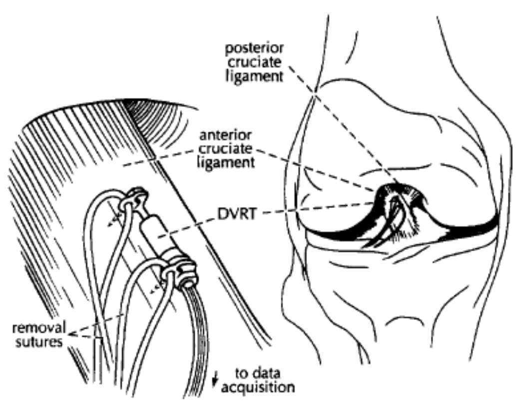

Figure 2.7: The Differential Variable Reluctance Transducer (DVRT) attached to the ACL with barbs (Fleming et al., 1998)

dynamic effects of muscles on the joint were either simplified or neglected. ACL loading patterns in those studies, therefore, did not necessarily represent the actual loading patterns in the living human. Quantifying the ACL strain in vivo could give useful insights in the ACL response to various joint loading conditions. Beynnon and group used implantable DVR transducers as shown in Figure 2.7 and studied in vivo ACL strain during different activities including squatting [Beynnon, et al. 1997], open and closed kinematic chain flexion exercise [Beynnon, et al. 1995], weight bearing knee flexion [Fleming, et al. 2001], stair climbing [Fleming, et al. 1999] etc. The transducer was implanted on the AMB of the ACL and the strain behavior was recorded while subjects performed the desired tasks. Li and associates [Li, et al. 2004] used live CT images to obtain the ACL insertion positions and subsequently used computational modeling techniques to calculate the ACL strain.

2.4.3.3 ACL Loading Estimated by Computer Simulations

All the in vivo and in vitro techniques above are invasive and can not be used to study dynamic sport movements. Also, it is not economically feasible to study the ACL injury mechanisms as each knee specimen can be injured only once. Cadaveric models are excellent guides to study the relationship between external loads applied on the joint and its distribution among the anatomical structures. As these structural loads are primarily affected by agonist and antagonist muscle activation patterns, cadaveric models are limited to passive joint mechanics as they do not include and/or mimic in vivo muscle loading patterns. It is very hard to get specimens of a desired age group, and the activity level of the specimen is always unknown. Limitations of the cadaveric models can be overcome by using computational models. These models can be injured again and again in order to study the underlying mechanisms. Computational modeling can take into consideration dynamic muscle activation patterns and offers unique potential to study injury events. Properly optimized and validated computational models can be used to estimate the forces in ligaments or its bundles. Due to these attractive advantages of computational modeling over cadaveric models, many researchers put in their efforts to develop computational models to study the knee joint biomechanics.

Computational models developed thus far are divided into movement mechanics models and joint mechanics models. Movement mechanics models predict overall forces produced at the knee joint. Computational models of joint mechanics estimate the loads

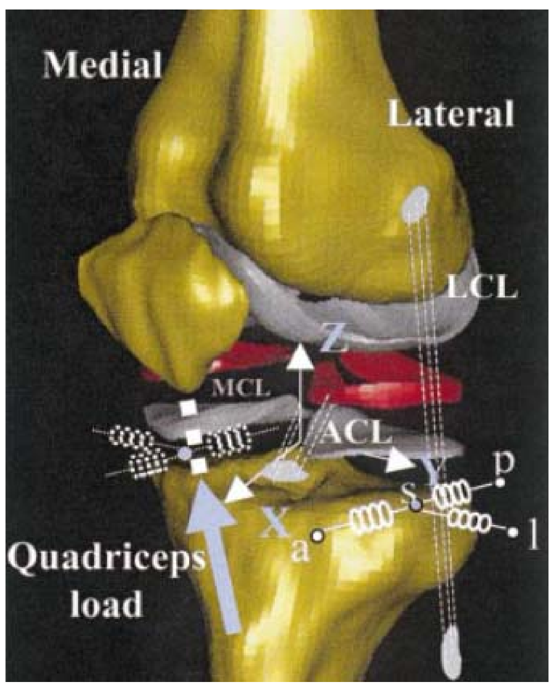

Figure 2.8: Finite element knee joint model developed from MRI scans
(Li et al., 2002)

experienced by the individual structure of the joint. McLean and associates [McLean, et al. 2003, McLean, et al. 2004] developed a forward dynamic, subject specific, musculoskeletal 3-D model to simulate the stance phase of first 200 ms of a side step cutting maneuver. After optimizing and validating each model, initial kinematic conditions were randomly perturbed for over 5000 trials. ACL injury was determined when any of the peak joint loads exceeded force and moment thresholds (2000 N and 210 Nm). Shelburne and associates [Shelburne, et al. 2004] developed an analytical model that had forward multibody dynamics combined with the joint mechanics. The model was not subject specific and not validated. Only a single movement simulation could be presented due to high a computational complexity. Li and colleagues [Li, et al. 2002] developed a validated 3-D finite element model as shown in Figure 2.8 to simulate ACL injured knee biomechanics. Generic finite element models of the knee joint already exist and have been used to simulate the ACL reconstruction techniques [Pena, et al. 2006], and active and passive knee biomechanics [Bendjaballah, et al. 1997, Bendjaballah, et al. 1998, Mesfar, et al. 2003, Mesfar, et al. 2005, Mesfar, et al. 2006a, Mesfar, et al. 2006b, Moglo, et al. 2003, Moglo, et al. 2005, Shirazi-Adl, et al. 2005]. Boisgard and group [Boisgard, et al. 1999] used computerized reconstruction from MRI scans to study the changes in ACL length from 0^0 to 75^0 flexion. Blankevoort and Huiskes [Blankevoort, et al. 1996] used quasi-static multibody modeling approach and developed a 3D model of the knee joint to simulate passive motion characteristics of the human knee joint. Cohen and associates used similar approach [Cohen, et al. 2003] to make subject specific patello-femoral joint models to simulate tibial tuberosity transfer procedures. Caruntu and Hefzy developed an anatomical dynamic model to determine the three dimensional dynamic response of human knee [Caruntu, et al. 2004]. The model was not subject specific and not validated. The model was used to study the knee flexion-extension exercise and analyze the loads experienced by ACL and PCL.

All these models were either generic or not validated and used to analyze normal ACL loading patterns during non-injurious movements. None of the above models were used to predict ACL injury mechanisms. Movement mechanics models [McLean, et al. 2004] did not have representation of ligaments and injury thresholds were based on the values reported in the literature. Joint mechanics models were simplified [Blankevoort, et al. 1996, Pena, et al. 2006] or not subject specific [Shirazi-Adl, et al. 2005, Caruntu, et al. 2004].

2.4.4 Discussion

There are varieties of techniques that quantify ACL loading using variety of techniques. Cadaveric models give basic insight to the underlying passive biomechanics of the joint. Computational models give important information about joint behavior under different loading conditions. Each study discussed above quantifies the ACL loading for particular purpose using particular loading or tissue property selection criteria. For effectively studying the ACL loading and injury mechanisms, cadaveric models are limited by high specimen costs, variability in strain rate, and inter specimen variability, whereas, computational models are limited by non subject specific joint geometry, assumed tissue properties, and high computational cost and time.

Methods for simulating joint mechanics under given external loads have been developed by our collaborator Dr. Leendert Blankevoort, and already being used for surgical simulations [Cohen, et al. 2003]. These are multi-body modeling approaches that use highly efficient algorithms to solve the mechanics of large structures. We propose to use these techniques in the current study to predict ligament forces in sports-like loading conditions. In this study, computational modeling techniques and multi-body quasi-static modeling domains are used to incorporate subject specific geometry, tissue properties, and neuromuscular control. Even though computational models are used, experiments are necessary to implement subject specificity and for validation. The models so developed are optimized for experimental data pertaining to the knee kinematic response to isolated loading conditions and then perturbed to simulate hazardous sports movements using interaction between joint geometry, tissue properties and neuromuscular control, to effectively study the ACL injury mechanisms.

CHAPTER III

EXPERIMENTAL ANALYSIS OF THE PASSIVE KNEE KINEMATICS AND THE ACL STRAIN DURING LAXITY AND COMBINED LOADING ON THE KNEE JOINT

In order to develop subject specific computational models, adequate experimental data were required to optimize model parameters as well as to validate model predictions. As collecting data on live humans was not in the scope of this study, we used five cadaveric knee joint specimens. Cadaveric experiments were performed using the Musculoskeletal Robotics and Mechanical Testing Core's (MRMTC) state-of-the-art six degree of freedom (DOF) motion platform Rotopod (R-2000, Parallel Robotic Systems Corp., Hampton, NH) and an in-house developed software interface in the LabVIEW (National Instruments Corp., Austin, TX). This chapter describes in detail the methodology and tools used to collect experimental kinematic and ACL strain data on each of the five cadaveric specimens.

3.1. INTRODUCTION TO ROTOPOD

Rotopod R-2000 is a hexapod that comes with an application program interface (API) for 6 DOF motion control robot. This robot uses six struts and motors to produce motion of its platform (Figure 3.1). Using this robot, one can achieve a high level of accuracy and stiffness. The robot has the ability to move all the six legs in a coordinated fashion giving it both a wide range of available motion and complete control of every DOF. Translation DOFs are named as X, Y and Z whereas rotational or orientation DOFs are named as roll, pitch and yaw. R-2000 has a positioning accuracy of 50μm and the remaining specifications are given in Appendix A (A1). This type of robotic system is now successfully used in biomechanics research (University of Calgary, University of Alberta, and Cleveland Clinic), flight simulators and many other industrial applications. In biomechanics, this device is mostly used to apply controlled 6 DOF motions to cadaveric specimens. In the Biomedical Engineering department of the Cleveland Clinic, the

Figure 3.1: Rotopod R2000 was used to conduct experiments on cadaveric specimens.

MRMTC has been developing different research protocols to study shoulder, knee and ankle joints using R-2000 robotic system. This study used the knee joint protocol that was made to mount the specimen, initialize the robot and transform the robot coordinate system in a suitable Joint Coordinate System (JCS) as explained by Grood and Suntay [Grood, et al. 1983]. The JCS provides a geometric description of three dimensional translations and rotations between the two rigid bodies for clinical perspective.

3.2 LabVIEW INTERFACE

Using the motion control API, MRMTC has developed a LabVIEW software system to use the robot both in motion or force control mode [Noble, et al. *In Press*]. This software interface served two purposes. First, it gave step-by-step instructions to the user to mount the specimen on the robot platform and create a JCS specific to the specimen. This was achieved by using a geostationary MicroScribe G2L digitizer (Immerson Corp., San Jose,

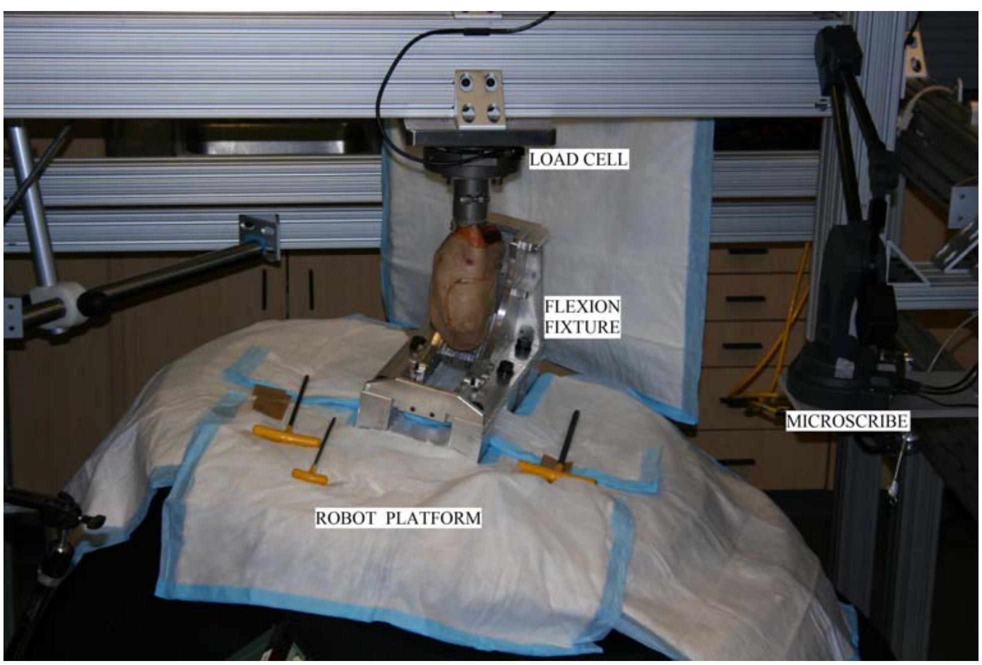

Figure 3.2: Experimental setup

CA) mounted on a metal rigid frame that was constructed around the robot. The MicroScribe specifications are given in Appendix A (A1). A universal force sensor (UFS) (SI-1500-240, ATI Industrial Automation, Apex, NC) was attached to this frame whereas a flexion fixture was attached to the robotic platform as shown in the Figure 3.2. The force sensor performance characteristics are given in Appendix A (A1) for reader's ready referral. The maximum allowable distance between the UFS and the robot platform can be adjusted depending on the type of the joint under study.

3.2.1 JCS

Data points were collected on and around the specimen. Specifically, for the knee joint studies, position vectors for load cell, flexion fixture, MicroScribe and knee joint specimen were collected by the MicroScribe stylus. The software interface then converted all the measured coordinates in such a way that the JCS was established. In this

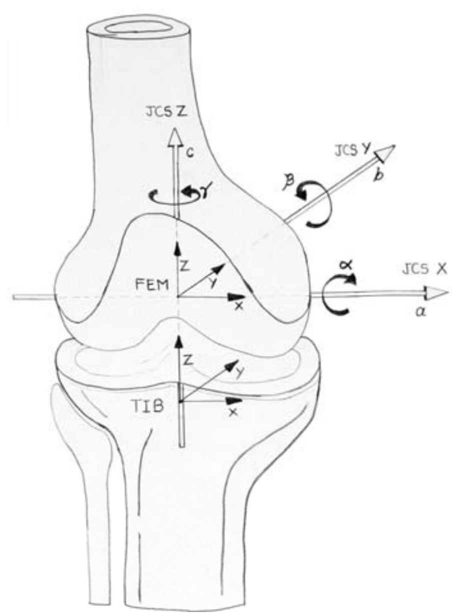

Figure 3.3: Schematic diagram explaining Joint Coordinate System

system, for the right knee, X-axis was pointing medially, Y-axis was pointing posteriorly and Z-axis was pointing superiorly. Figure 3.3 illustrates the schematic diagram of the knee joint with femur coordinate system FEM, tibia coordinate system TIB and JCS.

The origin of this coordinate system was the midpoint of two femoral epicondylar points collected using the MicroScribe. The JCS was defined by the flexion (X) axis in the knee and the internal rotation (Z) axis in the tibia. Directions were such that flexion, internal rotation, and valgus were positive angles. The flexion axis was fixed in the femur; the internal-external rotation axis was fixed in the tibia, and the floating axis for varus-valgus rotation was perpendicular to the other two. Medial translation was measured along the flexion axis, anterior translation along the floating axis and superior-inferior translation was measured along the tibia-fixed axis.

Thus, JCS had following DOFs:

a	medial translation of tibia
b	posterior translation of tibia
c	superior translation of tibia
α	flexion
β	valgus
γ	internal rotation

3.2.2 Robot Control

Second purpose of the software was to control the robot either in force or motion control mode. This was achieved using a feedback loop from the robot and the UFS. The interface continuously monitored the feedback data and controlled the robot position and orientation using a set of proportional-integral-derivative (PID) controllers. The velocity of the robot was controlled by controlling the gains of the PID controllers. When in force control mode, the interface gets a continuous feedback from the UFS and converts it into force and moment vector in the tibia coordinate system. The goal is to achieve user determined forces and/or moments in the tibia coordinate system. Using the feedback from the UFS and controlling the velocity of the robot, the interface tries to achieve the target in each DOF, in the tibia coordinate system and records corresponding joint kinematic data in the JCS. In motion control, the robot follows the user provided target positions and orientations, in each DOF, in the JCS, within stipulated time frame while recording the corresponding joint forces and moments in the tibia coordinate system. The interface also takes into account the user specified limits on DOFs and UFS. For e.g.,

Figure 3.4: Real time display of desired and actual forces and corresponding knee kinematics in left hand screen and corresponding PID controller gains and other robot data in right hand side screen.

user can set a limit of 30^0 on internal-external rotation and the robot would stop if this limit is reached while running any force control protocol. While running the robot in force control, the LabVIEW interface displays a real time view of the desired and actual loads (Figure 3.4) helping the user to adjust the controller gains during each run.

In the left screen of Figure 3.4, you can see four small windows. The upper left hand corner window displayed translations in tibia coordinate system whereas the lower left hand corner window displayed rotations (orientations) of the joint in JCS. The upper right hand corner window displayed the desired and actual forces applied to the joint and the lower right hand corner window displayed the desired and actual moments applied. The right hand screen displayed the PID controller gains. For motion control, the real time view of actual loads help user identify hazardous loading on the specimen and stop the robot.

3.3 SPECIMEN PREPARATION

3.3.1 Specimen Storage and Checking Joint Tissue Integrity

Five cadaveric knee specimens were used for this study. Four specimens were purchased from Life Legacy Foundation (Life Legacy Foundation, Inc, Tucson, AZ) and one from National Disease Research Interchange (NDRI, Philadelphia, PA). Prior to the study, Cleveland Clinic's Institutional Review Board's (IRB) exemption was obtained under category #4. The letter of exemption is attached in Appendix A (A2) for reader's ready referral. All the medical history and serology analysis data was obtained (Appendix A – A3 and A4) for each specimen to rule out any significant damage to the tissue due to any prior injury or medication and to maintain healthy working conditions in the laboratory. The details of each specimen are provided in Table 3.1.

Table 3.1: Details of each specimen

Specimen number	Sex	Age	Weight (kg)	Cause of death	Bone disorders
Knee 1124	F	70	77.2	Lung Cancer	None
Knee 1129	M	58	91.5	Laryngeal Cancer	Arthritis in hands
Knee 1131	M	58	91.5	Laryngeal Cancer	Arthritis in hands
Knee 1133	M	58	70	Small cell lung cancer	None
Knee 1135	M	58	70	Small cell lung cancer	None

Specimens were stored in a freezing storage at -20^{0}C before the start of the study. According to a study conducted by Woo and associates [Woo, et al. 1986], careful freezing of the tissue at -20^{0}C for up to 3 months would not have any effect on biomechanical properties of the ligaments. So we were assured of retaining the mechanical properties of the tissues. Each specimen was thawed overnight and MRI scans from all three anatomical planes viz. sagittal, coronal and axial were acquired. MRI scans were performed using 1T extremity scanner (ONI Corp., Santa Rosa, CA) located in the biomechanics laboratory. Readers are requested to turn to Chapter 4 to read the details of the MRI scans. The scans were visualized to confirm the ligament and cartilage integrity of the specimen. In all five specimens, MRI scans revealed intact ligaments and no significant damage to the cartilage. A medial parapatellar osteotomy was performed on each specimen to verify ligament and meniscal integrity and to document any arthritic damage to the cartilage. All the ligaments in all the specimens were found intact along with healthy cartilage.

3.3.2 Cross Referencing the Tibia and Femur Coordinate Systems

To compare the experimental data with model predictions, it was necessary to make sure that the experimental JCS in which the kinematic data was recorded, was an exact match with the computational model coordinate system. Ramakrishna and Kadaba [Ramakrishnan, et al. 1991] studied the effect of variations in joint coordinate systems on joint kinematics and showed that small uncertainties can significantly affect the joint kinematics. The only way to match the two coordinate systems was to have exactly same reference point while creating the coordinate systems. Since the origin of the femur coordinate system was determined by measuring coordinates of the medial and lateral epicondyles of the femur, we drilled 6-32 X ¾" vinyl screws in these epicondyles. These vinyl screws showed up as a dark contrast in the MRI scans and were then used as cross references while developing the joint model coordinate system. Using these screws as registration objects both in experiments as well as models; we believe that we would get a close matching of the coordinate systems.

3.3.3 Strain Gauge – Calibration and Mounting

As discussed in Chapter 2, strain gauges provide basic information about the strain experienced by the tissue under load. In our experiments, we used single Differential Variable Reluctance Transducer (DVRT) (MicroStrain, Inc., Williston, VT) to register the strain data in the AMB of the ACL of each specimen. In theory, application of multiple DVRTs could provide a detailed mapping of the strain distribution across the different bundles of the ACL, however, it was out of the scope of this thesis. The typical components of DVRT are shown in the Figure 3.5. The free end of the DVRT is called core and it slides inside the stainless steel shell. The ruby tip of the core and the distal end of the shell get attached to the tissue for which the strain data is needed. We used a

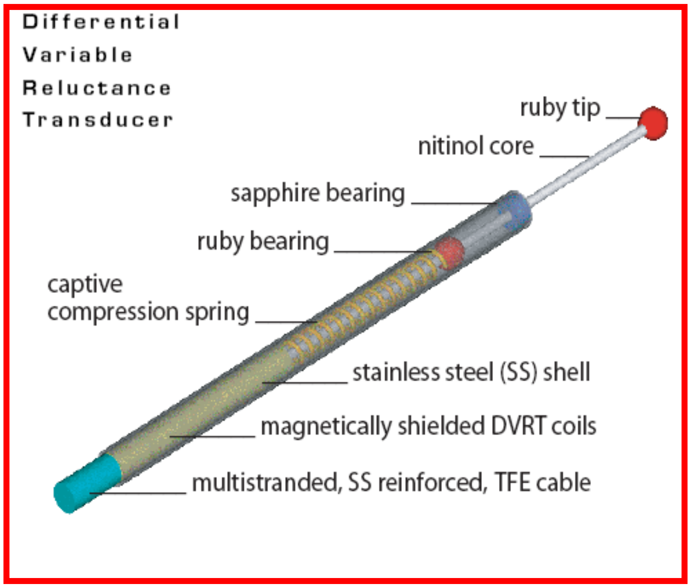

Figure 3.5: Components of DVRT (www.microstrain.com)

customized DVRT that came with barbs at ruby tip and distal shell ends. These barbs when pressed hard in the tissue would hold on to their position reducing the error in the strain data collection. The position of the core is detected by measuring the coil's differential reluctance.

The differential method used by MicroStrain provides a very sensitive measure of core's position and eliminates any temperature effects. Readers are requested to turn to A5 of Appendix A for further information on the DVRT product overview and specifications.

Before using the DVRT, it was necessary to calibrate this strain gauge and calculate it's functional as well as mid range for mounting purposes. We calibrated the DVRT starting the ruby tip from its fully closed position to fully open position. Linear relationship between the gauge length and gauge voltage was established by fitting a linear regression

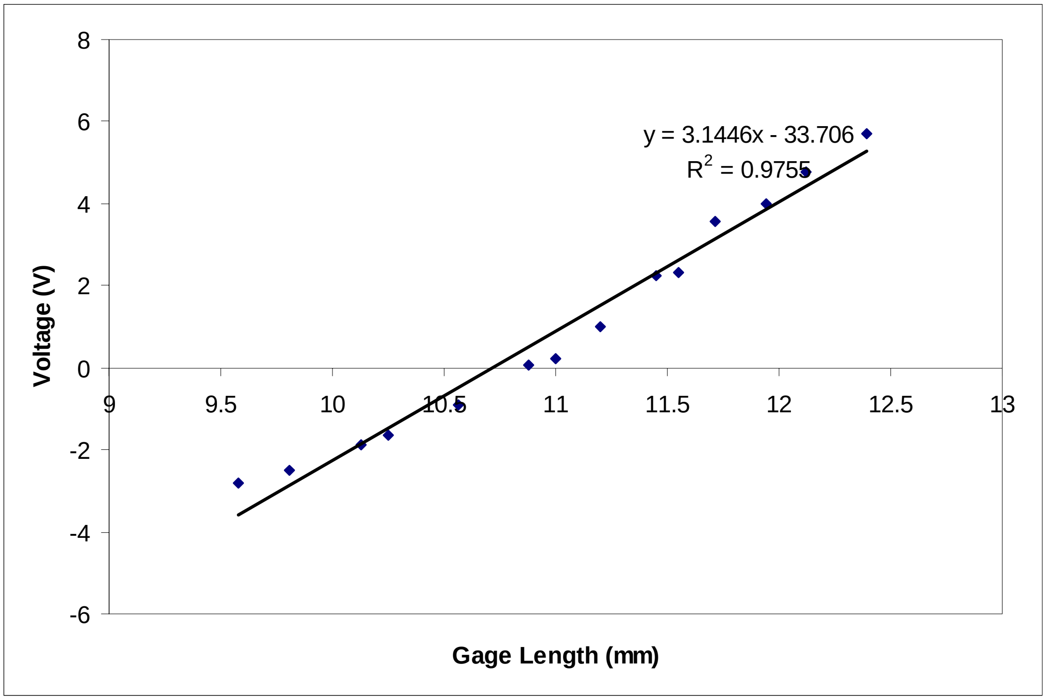

Figure 3.6: DVRT calibration graph. For this DVRT, slope = 3.144 V/mm and x intercept is -33.706

line through the data points with R^2 value equal to 0.9755 as shown in the Figure 3.6. It was determined from the graph that the safe linear range for this DVRT was between 9.8mm to 12.12mm with corresponding voltage ranging from -2.88V to 4.409V.

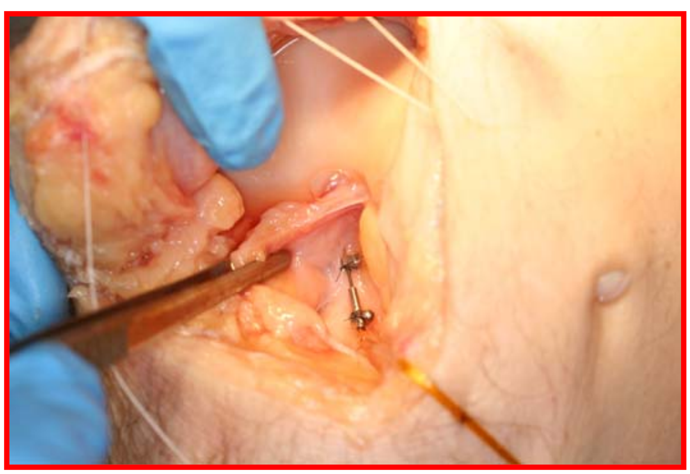

Figure 3.7: DVRT mounting on the AMB of ACL

After checking the ligament integrity through medial parapatellar osteotomy, the DVRT was mounted on the AMB of the ACL. To verify and isolate the AMB, knee specimen was flexed to 30^0 and cyclic anterior drawer force was applied on tibia that made the AMB taut [Beynnon, et al. 1995]. Barbs were inserted in the AMB in such a way that the distal barb of the DVRT was about 3 to 4mm above the tibial insertion of AMB. This was done to avoid the DVRT impingement against the femoral notch during full extension of the joint. To ensure the reproducibility of the DVRT output, it was necessary to do repeated normal tests before the beginning of actual data collection. Owing to the loading tests conducted on the specimen, we sutured each barb to the tissue using grade II polyethylene suture material as shown in the Figure 3.7. To ensure that the DVRT remained functional throughout the loading protocol, we had to mount the barbs at about mid point of its safe working range. This was achieved by suturing the first barb to its position and then placing the second barb while looking at the DVRT output at the same time.

3.4 SPECIMEN MOUNTING AND INITIALIZATION

For each specimen, joint capsule was left intact (approximately 6-7cm on each side of the joint line) and the remaining musculature and tissue was removed. Femur and tibia were potted in 50mm diameter pots and sealed with wood's metal (Lipowitz's alloy). Two drill bits were drilled transversely through the pots and left there intact to help wood's metal hold the bone and pot together. Tibia was fixed to the UFS and femur was moved in a fixture mounted on the robotic platform to achieve desired flexion angle as shown in Figure 3.8. The fixture is designed to flex the knee through series of flexion angles up to

120^0. A specimen initialization protocol was run which calculated coordinate transformations from robot coordinate system and UFS coordinate system to establish the knee JCS [Grood, et al. 1983] to record kinematics and the tibia coordinate system to apply and control forces and moments. Once femur was fixed to a desired flexion angle, robot was operated in force control mode and a neutral loading position of the joint was established. Neutral loading position was achieved to relieve the joint from any residual forces or moments. To establish a consistent neutral position, knee joint was biased using a small internal rotation moment of 0.001 Nm on tibia and allowing the robot to rest in a

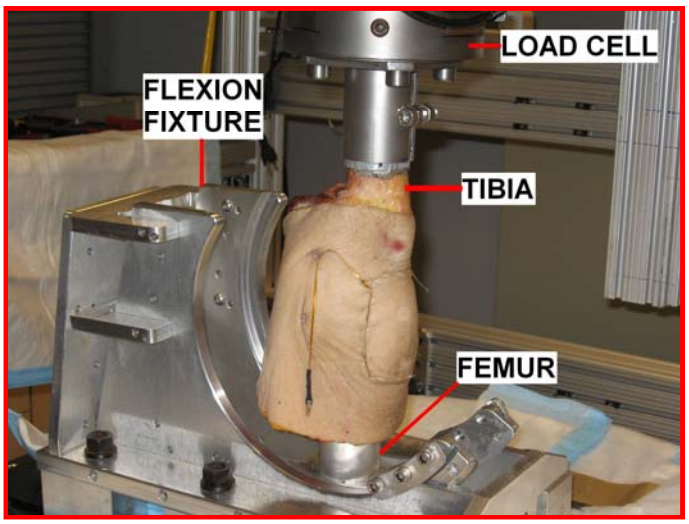

Figure 3.8: Flexion fixture – specimen – UFS (Load Cell) set-up.

position where the robot controller gains were not changing significantly. After this step, robot was operated in force control mode and loading trajectories were executed to determine 5 DOF kinematics of the knee joint. This is a standard methodology used for mechanical testing of knee joints using robot [Kanamori, et al. 2000].

3.5 JOINT KINEMATICS DATA COLLECTION

Once the preliminary set up was completed, the specimen underwent series of laxity loading trajectories and combined loading trajectories. For each flexion angle, laxity and combined loading trajectories were run under force control mode and corresponding kinematic in remaining 5 DOF was recorded in the JCS. For this study, we used four flexion angles viz. 0^0, 15^0, 30^0 and 45^0 on which the loading trajectories were applied. Each specimen was preconditioned by applying the laxity loading protocols before the start of data collection. Considering the viscoelastic nature of the ligaments, preconditioning made sure that the ligaments were free of any residual stress that might be present due to their stress relaxation property. Preconditioning protocol was also used to confirm the smooth behavior of the DVRT output. After all the kinematic data collection protocol was over, one flexion angle was randomly selected and either laxity or combined loading protocol was repeated. This was done to confirm the repeatability of experiments and to rule out the possibility of injury or damage to any of the joint structures.

3.5.1 Laxity Test Parameters

Joint laxity can be defined as a subject specific passive relationship between force or moment applied in an isolated DOF of the joint and corresponding movement of the joint. We will use this data as an optimization target for estimation of subject specific joint model parameters (Chapter 5). Joint laxity in 3 isolated DOFs was recorded as follows:

1) Internal-external (I-E) laxity was recorded by applying I-E rotation moment from 0 to $\pm$5 Nm in steps of 1 Nm at flexion angles from 0^0 to 45^0 in steps of 15^0.

2) Varus-Valgus (V-V) laxity was recorded by applying V-V rotation moment from 0 to $\pm$10 Nm in steps of 2.5 Nm at flexion angles from 0^0 to 45^0 in steps of 15^0.

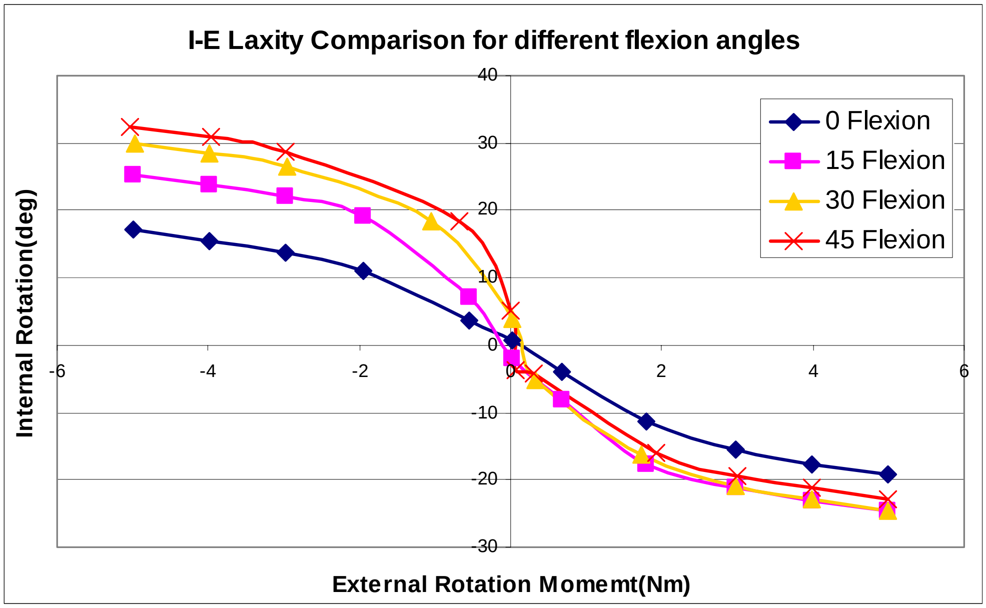

Figure 3.9: I-E laxity data for specimen # 1

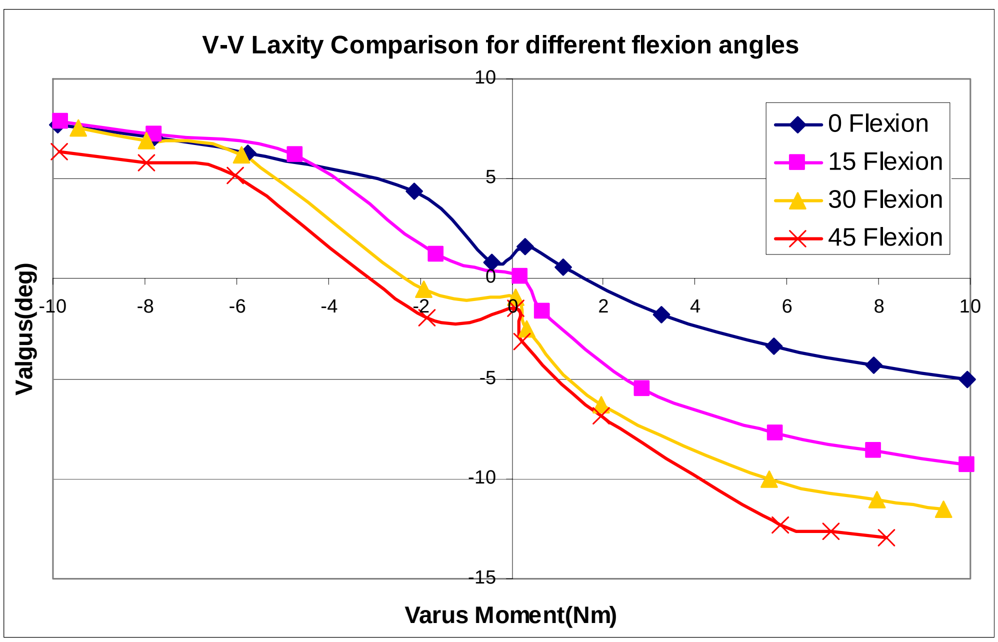

Figure 3.10: V-V laxity data for specimen # 1

3) Anterior-posterior (A-P) laxity was recorded by applying A-P force of 0 to $\pm$100 N in steps of 10 N at flexion angles from 0^0 to 45^0 in steps of 15^0.

This generated laxity data for total of 52+52+88 = 192 loading states. Joint kinematic data was recorded at each loading state by the LabVIEW interface. 192 Loading states

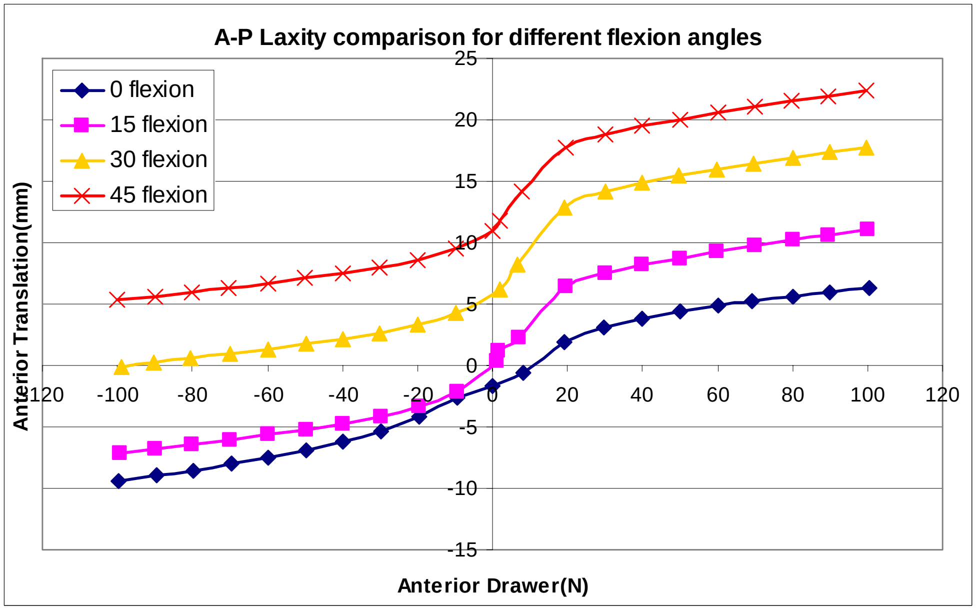

Figure 3.11: A-P laxity data for specimen # 1

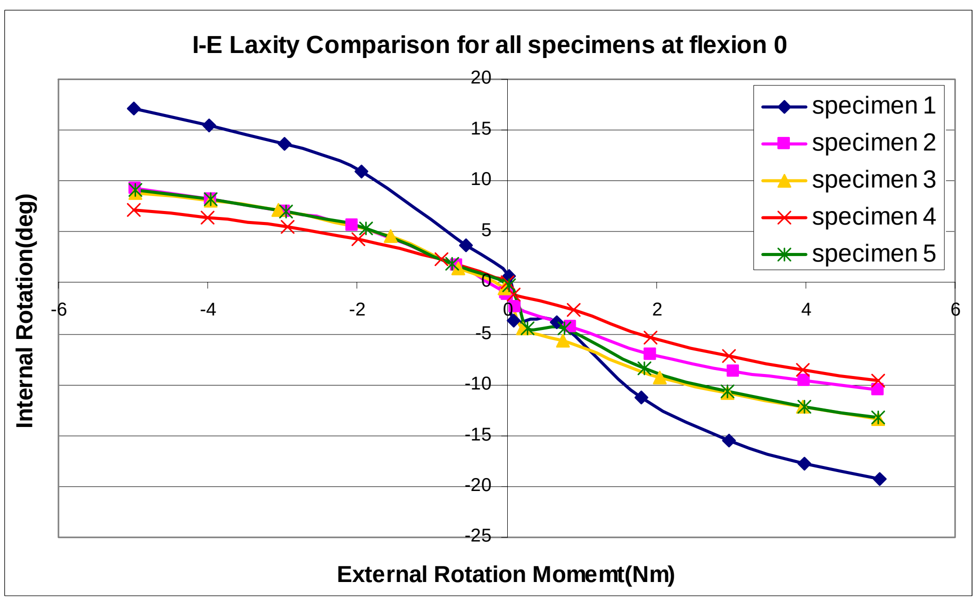

Figure 3.12: I-E laxity data for all knee specimens at flexion 0

included 28 neutral or near zero loading conditions, 7 for each flexion angle, that were recorded in between the switchover from one loading direction to another. Figure 3.9 shows I-E laxity data for knee specimen # 1 for all flexion angles.

Figure 3.10 shows V-V laxity data and Figure 3.11 shows A-P laxity data for the same specimen. We are reporting the data in terms of absolute values as recorded by the LabVIEW software.

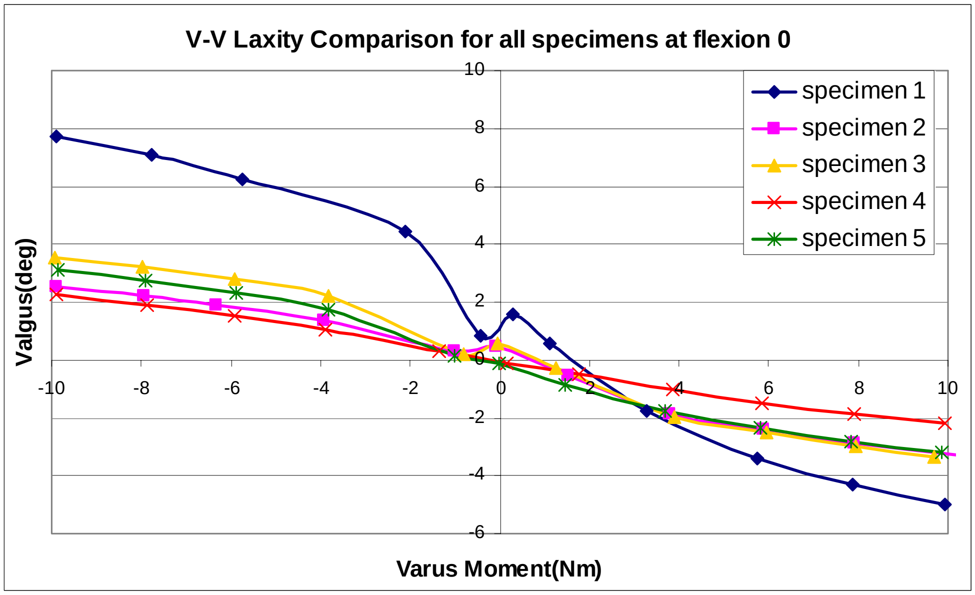

Figure 3.13: V-V laxity data for all knee specimens at flexion 0

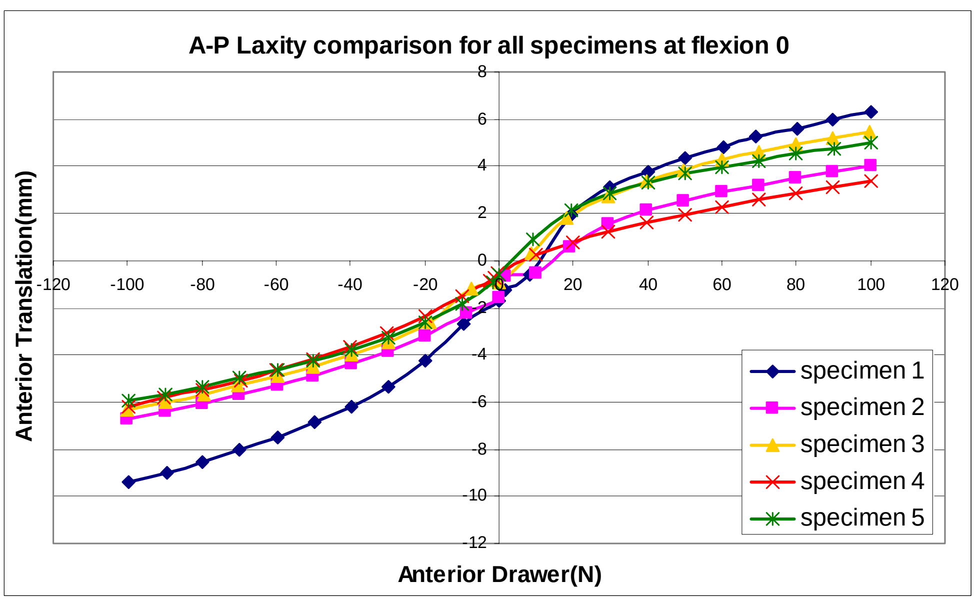

Figure 3.14: A-P laxity data for all knee specimens at flexion 0

Similar results were observed for all other specimens. For knee specimen # 1, internal rotation laxity was more pronounced for higher flexions (Figure 3.9) whereas the external rotation laxity did not change much with flexion angle. Varus laxity increased prominently as flexion angle increased (Figure 3.10). Even though there was a shift in A-P laxity curve (Figure 3.11), the relative laxity within each flexion angle remained constant. The shift was observed due to a roll back of femur on tibial plateau during flexion. Laxity values changed as specimen changed, but these overall observations remained the same. Based on the overall joint stiffness, laxity values differed from one specimen to another. Figure 3.12 shows comparison of I-E laxity data at 0^0 flexion angle for all the specimens. Figure 3.13 shows the same comparison for V-V laxity and Figure 3.14 shows A-P laxity comparison for all the specimens. As can be seen from these comparisons, specimen # 1 appears to be more lax than all the other specimens. The reason could be attributed to the age of the specimen. Specimen # 1 was from a 70 year old donor while all other specimens were from 58 year old donors. However there was no scientific study that particularly focused on the effect of gender or aging on joint laxity.

3.5.2 Combined Loading Test Parameters

After laxity loading tests, each specimen underwent series of combined loading tests at each of the four flexion angles. The combined loading consisted of permutations of I-E moment ranging from 0 to $\pm$5 Nm and V-V moment ranging from 0 to $\pm$10 Nm while under either anterior or posterior drawer force of 100 N. This data is more representative of sports movements and will be used for validating the joint models in chapter 6. The loading trajectory using anterior drawer force of 100 N is shown in the Figure 3.15. A typical kinematic response as recorded on specimen # 1 for 0^0 flexion angle is shown in Figure 3.16.

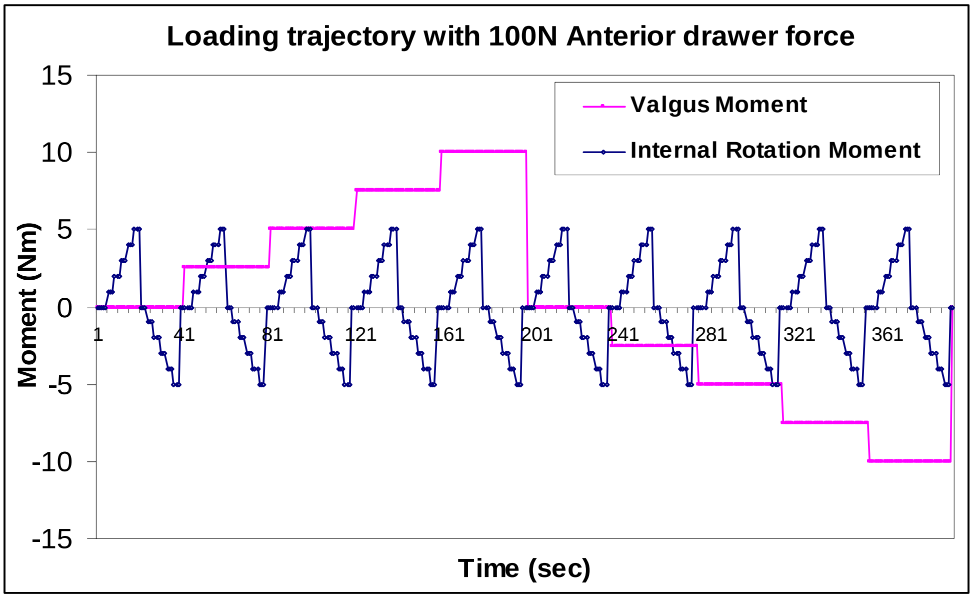

Figure 3.15: Combined loading trajectory

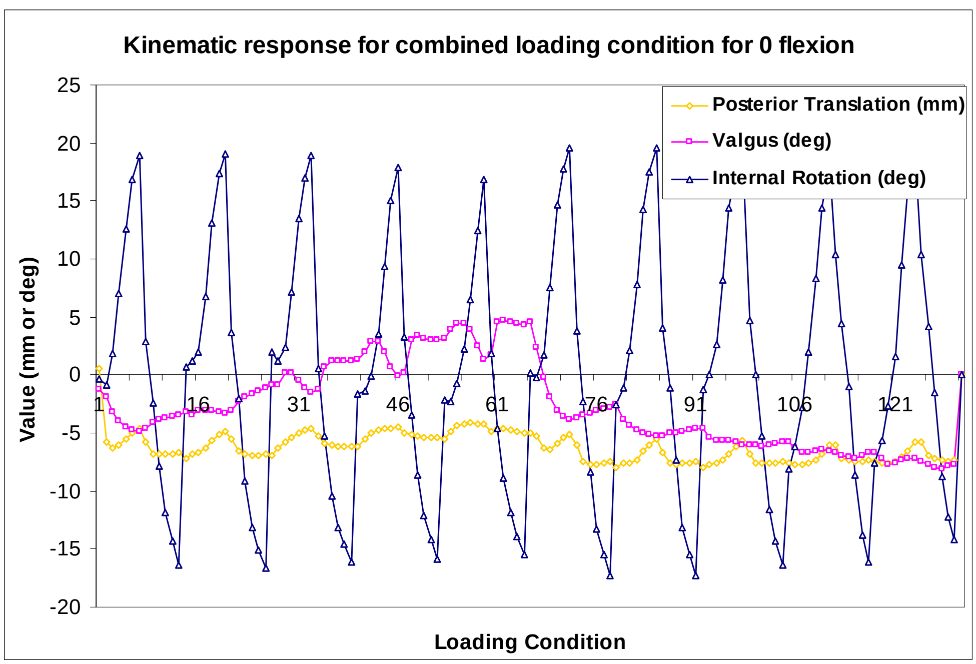

Figure 3.16: Kinematic response to combined loading trajectory by knee specimen # 1

Internal rotation angle peaks reduced as the valgus moment increased whereas anterior translation of the tibia seemed unaffected by the moments applied in combination. Again, similar observations were made for all the specimens. A complete combined loading trajectory for one flexion angle required 20 minutes 35 seconds to complete. Each specimen was kept moist throughout the entire testing protocol using saline solution.

3.6 ACL STRAIN DATA ANALYSIS

As described in Section 3.3 of this chapter, we collected ACL strain data on each of the laxity and combined loading conditions. The strain data was recorded in Volts and using the calibration graph, the actual gauge length to the corresponding voltage output was calculated. Strain data was not recorded for specimen # 3 because of the difficulties faced. For this specimen, even though DVRT was installed at its midrange, it was not functioning at 0^0 and 15^0 flexion angles.

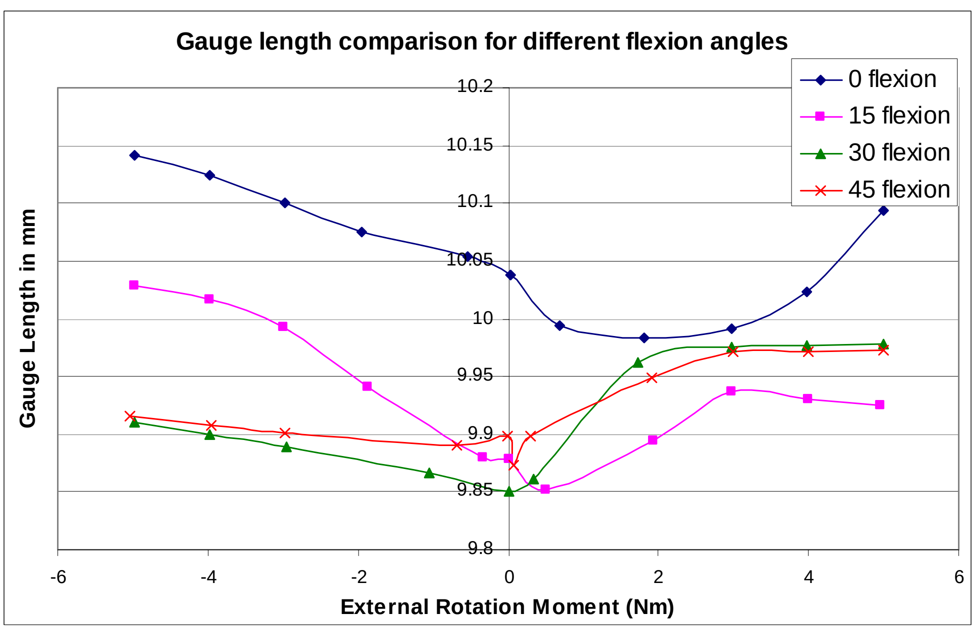

Figure 3.17: ACL strain in I-E rotation moment as determined by gauge length of DVRT – specimen # 1

This was due to the presence of a lump tissue near the ACL attachment site which we decided not to remove. Removal of this lump could have caused damage to the ACL jeopardizing the entire data. Figure 3.17 shows DVRT gauge length data against the I-E rotation moment.

Fleming and associates [Fleming, et al. 2001] recorded the ACL strain data on live human subjects at 20^0 flexion and reported that for non weight-bearing condition, an external torque of 10 Nm did not strain the ACL whereas an internal torque of 10 Nm strained the ACL up to 2%. Even though the actual strain percentage is not available, our strain data is in qualitative agreement with Fleming's study. Fleming and associates [Fleming, et al. 2001] did not observe any strain during 15 Nm V-V moment, whereas, we observed higher gauge length changes (Figure 3.18) at 0^0 flexion as compared to other flexion angles. The anterior drawer force strained the ACL and this was effectively

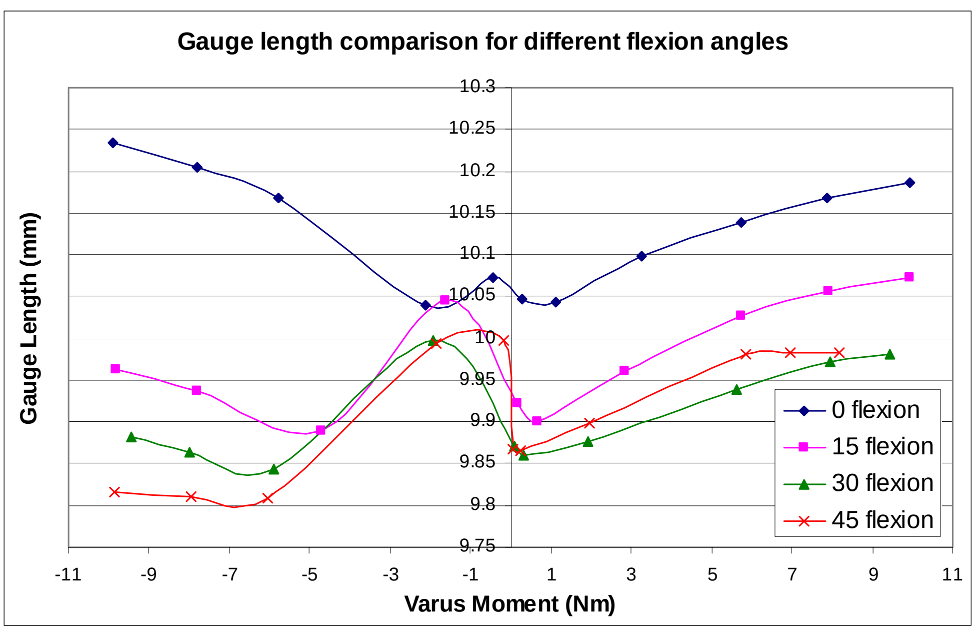

Figure 3.18: ACL strain in V-V rotation moment as determined by Gauge length of DVRT – specimen # 1

observed in our data (Figure 3.19). ACL strain was more pronounced at 0^0 flexion in comparison with other flexion angles.

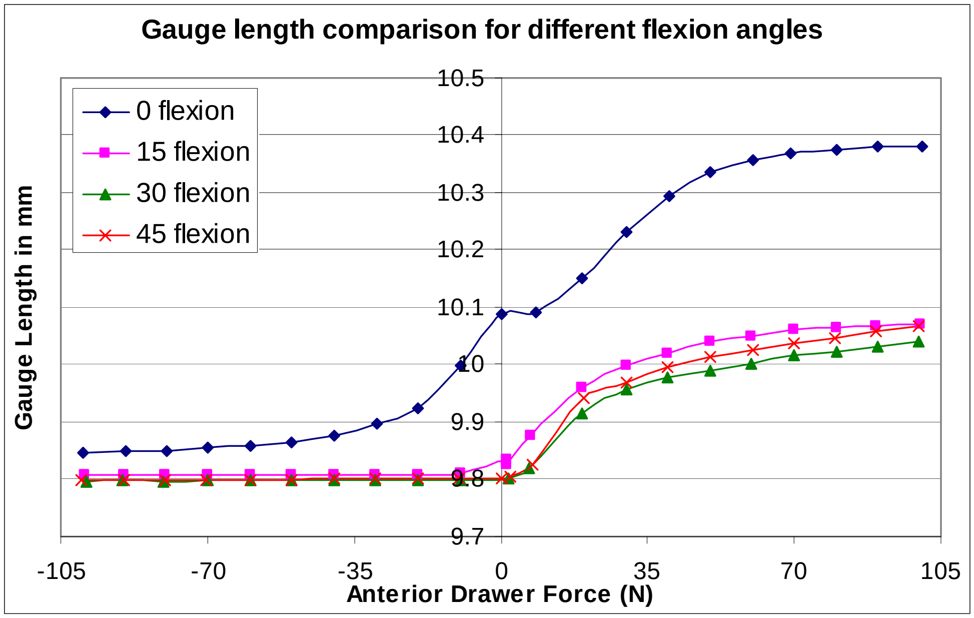

Figure 3.19: ACL strain in A-P drawer force as determined by Gauge length of DVRT – specimen # 1

3.7 SUMMARY OF EXPERIMENTS

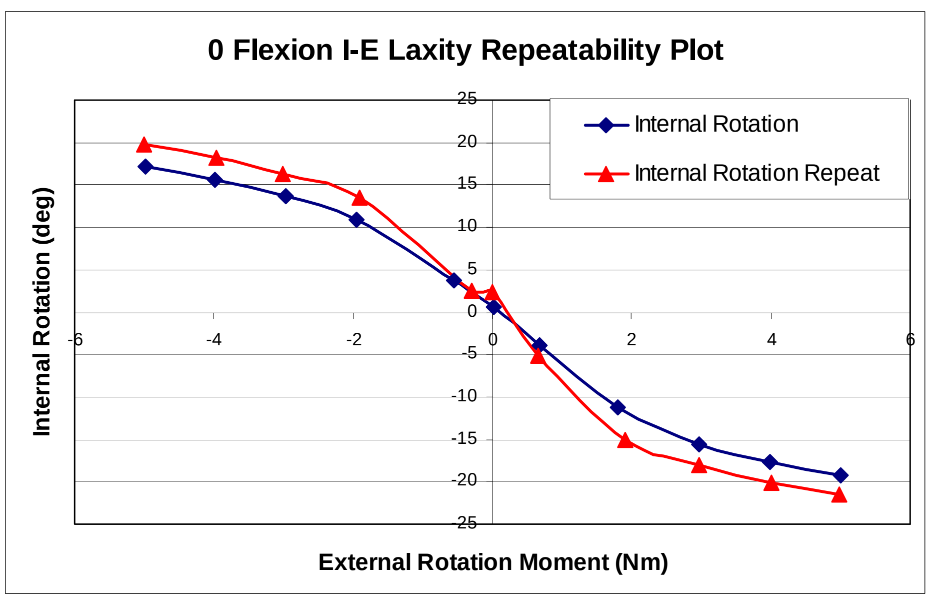

Figure 3.20: Repeatability test for internal rotation laxity for specimen # 1

The analysis performed on the experimental data shows typical behavior of the passive knee joint under applied laxity and combined loads and the joint laxity plots show qualitative comparison with the past studies conducted on the cadaveric specimens.

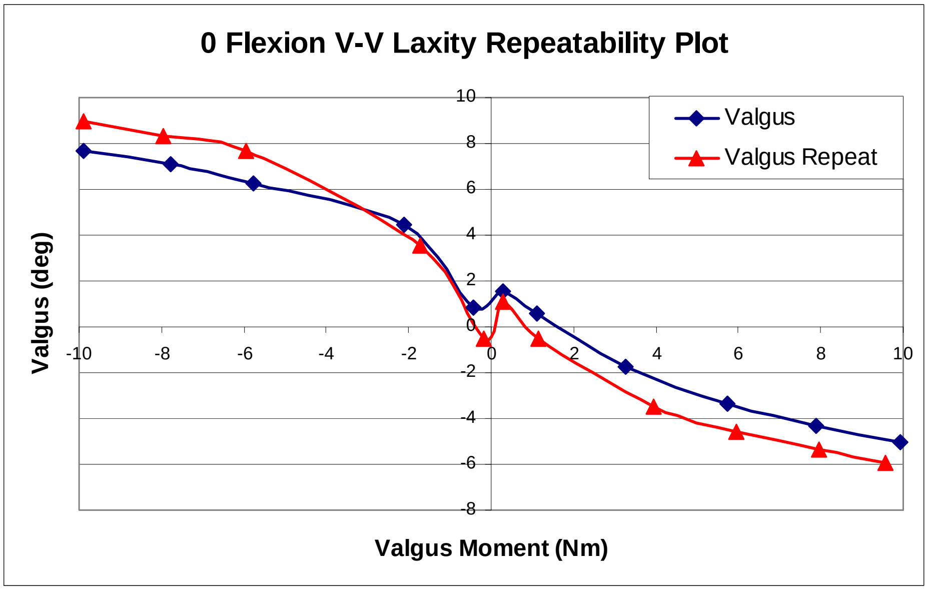

Figure 3.21: Repeatability test for valgus rotation laxity for specimen # 1

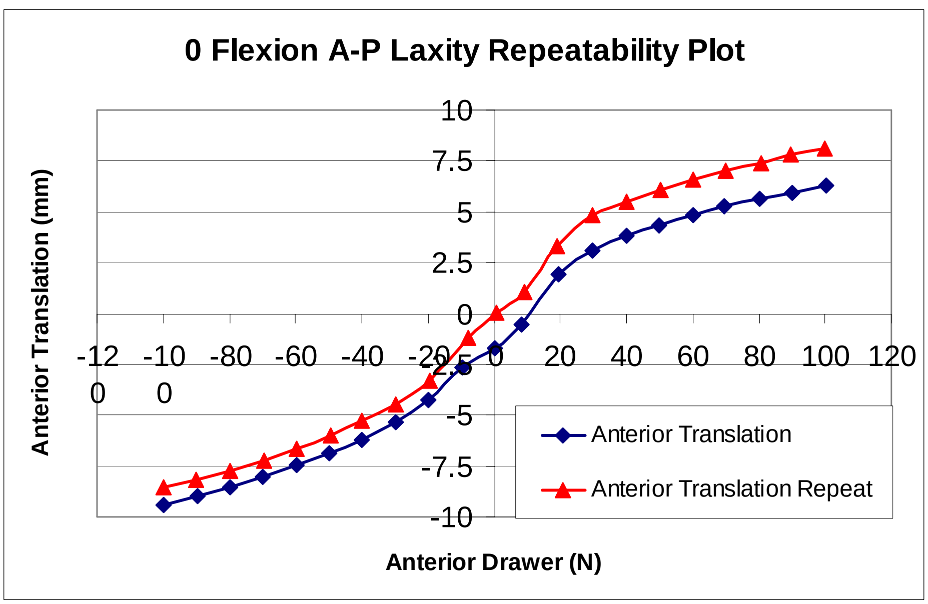

Figure 3.22: Repeatability test for anterior translation laxity for specimen # 1

Specimen # 1 was more lax as compared to the other specimens and demonstrated instability in the region of no loads. At low or zero loads, joint friction may play an important role in determining the region of instability. Our repeatability experiments showed no significant deviations in the pre and post experimental data.

Figures 3.20, 3.21 and 3.22 show the comparison of pre and post experimental laxity test conducted on specimen # 1 at 0^0 flexion. The maximum deviation in the internal rotation laxity, valgus rotation laxity and anterior translation laxity data was 2.1^0, 0.94^0 and 1.45 mm. Repeatability results for specimen # 1 were the worst among all repeatability tests since specimen # 1 was the most lax knee joint. Our next step is to develop the knee joint models and optimize the joint model parameters as discussed in chapters 4 and 5.

CHAPTER IV

DEVELOPMENT OF SUBJECT SPECIFIC KNEE JOINT MODELS

Answering clinical questions pertaining to the joint structure initiates the need for incorporating subject specific methodologies. Clinically, treatment of any pathological condition requires screening of the patient to understand the critical components of the pathology or to administer drug. Similar analogy should be applied while treating the injuries to one's joint. If the treatment of an injury or understanding injury itself involves modeling techniques then those models should incorporate the subject specific parameters. Whether to make the models subject specific depends largely on the end use of the model. In our research, we are trying to understand injury mechanisms to the ACL structure and it becomes inevitable to incorporate subject specificity in our models. Based on subject specific properties (both geometrical and mechanical) of the joints, certain external loading can prove hazardous to some individuals while others can still remain in the safe zone for the same loading. This chapter describes the methodologies used to develop MRI based knee joint models that reflect subject specific mechanical properties and geometry. These models are robust, cost effective and physics based that give thorough understanding of the underlying ACL injury mechanisms.

4.1 IMAGING

4.1.1 Basic Principles of Magnetic Resonance Imaging

MRI uses the interaction of an externally applied magnetic field and radio-waves to produce highly detailed images of the human body. The images are produced as slices through the anatomy being imaged. The slices are often described in terms of the imaging plane. The three main planes we consider are axial, sagittal and coronal. Human body consists of abundant hydrogen in its tissue, fat and water molecules. The hydrogen proton is positively charged and possesses a "spin" property and therefore behaves like a tiny bar magnet with north and south pole. When placed in a magnetic field, the hydrogen proton precesses (wobbles) about the direction of the magnetic field and the rate at which it precess depends upon the strength of the magnetic field. The magnetic field of the proton itself is very small and randomly oriented. However, when placed in the external magnetic field, all the protons align in the same direction as that of the magnet. The resultant magnetic field formed by addition of each proton's individual magnetic moments is called net magnetization.

When a joint being imaged is placed in the magnet, all the tissue's net magnetization is aligned parallel to the external magnetic field. The radio frequency (RF) coil present in the MRI machine then applies the RF energy pulse that tips the magnetic field in transverse plane and gets detected by the receiver coil. At the application of the RF pulse, the net magnetization spirals outward and tips completely in transverse plane. At this point, RF is turned off and due to the magnetic field; current is induced (Faraday's law of

Figure 4.1: OrthOne 1.0 T extremity scanner used to scan the knee joint.

induction) in the receiver coil which is placed in the transverse plane. The signal decays with time as the tissue magnetization goes to its normal orientation. There are two ways this relaxation of tissue magnetization happens. One is T1 relaxation and second is T2 relaxation. Depending on the tissue type, T1 and T2 decay (relaxation) timings vary and thus the signal they induce varies. For example, fat has a rapid T1 and T2 decay, whereas, water has long T1 and T2 decay. The signal induced in receiver coil is then sampled using different RF pulse sequences like spin echo which uses 180^0 RF pulse. In the scanning process, these sequences are repeated many times. The time between successive 90^0 pulse sequences is known as TR and the time between the 90^0 pulse and center of echo formation is known as TE. The TR and TE parameters are selected to control the contrast in the image based on the knowledge of T1 and T2 decay timings.

4.1.2 Imaging Protocol

The biomechanics laboratory of the Cleveland Clinic has 1.0T (Tesla) extremity MRI scanner (Figure 4.1 - ONI Corp., Wilmington, MA) to scan upper and lower extremities of up to 180mm diameter. All the MRI scans were conducted using this MRI facility. Using pilot data from different subjects, we developed a scanning protocol that gave a good contrast for articular cartilage and ligaments in the same scan. The specifics of this protocol are detailed in Appendix B (B1). We used five cadaveric knee specimens for this

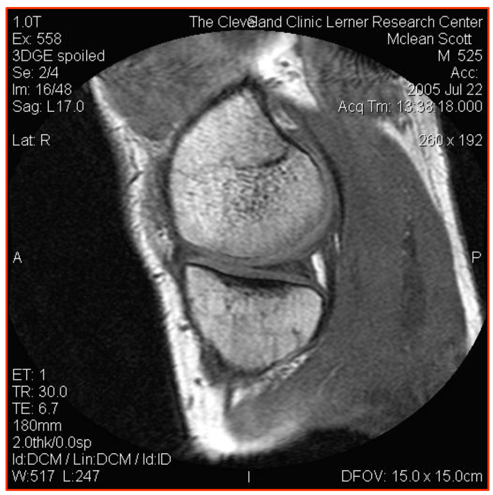

Figure 4.2: Sagittal plane MRI scan of the knee joint.

study. Four specimens were purchased from Life Legacy Foundation (Life Legacy Foundation, Inc, Tucson, AZ) and one from National Disease Research Interchange (NDRI, Philadelphia, PA). Specimens were stored in a cold storage at -20^{0}C. Each specimen was thawed for 24 hours before starting the testing protocol. After thawing to room temperature, each specimen underwent medial parapatellar arthrotomy to verify the ligamentous and meniscal integrity and to document any arthritic changes. Nylon registration screws were drilled in the femoral epicondyles of the knee specimen for cross referencing the coordinate system in the computational joint model.

In this protocol, the knee was kept in full extension position which was defined as the reference position of the joint model. Imaging technique used 3D spoiled gradient echo sequence with fat suppression, TR = 30, TE = 6.7, Flip Angle = 20^0, Field of View (FOV) = 150mm X 150mm, Slice Thickness = 1.5mm. Each knee specimen was scanned in three anatomical planes viz. axial, sagittal, and coronal. Total scanning time was approximately 18 minutes for each specimen. Selecting these specific sequence parameters produced images that highlighted articular cartilage such that it could be easily discriminated from surrounding bone and tissue, as shown in Figure 4.2.

4.1.3 Segmentation

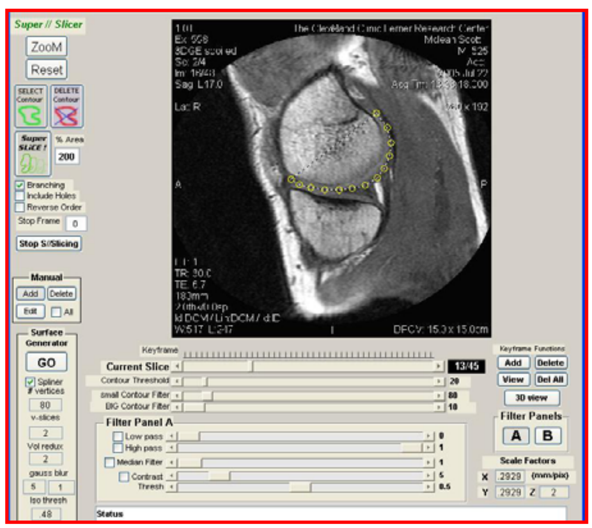

Figure 4.3: Digitization of sagittal plane MRI scans to extract cartilage surface geometry.

The MRI machine software produced DICOM files that were then imported in MATLAB (Mathworks Inc., Natick, MA) for subsequent segmentation. Sagittal plane scans were used to segment cartilage surface and ligament insertion points whereas scans in other planes were used by the user for visual confirmation of the ligament insertion areas. An in house MATLAB algorithm was used [Doehring, et al. 2005] to load sagittal scan images and segment the tibial and femoral articular cartilage. This MATLAB program enabled us to load all the sagittal plane images at one time and either manually or automatically segment the regions of interest using different segmenting parameters. We used manual segmenting option to yield the contours describing articular surfaces as shown in Figure 4.3. Contours of medial tibial plateau, lateral tibial plateau, femoral articular surface and medial bony edge were segmented in each scan for each of the articular surface individually. The medial bony edge is the surface of the tibia along the medial border of the tibial plateau and would be used to simulate the wrapping of MCL bundles around the bone. Segmented contours were subsequently saved as point clouds representing each cartilage surface. In the knee joint model, each ligament was represented by three bundles or line elements.

The joint model required insertion coordinates of 12 bundles to represent ligaments. The MRI scans would only show the insertion of the combined bundles within each ligament. We extracted an outline defining ligament insertion areas. To extract bundle insertion points from MRI scans, perimeters of the bundle insertions were traced using appropriate image scans inside this outline and using Harner et. al., [Harner, et al. 1999] as a guide for cruciates and Blankevoort and Huiskes, [Blankevoort, et al. 1991b] as a guide for collaterals. Centroids of these perimeters were computed as insertion points of these bundles on respective bones. However, this method to determine insertion points and separating bundles of the ligament was prone to human and digitization error. Because of this uncertainty, and because we found that model behavior was sensitive to this, the insertion coordinates were subsequently refined via optimization as described in Chapter 5. Perimeters of the medial and lateral epicondylar areas of the femur and femoral long axis point were obtained to calculate anatomical joint coordinate system of the model. The epicondyles were detected based on the registration screw contrast found in the image. The femoral long axis point on the other hand was detected based on manual determination of the image in which the femoral bone shaft was having maximum width and then picking up the extreme superior point on this image that was also the midpoint of the bone width.

4.2 ARTICULAR SURFACE DEVELOPMENT

Representing joint articular surfaces using mathematical models is a challenging task. Researchers have generally used piecewise bicubic surface patches [Scherrer, et al. 1979], cubic B-splines [Ronsky, et al. 1995], and quintic B-splines [Ateshian. 1993] for modeling three dimensional joint surfaces. Piecewise bicubic surface patches can not maintain continuity up to second derivative across the patch boundaries. Ronsky used cubic B-splines in each MRI slice but used linear interpolation in transverse slice direction that did not have continuity up to first derivative. Quintic B-splines had continuity up to 4^{th} derivative. The primary limitation of all the above techniques is that they are based on tensor products of curve fitting splines which requires the surface data to be nominally gridded and not randomly distributed [Boyd, et al. 1999]. Most of the joint surfaces, including knee joint surfaces, are non-uniformly distributed. To address this issue, a novel method to model these surfaces using thin plate splines was suggested by Boyd and colleagues [Boyd, et al. 1999].

Thin plate spline (TPS) is a classic interpolating function and uses radial basis function of the form $\Phi(r) = r^2 \ln(r)$. Boyd and colleagues [Boyd, et al. 1999] modified this TPS function to use it as smoothing function whenever desired. We have adopted this technique to use in our model. The set of articular surface coordinates (point cloud) obtained were processed into a smooth parametric surface model using thin plate spline fitting algorithm in MATLAB, developed by Boyd. Specifically, using the TPS function, we developed a surface fitting algorithm to fit a mathematical TPS surface to any point cloud. The Cartesian coordinates of the femoral point cloud were transformed to cylindrical coordinate system by finding the axis of the cylinder that best fitted the data.

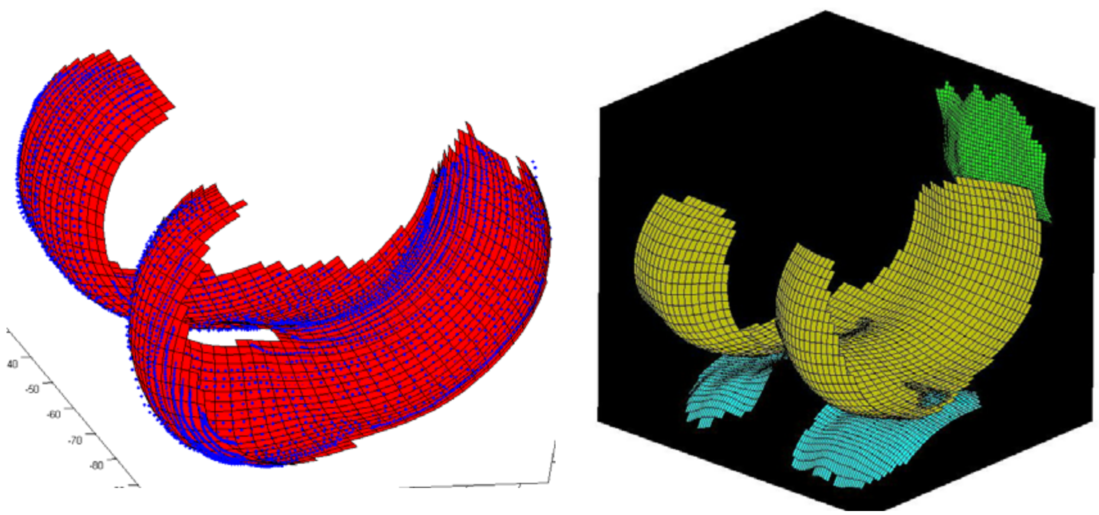

Figure 4.4: Resampled and trimmed TPS surfaces representing articular cartilages of the knee joint.

This transformation was necessary to reduce the curvature of the surface. After fitting smooth TPS to point cloud, femoral point cloud and TPS surface fit data was transformed back to Cartesian coordinate system and the fitted surface was resampled to get a rectangular mesh. These resampled points were processed through a discard algorithm that trimmed the mesh to the size of the original articular surface. Finally, the trimmed mesh was saved as a .3D file for further use in the joint model software. The surface fitting algorithm is given in Appendix B (B2) for reader's ready referral. The smoothing parameter was determined on the basis of desired root mean square (RMS) error value. To keep the subject specificity of the surfaces, we maintained the RMS error value within 0.35 mm.

Our preliminary studies successfully fitted thin plate spline surfaces to the point clouds of segmented cartilage surfaces (Figure 4.4). We tried different target RMS values ranging from 0.2 mm to 0.5 mm. Best results were obtained if the target RMS value was same as the noise in the coordinate data, which was equal to the MRI scan pixel size. Preliminary attempts to make the RMS value smaller than 0.3 mm did not produce smooth surfaces. Also, the RMS error of 0.35 mm worked well for smoothing and post use of the surfaces.

4.3 JOINT MODEL DEVELOPMENT

The purpose of the knee joint model is to give estimate of the ACL forces based on the external loads and torques applied to it. We used generic software written in FORTRAN and designed to formulate 3-dimensional, quasi-static and multi-body models of diarthrodial joints. This software was developed by Kwak and colleagues Kwak, et al. 2000] in Columbia University (Columbia University, New York, NY) in 2000.

The quasi-static multibody model software finds the bone positions and orientations in which there is equilibrium between ligament forces, muscle forces, contact forces and external loads. The model software distinguishes material bodies that can represent each of the bones, and particles that are embedded in soft tissue structures to allow wrapping of these structures around bones [Kwak, et al. 2000]. Material bodies have six DOF (three translations and three orientations), while particle bodies only have three translational DOF. All the other structures such as ligaments, tendons and muscles are defined as links joining two material bodies. These links can be modeled according to their use. Ligaments, for example, can be modeled as linear or non linear spring elements, whereas, muscles can be modeled as links producing constant force etc. To obtain the equilibrium state, each material body β will be forced to satisfy the following equations:

$$f^{\beta} = \sum_{i} f_{i}^{\beta} = 0 \qquad \text{..............................(1)}$$

$$m^{\beta} = \sum_{i} m_{i}^{\beta} = 0 \qquad \text{..............................(2)}$$

where f_i^{β} = force produced by link i on material body β and m_i^{β} = moment produced by link i on material body β. The summation is taken over all links i which insert into the material body β. It is assumed that all the forces are dependent only on the relative bony positions of the joint making the model elastic. A generalized force vector f is used to satisfy the above equations for all moving bodies where,

$$[f] = \left[f^{1}\, m^{1}\, f^{2}\, m^{2} \ldots f^{n}\, m^{n}\right]^{T} \qquad \text{......................(3)}$$

n being the total number of bodies. Similarly, DOFs of each material body are represented by a generalized DOF vector q as,

$$[q] = \left[a^{1}\, \theta^{1}\, a^{2}\, \theta^{2} \ldots a^{n}\, \theta^{n}\right]^{T} \qquad \text{....................(4)}$$

where a is translational vector and θ is an attitude vector for material bodies. Thus, the model solves system of nonlinear equations $f(q)$ = 0 for the unknown vector q. These equations are solved through the use of analytical Jacobians in the Newton-Raphson method. Convergence is achieved when the relative change in the magnitude of the generalized DOF vector q is less than 10^{-5} or when the magnitude of generalized force vector f is less than 10^{-7}. Thus, the input to the software is initial guess of DOF of material bodies and particles and external forces and moments acting on each one of the material bodies or particles, whereas, the output is the equilibrium state DOF of material bodies and particles and the forces and moments sustained by internal structures of the model. Software provides a graphical interface for changing the model parameters interactively.

Due to the quasi-static nature of the analysis, the model does not require mass and inertia properties of the bodies, or the damping properties which can not be easily obtained on subject specific basis. However, quasi-static analysis can be applied to joints in motion as long as inertial forces and viscous effects are negligible. Moreover, the model will be used to process thousands of movement simulations to analyze ACL injury. Considering the low computational time the model takes to solve for each simulations (few seconds), as against the time consumed by comparable finite element models (few hours), using this modeling approach seems more pertinent and pragmatic. Ideally, using this software and our imaging techniques, the whole knee joint model will consist of three material bodies viz. femur, patella and tibia, and of following structural elements (Figure 4.5):

1. Contact between tibia and femur, modeled using articular cartilage surfaces developed and the mechanical properties of cartilage [Blankevoort, et al. 1991]
2. Contact between femur and patella, modeled using articular cartilage surfaces developed and mechanical properties of cartilage [Cohen, et al. 2003].

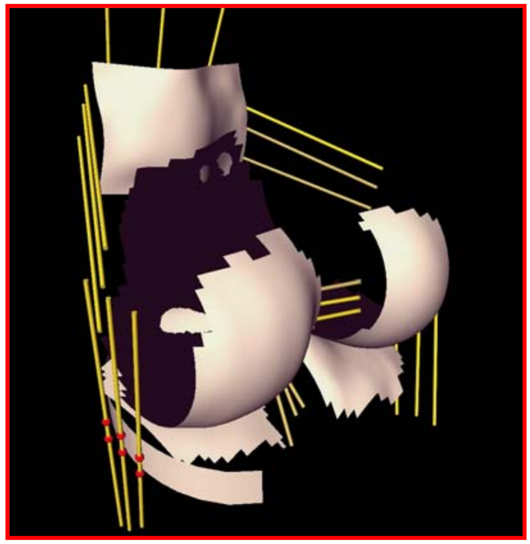

Figure 4.5: Knee joint model consisting of all the 8 structural elements.

3. 12 ligament bundles between femur and tibia: 3 bundles each for MCL, LCL, ACL, and PCL.
4. 6 ligament bundles between femur and patella: 3 bundles each for medial and lateral patello-femoral ligament.
5. 5 ligament bundles between patella and tibia to model patella tendon.
6. 3 line elements between patella and femur to model quadriceps muscle.
7. Contact between femur and particle bodies embedded in quadriceps (4 each).
8. Contact between tibial boney edge and particle bodies embedded in MCL bundles (2 each)

The joint model consisting of all the above structural elements will have at least 12 DOF for material bodies and 54 DOF for particle bodies. However, for the purpose of developing cadaver specific models and validating those, we considered tibio-femoral joint only. The reason being that the cadaveric specimen exhibited passive knee joint characteristics when mounted on robot. In other words, joint laxity tests carried out on the robot were not expected to be influenced by the presence of patella, patello-femoral ligaments, patella tendon, and quadriceps muscle since these were not loaded as a part of the experimental protocol. To mimic the similar characteristics in the joint model, we considered structural element nos. 1, 3 and 8 from above, to represent tibio-femoral joint. All the discussion henceforth would be made pertaining to this architecture of the joint model. An input file that loaded the surfaces and established the initial required bone and ligament position and interaction parameters and properties is attached in Appendix B (B3).

The original joint model software [Kwak, et al. 2000] was designed to solve the equilibrium positions and orientations of the moving rigid bodies and particles with respect to the ground rigid body for applied external forces and moments. Even though it was robust enough to solve equilibrium states, we did not have a direct control over the solution algorithm of the nonlinear system of equations or to extract the generalized force vector f whenever needed. A Material Transfer Agreement (MTA) was signed between the Columbia University, New York NY and the Cleveland Clinic, Cleveland OH to access the source code of the joint model software [Kwak, et al. 2000]. Once we received the source code, we worked on the solution algorithm of the nonlinear system of equations using inbuilt MATLAB solver functions. This gave us a unique opportunity to control, modify, and apply different solver functions and parameters while the software searched for the convergence. MATLAB provides a subjective interface to deal with external programs written in C or FORTRAN languages. C or FORTRAN subroutines can be called from MATLAB as if they were built in functions. This can be done effectively by using MEX-functions in MATLAB. MATLAB callable C and FORTRAN files are referred to as MEX-files. MEX-files are dynamically linked subroutines that the MATLAB interpreter can automatically load and execute. MEX-files just behave like MATLAB M-files and built in functions. Once created, they can be executed in MATLAB. To customize the model for our solution method and optimization approach, the joint model software was modified and accessed via the MATLAB MEX-function interface to provide the force imbalance (GF i.e. f in equation (3)) of the moving bodies as an output with the applied external loading condition i and initial rigid body positions as an input. A sample MEX function used for this project is attached in the Appendix B (B4) for reader's ready referral.

We started building the joint model MEX function using the open source GNU FORTRAN compiler (http://gcc.gnu.org/). After initial struggles and lot of debugging, we realized that the compiler produced incorrect behavior due to incompatibility with the older Fortran code from Columbia University and causing problems in our compilations. We switched over to Intel Fortran compiler and that solved our compiling problems.

4.4 SOFTWARE MODIFICATIONS

To customize the joint model software code to our needs, we modified many subroutines from the source code. We also found many small bugs in the original code. We will not discuss these bugs in detail, however we will briefly explain major modifications done in the source code. The *io_open.f* subroutine assigned values to unit names and opened files for input and output storage. The output was stored in a .lis file after static equilibrium was achieved. We changed this original code and deleted the part where it stored the output in .lis file. The *calc_model.f* subroutine was the major subroutine in the source code used for static multibody equilibrium analysis. The original source code checked the initialization of the input file, calculated the generalized force vector f looping through each material body and particle characteristic, created analytical jacobian matrix that corresponded to force vector f and finally solved the nonlinear system of equations employing Newton-Raphson method. Since we wanted to apply MATLAB provided solver functions, we modified this subroutine and deleted the Newton-Raphson solution algorithm from the code. The modified code thus provided the calculation of generalized force vector f and corresponding analytical jacobian matrix. The correctness of the matrices was checked from time to time by printing log files at each level of the code.

Model ligaments were defined as nonlinear tension only spring models. In the original code, the ligament behaved nonlinearly till a particular threshold strain and then linearly beyond that point. Spring behavior for zero or negative loads was not defined. This introduced singularities in the spring model during no load conditions. This caused trouble while optimizing the ligament resting lengths. As soon as the ligament was given a large enough resting length that remained slack during all loading conditions, the optimization algorithm never recruited it again because the algorithm could no longer detect that ligament properties could make a difference. This problem was solved previously by Blankevoort and Huiskes [Blankevoort, et al. 1996] using the estimate of the ligament strain. They started the optimization using the maximum strain length as initial guess. We used another approach to solve the problem. Discontinuities present in the modeling of the ligaments were eliminated by introducing a small linear elastic term thereby making the ligament model continuous (always positive stiffness) even when slack. This strategy helped recruiting the ligaments in all optimization iterations eliminating the risk of getting them inactive throughout the optimization process due to high slack lengths attributed in previous iterations. The new ligament subroutine was introduced in the original source code and the affected subroutines were modified accordingly.

4.5 COORDINATE SYSTEM CONVERSIONS

The experimental data was recorded in JCS as explained in 3.2.1. In the joint model software, all the rotations were reported using an attitude vector $\theta = \theta n$ where n is the unit direction vector about which the scalar rotation θ occurs [Kwak, et al. 2000]. To compare experimental data with model predicted kinematics, the experimental data was converted to attitude vector parameters. This was accomplished by using a MATLAB written algorithm which is provided in Appendix B (B5) for reader's ready referral.

4.6 PRELIMINARY STUDIES

As a part of our preliminary studies, we developed a tibio-femoral joint model and successfully demonstrated its use in understanding the isolated ACL injuries in the joint. Specifically, MR images of the right knee were acquired from a human subject (male, 35 years) with no prior history of knee injury. Imaging was performed with the Orthone 1.0 T extremity scanner. Articular cartilage was segmented manually from the sagittal scans using in-house MATLAB code. A thin plate spline surface was fitted through the femoral, lateral tibial, and medial tibial surfaces individually with smoothing adjusted to obtain a RMS fit error of 0.35 mm for all the surfaces. Anatomical insertion areas of cruciate ligaments, and collateral ligaments were manually digitized. Each ligament was represented by two line elements. Force-deformation properties for ligaments and articular cartilage were taken from earlier work (Blankevoort and Huiskes, 1996). Initially, zero ligament strain was defined to occur with the joint in its imaged position.

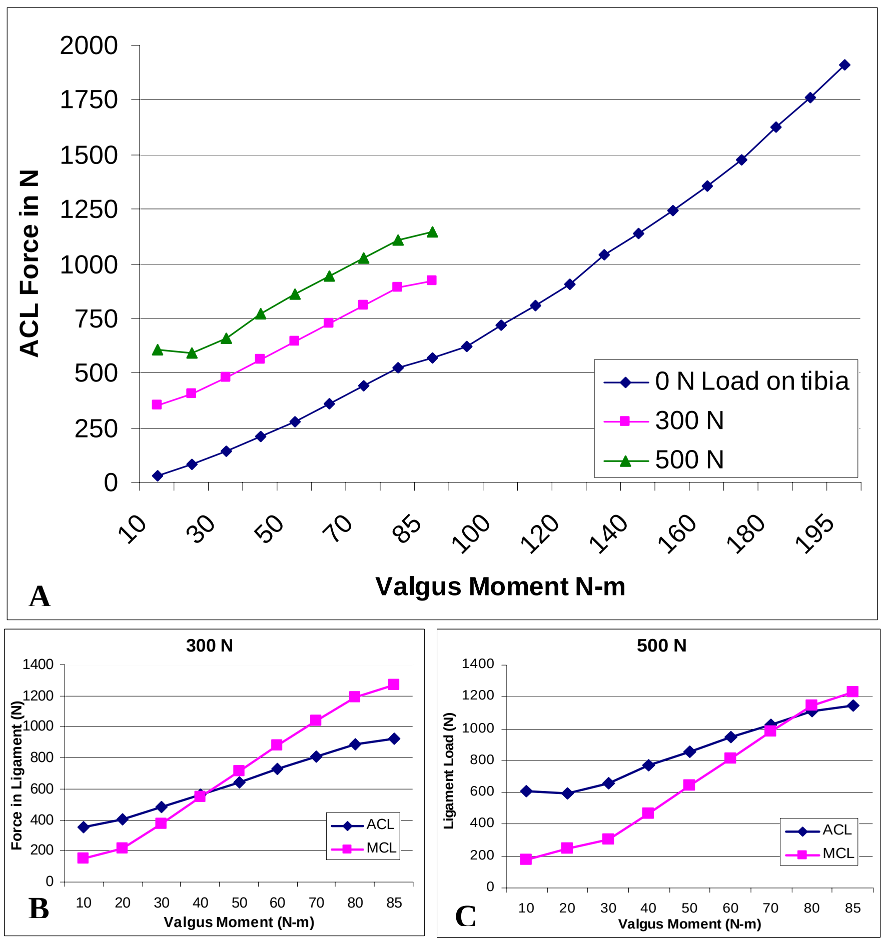

Figure 4.6: **A** shows model predicted ACL force due to combined valgus torque and anterior drawer force. **B** and **C** show MCL – ACL load sharing at two levels of anterior drawer force

The model had 15 degrees of freedom: six for tibio-femoral joint motion, and 9 for wrapping particles embedded in the MCL. To simulate ACL injury, we first applied valgus moment while the knee was constrained at 0º flexion. Valgus moment was increased in the steps of 10 Nm until the ACL reached 2000 N, which was assumed to be the ACL failure load. We repeated the same series in the presence of anterior drawer force of 300 N and 500 N.

ACL force increased with valgus load and anterior drawer force (Figure 4.6-A). With anterior drawer, solutions could not be obtained at valgus loads higher than 85 Nm, possibly due to rotational instability in the model. At 85 Nm valgus and 500 N anterior drawer, ACL force was 1145 N, which approaches the failure load for young females [Chandrashekar, et al. 2006]. Load sharing between the MCL and ACL was influenced by loading condition (Figure 4.6-B). In combined loading, the force in the ACL often exceeded that in the MCL. After consideration of their respective failure loads, this may explain why isolated ACL injury can occur during valgus loading, leaving the MCL unharmed. The loads applied during these simulations could potentially occur during sports movements, where valgus moments of 50 Nm valgus and 500 N anterior drawer have been reported. Equilibrium states were solved in less than 2 seconds, which is much less than a comparable finite element model.

CHAPTER V

AN OPTIMIZATION APPROACH TO GENERATE SUBJECT SPECIFIC KNEE JOINT MODELS

In the context of our study, optimization is a technique which minimizes the differences between the model predicted output and experimental data by varying the model parameters within their bounds. This chapter explain in detail the optimization procedures we applied to the joint model in order to determine subject specific model parameters. This chapter is divided into two sections. We used two gradient based optimization procedures and Section I of this chapter demonstrates comparison of these two optimization procedures and is written in a publication format. The methods part of this section gives summary of chapters 3 and 4 along with the optimization methods used. Only two out of five models are taken into account for the comparison done in section I. Section II identifies the best suitable optimization procedure for this study and provides detailed results of the optimization for all the five models.

5.1 SECTION I

5.1.1 Introduction

Computational modeling approach has long been used to address complex clinical, surgical or sports related problems of the knee joint. These models can be categorized as movement mechanics or joint mechanics models. Movement mechanics models take into consideration the human musculoskeletal system in either forward dynamic or inverse dynamic approaches. Based on the approach used, these models provide basic understanding of either joint movement (forward dynamics) or (muscle and) reaction forces (inverse dynamics) at the joint that balance the external loads exerted on the joint during the simulated activity [van den Bogert. 1994]. Joint mechanics models, on the other hand, provide information about distribution of these reaction forces among the internal joint structures in terms of stresses or strains.

Abnormal external joint loading causes diversity of problems to the knee joint ranging from joint pain, tissue damage and ligament injuries. There are many previous studies that use computational model as a tool to investigate knee joint problems. Cohen and colleagues [Cohen, et al. 2003], for example, used a multibody, quasi-static patello-femoral joint model to simulate tibial tuberosity transfer surgery. Pena and associates [Pena, et al. 2006] used a finite element modeling approach to asses tunnel angle in the Anterior Cruciate Ligament (ACL) reconstruction surgery. Halloran and colleagues [Halloran, et al. 2005] used explicit finite element models along with numerical simulations to predict relative motions or kinematics in different TKR designs. ACL forces in normal walking were predicted by a 3D dynamic musculoskeletal model developed by Shelburne and associates [Shelburne, et al. 2004]. These models have provided general (not subject specific) insights to the clinical problems under study. However, when considering the use of the computational joint models in clinical applications such as injury prevention or treatment planning, it becomes important that the model represents the biomechanics of a specific subject. Generic models are good enough to get insights into general joint biomechanics but not to predict subject specific treatment. Subject specific modeling approach calls for obtaining subject specific tissue properties and anthropometric data to be incorporated in the models. While geometry of the joint structures (ligaments and articular surfaces) can be measured non-invasively by imaging techniques, this is not the case for their mechanical properties. Only indirect information is available via whole joint mechanical testing. Subject specificity with regards to model parameters such as ligament zero-strain length or muscle activations can then be obtained by optimizing the model using the experimental data.

Developing subject specific modeling methodologies can necessitate increase in the complexity of the model with regards to its subject specific properties. The complexity of the model is further increased by processing multiple degrees of freedom (DOFs) and parametric control of each DOF by multiple design variables. As design variables and model complexity increase, optimization process can require thousands of function evaluations to achieve convergence and can end up soaking high computational cost. This is especially true when finite element modeling domains are used. Commercially available softwares that provide optimization solvers include GAMS (www.gams.com), TOMLAB (http://tomopt.com), MATLAB (www.mathworks.com), NEOS (http://www-neos.mcs.anl.gov/), ILOG-CPLEX (www.ilog.com) etc. Optimization methods typically involve small or medium scale algorithms with less than 100 design variables. Researchers generally use gradient based optimization methods or apply global optimization methods such as simulated annealing [Neptune. 1999] to optimize model parameters. Gradient based algorithms classically have quadratic convergence with iterative evaluation of the objective function and constraints but possess the risk of running into local minima. Global optimization algorithms, on the other hand, generally require significantly higher computational cost in lieu of less risk of encountering local minima.

Optimization algorithms have been used to solve human movement problems [Anderson, et al. 1999, Anderson, et al. 2001]. In their dynamic optimization study, Anderson and colleagues[Anderson, et al. 2001] reported the CPU time of 10000 hours using 32 processors from Cray T3E architecture for optimization of 810 control variables to the experimental gait data containing 15 time stamps at the interval of 37.3 ms. Using global simulated annealing optimization approach, McLean and associates [McLean, et al. 2004] reported the computational time of approximately 37 hours to optimize total 61 control variables of a forward dynamic musculoskeletal model over 200 time samples of experimental side-step cutting data. Recently, Koh and colleagues [Koh, et al. 2009] evaluated the performance of parallel particle swarm global optimization (PSO) algorithm to solve large scale human movement problems. They concluded that gradient based algorithms performed better than PSO in optimizing gait change predictions to reduce the left knee adduction torque of an inverse dynamic model from a nominal gait and issued a caution while using parallel PSO algorithms on large scale. Clearly, the use of these algorithms involving large number of variables is limited due to high computational costs involved.

The optimization algorithms used in above studies typically incorporate unconstrained objective functions to estimate model specific parameters such as tissue properties or muscle excitations. The large scale optimization algorithms on the other hand incorporate constrained objective functions for the parametric estimation of large number (millions) of variables including model parameters and have been used in systems governed by partial differential equations (PDE) [Ghattas, et al. 2004]. PDE-constrained large scale algorithms have been consistently used in finite element methods to solve optimal design problems for element shape control, boundary control or volume control parameters. Large scale algorithms are efficient and quickly gathering interest in science and engineering applications. These methods have potential applications in solving biomechanics problems such as optimal control of human movement or development of optimal joint mechanics models. However, the robustness and feasibility of large scale algorithms in addressing optimization problems in biomechanics research has not been evaluated. Considering these facts, the objectives of this study were (1) to institute a methodological approach to develop subject specific, 3-D, multi-body, quasi-static knee joint models from MRI scans, and (2) to introduce and evaluate a large-scale optimization approach that could cost effectively find the model parameters that minimized the difference between model predicted kinematics and experimental kinematics collected from a large set of whole joint load-deformation measurements.

5.1.2 Materials and Methods

5.1.2.1 Joint Model Development

Two fresh-frozen cadaveric knees with no history of knee injury or degenerative bone disease in the knee joint were used in this study. First knee specimen was a right knee, 70 year old, from a female donor and second knee specimen was a left knee, 58 year old, from a male donor. Both specimens were thawed at room temperature for 24 hours before testing [Woo, et al. 1986]. Both knees underwent medial parapatellar arthrotomy to verify ligamentous and meniscus integrity and to document any arthritic changes. We inserted nylon screws (6-32 X ¾") into the medial and lateral epicondyles (bony landmarks) of the femur and tibia of each specimen for future cross reference. Imaging was performed with OrthOne 1.0T extremity MRI scanner (ONI medical systems Inc., Wilmington, MA)

Figure 5.1: Tibio-femoral knee joint model developed from sagittal plane MRI scans

using 3D Gradient Echo pulse sequence. Sagittal plane MRI scans were acquired from each of the two cadaveric specimens at a resolution of 0.29 mm x 0.29 mm x 1.5 mm and with acquisition time ranging from 4 min. 31 sec to 4 min. 58 sec. Using sagittal plane MRI scans, two tibio-femoral joint models were developed (Figure 5.1), one for each specimen. Each model consisted of a deformable contact between articular cartilage, line elements for each of the four ligaments viz. Medial Collateral Ligament (MCL), Lateral Collateral Ligament (LCL), Anterior Cruciate Ligament (ACL), Posterior Cruciate Ligament (PCL), and wrapping of MCL around the bony medial tibial edge.

Articular cartilage was segmented manually from the sagittal scans using an in-house algorithm [Doehring, et al. 2005] written in MATLAB 7.1 (Mathworks Inc., Natick, MA). This algorithm enabled us to load all the sagittal plane images at one time and either manually or automatically segment the regions of interest using different segmenting parameters. We used manual segmenting option to yield the point contours describing articular surfaces. Using the digitized coordinates (point cloud), a thin plate spline surface [Boyd, et al. 1999] was fitted through the femoral, lateral tibial, medial tibial and medial tibial bony edge contours individually with smoothing adjusted to obtain a RMS fit error of 0.35 mm for all the surfaces. Anatomical insertion areas of the cruciate ligaments and collateral ligaments were manually digitized.

Each ligament was represented by three line elements. Force-deformation properties for ligaments and articular cartilage were selected from earlier work [Blankevoort, et al. 1996]. Initially, zero ligament strain or reference strain was defined to occur with the joint in its imaged position. All the kinematics was reported with respect to the femur with origin located at the midpoint of the line joining the medial and lateral bony landmarks. Each model had 23 degrees of freedom (DOF): five (three translations and two rotations) for tibio-femoral joint motion and 18 (three translations each) for six wrapping particles embedded in the MCL. Simulations were performed with a multi-body, quasi-static modeling software developed by Kwak and colleagues [Kwak, et al. 2000] for generalized joint modeling.

The joint model software [Kwak, et al. 2000] was a three-dimensional mathematical model that employed quasi-static force and moment equilibrium analysis to predict the position and orientation of interacting bones in diarthrodial joints. In this model, bones were treated as rigid bodies and soft tissues as nonlinear springs. Cartilage was assumed to have constant thickness of 5mm in all the models. Deformable contact was defined between the two rigid body surfaces. Quasi-static analysis eliminated the requirement of body parameters such as mass and inertia properties, or damping properties for which subject specific data could not be obtained. This approach could be applied to study the joints in motion as long as the inertial forces or viscous effects were negligible.

5.1.2.2 Experimental Data Collection

Immediately after MRI scanning, each knee specimen was prepared for experimental testing. For each specimen, joint capsule was left intact (approximately 10 cm on each side of the joint line) and remaining musculature and tissue was removed. The exposed tibia and femur were then potted (secured) in a 50 mm diameter aluminum cylinder using wood's metal (Lipowitz's alloy). Two drill bits were transversely drilled through each of the cylinders and left intact to hold the cylinder and bone together. All the experiments were performed using a robotic motion platform Rotopod R2000 (Parallel Robotic Systems Corp., Hampton, NH). Rotopod R2000 comes with 6 DOF motion control software, with an Application Program Interface (API). Using the API, the Musculoskeletal Research and Mechanical Testing Core (MRMTC) at the Cleveland Clinic has developed in-house software in LabVIEW (National Instruments Corp., Austin, TX) for mixed motion-force control in a standard joint coordinate system (JCS) [Grood, et al. 1983]. The force control mode of the robot applied desired loads and torques at the knee joint to determine 5 DOF kinematics of the knee joint, similar to Kanamori and associate's work [Kanamori, et al. 2000, Kanamori, et al. 2002].

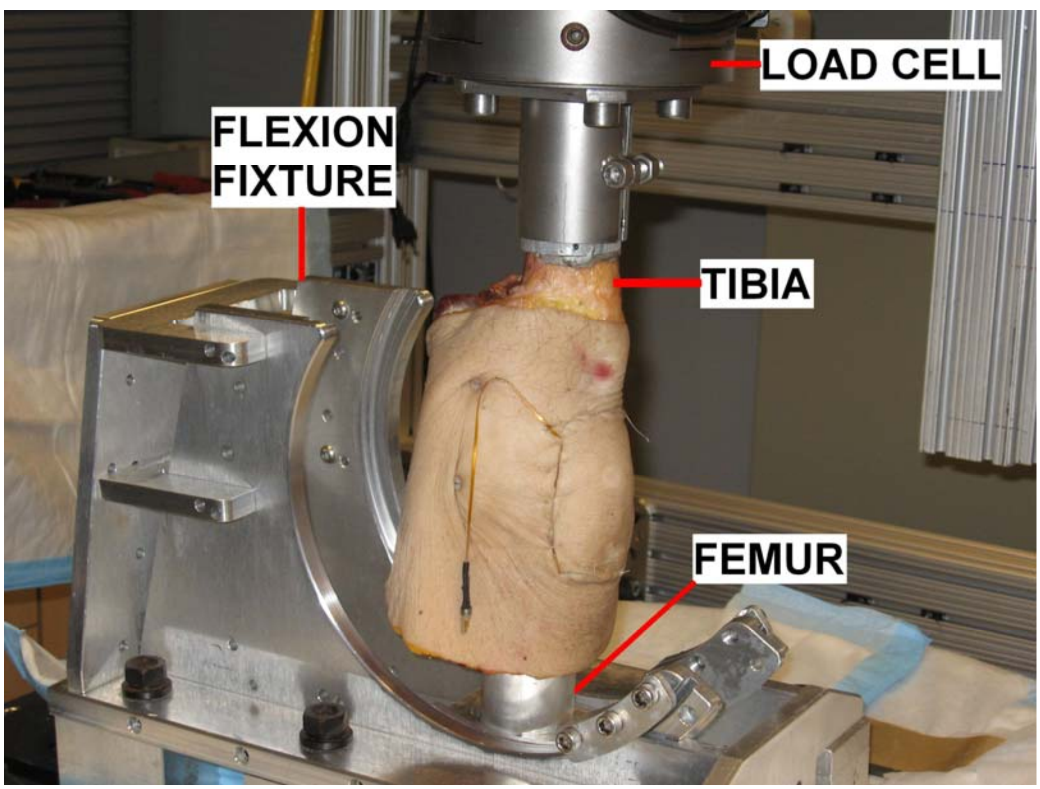

Figure 5.2: Flexion fixture – knee joint specimen – load cell set-up for expreiments

The tibia was mounted on a 6-component load cell (SI-1500-240, ATI Industrial Automation, Apex, NC) and femur was attached to the motion platform of Rotopod R2000 using a special fixture as shown in Figure 5.2. This fixture allowed changing the flexion angle and fixing it to a desired position. Force control was applied to the 3D force, internal-external (I-E) rotation moment, and varus-valgus (V-V) moment and joint laxity data was obtained from each of the specimen. Specifically, I-E rotation torque (+/-5 Nm in steps of 1 Nm), V-V torque (+/-10 Nm in steps of 2.5 Nm) and anterior-posterior (A-P) drawer force (+/-100 N in steps of 10 N) were applied in tibia coordinate system in isolated manner and the corresponding kinematic data was recorded by LabVIEW interface. The joint laxity data was essentially used as a prediction target for optimization of the joint model. This loading was repeated for four flexion angles viz. 0^0,15^0,30^0, and 45^0. Before starting the laxity loading protocol, each joint was neutralized from residual stresses and preconditioned at 0^0 flexion using loads equivalent to laxity loads. At the end of the loading protocol, one set of laxity loading conditions was repeated at one of the four flexion angles and the results were compared with previous run to ensure that there was no damage to knee structures during the protocol.

5.1.2.3 Optimization Method

Our optimization goal was to find the 12 ligament line element reference strains that minimized the difference between the simulated and measured tibio-femoral kinematics (3 translations and 2 rotations) for each laxity loading condition. The original joint model software [Kwak, et al. 2000] was designed to solve the equilibrium positions and orientations of the moving rigid bodies and particles with respect to the ground rigid body for applied external forces and moments. A Material Transfer Agreement was signed between the Columbia University, New York NY and the Cleveland Clinic, Cleveland OH to access the source code of the joint model software (Kwak et al., 2000). To customize the model for the optimization approach, the joint model software was modified and accessed via the MATLAB MEX-function interface to provide the force imbalance (*GF*) of the moving bodies as an output with the applied external loading condition *i* and initial rigid body positions as an input. Using the MEX function set-up, we applied two optimization approaches, first MATLAB solver based small scale optimization (SSO) approach and second TOMLAB/SNOPT (Sparse Nonlinear OPTimizer) solver based large scale optimization (LSO) approach.

5.1.2.4 *Small Scale Optimization (SSO)*

This was the conventional optimization approach where a MATLAB solver algorithm based on Levenberg-Marquardt [Levenberg, 1944, Marquardt, 1963] methods for estimation of non-linear parameters using least-squares was used. Reference strains of 12 ligament line elements were used as optimization parameters and the kinematic response of the knee to different loading conditions during laxity tests were employed as prediction target. The corresponding objective function was given by,

$$\min f(p) = \sum_{i=1}^{n} \left\| \vec{S}_i(p) - \vec{M}_i \right\|^2 \qquad \ldots\ldots\ldots\ldots\ldots\ldots\ldots\ldots\ldots(1)$$

where,

p = unknown model parameter (ligament zero-strain lengths),

$\vec{K}_i$ = a vector with model position and orientation variables for moving bodies at *i,*

$\vec{M}_i$ = a vector with measured kinematic variables for loading condition i,

$\vec{S}_i$ = a vector with corresponding kinematic variables in the model, a subset of K_i.

In this optimization approach, the solver algorithm had to solve the joint model force imbalance ($GF = f_i(K_i, p) = 0$) at each laxity loading condition i to get the equilibrium of internal and external forces and moments and corresponding model kinematic variables S_i for the initial values of p. Corresponding square of the difference between predicted and measured kinematics at each laxity loading condition i was then acquired and if the difference did not meet the stopping criterion, then p values were perturbed within the bounds to get a new residual. This process was run in optimization loop until one of the stopping criterions was met.

5.1.2.5 Large Scale Optimization (LSO)

LSO implemented parametric estimation of a large set of variables X comprising m number of model parameters p and model position and orientation variables K_i (at each loading condition i) for n loading conditions. Thus, $X = (K_1,\ldots,K_n,\ p_1,\ldots,p_m)$. In this approach, using the MEX interface, we acquired the force imbalance (GF) at each loading condition i such that,

$$C_i(X) \equiv GF(K_i) \qquad \ldots\ldots\ldots\ldots\ldots\ldots\ldots\ldots\ldots\ldots\ldots\ldots(2)$$

Analytical derivatives of GF with respect to K_i were obtained from the joint model software using the MEX interface. The objective function that quantified the model difference with respect to the experiments was given by:

$$f(X) = \sum_{i=1}^{n} (\vec{S}_i - \vec{M}_i)^2 \quad \ldots\ldots\ldots\ldots\ldots\ldots\ldots\ldots\ldots\ldots\ldots\ldots (3)$$

This was a large-scale constrained optimization problem which was solved by the TOMLAB/SNOPT solver (http://tomopt.com) to minimize the objective function (3) while satisfying the constraints $C_i\ (X) = 0$. The SNOPT solver linearizes the constraints of the original problem into a sequence of quadratic programming subproblems, and the objective function of the subproblem is a quadratic approximation to the Lagrangian function exploiting the sparsity in the constraint jacobian [Gill, et al. 2005]. The QP subproblems are then solved using an inertia-controlling reduced-Hessian active-set method Sequential Quadratic OPTimizer (SQOPT).

In our typical LSO problem using the entire experimental joint laxity data,

n = number of loading conditions = 192,

m = number of unknown model parameters = 12,

$dim(M_i) = 5$ (3 femur positions and 2 orientations) for each loading condition i,

$dim(K_i) = dim(C_i) = 23$ for each loading condition i.

This required the SNOPT solver to solve for $dim(X) = (192*23) + 12 = 4428$ parameters. We started the optimization with an initial guess of X where all the K_i variables satisfied the static equilibrium conditions $C_i\ (X) = 0$ for an initial guess of model parameters p based on the ligament lengths as seen in the MRI scans.

We conducted series of preliminary trials on two joint models to understand the effect of different optimization parameters and determine the sensitivity of model parameters with respect to the joint kinematics. In these trials, the model appeared stiffer than the experiments in the regions where the kinematic parameter was the primary response (peaks) to the isolated loading condition (Figure 5.3 and 5.4). The model behavior in the

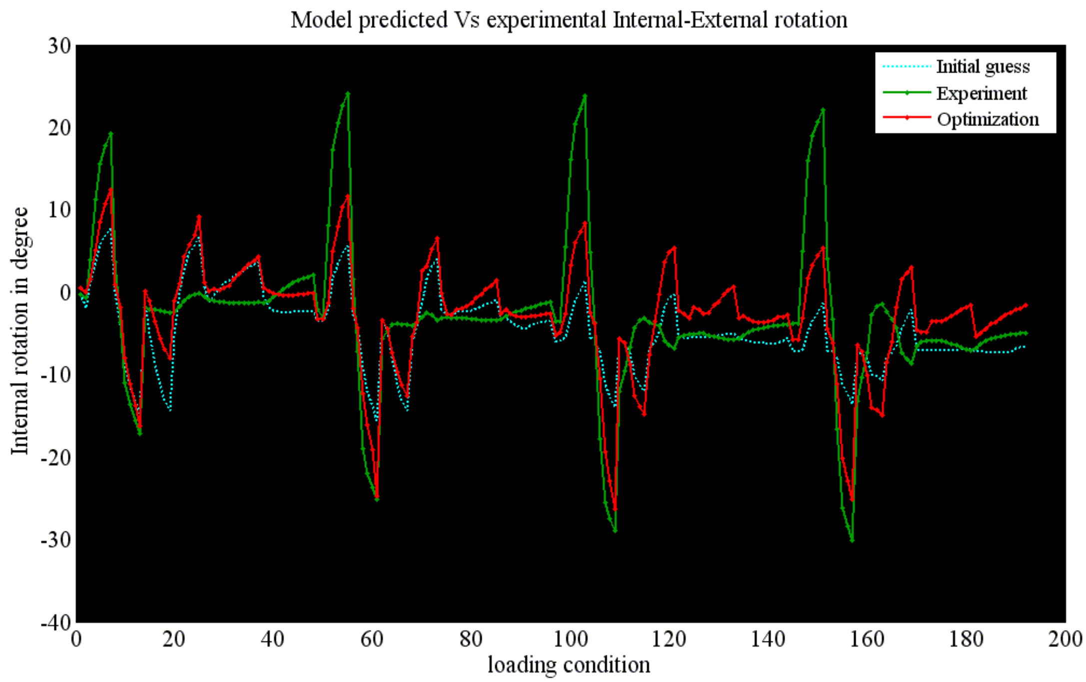

Figure 5.3: Preliminary results showing model fit to experimental I-E kinematic data for pre and post optimized parameters

secondary response parameter corresponding to the isolated loading condition (e.g. anterior translation in response to rotation torque) did not appear to be in qualitative agreement with the experiments.

Sensitivity analysis pointed towards ligament insertion points being responsible. Considering the human element of error of up to 3 mm in determining the insertion points from MRI scans, we employed 24 insertion points as additional optimization parameters in both the LSO and SSO approaches. This increased the number of optimization

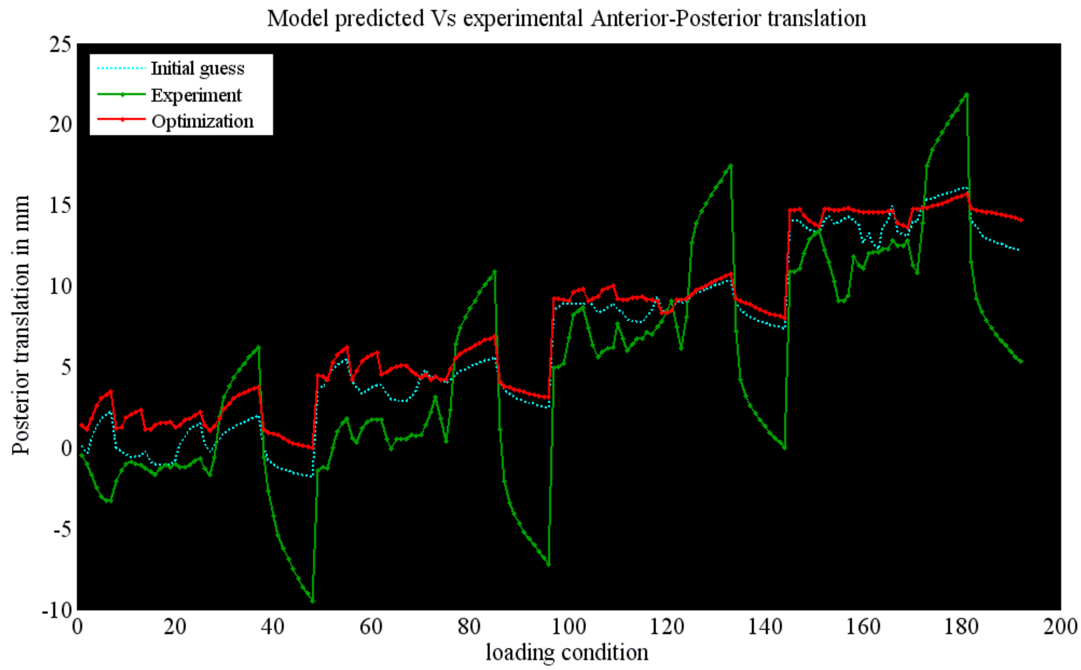

Figure 5.4: Preliminary results showing model fit to experimental A-P kinematic data for pre and post optimized parameters

parameters for SSO from 12 to 36 and LSO parameters from 4428 to 4452. The ligament insertion coordinates were allowed to vary within ±4.5 mm (3 scans) of the originally digitized insertion points in each direction. The reference strains were allowed to vary up to ±30% of their initial guess. For each ligament insertion site, only one insertion point out of three ligament elements was varied and the insertion points of the remaining two elements were tagged along with the first one to have equal variations and avoid redundancy in the solutions.

Table 5.1: Description of optimization sets run using both MATLAB and SNOPT solvers

	Objective function fits	**Loading conditions**	**Unknown model parameters**	**Optimization parameters for SSO approach**	**Optimization parameters for LSO approach**
Set 1	I-E kinematics	52	36	36	1232
Set 2	I-E and A-P kinematics	52	36	36	1232
Set 3	I-E, A-P and V-V kinematics	192	36	36	4452

To demonstrate the computational efficiency of the LSO approach, we performed three sets of optimizations varying the number of loading conditions and objective function in each set. The first set considered only I-E laxity loading conditions and the objective function was to minimize the difference between model predicted and experimental I-E rotations for these loading conditions. The second set also considered only I-E laxity loading conditions but this time the objective function was to minimize the difference between model predicted and experimental I-E rotations together with A-P translations for I-E loading conditions. The third set considered all A-P, I-E and V-V loading conditions and the objective function was to minimize the difference between model predicted and experimental primary response to primary loading condition (for e.g., A-P translation with respect to A-P loading). These three sets are summarized in Table 5.1.

5.1.3 Results

All the optimizations were performed on Intel Pentium IV, 1.86 GHz processors. Not all the LSO algorithms reached the stopping criteria. The LSO algorithms that stopped after facing numerical difficulties were restarted with different initial guess or initial guess extracted from the solution of the previous run. The RMS error achieved by the LSO approach was close to the corresponding RMS error achieved by the SSO approach. The computational time required to optimize model parameters of the first model for each set using each solver is summarized in Tables 5.2 & 5.3. SNOPT solver required approximately 1/3rd computational time as compared to MATLAB solver for similar optimization problem and to achieve similar RMS error level.

Table 5.2: MATLAB solver optimization details

	Set 1	**Set 2**	**Set 3**
	I-E optimization	I-E with A-P optimization	A-P, I-E and V-V separate optimization
Time (hrs)	54	96	189
RMS Error	2.14	3.07	4.07

Table 5.3: TOMLAB/SNOPT solver optimization details

	Set 1	**Set 2**	**Set 3**
	I-E optimization	I-E with A-P optimization	A-P, I-E and V-V separate optimization
Time (hrs)	18.5	29	71
RMS Error	2.42	3.28	4.85

5.1.4 Discussion

This study demonstrated the use of LSO algorithms to find subject specific modeling parameters for the knee joint loading while significantly reducing the computational time. As there was no need to achieve equilibrium at each function evaluation, the LSO approach was faster than the conventional SSO approach. Since optimization is the only available non invasive tool to find subject specific model parameters, it is worth the time and effort to find algorithms that are computationally low cost and efficient. The SNOPT solver used in the LSO algorithm to optimize model parameters of a quasi-static multi-body model can be effectively used in dynamic musculoskeletal models to solve optimal control problems. Previous optimization studies focus on reducing the computational cost of optimization by deploying parallel algorithms in gradient based [Anderson, et al. 1999, Anderson, et al. 2001] as well as global optimization based [Higginson, et al. 2005] routines. However, global optimization algorithms are always computationally costly compared to gradient based algorithms.

The convergence and performance of gradient based optimizations such as the LSO method presented here depends heavily upon the accuracy and availability of first partial derivatives of the constraints as well as the initial guess of optimizing variables. Nonlinearities and discontinuities present in the model behavior pose serious computational difficulties in any gradient based optimization algorithms [Pandy, et al. 1992]. Many modeling and optimization studies approximate the first derivatives by initiating a complex and time consuming approximation process that may cause infeasibilities in optimization algorithms if not properly deployed. In the current study, the constraint jacobians were provided analytically by the joint model software eliminating the need for approximation and further reducing the computational time.

In all the LSO runs, the RMS error levels achieved were equivalent to the RMS error levels achieved in the SSO runs. However, the optimized values of model parameters were not in qualitative agreement in corresponding optimization sets indicating either or both the algorithms may have reached local minima. In certain cases, the LSO algorithm stopped after running into infeasible constraint conditions and we had to rerun the algorithm which required additional computational time. The LSO runs did not converge to the stopping criterions set by feasibility and optimality conditions (10^{-4}) but came closer to it before running into constraint infeasibilities. We believe that this problem can be resolved by customizing the LSO algorithm options set by SNOPT solver or reducing the number of model optimization parameters from 36 to 12. A two step optimization approach can be implemented in which the first step would optimize the 12 reference strains and the second step would use the optimized values of these 12 parameters along with 24 insertion parameters to conduct further optimization. This process would give robustness to the optimization algorithm.

5.2 SECTION II

Even though LSO algorithm was computationally cost effective, it did not always converge to an optimal solution. The sequential QP approach used in the LSO was sensitive to the initial guess of the optimization variables causing convergence problems and ultimately increasing the computational cost. There were many optimization parameters for example, scaling options or minor iteration feasibility tolerances that were set to default values by SNOPT solver. These parameters needed to be customized for the problem under study to make the solver more robust and eliminate some of the convergence problems. Despite these limitations, the LSO approach is by far an effective and computationally low cost alternative to SSO. With correct set of optimization parameters and with sufficient time to find those parameters to make the optimization algorithm more robust, LSO method would be our first choice for optimizations. However, owing to the time constraints, we had to switch back to the SSO algorithm for optimizing the rest of our models. In the current situation, SSO approach is more robust even though computationally expensive. To maintain the continuity in our methods, we applied SSO algorithm to all 5 joint models and used the optimized reference strains and insertion points for the subsequent use of the model in the validation and simulation studies. This section gives a detailed description of different levels of SSO optimizations applied to each model and results obtained.

5.2.1 Optimization Sets

The ultimate goal of our optimization objective function was to minimize the difference between A-P translation, I-E and V-V rotation kinematics in all the joint laxity loading conditions. In each model, this objective function had 576 residuals from 192 loading conditions to calculate the optimized values of 36 optimization variables. In order to eliminate any problems related to the optimization procedures and understand the isolated or combined effect of each DOF on optimization, we applied different objective functions and compared the results.

Table 5.4: Details of optimization trials conducted on each models

Sr. No.	Objective Function Name	Description	# loading conditions	# Residuals minimized
1	**AP Only**	Fit A-P kinematics w.r.t. corresponding A-P laxity loading conditions.	88	88
2	**IE Only**	Fit I-E kinematics w.r.t. corresponding I-E laxity loading conditions.	52	52
3	**VV Only**	Fit V-V kinematics w.r.t. corresponding V-V laxity loading conditions.	52	52
4	**AP-IE-VV separate**	Fit A-P kinematics w.r.t. corresponding A-P laxity, I-E kinematics w.r.t. corresponding I-E laxity loading and V-V kinematics w.r.t. corresponding V-V laxity loading conditions	192	192
5	**AP with IE and VV**	Fit A-P, I-E and V-V kinematics w.r.t. corresponding A-P laxity loading conditions	88	264
6	**AP with IE**	Fit A-P and I-E kinematics w.r.t. corresponding A-P laxity loading conditions	88	176
7	**IE with AP and VV**	Fit A-P, I-E and V-V kinematics w.r.t. corresponding I-E laxity loading conditions	52	156
8	**IE with AP**	Fit I-E and V-V kinematics w.r.t. corresponding I-E laxity loading conditions	52	104
9	**AP-IE-VV combined**	Fit A-P, I-E and V-V kinematics w.r.t. all corresponding laxity loading conditions	192	576

Specifically, models 1 and 2 were subjected to 9 different objective functions and models 3, 4 and 5 were subjected to 4 objective functions as illustrated in the table 5.4 here.

The first three sets of objective functions (**AP only, IE only and VV only**) guaranteed us that the model was able to converge to an optimized solution in each isolated DOF for corresponding loading conditions. Set # 4 (**AP-IE-VV separate**) was conducted to ensure that optimization sequence was working when the first three objective functions were combined in one objective function. Set # 5 and 6 (**AP with IE and VV, AP with IE**) studied the effect of including or excluding V-V kinematics in objective function when using A-P laxity loading. Set # 7 and 8 (**IE with AP and VV, IE with AP**) studied the effect of including or excluding V-V kinematics in objective function when using I-E laxity loading conditions. The objective function of the final set (**AP-IE-VV combined**) reflected the ultimate aim of our optimization and the optimization results from this set would be used for validation and simulation studies.

5.2.2 Optimization Results

Table 5.5: RMS error values achieved in each optimization set for each model

Optimization Set	Model 1	Model 2	Model 3	Model 4	Model 5
AP Only	2.133	1.467	N/A	N/A	N/A
IE Only	2.149	1.721	N/A	N/A	N/A
VV Only	2.086	1.883	N/A	N/A	N/A
AP-IE-VV separate	4.073	3.481	2.926	2.081	2.429
AP with IE and VV	3.283	1.677	N/A	N/A	N/A
AP with IE	2.613	2.794	1.683	1.722	1.756
IE with AP and VV	3.732	2.136	N/A	N/A	N/A
IE with AP	3.071	1.859	2.114	1.183	0.946
AP-IE-VV combined	4.001	2.972	2.967	2.594	2.587

Models 1 and 2 were evaluated for all the optimization sets to ensure the capability of both model and optimization algorithms to work in all the procedures. Table 5.5 gives summary of optimization sets performed on each model and the corresponding RMS error achieved in each set for each model.

Optimized reference strains of the ligaments corresponding to **AP-IE-VV combined** set of objective function for each model are summarized in table 5.6. We optimized 36 parameters including 12 reference strains and 24 insertion points however; values of 12 optimized reference strains are reported in Table 5.6 and values of insertion optimized insertion points are reported in Table 5.7. Each value of the reference strains indicates the initial strain each ligament should be set to when in its reference position (full extension). The corresponding ligament length is the zero strain length indicating that the ligament will be strained if the model predicted length of the ligament increases above this value. Positive value of the strain indicates tight ligament whereas negative value indicates slackness in the ligament with respect to its initial guess. As can be illustrated from table 5.6, each model suggests considerable different reference strains and there is no particular pattern observed in the optimizations.

Table 5.6: Optimized reference strain values for each model

	Reference strains from optimizations (%)				
Ligament Type	**Model 1**	**Model 2**	**Model 3**	**Model 4**	**Model 5**
MCL1	-5.24	-5.96	-12.70	-2.00	-1.02
MCL2	-4.14	-0.11	-7.68	2.07	2.39

	Reference strains from optimizations (%)				
Ligament Type	Model 1	Ligament Type	Model 1	Ligament Type	Model 1
MCL3	-10.16	4.98	3.25	1.66	1.54
LCL1	0.12	-1.58	0.73	3.40	2.07
LCL2	-20.44	-7.88	3.22	2.08	3.75
LCL3	0.80	4.32	5.53	0.58	-4.65
ACL1 – AMB	0.54	-6.87	1.63	1.78	-6.25
ACL2 – MB	5.23	6.25	-2.20	3.33	2.42
ACL3 – PLB	6.86	-0.66	-7.50	2.53	0.52
PCL1 – ALB	-20.46	-19.30	-31.28	-16.51	-12.20
PCL2 – MB	-9.55	-4.84	-17.06	-11.10	-8.93
PCL3 – PMB	-0.04	-0.88	-19.11	-2.75	-1.56

Table 5.7: Optimized insertion point values for each model

	Insertion points from optimizations (mm)				
Ligament type	Model 1	Model 2	Model 3	Model 4	Model 5
MCL–X on tibia	-56.3655	-59.1098	-60.5985	-62.6768	-83.7333
MCL–Y on tibia	22.6296	29.8426	26.6855	17.7639	7.2453
MCL–Z on tibia	27.5028	-10.4195	-8.6732	-8.1861	-2.9245
PCL–X on tibia	-30.6634	-41.3824	-39.6720	-40.8318	-35.1520
PCL–Y on tibia	-6.9061	-0.1498	0.9245	-10.5441	-4.2350

	Insertion points from optimizations (mm)				
Ligament type	**Model 1**	**Model 2**	**Model 3**	**Model 4**	**Model 5**
PCL–Z on tibia	42.4750	10.3421	14.1850	14.8489	22.1881
ACL–X on tibia	-36.7486	-35.6501	-21.2191	-28.5742	-26.7984
ACL–Y on tibia	-2.8000	-0.3020	11.0363	-9.6665	-3.4450
ACL–Z on tibia	12.8231	-20.5367	-20.0016	-12.7884	-6.0331
LCL–X on tibia	-46.1264	-62.4970	-52.5967	-57.4490	-67.1271
LCL–Y on tibia	-33.5934	-51.8830	-51.9182	-60.3667	-56.5201
LCL–X on tibia	41.8307	6.9760	-5.1761	16.9643	34.8362
MCL–X on femur	-7.2384	-7.2040	2.3635	-7.3368	-5.0955
MCL–Y on femur	39.4615	46.0640	51.8823	45.4048	46.1108
MCL–Z on femur	9.9368	-2.1876	3.2912	-4.7363	-0.6782
PCL–X on femur	-16.9697	-18.9304	-16.0280	-15.0086	-9.9207
PCL–Y on femur	8.0564	6.5319	17.6913	3.7636	2.7566
PCL–Z on femur	13.3192	-2.2952	3.6805	-4.1743	1.4319
ACL–X on femur	0.4592	-4.1635	9.3098	-3.1807	1.2203
ACL–Y on femur	-9.1395	-8.9460	2.2412	-0.4561	-3.9625
ACL–Z on femur	18.4410	13.3579	12.3552	5.9432	10.4313
LCL–X on femur	-10.1485	-10.4619	6.5851	1.6850	2.4354
LCL–Y on femur	-33.8295	-43.6745	-42.2052	-46.1757	-43.7955
LCL–Z on femur	11.4288	4.1994	-0.9150	8.4142	7.2116

Models 1 and 2 provide excellent analysis of model behavior under different optimization sets. When single kinematic parameter was used in objective function (sets **AP only, IE only and VV only**), model showed good fit to the experimental data with RMS error value as low as 1.46 mm.

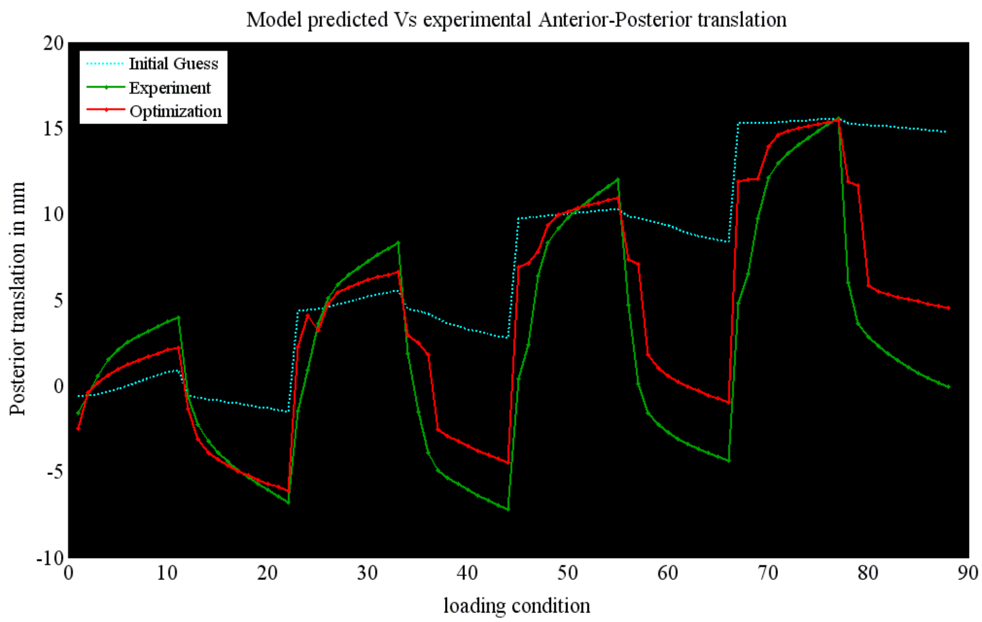

Figure 5.5: Model fit to A-P kinematic data for model # 2 using **AP only** set

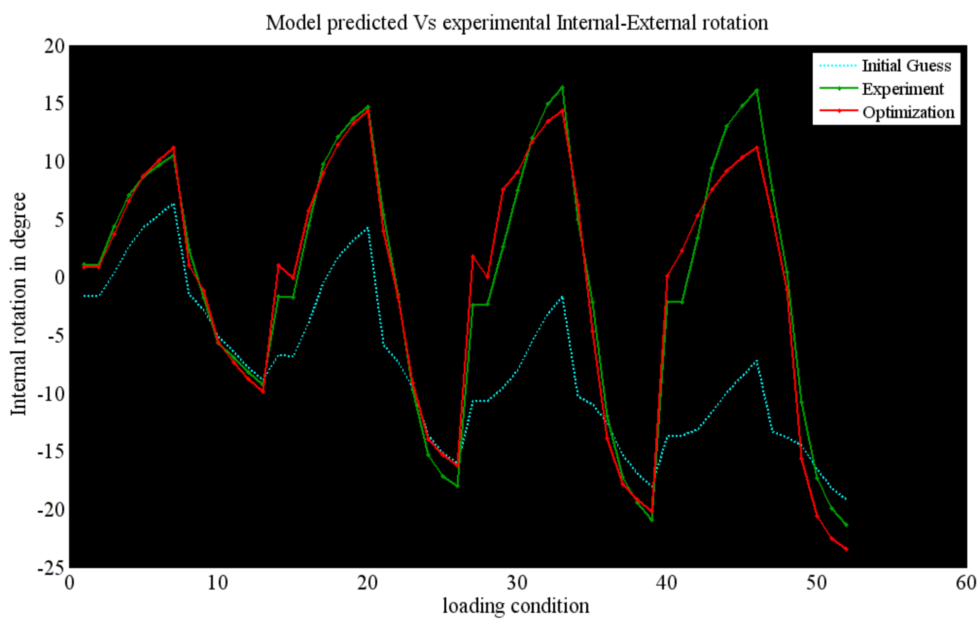

Figure 5.6: Model fit to I-E kinematic data for model # 2 using **I-E only** set

This was because the secondary kinematic effects of the primary loading condition were neglected. Figure 5.5 shows optimized fit for model 2 using **AP only** set and Figure 5.6

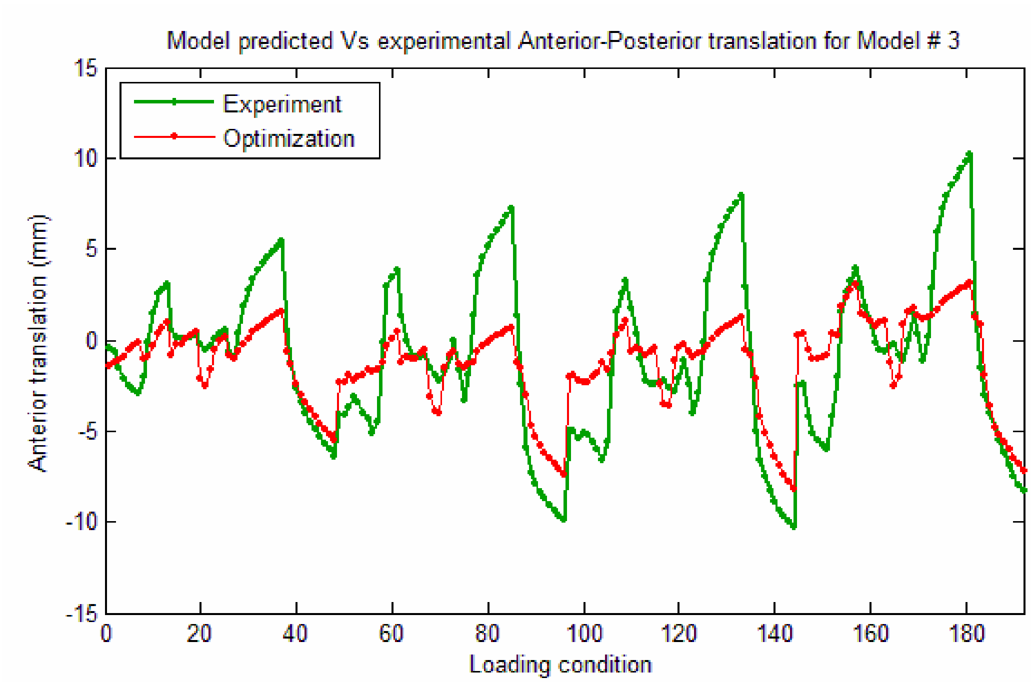

Figure 5.7: A-P translation optimization fit for **AP-IE-VV combined** set

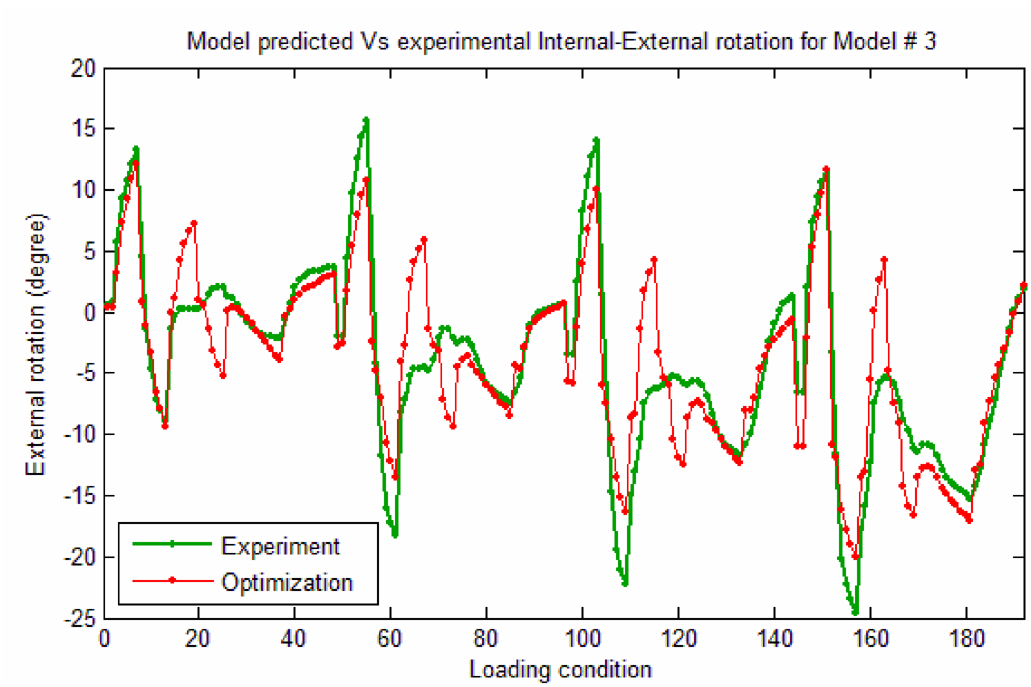

Figure 5.8: I-E rotation optimization fit for **AP-IE-VV combined** set

shows optimization fit for model 2 using **IE only** set.

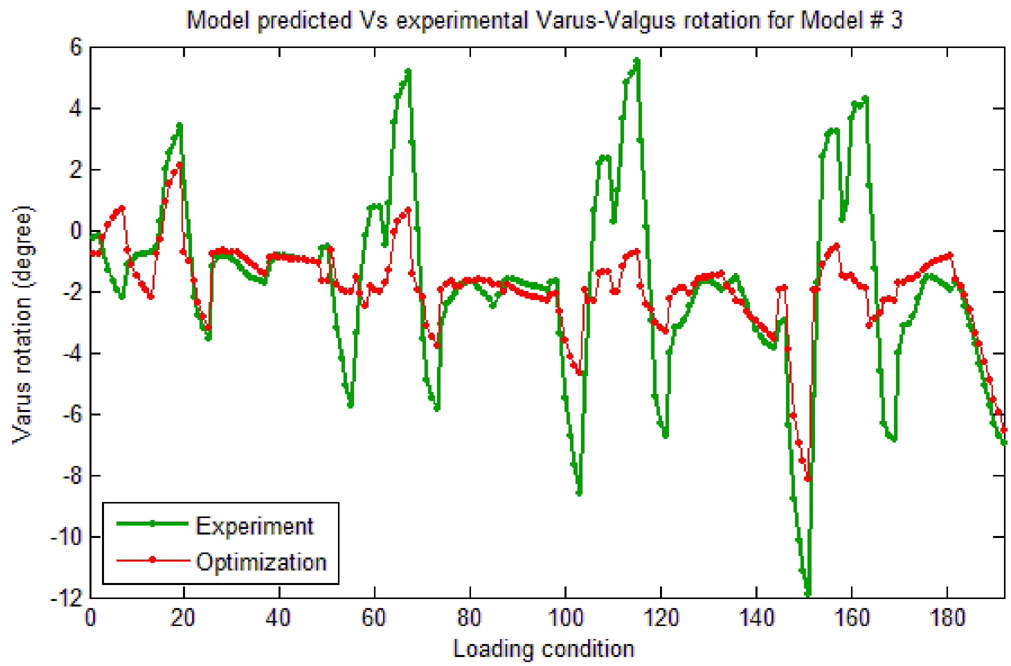

Figure 5.9: V-V rotation optimization fit for **AP-IE-VV combined** set

Optimization fit for **AP-IE-VV combined** set for model # 3 is shown in Figures 5.7, 5.8 and 5.9 for A-P, I-E and V-V kinematics respectively.

There are 192 laxity loading conditions in each plot applied to four flexion angles of the joint. Each flexion angle constitutes 48 loading conditions. Plots showing optimization fit for the remaining models are provided in Appendix C.

5.2.3 Optimization Analysis

As illustrated in Figures 5.7, 5.8 and 5.9, the model behavior in the secondary axis corresponding to the loading condition in primary axis (A-P translation to I-E laxity loading in Figure 5.7) was poorly optimized. These coupled motions are sensitive to the changes in the joint coordinate system and we believe that this could be the effect of coordinate system mismatch between the experimental data and the model. Even though cross referencing screws were embedded in the cadaver knees, there could be a mismatch in the femoral (longitudinal) axis of the model and experiments leading to over or under prediction of ligament strains to match the joint kinematics. As we define the coordinate systems keeping the joint in full extension, these mismatches could accumulate as flexion angle increases. Small uncertainties in defining the coordinate systems have been shown to significantly affect the joint kinematics by Ramakrishna and Kadaba [Ramakrishnan, et al. 1991]. Regardless, optimized reference strains from this set (**AP-IE-VV combined**) will be used to validate the model predictions to the experimental data recorded for combined loading conditions. The RMS errors achieved in each DOF for this set of objective functions are listed in table 5.8.

Table 5.8: RMS errors observed for each model in each A-P, I-E and V-V kinematics for objective function set **AP-IE-VV combined**.

	Model 1	**Model 2**	**Model 3**	**Model 4**	**Model 5**
I-E rotation	5.484	3.047	3.707	2.722	3.198
V-V rotation	2.299	1.838	2.150	2.238	1.773
A-P translation	3.580	3.738	2.843	2.788	2.614

In all the models, V-V kinematic fit was better than the other two indicating that optimizations favored V-V kinematics. We used degree and mm units while calculating the residuals during optimization algorithm. The range of motion for each knee in our experiments was within one decimal point when measured in degree and mm. However, scaling can be controlled more efficiently by using weight factors in the objective functions.

We conducted sensitivity analysis on the model parameters by manually changing the parameter values and recording its effect on model response. This analysis revealed that model simulations were sensitive to ligament insertion points and ligament zero strain lengths and less sensitive to the ligament and cartilage stiffness parameters. Blankevoort and Huiskes [Blankevoort, et al. 1996] conducted a sensitivity analysis of cartilage stiffness parameters and proved that cartilage stiffness was not a critical parameter to be optimized and we concluded that a subject specific estimate of cartilage stiffness was not needed. Thus, we included only insertion coordinates and zero strain lengths of the ligament bundles in our optimizations.

Typical data never exactly fit the model that is being used, even when model is correct. A fitting procedure should ideally provide (1) parameters, (2) error estimates on the parameters, and (3) a statistical measure of goodness of fit. There are ways and means to assess whether or not the model is appropriate and we need to test the goodness of fit against certain useful statistical standard. Although RMS error number provides some measure of goodness of fit, it does not quantify the model predictive abilities and a much advanced analysis is warranted in future studies. Here we theoretically discuss how this analysis would be conducted on the optimized parameters. The joint model developed in this study depends nonlinearly on the set of optimization parameters p_i, $i = 1,2,\ldots,36$. A least square objective function given in equation (1) finds the parameters that minimize the difference between the experimental data and model predicted data. This is equivalent to a maximum likelihood estimation of the fitted parameters if the measurement errors are independent and normally distributed with constant standard deviation. The uncertainties in the estimated parameters can be described by a covariance matrix *C*. In case of nonlinear model, this covariance matrix can be calculated using the Hessian matrix of the objective function (http://www.nrbook.com/a/bookcpdf/c15-5.pdf) [Press, et al., 1992]. From the given objective function in equation (1), the Hessian matrix is given by the second partial derivative of the objective function *f*,

$$H_{ij} = \frac{\partial^2 f}{\partial p_i \partial p_j}$$

In the specific case of a least squares objective function, the hessian can be approximated by the Jacobian J of model residuals (http://www.nrbook.com/a/bookcpdf/c15-5.pdf) [Press, et al., 1992]:

$$H = J^T J \qquad \textit{(this is short for: } H_{ij} = \sum_k J_{ki} J_{kj} \textit{)}$$

The Jacobian matrix *J* is already available from the joint model software. The covariance matrix *C* is given by,

$$C = H^{-1}$$

The diagonal elements of *C* are the variances (uncertainties) of the fitted parameters *p,* normalized to the variance of experimental data. Similarly, the off-diagonal elements C_{ij} represent the covariances between p_i and p_j. High values on the diagonal indicate possibly redundant parameters, high off-diagonal values indicate parameters that may have similar effect on the model, and one of them may be redundent. In our model, this can happen if one bundle of a ligament becomes longer and the second one shorter and the joint mechanics is largely unchanged. The covariance matrix provides insight into these model properties, and can be further used to estimate confidence limits on the estimated parameters (http://www.nrbook.com/a/bookcpdf/c15-5.pdf) [Press, et al., 1992] . The covariance matrix contains all the details of the probability distribution of errors in parameter estimation whereas confidence limits summarize this distribution on the 36 dimensional space of parameters *p,* based on the assumption that measurement errors are normally distributed. This detailed error analysis on optimized parameters should be included in future studies.

Comparing the results from the optimization sets **AP with IE and VV** and **AP with IE** highlighted the adverse effect of introducing V-V kinematics in the objective function. In earlier studies, V-V motion was regarded as coupled motion and not sensitive to ligament reference lengths [Blankevoort, et al. 1996]. We observed similar findings in our optimizations. The magnitude of V-V rotation as a coupled motion was very small and can be susceptible to the coordinate system mismatch error. As illustrated from table 5.5, the optimization sets not including V-V kinematics achieved lower RMS errors. We also observed a reverse trend in model 2 where **AP with IE and VV** set had lower RMS error than **AP with IE** set. We cross checked the solution of **AP with IE and VV** set by putting it in **AP with IE** set and observed the RMS error to be 2.87 indicating that the optimization results in **AP with IE and VV** set favored reducing V-V kinematics. This also confirmed that the optimization results in **AP with IE** set did not reach local minimum, although whether it reached global minimum can not be confirmed. The adverse effect of V-V kinematics on optimization can be controlled by using weight factors in the objective function favoring the kinematics corresponding to primary load for each loading condition. However, this is not in the scope of the thesis and will be regarded as future work.

All the optimized models demonstrated a good fit to the kinematic data corresponding to the primary loads (for example, I-E rotation to I-E loading). One may ask how this optimization model will respond to a set of combination of loads applied in all A-P, I-E and V-V axes of the joint model. We will demonstrate that in our next Chapter.

CHAPTER VI

MULTI-AXIAL VALIDATION OF THE KNEE JOINT MODELS USING JOINT KINEMATICS AND ACL STRAIN FROM COMBINED LOADING TESTS

6.1 INTRODUCTION

Each human knee joint is unique with regards to its morphological structure and tissue properties and there are many extrinsic factors responsible for its uniqueness. Age, gender and life style form one such triad of extrinsic factors based on which the joint structure and properties vary. This complex structure gets injured most of the times during any sports that involves ground contact and cutting or maneuvering tasks. On the other hand, debilitating joint diseases such as arthritis damage the cartilage surface of the joint and needs surgical treatment to replace it with artificial surfaces. It is obvious that the knee joint bears complex loading conditions in the event of injury and similarly, an arthritic knee joint exhibits changed loading pattern than the normal knee joint. Computational modeling provides a non-invasive approach to understand the forces acting on the knee joint or distribution of these forces within the tissue structures of the joint. However, to prevent the injuries to the knee joint requires understanding of the injury mechanisms. Although subject specific models lend insights to the force or stress variations due to subject specificity, they can not be confidently used as predictive tools in the treatment planning or injury prevention programs unless properly validated. Experimental validation of subject specific model simulations constitutes important step towards building the credibility in the model's predictive capability.

Validation is the process to evaluate the model predictions with sufficient accuracy keeping in mind the intended use of the model [Babuska, et al. 2004]. As suggested by early studies, validation stands for acceptable correlation of the model predictions with the observed facts [Wismans, et al. 1980]. Previous validation studies were targeted towards understanding the performance of the models for either isolated loading conditions [Blankevoort, et al. 1996, Li, et al. 1999] or small set of combined loading in two axes [Mommersteeg, et al. 1996]. In both the studies, Blankevoort and Huiskes and Li and associates validated their models using experimental data from the literature and not from the same knee specimen from which their respective models were generated. Mommersteeg and associates developed single tibio-femoral joint model and focused on verifying their model rather than validating it and also acknowledged that the number of loading conditions applied for the verification purpose were limited due to the subluxation problem faced by the specimen. In all the above studies, internal external rotations of the models were constrained while evaluating the model performances restricting the use of these models to constrained situations only.

We have developed MRI based subject specific tibio-femoral knee joint models (Chapter 4) to understand the injury mechanisms to the anterior cruciate ligament (ACL). Using the experimental data from corresponding cadaveric knee specimens, we have conducted series of parametric optimization procedures (Chapter 5) in order to incorporate subject specific properties to the model parameters. The aim of this study was to validate the optimized tibio-femoral knee joint models to experimental data with respect to 1) knee kinematic response to large data set of combined loading conditions and 2) corresponding ACL strain data collected during these loading conditions.

6.2 MATERIALS AND METHODS

Subject specific 3D mathematical knee joint models were used in this study. Specifically, five quasi-static, multi-body tibio-femoral knee joint models were developed from MRI scans of the cadaveric specimens. Details of each specimen are given in Table 6.1.

Table 6.1: Specimen details

Specimen Number	sex	age	weight (kg)	cause of death	bone disorders
Knee 1124	F	70	77.2	Lung Cancer	None
Knee 1129	M	58	91.5	Laryngeal Cancer	Arthritis in hands
Knee 1131	M	58	91.5	Laryngeal Cancer	Arthritis in hands
Knee 1133	M	58	70	Small cell lung cancer	None
Knee 1135	M	58	70	Small cell lung cancer	None

The details of the experiments and model development methods were previously explained in Chapters 3 & 4. Briefly, each specimen was thawed overnight and underwent medial parapatellar arthrotomy to check ligament and cartilage integrity. Cross referencing nylon screws were embedded in the medial and lateral femoral epicondyles to match the coordinate system of the experiments and corresponding computational model. MRI scans were performed using 1.0 Tesla MRI extremity scanner (ONI Corp., Santa Rosa, CA) with knee joint in its full extension. The full extension or 0^0 flexion position was referred as the reference position of the joint for modeling purpose. Sagittal plane MRI scans were used to digitize femoral condylar articular cartilage and medial and lateral tibial articular cartilage using an in house MATLAB (Mathworks Inc., Natick, MA) algorithm [Doehring, et al. 2005]. In addition, insertion points of the four major ligaments of the knee joint viz. anterior cruciate ligament (ACL), posterior cruciate ligament (PCL), medial collateral ligament (MCL), and lateral collateral ligament (LCL) were also digitized from the sagittal MRI scans. A mathematical surface fitting algorithm written in MATLAB [Boyd, et al. 2000] was used to fit a smooth parametric surface model of the form $\Phi(r) = r^2 \ln(r)$ (thin plate spline) to the digitized point cloud of each of the femoral and tibial cartilage.

The mathematical surface was resampled to generate rectangular mesh for each of the articular cartilage as shown in Figure 6.1. Resampled surface was stored in a specific .3D file format as required and specified by the joint modeling software. Using the .3D files and insertion points of the four ligaments, a tibio-femoral knee joint model was developed. In this model, each ligament bundle was represented by three line elements.

The joint model featured a deformable contact between articular cartilages; non-linear piecewise springs to represent three line elements of each ligament bundle and particles

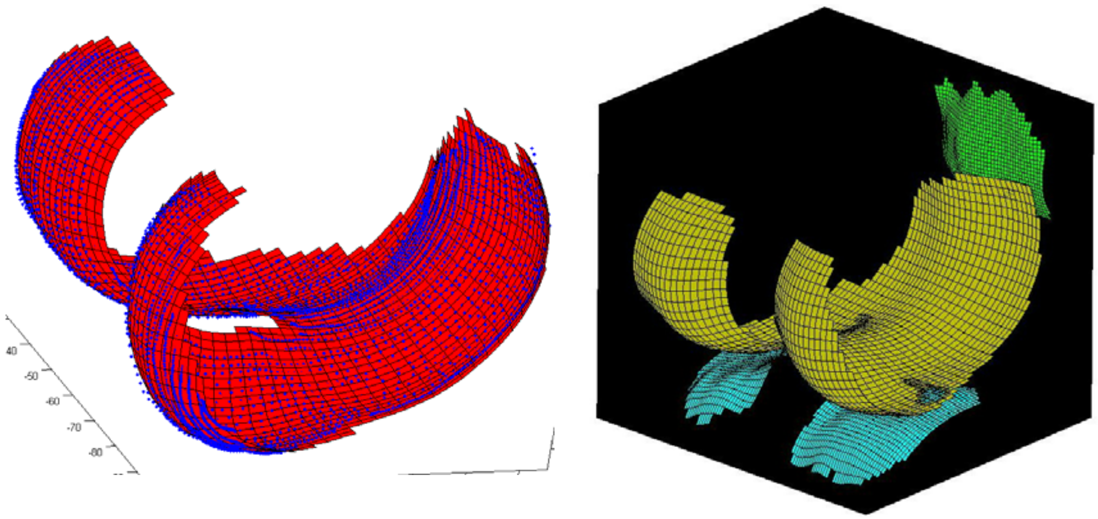

Figure 6.1: Resampled and trimmed TPS surfaces representing articular cartilages of the knee joint.

bodies embedded in the MCL line elements to wrap around the medial bony edge of the tibia [Kwak, et al. 2000]. Force-deformation properties of the ligaments and articular cartilage were adapted from the literature [Blankevoort, et al. 1991a]. Five models were developed using this methodology. Each joint model consisted of 23 degrees of freedom (DOF). A general formulation for 3D quasi-static multi-body modeling developed by Kwak and colleagues [Kwak, et al. 2000] was used to simulate and analyze joint mechanics (Details in Chapter 4). The quasi-static multibody model software finds the bone positions and orientations in which there is an equilibrium between the internal structures of the joint (ligament forces, muscle forces, contact forces etc.) and external forces and moments applied to the joint. All the model kinematics was reported with respect to the tibia with origin located at the midpoint of the line joining the medial and lateral femoral epicondyles.

Experimental data were collected on each specimen using a 6 DOF robotic motion platform Rotopod (R2000, Parallel Robotics Systems Corp., Hampton, NH) along with

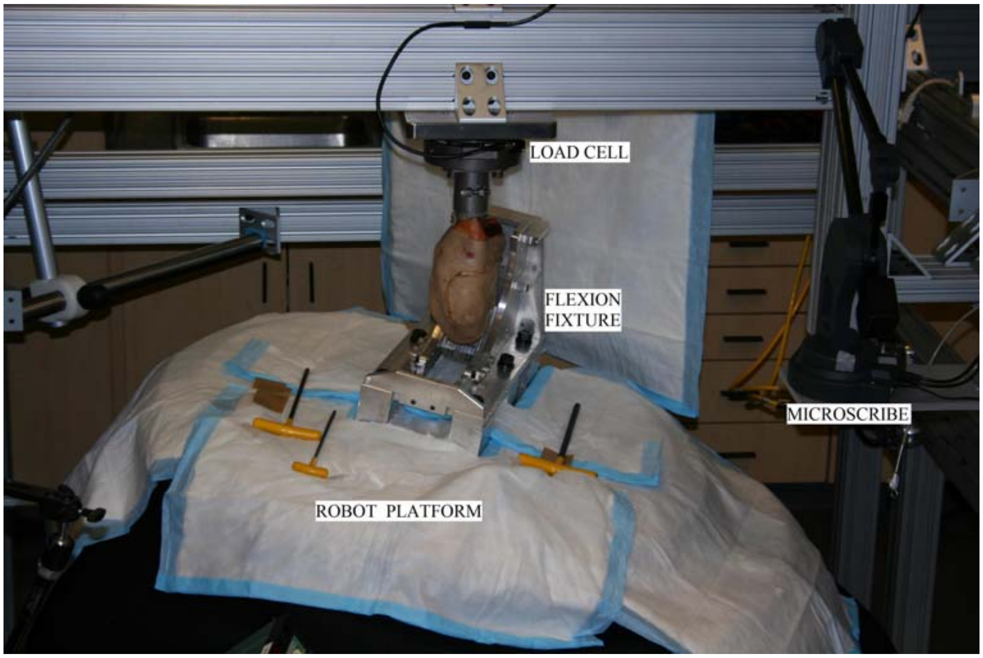

Figure 6.2: Experimental setup

an application program interface developed in the LabVIEW (National Instruments Corp., Austin, TX) by the Musculoskeletal Research and Mechanical Testing Core (MRMTC) at the Cleveland Clinic. The software interface served two purposes. First, it provided step-by-step instructions to the user to mount the specimen on the robot platform and create a Joint Coordinate System (JCS) [Grood, et al. 1983] specific to the specimen. This was achieved by using a geostationary MicroScribe G2L digitizer (Immerson Corp., San Jose., CA) mounted on a rigid metal frame which in turn was constructed around the robot. A universal force sensor (UFS) (SI-1500-240, ATI Industrial Automation, Apex, NC) was attached to this frame whereas a flexion fixture was attached to the robotic platform as shown in the Figure 6.2.

The second purpose of the interface was to operate the robot either in force or motion control mode. This was achieved using a feedback loop from the robot and the UFS. When in force control mode, the interface receives a continuous feedback from the UFS and converts it into force and moment vector in tibia coordinate system. The goal is to achieve user determined forces and/or moments in the tibia coordinate system and record corresponding joint kinematics data in the JCS. In motion control, the robot follows the user provided target positions and orientations, in each DOF, in the JCS, within stipulated time frame while recording the corresponding joint forces and moments in the tibia coordinate system.

In our experiments, we used single Differential Variable Reluctance Transducer (DVRT) (MicroStrain, Inc., Williston, VT) to register the strain data in the antero-medial bundle (AMB) of the ACL of each specimen. After confirming the ligament integrity, a pre-calibrated DVRT was mounted on the AMB of the ACL. To verify and isolate the AMB, knee specimen was flexed to 30^0 and cyclic anterior drawer force was manually applied on the tibia that induced strain on AMB making it taut [Beynnon, et al. 1995]. DVRT barbes were inserted and sutured to the AMB in such a way that the distal barb of the DVRT was about 3 to 4 mm above the tibial insertion of AMB. This was done to avoid the DVRT impingement against the femoral notch during full extension of the joint. Repeated loading tests were performed before and at the end of the data collection protocol to ensure the reproducibility of the DVRT output. During the experiments, it was noted that the DVRT output for model # 3 was not responding to the applied loads.

Thus, we would not be using the ACL strain data from model 3 for any further evaluation.

To mount the specimen on the robot, joint capsule was left intact until 7 cm on each side of the joint line and all the remaining musculature and tissue was removed. Tibia and femur of each specimen was secured in 50mm diameter aluminum cylinder, using Lipowitz's alloy and two transversely drilled screws. Tibia was mounted on the UFS and femur was mounted on the flexion fixture. Data points were collected using the MicroScribe stylus to obtain the position vectors of the UFS, flexion fixture, MicroScribe and the knee joint specimen. A knee JCS was established using this data. In this JCS, for the right knee, X-axis was pointing medially, Y-axis was pointing posteriorly and Z-axis was pointing superiorly. The origin of this coordinate system was the midpoint of two femoral epicondylar points collected using the microscribe. The JCS was defined by the flexion (X) axis in the femur and the internal rotation (Z) axis in the tibia such that

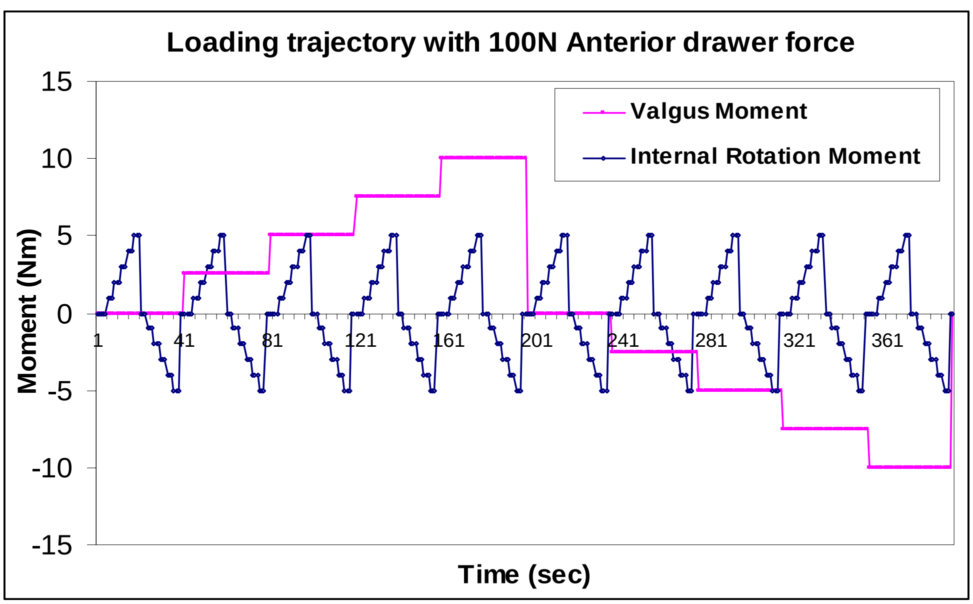

Figure 6.3: Combined loading trajectory

flexion, internal rotation, and valgus were positive angles and the floating valgus axis was perpendicular to the other two [Grood, et al. 1983].

Using this set-up and operating the robot in force control mode, two loading protocols were conducted on each joint viz. laxity loading protocol and combined loading protocol. The laxity loading protocol is explained in detail in chapter 3 and consisted of joint loading in isolated DOF. In combined loading protocol, permutations of anterior-posterior (A-P) drawer force, varus-valgus (V-V) moment and internal-external (I-E) moment were applied to the tibia while recording the corresponding joint kinematics and AMB strain data for flexion angles 0^0, 15^0, 30^0 and 45^0. Specifically, $\pm$100 N A-P drawer force was applied along with variations of $\pm$10 Nm of V-V moment in steps of 2.5 Nm and $\pm$5 Nm of I-E moment in steps of 1 Nm. The typical loading trajectory for 100 N anterior drawer force is shown in Figure 6.3. These loading conditions test the overall joint response to combined external loading conditions and represent the physiological external loads experienced by any person in their daily activities. Laxity data were used to optimize each tibio-femoral joint model as described in Chapter 5.

Finally, each optimized model was used to evaluate its kinematic response to combined loading conditions in A-P translation, V-V and I-E rotation kinematics and compared against the experimental data. We also used ACL strain data obtained from the experiments for the validation of the ACL force predicted by the model. A force-deformation relationship between the model predicted force and corresponding DVRT gauge length was plotted first. Roughly estimating the zero strain length of the strain gauge from these plots, we plotted model predicted AMB strain against experimentally measured % strain in the DVRT. A linear regression line was fitted through each scatter and using the equation of the line, an RMS error of regression was calculated for each model. We called this error as an RMS fit error for strain data which is simply a measure of how model predicted strain deviates from a linear regression line. To confirm the subject specificity of each joint model, we compared the validation error within the specimen to the validation error between the specimens. For this purpose, using one model with its optimized parameters, we calculated model response for combined loading conditions and compared it with the corresponding experimental kinematics recorded for each of the four specimens simultaneously calculating the RMS error in the kinematics and RMS fit error in the AMB strain. Paired student t-test was used to compare the validation error achieved using subject specific specimens and using single specimen.

6.3 RESULTS

Figure 6.4 illustrates the comparison between the experimental and model predicted V-V rotation data for combined loading conditions for all the five models. There are total 1056 combined loading conditions and four flexion angles in each plot. Figure 6.4-F however represents a zoom in view of the data from model 5 at 30^0 flexion and 100N anterior drawer loading conditions as indicated on the Figure 6.4-E. Model 1 seems over predictive in all flexion angles and at all loading conditions. Model 3 on the other hand is over predictive in the presence of anterior drawer load at 0^0 flexion and remains under predictive for all the remaining loading conditions.

Figure 6.5 illustrates comparison between the experimental and model predicted I-E rotation data for combined loading conditions for all the five models. Model 1 is under predictive at all flexion angles as compared to the remaining models. Figure 6.5-F represents a zoom in view of the data from model 5 at 30^0 flexion and 100N anterior drawer force.

Figure 6.6 illustrates comparison between the experimental and model predicted A-P translation kinematics for combined loading conditions for all the five models. Even though model predicted I-E kinematics was in good agreement with experiment; that was not the case with the A-P kinematics. In A-P kinematics, all the models were highly under predictive than the experiments suggesting the need to focus on this region in future optimizations. We used millimeters and degrees as the units for translations and rotations to take care of scaling. Table 6.2 identifies the RMS error obtained in I-E rotation (degree), V-V rotation (degree) and A-P translation (mm) for each model during validation. It can be noted that models 2 and 4 give lowest possible RMS error values.

Table 6.2: RMS errors observed for each model in each A-P, I-E and V-V kinematics

RMS Error in	Model 1	Model 2	Model 3	Model 4	Model 5
I-E rotation	9.2195	3.4667	4.7475	3.4438	4.7287
V-V rotation	3.2825	2.0415	3.1381	2.4022	2.0559
A-P translation	6.9883	5.7484	4.7211	5.1925	3.7707

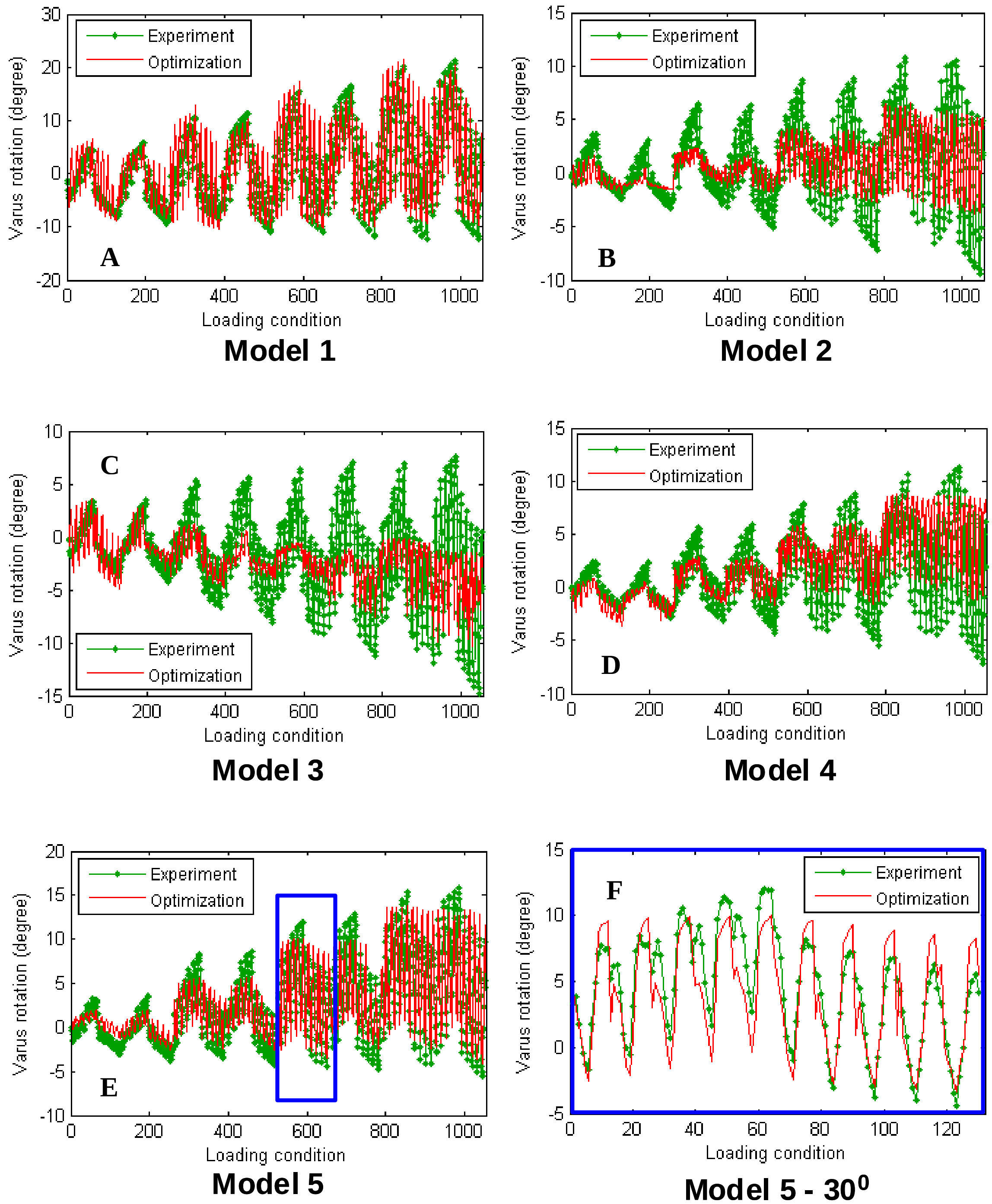

Figure 6.4: Model validations with respect to the experimental V-V kinematics. Plot F (Model 5 – 30^0) shows the zoom in view from plot E.

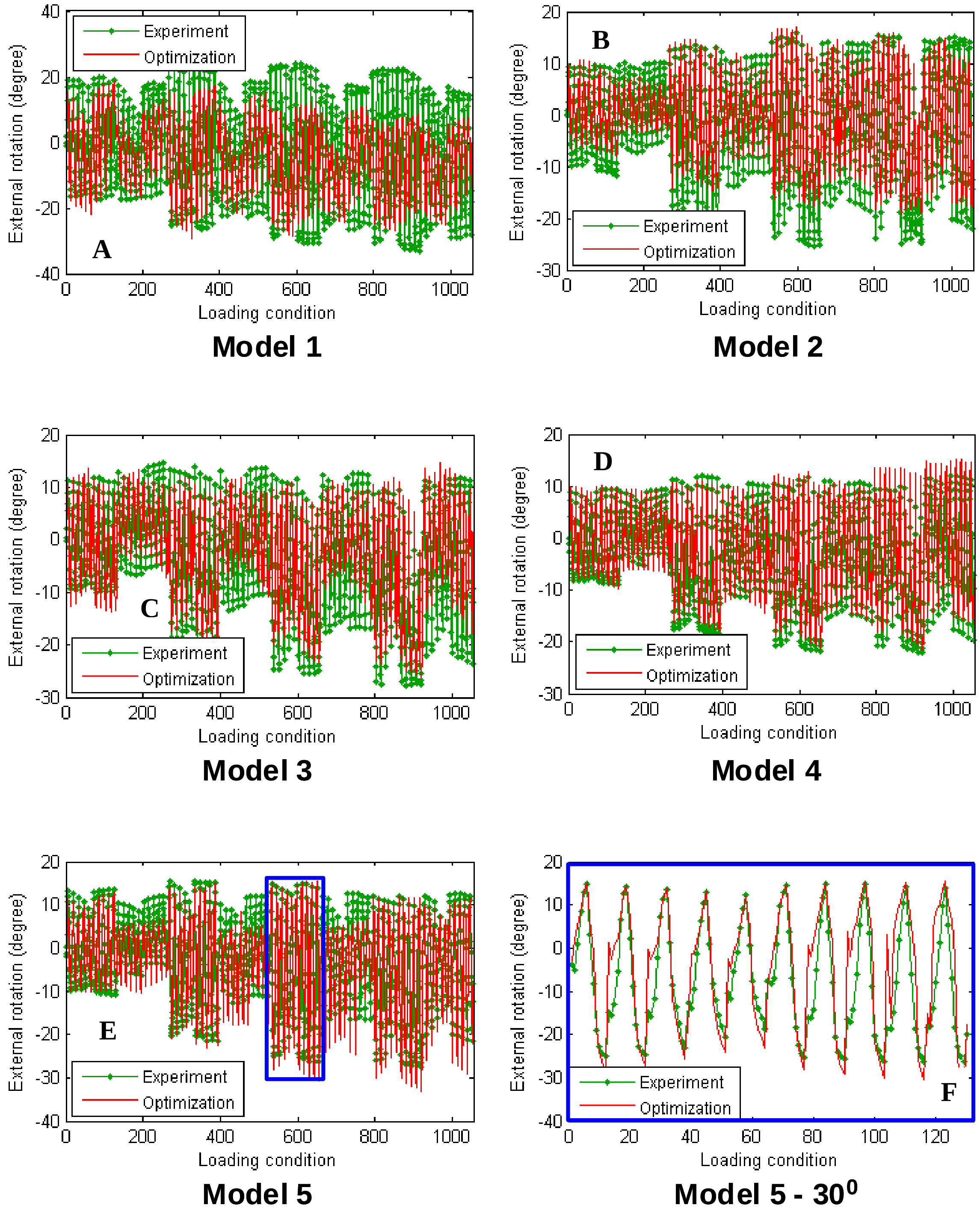

Figure 6.5: Model validations with respect to the experimental I-E kinematics. Plot F (Model 5 – 30^0) shows the zoom in view from plot E.

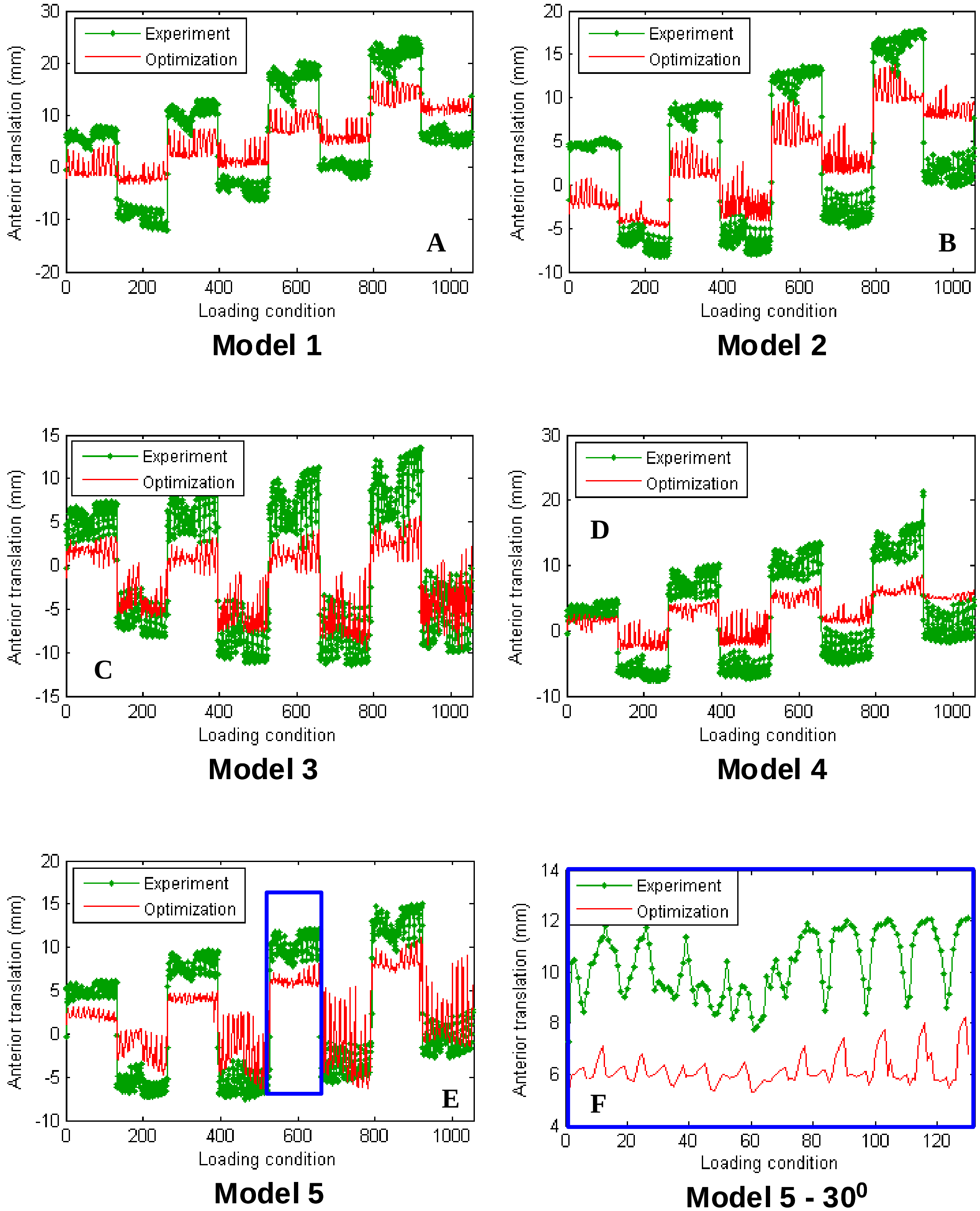

Figure 6.6: Model validations with respect to the experimental A-P kinematics. Plot F (Model 5 – 30^0) shows the zoom in view from plot E.

We conducted two more levels of optimizations using different objective functions each time. In the first level, the objective function was to minimize the difference between the A-P, I-E and V-V kinematics to the laxity loading condition considering only those situations where the kinematic parameter was the primary response to the laxity loading condition (e.g. anterior translation in response to anterior drawer force). This optimization produced different results for reference strains and insertion points. We observed that the model behavior in the secondary response parameter corresponding to the isolated loading condition (e.g. anterior translation in response to internal rotation moment) was not in agreement with the experiments. In the second level of optimizations, we selected one laxity loading and optimized the corresponding kinematic

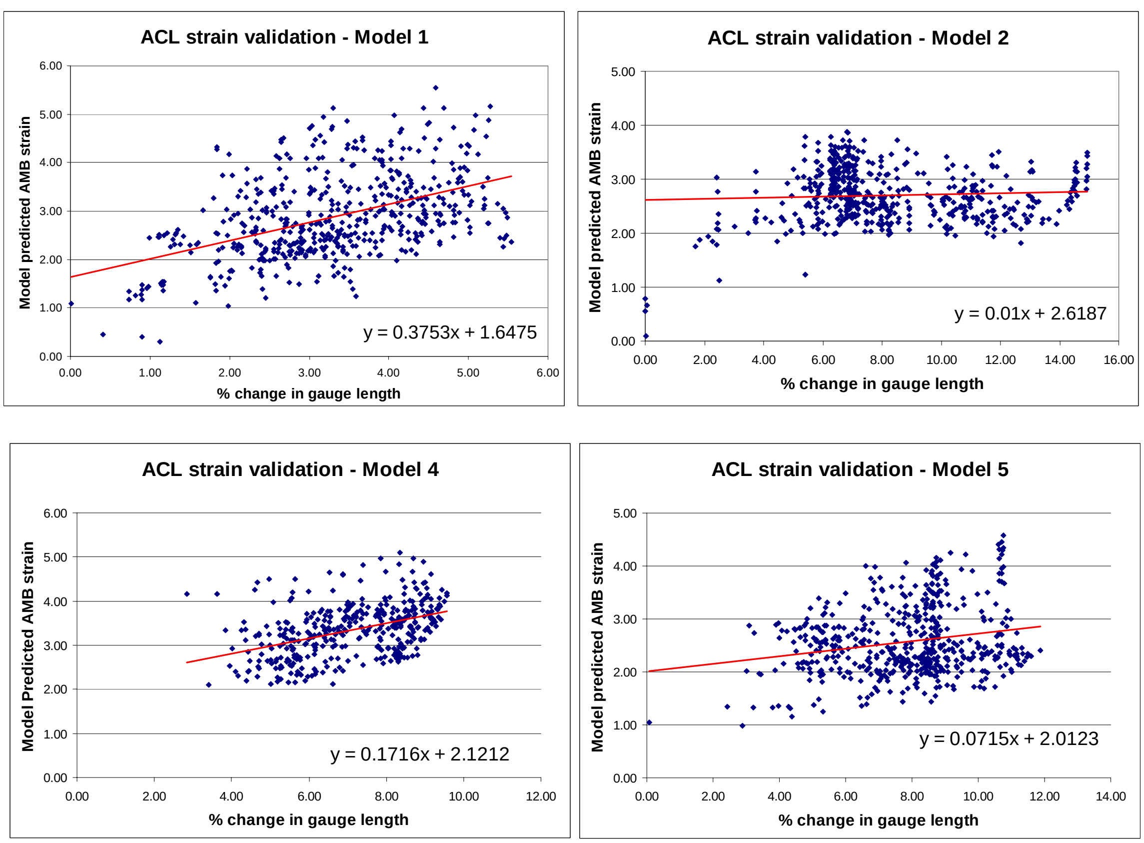

Figure 6.7: Model AMB strain validation with respect to the strain recorded by DVRT

parameter and one secondary response (e.g., internal rotation and anterior translation in response to internal rotation moment) as an objective function to minimize. This optimization provided yet another set of reference strains considerably different from the previous two.

Since the validated models would be used to simulate the ACL injuries, it was necessary to evaluate the ACL force predictions by comparing them with the ACL strain data collected on the AMB of each specimen. Figure 6.7 demonstrates the AMB strain validation plots where model predicted strain on the AMB is plotted against the estimated % change in gauge length, for all the models except model 3. We could not run the strain validation analysis on model 3 as strain data was not recorded on specimen 3 due to technical difficulties. Only those combined loading conditions that involve anterior drawer load of 100 N were considered for this validation. There are 528 loading conditions and as many data points in each plot. For the RMS fit error calculation, we used n = 528 data points from each plot. Suppose, the n pairs of dataset are given by,

$$(x_1, y_1), (x_2, y_2) \ldots (x_n, y_n),$$

and the equation of the regression line is given by,

$$y = f(x) = a\,x + b,$$

then the RMS fit error is calculated as

$$\text{RMS\_FE} = \sqrt{\frac{1}{n}\sum_{i=1}^{n}\left(y_i - f(x_i)\right)^2}$$

Table 6.3 shows an RMS fit error calculated for each of the model.

Table 6.3: RMS fit error achieved for AMB strain data prediction for each model

	Model 1	Model 2	Model 4	Model 5
RMS fit error for AMB strain	0.7722	0.4889	0.5385	0.6368

The RMS error achieved in each specimen using model 4 and comparing with specimen specific kinematic and strain data is shown in Table 6.4. A paired t-test was performed to test whether the RMS error (Table 6.2) and RMS fit error in strain data (Table 6.3) achieved using subject specific joint model were higher than the corresponding error achieved using one optimized joint model (model 4). At 95% confidence interval, the predictions using subject specific model were statistically significant ($p = 0.0195$) than the predictions using another subject's model. This confirms the statistical validation of subject specificity of the joint models.

Table 6.4: Validation error values using one model (model # 4) for all specimens

RMS error in	**Error values for model 4**				
	Specimen 1	**Specimen 2**	**Specimen 3**	**Specimen 4**	**Specimen 5**
I-E rotation	7.7366	3.7878	4.3988	3.4438	4.5344
V-V rotation	5.7069	3.1183	5.7433	2.4022	3.8429
A-P rotation	8.2967	5.9674	7.0092	5.1925	6.2284
AMB strain	0.9295	0.4889	N/A	0.5385	0.7472

6.4 DISCUSSION

Subject specific model development is important to understand the injury mechanisms or evaluate the treatment outcome. However, validating the subject specific models to experimental data becomes more important when one enters into the next era of simulation based medicine. We developed subject specific knee joint models and this study was the first attempt towards validation of the models with respect to a very large experimental data that consisted kinematic as well as strain data. Quasi-static nature of the model did not require mass and inertia properties of the bodies, or the damping properties which could not be easily obtained on subject specific basis. However, quasi-static analysis can be applied to joints in motion as long as inertial and viscous forces are negligible. Considering the low computational time required to solve for each simulation (few hundred milliseconds) as against the time consumed by comparable finite element models (few hours), using this modeling approach seemed more pertinent and pragmatic.

Blankevoort and Huiskes [Blankevoort, et al. 1996] used similar modeling approach and validated four tibio-femoral joint models. They optimized the reference strains in the model ligaments with respect to I-E rotations and A-P translations recorded for I-E moment of $\pm$3 Nm and for flexion angles ranging from full extension to 90^0. The optimized models were then submitted to the validation using the results from yet another study by Markolf and associates [Markolf, et al. 1976, Markolf, et al. 1978]. Specifically, they validated the models for A-P translations at A-P force of $\pm$100 N at 20^0 and 90^0 of flexion and for V-V rotations at V-V moment of $\pm$20 Nm at full extension and 20^0 of flexion. Flexion and I-E rotations were constrained during validations to match the model with experimental conditions of Markolf's study. Using this approach, they found good fit with Markolf's data for both A-P and V-V laxity even though huge variations were reported between each model. In another study by Li and colleagues [Li, et al. 2004], a finite element model of the tibio-femoral joint of the model was developed from MRI scans. The ligament stiffness and reference strains in the model were optimized by minimizing the difference between model predicted and experimental A-P translation from 0 to $\pm$100 N A-P load at 0^0 and 30^0 of flexion. The optimized model was then evaluated by comparing its kinematic predictions to the I-E moment of 10Nm for which the data was obtained from the literature [Kanamori, et al. 2000, Kanamori, et al. 2002, Markolf, et al. 1995].

Compared to these two studies, we optimized the ligament reference strains and insertion points with respect to A-P, I-E and V-V laxity kinematics simultaneously and at four flexion angles. Even though V-V rotations were considered as coupled motions [Blankevoort, et al. 1996], their sensitivity to the variations of the reference strains, however low it may be, can not be completely neglected. This is specifically true when optimizing the ligament reference strains based on the joint laxity data. General validation was achieved in these two studies based on the data from the literature and while doing that, subject specificity of the model was compromised. These models can not be used with confidence for predictive evaluations of tissue loads or stress in the areas where models are not validated. Our validation approach on the other hand consisted of systematic exploration of the model behavior to large experimental data set of combined loading conditions applied on the same knee specimen from which the computational model was developed. This makes the model more trustworthy in predictive mode. Validated models such as these have a huge potential in many clinical as well as research applications let alone understanding the injury mechanisms of particular tissue.

Selecting the initial reference strains or bounds on the initial values can become a tricky situation leading the optimization to a local minimum. We used two initial guesses in two of the five models and confirmed that the optimization algorithm converged to the same solution in each case, although, it might not guarantee that the global minimum was achieved. The two levels of optimizations conducted on each model gave us valuable insights in understanding model behavior as well as ligament behavior under different reference strains. Results from the level one optimization suggested that models optimized to isolated loading conditions may not be accurate in predicting the secondary responses leading to false distribution of forces and compensation mechanisms. Results from the level two optimization suggested that it was difficult to achieve combined complex behavior of the joint by using relatively simpler models where the absence of joint structures such as meniscus can not be compensated for by the structures present in the model. This was in accordance with the observations made by Blankevoort and Huiskes [Blankevoort, et al. 1996]. Optimized reference strain values for PCL indicate that some line elements of the model PCL might never be used in any loading condition and remain slack throughout the range of motion. To check this theory, we applied posterior load to the tibia that were known to recruit PCL in the real knee. As a result, all line elements of the PCL in all the models were recruited except for model 3. In this model, PMB of PCL was never recruited suggesting the redundancy in the ligament configuration within the knee model [Blankevoort, et al. 1996].

Even though we used a robust approach to develop and validate subject specific models of the knee, whether or not our models achieved sufficient validation criteria to be used in predictive situations is an entirely different issue. Looking at the validation RMS error values for each model, one might argue the feasibility of the model itself to be used as a simulation tool. The strain and kinematic predictions using subject specific model were statistically significant than with another subject's model, but the improvements were not spectacular and may not justify all the work that is needed to create a subject specific model. However, we expect with future improvements of the modeling and optimization methods that the subject specificity will become much better. There could be two types of measurement errors introduced in the data. The first error corresponded to the error due to measuring accuracy of the robotic equipment while recording the experimental data and the second error corresponded to the error introduced by the gradual increase in specimen laxity over its usage during the loading protocol. The position accuracy of the Rotopod was 50 μm (Chapter 3) indicating that it would be negligible error compared to the second error. We estimated that the average measurement errors due to laxity could be 0.85^0, 0.47^0, and 0.72 mm in the internal rotation, valgus rotation and anterior translation data respectively (Chapter 3). These values were much lower than the RMS error values observed during the optimization and validation indicating that the RMS errors were caused mainly due to modeling errors. Furthermore, the primary purpose of the models was to estimate ACL injury and not the joint kinematics. Joint kinematics was used only to drive the optimization and quantify validity. Based on the length of the ACL, 1 mm error in translational motion may cause certain % error in the corresponding ACL strain, but when simultaneous translation and rotation motions are applied, this interpretation is not straightforward. This exemplifies the need to validate the models to the ACL strain data and RMS errors reported in the kinematics validation can be regarded as a guideline.

Human knee joint represent a mechanically redundant system suggesting that the forces experienced by the ligaments can not be uniquely determined unless these structures are simplified. In an attempt to solve this system and get a unique solution, we sometimes overlook what each structure of the joint is capable of. Conducting different levels of optimizations showed us exactly how the knee joint system would behave under given circumstances. The word 'given circumstances' is important here as it determines the present state of the system. In validation evaluations of all our models, we observed under prediction of A-P translations and V-V rotations and these errors increased as the flexion angle increased. There are several reasons that can be attributed to this and other behavior. Although we used cross referencing screws to match the model coordinate system with the experiments, there was a possibility of human error when selecting the correct slice on the MRI scans while creating the coordinate system for the model. It has been previously shown that small variability in defining the coordinate system can significantly affect the joint kinematic response [Ramakrishnan, et al. 1991]. The joint model did not have meniscus modeled in its structure. This affected the ability of the model to restrain rotations at lower flexion angles and they were always over predicted by the model. The A-P translations were always under predicted. Lack of meniscus caused over prediction of ACL strains in an attempt to compensate for meniscus. This in turn caused the models to remain under predictive in anterior direction.

Ligament behavior was modeled as a piecewise function with up to 6% strain on the ligament modeled as having nonlinear (quadratic) relationship with the force and anything above 6% strain as linear. All the loads in combined loading protocol were carefully chosen in such a way that no ligament of the joint would get excessively strained. In this loading protocol, it is possible to get up to 6 or 7% strain in the ACL. This clearly indicates that almost 90% of the data points lie in the non linear region of the ligament behavior. The force-deformation plots (Figure 6.7) show a scattered data indicating that either DVRT strain gauge or joint model behaved erratically. However, when we extract the data points from this plot that correspond to internal rotation moment from 0 to 5 Nm applied along with the anterior drawer force of 100 N while keeping the

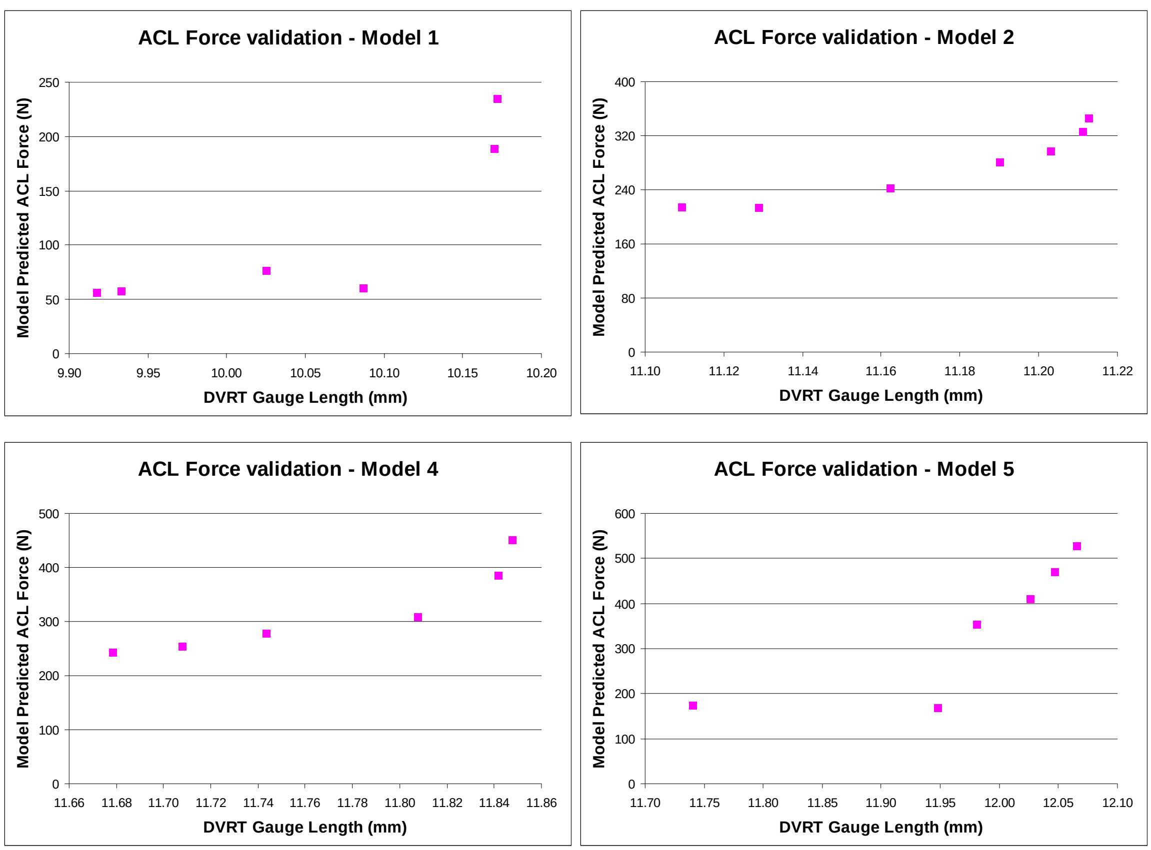

Figure 6.8: ACL force validation with respect to the isolated loading condition

V-V rotation moment constant at 0 Nm and flexion at 0^0, we get the plots shown in Figure 6.8. Each plot in Figure 6.8 illustrates typical load-elongation curve for a ligament as seen in Figure 2.5 in chapter 2. This may suggest that a validated model for isolated loading might not be valid for complex loading conditions. Earlier studies performed validations of the model using isolated loading conditions and that may not be enough to validate the model for complex loads. This highlights the importance of validation in complex loading conditions. Nevertheless, experimental strain data should be carefully collected to avoid any sources of error. DVRT is sensitive to impingement which we observed in specimen # 3. In the strain data for specimen # 3, we found that there was a DVRT impingement against the femoral notch during this data collection. Impingement causes erratic behavior of the strain gauge at full extension as per the studies conducted by Beynnon and associates [Beynnon, et al. 1995]. DVRT output could be sensitive to rotation as the rotation of the sliding cylinder of the DVRT may also cause erratic output. There is a possibility that DVRT may be on fibers that are not representative of the whole ligament loading. Although we believe that the main source of error was model error, these other errors prevent us from properly quantifying the model error with respect to predicting ACL load. Optimization of reference strains can result in varying ligament contributions at different loading conditions. For example, there is a possibility that optimization algorithm may favor the MCL recruitment over ACL causing the ACL to go slack in higher flexion angles and not restraining the coupled motions thereby over predicting the internal rotation for higher flexion angles but under predicting varus-valgus rotations.

Finally, validation is an important step in confirming the credibility of the model to use it in a predictive mode. We successfully conducted validation tests to make our models more robust to predict ACL injury mechanisms. Even though the credibility of our models can be argued in the light of errors, this study can be regarded as a first step towards developing more robust and sophisticated models for predictive purpose. The high error values found in our study can be attributed to optimization methods, lack of important joint structures such as meniscus and coordinate system mismatches. We strongly believe that validated models using this methodology can become strong contenders in future simulation based medicine programs.

CHAPTER VII

SIMULATION OF ACL INJURY MECHANISMS USING VALIDATED AND SUBJECT SPECIFIC KNEE JOINT MODELS

7.1 INTRODUCTION

Anterior Cruciate Ligament (ACL) injuries are common in any organized or recreational sports regardless of age, gender or playing level. The outbreak of ACL injuries is major concern among the college level or professional athletes from different organized sports such as soccer, basketball, team handball, volleyball, football, lacrosse, field hockey, gymnastics and softball. The ACL reconstruction surgery has a compounding impact on the athlete and the society. Early onset of osteoarthritis [Maletius, et al. 1999, Messner, et al. 1999, Lohmander, et al. 2004] and lengthy rehabilitation programs are areas of concern for the athlete whereas, higher rate of ACL injuries in female athletes [Griffin, et al. 2000] and overall surgery and rehabilitation cost surmounting 2 billion dollars are areas of concern for researchers, health professionals and government alike. Seventy percent of the ACL injuries are non-contact injuries [Boden, et al. 2000] involving ground contact and its effect on the knee during landing or cutting tasks.

ACL injury studies typically concentrate on finding the structural, biomechanical and neuromuscular risk factors involved [Griffin, et al. 2000, Uhorchak, et al. 2003, Lephart, et al. 2002, Hewett, et al. 2005, Hewett, et al. 1996, Borotikar, et al. 2008]. Using statistical design approach, these studies have identified certain key risk factors to ACL injury such as body mass index, joint laxity, femoral inter-condylar notch width, initial contact knee and hip flexion and valgus, initial contact hip internal rotation and neuromuscular fatigue. Using the key findings in these studies, there has been a subsequent development of neuromuscular training programs designed to prevent ACL injury [Mandelbaum, et al. 2005, Beynnon, et al. 2005, Hewett, et al. 2001, Hewett, et al. 2005, Myer, et al. 2004]. However, despite increases in prevention and strength training programs over past 10 years, a decreasing trend in ACL injuries and injury rates can not be identified [Agel, et al. 2007]. The presumable increase in the fitness and core strength of the athletes over the years has not made any significant impact on reducing the risk of injury. ACL injuries are still growing in epidemic proportions indicating that these studies are missing key factors in addressing the ACL injury problem. One such key factor lies in understanding the actual ACL injury mechanisms and its correlation to the external knee joint loads experienced by the athlete.

Current ACL injury studies involving cadaveric specimens [DeMorat, et al. 2004, Hashemi, et al. 2007, Meyer, et al. 2008] focus only on specific joint loading conditions known to injure ACL, leaving out the other loading conditions that may put hazardous strains on the ACL. Evidently, cadaveric experiments to study ACL injury mechanisms are not feasible since ACL failure can only be studied once in each specimen. To date there are no computational modeling attempts to understand ACL injury mechanisms and analyze the effect of subject variability on the injury mechanisms. The need for developing robust computational models that can evolve as a tool for studying the underlying mechanisms of injury has already been discussed previously [Borotikar, et al. 2008, van den Bogert, et al. 2007]. Large variability in anatomical shapes of knee structures [Biscevic, et al. 2005], anthropometric data, and tissue mechanical properties [Woo, et al. 1991] between individuals restricts the use of the generic models and calls for incorporating subject specificity in each model with regards to these factors while evaluating injury mechanisms.

Owing to above facts, the aim of this study was to analyze different ACL injury mechanisms using quasi-static, multi-body 3D tibio-femoral knee joint models. We have developed subject specific models (Chapter 4) to represent tibio-femoral knee joint of five cadaveric specimens. Using novel optimization approaches (Chapter 5), we have determined subject specific reference strains of model ligaments that minimized the error between model behavior and experimental data collected during joint laxity tests. The optimized models have been validated evaluating the kinematic behavior and the ACL load predictions of the models to the corresponding large data set of combined external loading conditions on each cadaveric specimen (Chapter 6). In this study, the validated models were used to simulate and study different injury mechanisms.

7.2 MATERIALS AND METHODS

The development, optimization and validation of the computational joint models have been discussed in detail in previous Chapters. The methods are briefly explained here. Mechanical testing was performed on five cadaveric knee specimens using a state-of-the art six degrees of freedom (DOF) motion platform (R2000, Parallel Robotic Systems Corp., Hampton, NH) and an in-house developed software interface in LabVIEW (National Instruments Corp., Austin, TX). Tibio-femoral rotation and translation were measured in each specimen at four flexion angles (0^0, 15^0, 30^0, and 45^0) during application of two sets of external loading protocols. The first set comprised of joint laxity loading with isolated loads on anterior-posterior (A-P), internal-external (I-E), and varus-valgus (V-V) axis of the joint. The second set consisted of combined loads in the above three axes keeping the flexion axis constrained. A Differential Variable Reluctance Transducer (DVRT) strain gauge (Microstrain, Burlington, VT) was mounted on the antero-medial bundle (AMB) of the ACL in each specimen and strain data was recorded during each loading condition of the two loading sets.

Each specimen was imaged using sagittal plane MRI scans (OrthOne 1.0T scanner, ONI medical systems, Wilmington, MA). Computational tibio-femoral knee joint models were generated using the modeling techniques and parameters described in Chapter 4. The model was implemented using existing software for 3D quasi-static joint modeling [Kwak, et al. 2000]. Each joint model represented total 12 line elements for four ligaments (2 cruciates and 2 collaterals), deformable articular contact and wrapping of the medial collateral ligament around the medial tibial bony edge. The optimization goal was to find reference strains of 12 ligament line elements and insertion points of these line elements that minimized the difference between the simulated and measured tibio-femoral kinematics for joint laxity loading conditions as described in Chapter 5. The joint model software [Kwak, et al. 2000] was accessed via the MATLAB MEX-function interface (Mathworks Inc., Natick, MA) to provide the force imbalance (*GF*) of the bodies as an output for the applied external loading condition and initial rigid body positions as an input. Different RMS error values were achieved for each model as the result of optimization and are shown in Table 7.1.

Table 7.1: RMS error values achieved in optimization in degree and mm

	Model 1	**Model 2**	**Model 3**	**Model 4**	**Model 5**
RMS Error	4.00	2.97	2.96	2.59	2.58

Based on the RMS error values, it could be determined that models 4 and 5 were more accurate than models 2 and 3 and model 1 was worst with combined RMS error of 4.00 (degree and mm).

Each optimized model was then evaluated for 1056 combined loading conditions as detailed in Chapter 6. These loading conditions were representative of forces and moments experienced by the knee joint during sports activities. Specifically, joint kinematics (A-P translation, V-V and I-E rotation) and ACL force data predicted by each model was compared against the corresponding experimental data for each combined loading condition. Table 7.2 shows RMS error values observed in predicting A-P translations, V-V rotations and I-E rotations by each model. Validation confirmed the credibility of each model to use it in injury simulations.

Table 7.2: RMS errors observed for each model in each A-P, I-E and V-V kinematics

	Model 1	**Model 2**	**Model 3**	**Model 4**	**Model 5**
I-E rotation	9.2195	3.4667	4.7475	3.4438	4.7287
V-V rotation	3.2825	2.0415	3.1381	2.4022	2.0559
A-P translation	6.9883	5.7484	4.7211	5.1925	3.7707

To understand the injury mechanisms, each validated model was simulated with a large set of combined loading conditions applied to four axes of the joint while keeping the flexion angle constrained. To apply the simulation loads, a factorial design approach including five factors was used in which four factors were represented by loads in four axes of the joint and the fifth factor was flexion angle. The four factors consisted of anterior drawer force, joint compression force, I-E rotation moment and V-V rotation moment. All the loads applied are reported here with respect to tibia. Each factor was further evaluated at different levels. Anterior drawer force had 6 levels with force ranging from 0 to 320 N, joint compressive force had 3 levels with force ranging from 0 to 1500 N, I-E rotation moment had 17 levels with rotation moment ranging from 0 to $\pm$40 Nm, V-V rotation moment had 9 levels with rotation moment ranging from 0 to $\pm$ 160 Nm and flexion factor had 2 levels with flexion angle set to 0^0 or 30^0. The force and moment ranges in each of the I-E and V-V rotation moment factors were selected in such a way that extreme values in each level caused injuries to the ACL when applied as isolated loading conditions [Seering, et al. 1980, Meyer, et al. 2008]. The factorial design generated 5508 loading combinations systematically exploring the combination of high combined loading conditions that typically occur in any sports movement like stop jump or side step cutting maneuver. Figure 7.1 shows the 3D space mapped by simulations at each flexion angle and at each level of compression. We called it the region of interest.

For each simulation, ACL force predicted by the joint model was recorded and an injury threshold was set. Woo and associates [Woo, et al. 1991] reported that a young cadaveric ACL (age 22 to 35 years) can withhold up to 2160 (±157) N tensile force before failure. Considering these values from the literature, each model was evaluated at a threshold value of 2000 N.

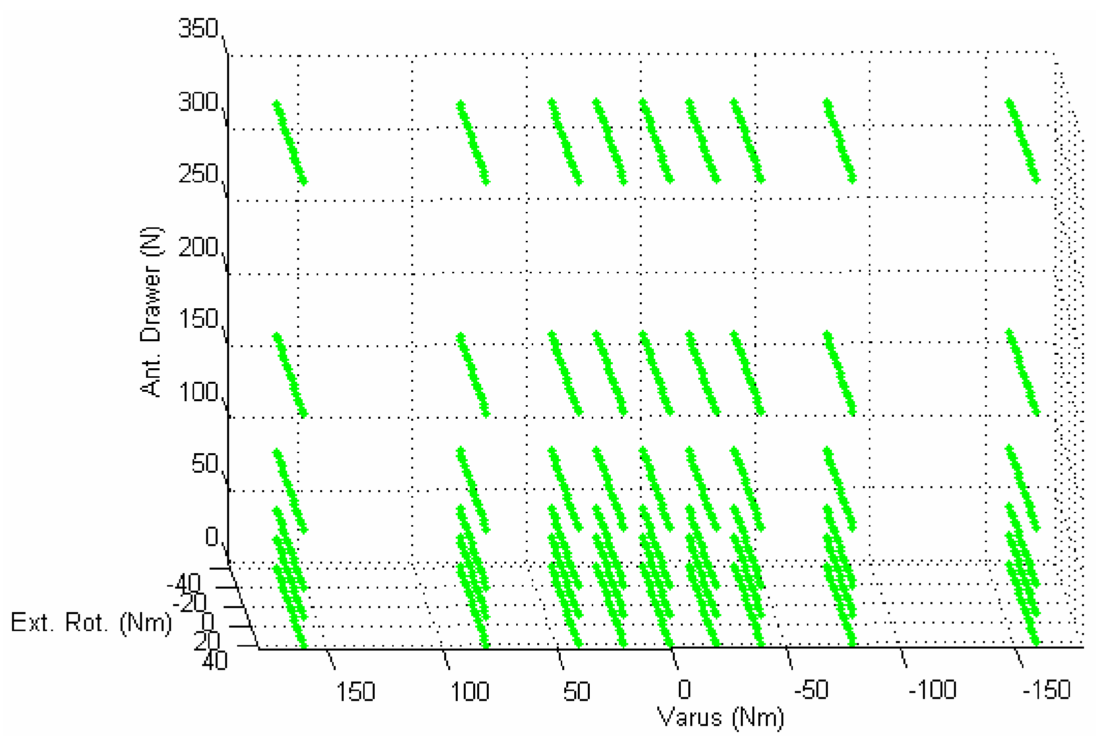

Figure 7.1: Simulation loading conditions used on each knee joint model

7.3 RESULTS

Injury simulations for each model were explained using four different scenarios covering two flexion angles and two levels of compressive forces in each flexion angle. Figure 7.2 illustrates 4 plots explaining injury simulations in each of the four scenarios for model 1. The green colored points represent the loading conditions simulated by the model and the red colored points represent the loading conditions in which model predicted loads were higher than the threshold of 2000 N. There were less injury loads in the region of interest when compression load was applied as compared to no compression plots in both 0^0 and 30^0 flexion angles. Figures 7.3, 7.4, 7.5 and 7.6 illustrate injury loads predicted in the region of interest by joint models 2, 3, 4 and 5 respectively. Contrary to the model 1 predictions, these models predicted more injury loads in the region of interest when compression load was applied.

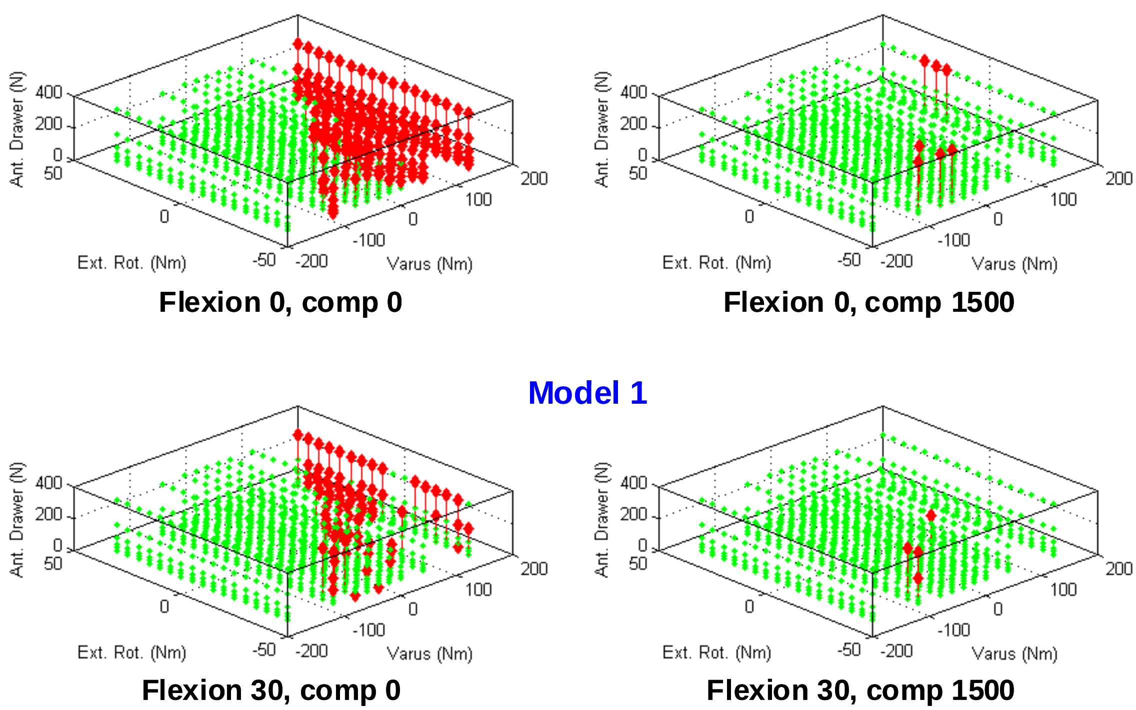

Figure 7.2: Injury loads as predicted by model 1

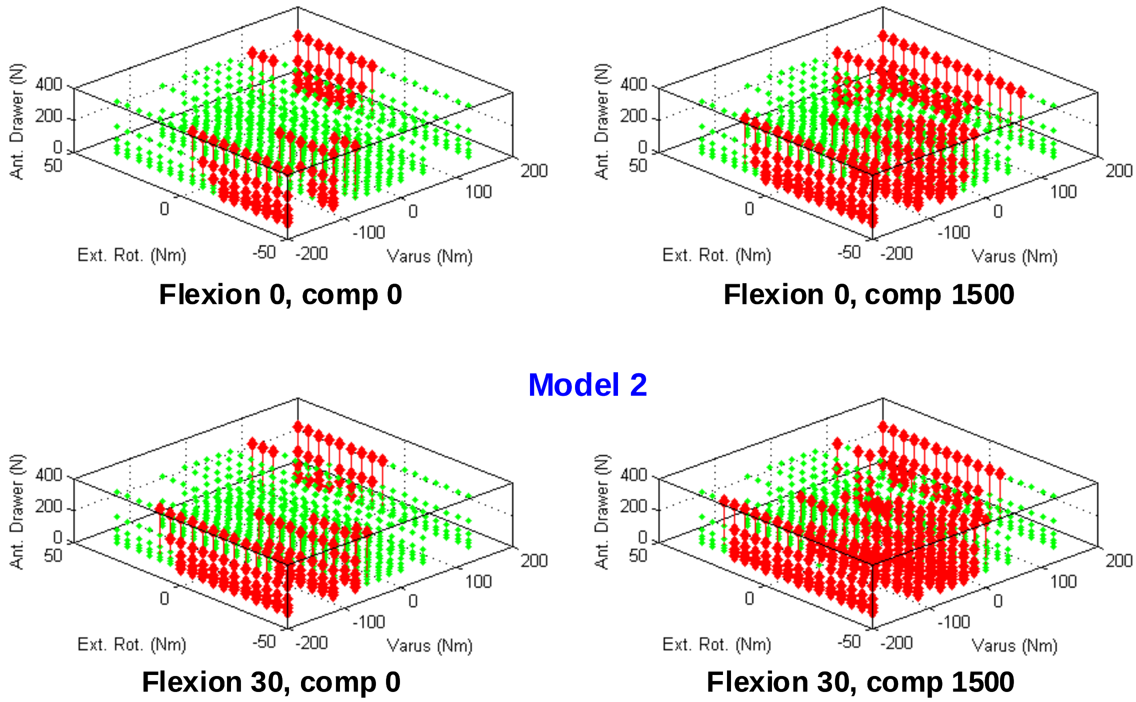

Figure 7.3: Injury loads as predicted by model 2

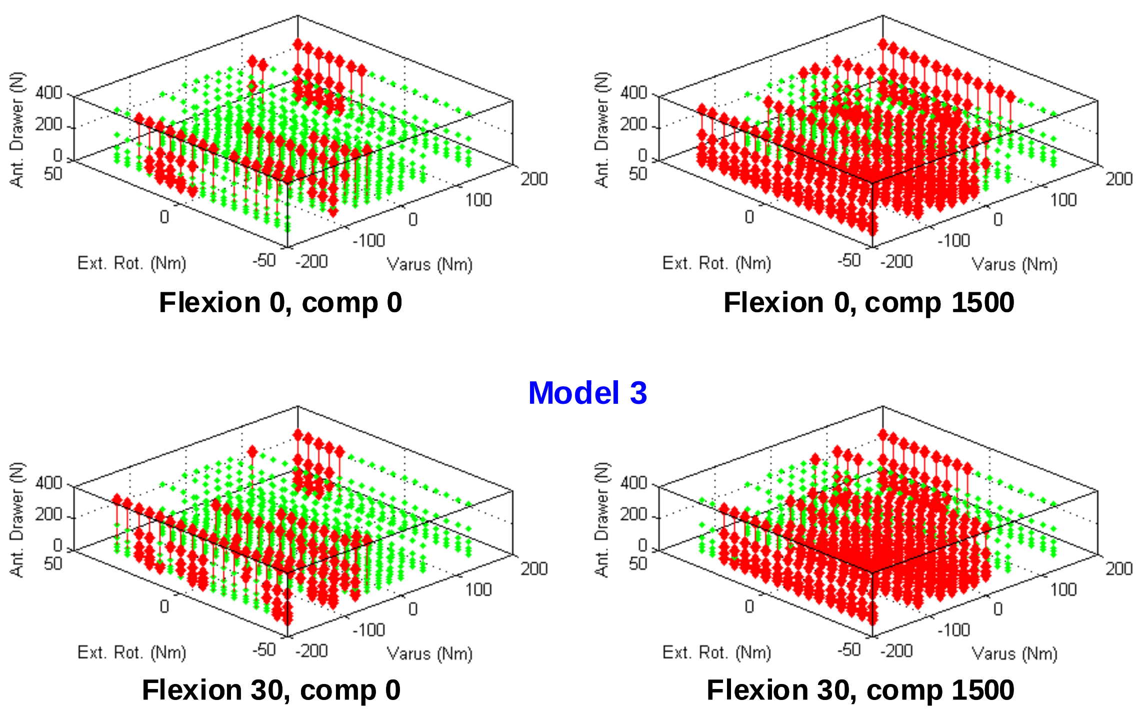

Figure 7.4: Injury loads as predicted by model 3

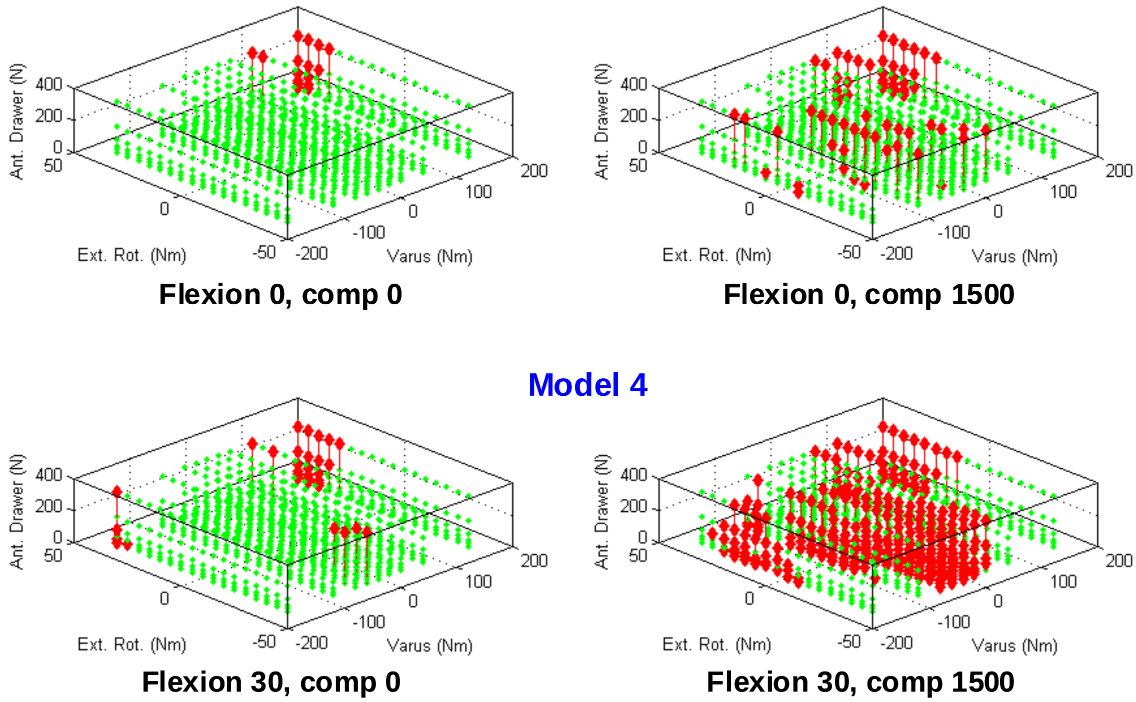

Figure 7.5: Injury loads as predicted by model 4

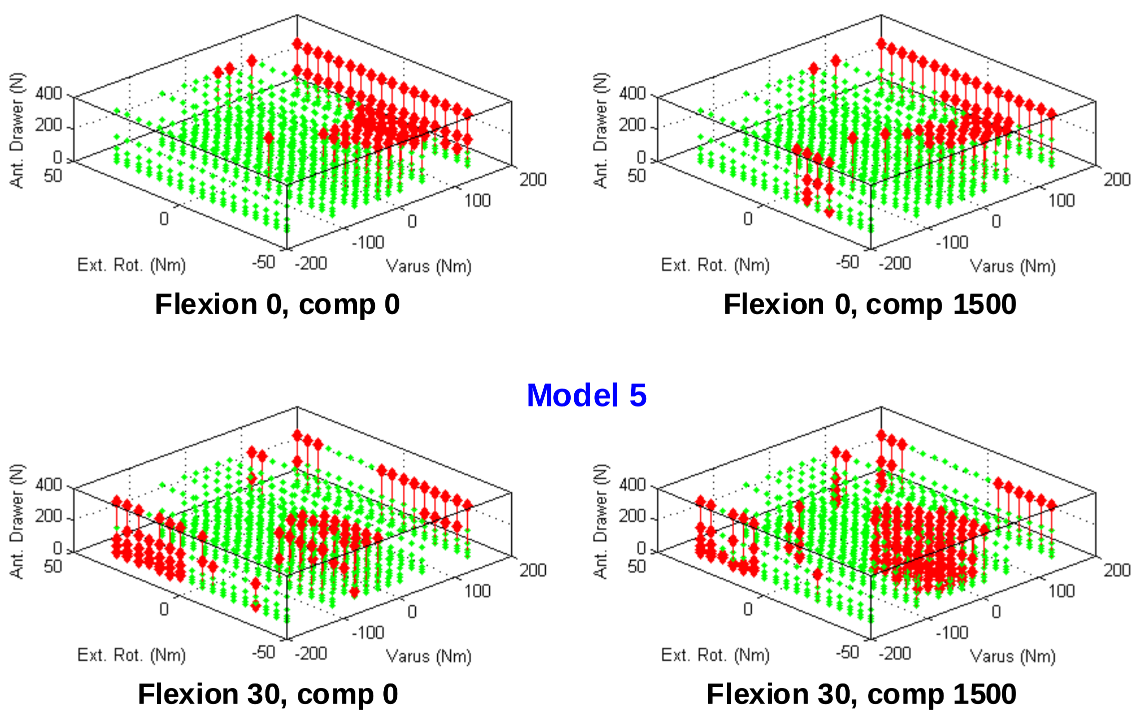

Figure 7.6: Injury loads as predicted by model 5

7.1 DISCUSSION

This study demonstrated the application of computational joint models to evaluate mechanisms of the ACL injury on individual basis. Validated computational models were used as tools to evaluate the injury mechanisms at the functional load levels. As illustrated in the results, ACL injury loads varied based on the subject specific model behavior. This study demonstrated the unique advantage of computational models over cadaveric studies. Each red colored point in each of the plots represented an injury. If we had to use cadaveric specimens, we would have needed as many of them as each specimen could be injured only once. The injury pattern itself in each region of interest was very non-linear indicating the non-linear behavior of the knee joint itself.

Previous studies used different techniques to predict external loads experienced by the knee joint. Inverse dynamics approach was used by many researchers [Erdemir, et al. 2007, Winter. 2005] to calculate the joint forces and moments from joint kinematic data and ground reaction forces. Lloyd and Besier [Lloyd, et al. 2003] used EMG driven inverse dynamic muscle models to predict joint moments and muscle forces and these models were further evaluated by Buchanan and associates [Buchanan, et al. 2005]. Forward dynamic musculoskeletal models were developed and validated by McLean and associates [McLean, et al. 2003] to estimate the resultant knee joint forces and moments and were further used to evaluate ACL injuries during simulated side-step cutting movements [McLean, et al. 2004]. Thelen and Anderson [Thelen, et al. 2006] used computed muscle control and forward dynamic musculoskeletal models to simulate human walking. All the above studies predicted the resultant knee joint forces in their respective simulations and acknowledged the need for analyzing the distribution of these forces within the knee joint structures (cartilage and ligaments). Our modeling and simulation techniques act as complementary tools that provide the distribution of the external resultant forces within the knee joint structures for a wide range of isolated or combined loads. To our knowledge, this is the first attempt to understand the ACL injury mechanisms using experimentally validated, physics based model and simulating the model for wide range of loading conditions.

Model 1 was the only model developed from a female knee joint specimen. The injury loads predicted by model 1 were different than the remaining models that represented male knee joints. There are differences in anatomical shapes [Biscevic, et al. 2005] and structural properties [Chandrashekar, et al. 2006] between male and female knees. Even though subject specific morphological differences may seem to have impact on mechanical response in male and female models, it could not be regarded as a risk factor based on this study. The number of specimens (n = 5) used in this study was too small to show correlations with the anatomy. With more number of specimens, it would be possible to find such relationship and this would be of great clinical value as morphology alone (without the entire modeling procedure) would already give potential injury risk information. Nevertheless, model 1 predicted higher ACL injuries in absence of compression and this phenomenon was entirely different in other male models. Although there was a potential for experimental error in this study, model 1 gave insights to the female ACL injury mechanisms. For 0^0 flexion and no compression, model predicted injury loads were concentrated in the area where combined loading of varus moment and internal rotation moment was applied on the tibia. When compression was applied, there were fewer injury loads in the region of interest as if the compression load worked towards stabilizing the knee. Similar observations were made at 30^0 flexion and with or with no compression. In the absence of compressive forces, injury causing ACL loads were predicted with the combination of low internal rotation moments and low valgus moments, a situation commonly observed in step-cutting or pivoting maneuvers in sports. Model predictions under compression may have been affected by the lack of meniscus. While presence of meniscus would stabilize the knee joint at high compressions, its absence may over predict the ACL force in the scenarios where anterior drawer and compressive loads were applied on the tibia.

For the remaining models however, model predicted injury loads were split into two locations within the region of interest. These locations comprised of combination of valgus and internal rotation moment or varus and external rotation moment and could be clearly identified in 'no compression' plots of each model. Also, when the compression was applied, unlike model 1, injury loads were increased within the region of interest. The minimum combined loads required to predict the ACL injury for model 2 were 40 Nm valgus moment, 30 Nm internal rotation moment and 320 N anterior drawer force. Similar injury loads were observed in models 3, 4 and 5. These predictions were in congruence with the observations made by other researchers in their studies focusing on ACL injuries [Boden, et al. 2000, Meyer, et al. 2008, Bahr, et al. 2005]. Models 2, 3, 4 and 5 also predicted that injuries happen when combination of varus moment (as low as 80 Nm for model 2), external rotation moment (as low as 30 Nm for model 2) and anterior drawer force (320 N for model 2) was applied. Combined loads such as these are commonly observed in various sports involving drop landing or sudden cutting tasks. External rotation moment is caused by planting the foot in one direction and turning the upper body in the other direction. Compression on the other hand is caused by landing and/or quadriceps muscle contraction. Valgus moment is caused during side stepping while planting the foot on one side and cutting on the other. These sports movements tend to produce high knee joint loading that in turn induce high ACL forces. A combined internal rotation moment of 50 Nm, valgus moment of 160 Nm and anterior drawer force of 320 N for example, induces high strains in the ACL as confirmed by many studies [Meyer, et al. 2008, Seering, et al. 1980, Markolf, et al. 1995].

These injury loads leave a space of green colored data points in the middle region of each plot which can be regarded as a safe zone for each knee joint and the boundaries of this safe zone are narrow or wide depending on each individual's knee structure and tissue properties. This can be very easily demonstrated in each of the models 2, 3, 4 and 5 where this safe zone varies as the subject specificity of the joint model varies. In this study, we reported the load combinations that cause the model ACL force above 2000 N. However, Chandrashekar and colleagues found that [Chandrashekar, et al. 2006] female cadaveric ACL (average age 37 years) can withhold only up to 1266 N tensile force. This considerably narrows the safe zone for female athletes making them more vulnerable to ACL injuries. This also limited the capability of our models to predict injury in specific situation as the failure properties of each ligament were not known a priori. In future studies, non-invasive and non-destructive tests can be employed to estimate the failure properties although they may not be feasible in each scenario. Our models, however, can be effectively used to understand which regions of the loading space can be of high risk for this subject and avoiding these regions via neuromuscular training.

Earlier studies found that compression loads (weight bearing) stabilize the knee joint reducing the risk of injury. However, models 2, 3, 4 and 5 predicted that knee joint was more susceptible to ACL injury in the presence of compressive forces. We speculate that in the presence of combined loads such as anterior drawer force or internal rotation moment on tibia, the femoral condyle would be translated and rotated to in the posterior region of the medial and lateral plateaus of the tibia. The posteriorly oriented slope of the tibia adds to the forward translation of the tibia when compressive force is applied and the only restraint is offered from the ACL. A higher strain causes the ACL to rupture.

Even though we used near injury loads for V-V and I-E rotation moment, lower A-P drawer forces (320 N) were used in our simulations. This was done to ensure the convergence of the model for each simulation. Anterior drawer loads as high as 1500 N along with other combined loads caused the model femur to subluxate from the tibial plateau introducing convergence problems. We selected 320 N to restrict the number of simulations in each model as increase in one level of loads could have increased the number of simulations by 1000. Meniscus was not modeled in our joint models and this could have caused over estimation of ligament forces as the modeled structures compensated for the function of meniscus in its absence, specifically when the anterior drawer force or compressive force was applied to tibia. The viscoelastic properties of the ligaments were not modeled limiting the ligament behavior purely elastic. We evaluated the models to analyze complete ACL ruptures. Some loading scenarios in the simulations may cause partial rupture of the ACL bundles; however, no data is available on failure loads in individual ACL bundles and thus it is not included in this study. We can estimate the failure load of one bundle as $1/3^{rd}$ of total ligament failure load and analyze the injury loads. This should be done in future studies as it will give specific insights in ACL injury mechanisms.

Despite these limitations, the joint model lends insights to the ACL injury mechanisms and future studies should be focused on building more complex models eliminating the limitations observed in this study. Understanding the ACL injury mechanisms on individual basis gives a unique opportunity to study the injury patterns and develop individual prevention strategies. The techniques used in this study can be employed in a clinical study to determine the risk of ACL injury to the live human beings.

CHAPTER VIII

SUMMARY

8.1 BRIEF SUMMARY OF THE STUDY

The knee joint is a complex joint involving multiple interactions between cartilage, bone, muscles, ligaments, tendons and neural control. The Anterior Cruciate Ligament (ACL) is one ligament in the knee joint that frequently ruptures during various sports or recreational activities. Obviously, ACL is subjected to hazardous loads during these activities. Understanding these injury loads a priori to the development of injury prevention programs is required to implement subject specific strategies as well as to generate large dataset of knowledge based injury causing loads. Computational modeling is an effective tool to analyze such clinical problems. Researchers use different modeling domains based on the clinical problem under study and the end use of the model. To understand the ACL injury mechanisms, we used a quasi-static, multi-body modeling approach and developed MRI based tibio-femoral knee joint models. Each model was subsequently optimized and validated using experimental data and injury simulations were performed using factorial design approach comprising of multiple factors and levels to replicate a large and rich set of loading states. These loading states represented sports-like loading on the knee joint. The injury simulations confirmed many known injury loads and unveiled many unknown scenarios as well. This thesis is an extensive work covering all the details of the ACL injury project explained above and highlighting the importance of 1) computational modeling in injury biomechanics, 2) incorporating subject specificity in the models, and 3) validating the models to establish credibility.

The aim of this study was twofold. The first part was focused on developing and experimentally validating the tibio-femoral knee joint models and the second part was focused on simulating the ACL injuries using sports-like loading scenarios. Five cadaveric specimens were used for this study. Experiments were performed using state-of-the-art robot technology. The joint laxity kinematic data was used to optimize model specific ligament resting lengths and ligament insertions thus generating subject specific models. A large-scale optimization approach was evaluated for the first time in the area of joint mechanics studies. Even though this approach was not used for further optimizations due to time constraints, future work should be focused on developing cost effective optimization algorithms using this approach. For the conventional small scale optimization approach, optimization fit was within RMS error of 4 units (mm or degree) and as low as 2.6 units (mm or degree), although the global convergence of optimization was not confirmed. In general, optimization fit was good when the kinematic parameter was the primary response to the isolated laxity loading condition. Future work should be devoted to employing customized optimization strategies such as penalty functions or weight factors to make the optimization more robust and to reduce RMS errors further. Experimental validation was accomplished by using the optimized parameters in each model and evaluating the model against the experimental data generated using combination of loading states. The experimental data comprised of knee kinematics and ACL strain for combined loading states. Although there was a relatively high RMS error observed in our validation studies, model behavior was in good agreement with experimental data for combined loads and with further developments in optimizations in future, we strive for better results. Subject specificity of each model was also evaluated and found in qualitative agreement as the validation error within specimen was smaller than the variation between specimens for each model.

The injury simulation studies focused on analyzing the mechanisms rather than the injury predictions, thus studying the relative injury risk over absolute risk. Injury simulations using the validated models revealed many interesting facts. Generally, compressive load on the knee joint help stabilize it but in our simulations, four out of five models predicted that compression loads in combination with the loads in other axes of the joint increase the risk of injury by almost twofold. The only female model developed in this study predicted that injuries the ACL was vulnerable to high injury-like loads when there was no compressive force acting on the tibia. This may suggest a difference in injury mechanisms than male knee, but the validity of this behavior should be confirmed using a larger number of male and female specimens. Simulations also predicted that any knee joint operates safely within a specific safe zone and crossing that zone in certain direction would cause ACL injury. The extent of this safe zone appears to depend highly on subject specific structural and mechanical properties of the joint.

8.2 LIMITATIONS

While developing subject specific knee joint models and validating them, this study battled limitations on various fronts. On the modeling front, the viscoelastic nature of the ligaments and cartilage was not modeled and this may have caused certain error in optimizations. Even though we observed good repeatability between pre and post joint loading protocols, increase in the joint laxity over time may have induced a systematic error in the experimental data. The meniscus was not included in the joint model and this caused two problems. First, this required other structures in the model to compensate for its absence, suggesting that ligament forces may be over predicted. Second, in high loading conditions, we sometimes observed that the model femur subluxated from the tibial plateau causing difficulties in convergence and making the model unstable in certain simulation loading conditions. On the experimental front, there was a coordinate system mismatch between the model and the experimental data causing difficulties in optimizations, especially in optimizing the coupled motions for primary loading conditions.

Limitations in this study should also be looked at from its use in clinical applications and how the methods used in this study affect its use in our long term vision. Generally, sports injuries take place at high speeds. During these events, the ACL is subjected to higher loading rates and it is thought that high loading rates are responsible for ACL ruptures. Our model predictions could be accurate enough in situations where the inertial and viscous effects on these structures are negligible. While joint friction can be assumed negligible, it might not be the case in these high loading rate scenarios. Future models should at least incorporate viscoelastic properties of ligaments to eliminate this limitation. Joint laxity changes pre and post exercise due to relaxation property of the ligaments and post exercise laxity is always higher than pre-exercise laxity. This may lead to changes in neuromuscular strategies by changing the muscle activations and muscle forces. As each subject specific model would be optimized only once before exercise, it may not accurately predict the force distribution in the ligaments. This error, if not completely eliminated, can be reduced by recording laxity data at two time points – one pre and one post exercise and using the average laxity data to optimize the model. In the current study, each model is developed using manually digitized points from MRI scans. This study did not take into consideration the repeatability and reproducibility of this process, which may affect the model behavior. In future studies, effects of repeatability and reproducibility should be quantified before implementing these techniques in clinical settings.

8.3 FUTURE STUDIES

More complex models should be developed to eliminate some of the limitations observed in this study. Models should include meniscus and represent the patello-femoral joint as well. To represent the passive knee as tested experimentally, the patello-femoral joint was not included in the models. Dynamic sports movements involve high quadriceps forces delivered to the femur through patello-femoral contact and patella tendon attachment on the tibia. At this point, our models have the capability to include these as external forces, but not their subject specific point of application and orientation. Future studies should incorporate the whole tibio-patello-femoral knee joint to overcome this limitation. The meniscus plays important role in constraining the translations and rotations of the femur along the tibial plateau and help reduce the forces on the ligaments. To understand the injury causing loading combinations, it is important to incorporate meniscus in future studies. Meniscus can be modeled as spring elements attached along the edge of the tibia having different stiffness properties that represent meniscal behavior. The stiffness parameters can be derived using optimization procedures.

To eliminate the coordinate system mismatch observed in this study, three markers should be attached to each specimen that can be cross-referenced both in the experiments as well as in the MRI scans. Future studies should also incorporate enough number of specimens from both male and female population to understand and analyze the differences due to anatomy.

8.4 CLINICAL APPLICATIONS

Non-invasive methods to understand human knee joint biomechanics can have a major impact on evaluating pre-surgical healthcare and developing protocols to prevent injuries. As discussed in Chapter 1, strategies to understand external knee joint loading during sports activities have already been developed by other researchers. What they lack is the understanding of how this external loading affects the internal distribution of forces and injury risk on a subject specific basis. This study exactly answers these two questions.

We have demonstrated the technical capability to perform subject specific analysis on the knee joint, although the validity of the injury predictions may not be good enough yet for clinical applications. The proposed approach in this study has a potential to be used in larger studies involving live human population. In the long term, the techniques used in this study could be easily extracted to conduct clinical studies on live human subjects. However, cautious design of the clinical study is warranted. To employ computational modeling in clinical setting, the models must be cost effective, user friendly and most importantly thoroughly validated to have confidence in their predictions. Even though gender specific injury risk was not specifically studied in this study, it can be easily incorporated in future studies.

Nevertheless, the use of this technique in the long term vision of the ACL injury prevention is presented here. In a clinical setting, data must be collected on each subject. Each subject will undergo an MRI test to collect the morphological data of the knee joint to develop joint models. Joint laxity data will be collected using a laxity measurement equipment similar to the one developed by Un and associates [Un, et al. 2001] at the University of Vermont. Using the laxity tests, joint models will be optimized to obtain model parameters that are subject specific. Simultaneous motion analysis and ground reaction force data will be collected on each subject while performing certain jumping or cutting tasks. An inverse dynamic musculoskeletal model will be developed as discussed in Erdemir and associates [Erdemir, et al., 2007]. This model will give external forces and moments acting on the knee joint at each sampled time stamp during the stance phase of the cutting or jumping task. For each time stamp, the optimized joint model will predict the distribution of these forces to the internal structures of the joint and ultimately report ACL force as an output. Depending on the subject specific model's ACL force response, it can be determined whether certain activities are leading to higher ACL force. Based on these findings, a subject specific neuromuscular training strategy can be developed.

REFERENCES

Agel, J., Olson, D. E., Dick, R., Arendt, E. A., Marshall, S. W., & Sikka, R. S. (2007). Descriptive epidemiology of collegiate women's basketball injuries: National Collegiate Athletic Association Injury Surveillance System, 1988-1989 through 2003-2004. *Journal of athletic training,* 42(2), 202-210.

Ahmed, A. M., Burke, D. L., Duncan, N. A., & Chan, K. H. (1992). Ligament tension pattern in the flexed knee in combined passive anterior translation and axial rotation. *Journal of orthopaedic research : official publication of the Orthopaedic Research Society,* 10(6), 854-867.

Ahmed, A. M., Hyder, A., Burke, D. L., & Chan, K. H. (1987). In-vitro ligament tension pattern in the flexed knee in passive loading. *Journal of orthopaedic research : official publication of the Orthopaedic Research Society,* 5(2), 217-230.

Amis, A. A., & Dawkins, G. P. (1991). Functional anatomy of the anterior cruciate ligament. Fibre bundle actions related to ligament replacements and injuries. *The Journal of bone and joint surgery.British volume,* 73(2), 260-267.

Anderson, F. C., & Pandy, M. G. (1999). A Dynamic Optimization Solution for Vertical Jumping in Three Dimensions. *Computer methods in biomechanics and biomedical engineering,* 2(3), 201-231.

Anderson, F. C., & Pandy, M. G. (2001). Dynamic optimization of human walking. *Journal of Biomechanical Engineering,* 123(5), 381-390.

Arendt, E., & Dick, R. (1995). Knee injury patterns among men and women in collegiate basketball and soccer. NCAA data and review of literature. *The American Journal of Sports Medicine,* 23(6), 694-701.

Arnoczky, S. P. (1983). Anatomy of the anterior cruciate ligament. *Clinical orthopaedics and related research,* (172)(172), 19-25.

Ateshian, G. A. (1993). A B-spline least-squares surface-fitting method for articular surfaces of diarthrodial joints. *Journal of Biomechanical Engineering,* 115(4A), 366-373.

Babuska, i., & Oden, T. J. (2004).Verification and validation in computational engineering and science: basic concepts. *Computer Methods in Applied Mechanics and Engineering,* 193, 4057-4066.

Bach, J. M., & Hull, M. L. (1995). A new load application system for in vitro study of ligamentous injuries to the human knee joint. *Journal of Biomechanical Engineering,* 117(4), 373-382.

Bach, J. M., Hull, M. L., & Patterson, H. A. (1997). Direct measurement of strain in the posterolateral bundle of the anterior cruciate ligament. *Journal of Biomechanics,* 30(3), 281-283.

Bahr, R., & Krosshaug, T. (2005). Understanding injury mechanisms: a key component of preventing injuries in sport. *British journal of sports medicine,* 39(6), 324-329.

Bendjaballah, M. Z., Shirazi-Adl, A., & Zukor, D. J. (1997). Finite element analysis of human knee joint in varus-valgus. *Clin.Biomech.(Bristol, Avon),* 12(3), 139-148.

Bendjaballah, M. Z., Shirazi-Adl, A., & Zukor, D. J. (1998). Biomechanical response of the passive human knee joint under anterior-posterior forces. *Clin.Biomech.(Bristol, Avon),* 13(8), 625-633.

Besier, T. F., Lloyd, D. G., Ackland, T. R., & Cochrane, J. L. (2001). Anticipatory effects on knee joint loading during running and cutting maneuvers. *Medicine and science in sports and exercise,* 33(7), 1176-1181.

Besier, T. F., Lloyd, D. G., Cochrane, J. L., & Ackland, T. R. (2001). External loading of the knee joint during running and cutting maneuvers. *Medicine and science in sports and exercise,* 33(7), 1168-1175.

Beynnon, B. D., Fleming, B. C., Johnson, R. J., Nichols, C. E., Renstrom, P. A., & Pope, M. H. (1995). Anterior cruciate ligament strain behavior during rehabilitation exercises in vivo. *The American Journal of Sports Medicine,* 23(1), 24-34.

Beynnon, B. D., Johnson, R. J., Abate, J. A., Fleming, B. C., & Nichols, C. E. (2005). Treatment of anterior cruciate ligament injuries, part 2. *The American Journal of Sports Medicine,* 33(11), 1751-1767.

Beynnon, B. D., Johnson, R. J., Fleming, B. C., Stankewich, C. J., Renstrom, P. A., & Nichols, C. E. (1997). The strain behavior of the anterior cruciate ligament during squatting and active flexion-extension. A comparison of an open and a closed kinetic chain exercise. *The American Journal of Sports Medicine,* 25(6), 823-829.

Beynnon, B. D., Pope, M. H., Wertheimer, C. M., Johnson, R. J., Fleming, B. C., Nichols, C. E. et al. (1992). The effect of functional knee-braces on strain on the anterior cruciate ligament in vivo. *The Journal of bone and joint surgery.American volume,* 74(9), 1298-1312.

Biscevic, M., Hebibovic, M., & Smrke, D. (2005). Variations of femoral condyle shape. *Collegium antropologicum,* 29(2), 409-414.

Blankevoort, L., & Huiskes, R. (1991). Ligament-bone interaction in a three-dimensional model of the knee. *Journal of Biomechanical Engineering,* 113(3), 263-269.

Blankevoort, L., & Huiskes, R. (1996). Validation of a three-dimensional model of the knee. *Journal of Biomechanics,* 29(7), 955-961.

Blankevoort, L., Huiskes, R., & de Lange, A. (1988). The envelope of passive knee joint motion. *Journal of Biomechanics,* 21(9), 705-720.

Blankevoort, L., Huiskes, R., & de Lange, A. (1991). Recruitment of knee joint ligaments. *Journal of Biomechanical Engineering,* 113(1), 94-103.

Blankevoort, L., Kuiper, J. H., Huiskes, R., & Grootenboer, H. J. (1991). Articular contact in a three-dimensional model of the knee. *Journal of Biomechanics,* 24(11), 1019-1031.

Boden, B. P., Dean, G. S., Feagin, J. A.,Jr, & Garrett, W. E.,Jr. (2000). Mechanisms of anterior cruciate ligament injury. *Orthopedics,* 23(6), 573-578.

Boisgard, S., Levai, J. P., Geiger, B., Saidane, K., & Landjerit, B. (1999). Study of the variations in length of the anterior cruciate ligament during flexion of the knee: use of a 3D model reconstructed from MRI sections. *Surgical and radiologic anatomy : SRA,* 21(5), 313-317.

Borotikar, B. S., Newcomer, R., Koppes, R., & McLean, S. G. (2008). Combined effects of fatigue and decision making on female lower limb landing postures: central and peripheral contributions to ACL injury risk. *Clinical biomechanics (Bristol, Avon),* 23(1), 81-92.

Boyd, S. K., Ronsky, J. L., Lichti, D. D., Salkauskas, K., & Chapman, M. A. (1999). Joint surface modeling with thin-plate splines. *Journal of Biomechanical Engineering,* 121(5), 525-532.

Buchanan, T. S., Lloyd, D. G., Manal, K., & Besier, T. F. (2005). Estimation of muscle forces and joint moments using a forward-inverse dynamics model. *Medicine and science in sports and exercise,* 37(11), 1911-1916.

Butler, D. L., Kay, M. D., & Stouffer, D. C. (1986). Comparison of material properties in fascicle-bone units from human patellar tendon and knee ligaments. *Journal of Biomechanics,* 19(6), 425-432.

Butler, D. L., Sheh, M. Y., Stouffer, D. C., Samaranayake, V. A., & Levy, M. S. (1990). Surface strain variation in human patellar tendon and knee cruciate ligaments. *Journal of Biomechanical Engineering,* 112(1), 38-45.

Caruntu, D. I., & Hefzy, M. S. (2004). 3-D anatomically based dynamic modeling of the human knee to include tibio-femoral and patello-femoral joints. *Journal of Biomechanical Engineering,* 126(1), 44-53.

Cerulli, G., Benoit, D. L., Caraffa, A., & Ponteggia, F. (2001). Proprioceptive training and prevention of anterior cruciate ligament injuries in soccer. *The Journal of orthopaedic and sports physical therapy,* 31(11), 655-60; discussion 661.

Chandrashekar, N., Mansouri, H., Slauterbeck, J., & Hashemi, J. (2006). Sex-based differences in the tensile properties of the human anterior cruciate ligament. *Journal of Biomechanics,* 39(16), 2943-2950.

Cohen, Z. A., Henry, J. H., McCarthy, D. M., Mow, V. C., & Ateshian, G. A. (2003). Computer simulations of patellofemoral joint surgery. Patient-specific models for tuberosity transfer. *The American Journal of Sports Medicine,* 31(1), 87-98.

Cohen, Z. A., Mow, V. C., Henry, J. H., Levine, W. N., & Ateshian, G. A. (2003). Templates of the cartilage layers of the patellofemoral joint and their use in the assessment of osteoarthritic cartilage damage. *Osteoarthritis and cartilage / OARS, Osteoarthritis Research Society,* 11(8), 569-579.

Cowling, E. J., Steele, J. R., & McNair, P. J. (2003). Effect of verbal instructions on muscle activity and risk of injury to the anterior cruciate ligament during landing. *British journal of sports medicine,* 37(2), 126-130.

Darcy, S. P., Kilger, R. H., Woo, S. L., & Debski, R. E. (2006). Estimation of ACL forces by reproducing knee kinematics between sets of knees: A novel non-invasive methodology. *Journal of Biomechanics,* 39(13), 2371-2377.

DeMorat, G., Weinhold, P., Blackburn, T., Chudik, S., & Garrett, W. (2004). Aggressive quadriceps loading can induce noncontact anterior cruciate ligament injury. *The American Journal of Sports Medicine,* 32(2), 477-483.

Doehring, T., Thangudu, P., Considine, J., & Cavanagh, P. (2005). *New Open-Source Tools for 3D Reconstruction of Medical Images.*

Dye, S. F., & Cannon, W. D.,Jr. (1988). Anatomy and biomechanics of the anterior cruciate ligament. *Clinics in sports medicine,* 7(4), 715-725.

Erdemir, A., McLean, S., Herzog, W., & van den Bogert, A. J. (2007). Model-based estimation of muscle forces exerted during movements. *Clinical biomechanics (Bristol, Avon),* 22(2), 131-154.

Fleming, B. C., Beynnon, B. D., Renstrom, P. A., Johnson, R. J., Nichols, C. E., Peura, G. D. et al. (1999). The strain behavior of the anterior cruciate ligament during stair climbing: an in vivo study. *Arthroscopy : The Journal of Arthroscopic & Related Surgery : Official Publication of the Arthroscopy Association of North America and the International Arthroscopy Association,* 15(2), 185-191.

Fleming, B. C., Renstrom, P. A., Beynnon, B. D., Engstrom, B., Peura, G. D., Badger, G. J. et al. (2001). The effect of weightbearing and external loading on anterior cruciate ligament strain. *Journal of Biomechanics,* 34(2), 163-170.

France, E. P., Daniels, A. U., Goble, E. M., & Dunn, H. K. (1983). Simultaneous quantitation of knee ligament forces. *Journal of Biomechanics,* 16(8), 553-564.

Frankel, V., & Nordin, M. (Eds.). (1980). *Bone Biomechanics of the Skeletal System.* Philadelphia: Lea and Febiger.

Fu, F. H., Harner, C. D., Johnson, D. L., Miller, M. D., & Woo, S. L. (1994). Biomechanics of knee ligaments: basic concepts and clinical application. *Instructional course lectures,* 43, 137-148.

Ghattas, O., Biegler, L. T., Heinkenschloss, M., & van Bloemen Waanders, B. (2004). Large Scale PDE-constrained Optimization - An Introduction. *Large Scale PDE Constrained Optimization Workshop, Santa Fe, Nm,* .

Gill, P. E., Murray, W., & Saunders, M. A. (2005). SNOPT: An SQP algorithm for large-scale constrained optimization. *SIAM Review,* 47(1), 99-131.

Girgis, F. G., Marshall, J. L., & Monajem, A. (1975). The cruciate ligaments of the knee joint. Anatomical, functional and experimental analysis. *Clinical orthopaedics and related research,* (106)(106), 216-231.

Griffin, L. Y., Agel, J., Albohm, M. J., Arendt, E. A., Dick, R. W., Garrett, W. E. et al. (2000). Noncontact anterior cruciate ligament injuries: risk factors and prevention strategies. *The Journal of the American Academy of Orthopaedic Surgeons,* 8(3), 141-150.

Grood, E. S., Stowers, S. F., & Noyes, F. R. (1988). Limits of movement in the human knee. Effect of sectioning the posterior cruciate ligament and posterolateral structures. *The Journal of bone and joint surgery.American volume,* 70(1), 88-97.

Grood, E. S., & Suntay, W. J. (1983). A joint coordinate system for the clinical description of three-dimensional motions: application to the knee. *Journal of Biomechanical Engineering,* 105(2), 136-144.

Halloran, J. P., Petrella, A. J., & Rullkoetter, P. J. (2005). Explicit finite element modeling of total knee replacement mechanics. *Journal of Biomechanics,* 38(2), 323-331.

Harner, C. D., Baek, G. H., Vogrin, T. M., Carlin, G. J., Kashiwaguchi, S., & Woo, S. L. (1999). Quantitative analysis of human cruciate ligament insertions. *Arthroscopy : The Journal of Arthroscopic & Related Surgery : Official Publication of the Arthroscopy Association of North America and the International Arthroscopy Association,* 15(7), 741-749.

Hashemi, J., Chandrashekar, N., Jang, T., Karpat, F., Oseto, M., & Ekwaro-Osire, S. (2007). An alternative mechanism of non-contact anterior cruciate ligament injury during jump-landing: In-vitro simulation. *Experimental Mechanics,* 47(3), 347-354.

Hewett, T. E., Myer, G. D., & Ford, K. R. (2001). Prevention of anterior cruciate ligament injuries. *Current women's health reports,* 1(3), 218-224.

Hewett, T. E., Myer, G. D., & Ford, K. R. (2005). Reducing knee and anterior cruciate ligament injuries among female athletes: a systematic review of neuromuscular training interventions. *The journal of knee surgery,* 18(1), 82-88.

Hewett, T. E., Myer, G. D., Ford, K. R., Heidt, R. S.,Jr, Colosimo, A. J., McLean, S. G. et al. (2005). Biomechanical measures of neuromuscular control and valgus loading of the knee predict anterior cruciate ligament injury risk in female athletes: a prospective study. *The American Journal of Sports Medicine,* 33(4), 492-501.

Hewett, T. E., Stroupe, A. L., Nance, T. A., & Noyes, F. R. (1996). Plyometric training in female athletes. Decreased impact forces and increased hamstring torques. *The American Journal of Sports Medicine,* 24(6), 765-773.

Higginson, J. S., Neptune, R. R., & Anderson, F. C. (2005). Simulated parallel annealing within a neighborhood for optimization of biomechanical systems. *Journal of Biomechanics,* 38(9), 1938-1942.

Hollis, J. M., Takai, S., Adams, D. J., Horibe, S., & Woo, S. L. (1991). The effects of knee motion and external loading on the length of the anterior cruciate ligament (ACL): a kinematic study. *Journal of Biomechanical Engineering,* 113(2), 208-214.

Huston, L. J., Greenfield, M. L., & Wojtys, E. M. (2000). Anterior cruciate ligament injuries in the female athlete. Potential risk factors. *Clinical orthopaedics and related research,* (372)(372), 50-63.

Kanamori, A., Woo, S. L., Ma, C. B., Zeminski, J., Rudy, T. W., Li, G. et al. (2000). The forces in the anterior cruciate ligament and knee kinematics during a simulated pivot shift test: A human cadaveric study using robotic technology. *Arthroscopy : The Journal of Arthroscopic & Related Surgery : Official Publication of the Arthroscopy Association of North America and the International Arthroscopy Association,* 16(6), 633-639.

Kanamori, A., Zeminski, J., Rudy, T. W., Li, G., Fu, F. H., & Woo, S. L. (2002). The effect of axial tibial torque on the function of the anterior cruciate ligament: a biomechanical study of a simulated pivot shift test. *Arthroscopy : The Journal of Arthroscopic & Related Surgery : Official Publication of the Arthroscopy Association of North America and the International Arthroscopy Association,* 18(4), 394-398.

Kennedy, J. C., Alexander, I. J., & Hayes, K. C. (1982). Nerve supply of the human knee and its functional importance. *The American Journal of Sports Medicine,* 10(6), 329-335.

Kennedy, J. C., Hawkins, R. J., & Willis, R. B. (1977). Strain gauge analysis of knee ligaments. *Clinical orthopaedics and related research,* (129)(129), 225-229.

Kennedy, J. C., Weinberg, H. W., & Wilson, A. S. (1974). The anatomy and function of the anterior cruciate ligament. As determined by clinical and morphological studies. *The Journal of bone and joint surgery.American volume,* 56(2), 223-235.

Koh, B. I., Reinbolt, J. A., George, A. D., Haftka, R. T., & Fregly, B. J. (2009). Limitations of parallel global optimization for large-scale human movement problems. *Medical engineering & physics,* 31(5), 515-521.

Kurosawa, H., Yamakoshi, K., Yasuda, K., & Sasaki, T. (1991). Simultaneous measurement of changes in length of the cruciate ligaments during knee motion. *Clinical orthopaedics and related research,* (265)(265), 233-240.

Kurosawa, H., Yasuda, K., Yamakoshi, K., Kamiya, A., & Kaneda, K. (1991). An experimental evaluation of isometric placement for extraarticular reconstructions of the anterior cruciate ligament. *The American Journal of Sports Medicine,* 19(4), 384-388.

Kwak, S. D., Blankevoort, L., & Ateshian, G. A. (2000). A Mathematical Formulation for 3D Quasi-Static Multibody Models of Diarthrodial Joints. *Computer methods in biomechanics and biomedical engineering,* 3(1), 41-64.

Kwan, M. K., Lin, T. H., & Woo, S. L. (1993). On the viscoelastic properties of the anteromedial bundle of the anterior cruciate ligament. *Journal of Biomechanics,* 26(4-5), 447-452.

Lephart, S. M., Ferris, C. M., & Fu, F. H. (2002). Risk factors associated with noncontact anterior cruciate ligament injuries in female athletes. *Instructional course lectures,* 51, 307-310.

Lew, W. D., & Lewis, J. L. (1978). A technique for calculating in vivo ligament lengths with application to the human knee joint. *Journal of Biomechanics,* 11(8-9), 365-377.

Lewis, J. L., Lew, W. D., Hill, J. A., Hanley, P., Ohland, K., Kirstukas, S. et al. (1989). Knee joint motion and ligament forces before and after ACL reconstruction. *Journal of Biomechanical Engineering,* 111(2), 97-106.

Li, G., DeFrate, L. E., Sun, H., & Gill, T. J. (2004). In vivo elongation of the anterior cruciate ligament and posterior cruciate ligament during knee flexion. *The American Journal of Sports Medicine,* 32(6), 1415-1420.

Li, G., Gil, J., Kanamori, A., & Woo, S. L. (1999). A validated three-dimensional computational model of a human knee joint. *Journal of Biomechanical Engineering,* 121(6), 657-662.

Li, G., Suggs, J., & Gill, T. (2002). The effect of anterior cruciate ligament injury on knee joint function under a simulated muscle load: a three-dimensional computational simulation. *Annals of Biomedical Engineering,* 30(5), 713-720.

Li, G., Zayontz, S., Most, E., DeFrate, L. E., Suggs, J. F., & Rubash, H. E. (2004). In situ forces of the anterior and posterior cruciate ligaments in high knee flexion: an in vitro investigation. *Journal of orthopaedic research : official publication of the Orthopaedic Research Society,* 22(2), 293-297.

Lloyd, D. G., & Besier, T. F. (2003). An EMG-driven musculoskeletal model to estimate muscle forces and knee joint moments in vivo. *Journal of Biomechanics,* 36(6), 765-776.

Lohmander, L. S., Ostenberg, A., Englund, M., & Roos, H. (2004). High prevalence of knee osteoarthritis, pain, and functional limitations in female soccer players twelve years after anterior cruciate ligament injury. *Arthritis and Rheumatism,* 50(10), 3145-3152.

Maletius, W., & Messner, K. (1999). Eighteen- to twenty-four-year follow-up after complete rupture of the anterior cruciate ligament. *The American Journal of Sports Medicine,* 27(6), 711-717.

Mandelbaum, B. R., Silvers, H. J., Watanabe, D. S., Knarr, J. F., Thomas, S. D., Griffin, L. Y. et al. (2005). Effectiveness of a neuromuscular and proprioceptive training program in preventing anterior cruciate ligament injuries in female athletes: 2-year follow-up. *The American Journal of Sports Medicine,* 33(7), 1003-1010.

Markolf, K. L., Bargar, W. L., Shoemaker, S. C., & Amstutz, H. C. (1981). The role of joint load in knee stability. *The Journal of bone and joint surgery.American volume,* 63(4), 570-585.

Markolf, K. L., Burchfield, D. M., Shapiro, M. M., Shepard, M. F., Finerman, G. A., & Slauterbeck, J. L. (1995). Combined knee loading states that generate high anterior cruciate ligament forces. *Journal of orthopaedic research : official publication of the Orthopaedic Research Society,* 13(6), 930-935.

Markolf, K. L., Gorek, J. F., Kabo, J. M., & Shapiro, M. S. (1990). Direct measurement of resultant forces in the anterior cruciate ligament. An in vitro study performed with a new experimental technique. *The Journal of bone and joint surgery.American volume,* 72(4), 557-567.

Markolf, K. L., Graff-Radford, A., & Amstutz, H. C. (1978). In vivo knee stability. A quantitative assessment using an instrumented clinical testing apparatus. *The Journal of bone and joint surgery.American volume,* 60(5), 664-674.

Markolf, K. L., Mensch, J. S., & Amstutz, H. C. (1976). Stiffness and laxity of the knee--the contributions of the supporting structures. A quantitative in vitro study. *The Journal of bone and joint surgery.American volume,* 58(5), 583-594.

McLean, S. G., Huang, X., Su, A., & Van den Bogert, A. J. (2004). Sagittal plane biomechanics cannot injure the ACL during sidestep cutting. *Clinical biomechanics (Bristol, Avon),* 19(8), 828-838.

McLean, S. G., Su, A., & van den Bogert, A. J. (2003). Development and validation of a 3-D model to predict knee joint loading during dynamic movement. *Journal of Biomechanical Engineering,* 125(6), 864-874.

Mesfar, W., & Shirazi-Adl, A. (2005). Biomechanics of the knee joint in flexion under various quadriceps forces. *The Knee,* 12(6), 424-434.

Mesfar, W., & Shirazi-Adl, A. (2006a). Biomechanics of changes in ACL and PCL material properties or prestrains in flexion under muscle force-implications in ligament reconstruction. *Computer methods in biomechanics and biomedical engineering,* 9(4), 201-209.

Mesfar, W., & Shirazi-Adl, A. (2006b). Knee joint mechanics under quadriceps--hamstrings muscle forces are influenced by tibial restraint. *Clinical biomechanics (Bristol, Avon),* 21(8), 841-848.

Mesfar, W., Shirazi-Adl, A., & Dammak, M. (2003). Modeling of biomedical interfaces with nonlinear friction properties. *Bio-medical materials and engineering,* 13(1), 91-101.

Messner, K., & Maletius, W. (1999). Eighteen- to twenty-five-year follow-up after acute partial anterior cruciate ligament rupture. *The American Journal of Sports Medicine,* 27(4), 455-459.

Meyer, E. G., & Haut, R. C. (2008). Anterior cruciate ligament injury induced by internal tibial torsion or tibiofemoral compression. *Journal of Biomechanics,* 41(16), 3377-3383.

Moglo, K. E., & Shirazi-Adl, A. (2003). Biomechanics of passive knee joint in drawer: load transmission in intact and ACL-deficient joints. *The Knee,* 10(3), 265-276.

Moglo, K. E., & Shirazi-Adl, A. (2005). Cruciate coupling and screw-home mechanism in passive knee joint during extension--flexion. *Journal of Biomechanics,* 38(5), 1075-1083.

Mommersteeg, T. J., Huiskes, R., Blankevoort, L., Kooloos, J. G., Kauer, J. M., & Maathuis, P. G. (1996). A global verification study of a quasi-static knee model with multi-bundle ligaments. *Journal of Biomechanics,* 29(12), 1659-1664.

Myer, G. D., Ford, K. R., & Hewett, T. E. (2004a). Methodological approaches and rationale for training to prevent anterior cruciate ligament injuries in female athletes. *Scandinavian journal of medicine & science in sports,* 14(5), 275-285.

Myer, G. D., Ford, K. R., & Hewett, T. E. (2004b). Rationale and Clinical Techniques for Anterior Cruciate Ligament Injury Prevention Among Female Athletes. *Journal of athletic training,* 39(4), 352-364.

Neptune, R. R. (1999). Optimization algorithm performance in determining optimal controls in human movement analyses. *Journal of Biomechanical Engineering,* 121(2), 249-252.

Noble, L.D., Colbrunn, R.W., Lee, D. G., van den Bogert, A. J., Davis, B. L. (2009) Design and validation of a general purpose robotic testing system for musculoskeletal applications. *Journal of Biomechanical Engineering,* in press.

Norwood, L. A., & Cross, M. J. (1979). Anterior cruciate ligament: functional anatomy of its bundles in rotatory instabilities. *The American Journal of Sports Medicine,* 7(1), 23-26.

Noyes, F. R., Butler, D. L., Grood, E. S., Zernicke, R. F., & Hefzy, M. S. (1984a). Biomechanical analysis of human ligament grafts used in knee-ligament repairs and reconstructions. *The Journal of bone and joint surgery.American volume,* 66(3), 344-352.

Noyes, F. R., Keller, C. S., Grood, E. S., & Butler, D. L. (1984b). Advances in the understanding of knee ligament injury, repair, and rehabilitation. *Medicine and science in sports and exercise,* 16(5), 427-443.

Odensten, M., & Gillquist, J. (1985). Functional anatomy of the anterior cruciate ligament and a rationale for reconstruction. *The Journal of bone and joint surgery.American volume,* 67(2), 257-262.

Pandy, M. G., Anderson, F. C., & Hull, D. G. (1992). A parameter optimization approach for the optimal control of large-scale musculoskeletal systems. *Journal of Biomechanical Engineering,* 114(4), 450-460.

Pandy, M. G., & Sasaki, K. (1998). A Three-Dimensional Musculoskeletal Model of the Human Knee Joint. Part 2: Analysis of Ligament Function. *Computer methods in biomechanics and biomedical engineering,* 1(4), 265-283.

Pandy, M. G., Sasaki, K., & Kim, S. (1998). A Three-Dimensional Musculoskeletal Model of the Human Knee Joint. Part 1: Theoretical Construct. *Computer methods in biomechanics and biomedical engineering,* 1(2), 87-108.

Pandy, M. G., & Shelburne, K. B. (1997). Dependence of cruciate-ligament loading on muscle forces and external load. *Journal of Biomechanics,* 30(10), 1015-1024.

Pena, E., Calvo, B., Martinez, M. A., & Doblare, M. (2006). A three-dimensional finite element analysis of the combined behavior of ligaments and menisci in the healthy human knee joint. *Journal of Biomechanics,* 39(9), 1686-1701.

Pena, E., Calvo, B., Martinez, M. A., Palanca, D., & Doblare, M. (2006). Influence of the tunnel angle in ACL reconstructions on the biomechanics of the knee joint. *Clinical biomechanics (Bristol, Avon),* 21(5), 508-516.

Pflum, M. A., Shelburne, K. B., Torry, M. R., Decker, M. J., & Pandy, M. G. (2004). Model prediction of anterior cruciate ligament force during drop-landings. *Medicine and science in sports and exercise,* 36(11), 1949-1958.

Pioletti, D. P., Heegaard, J. H., Rakotomanana, R. L., Leyvraz, P. F., & Blankevoort, L. (1995). Experimental and mathematical methods for representing relative surface elongation of the ACL. *Journal of Biomechanics,* 28(9), 1123-1126.

Piziali, R. L., Rastegar, J., Nagel, D. A., & Schurman, D. J. (1980). The contribution of the cruciate ligaments to the load-displacement characteristics of the human knee joint. *Journal of Biomechanical Engineering,* 102(4), 277-283.

Press, W. H., Teukolsky, S. A., Vetterling, W. T., Flannery, B. P. (1992). *Numerical Recipes in C: The Art of Scientific Computing.* (Second Edition) Cambridge University Press, Cambridge, New York, NY.

Ramakrishnan, H. K., & Kadaba, M. P. (1991). On the estimation of joint kinematics during gait. *Journal of Biomechanics,* 24(10), 969-977.

Raunest, J., Sager, M., & Burgener, E. (1996). Proprioceptive mechanisms in the cruciate ligaments: an electromyographic study on reflex activity in the thigh muscles. *The Journal of trauma,* 41(3), 488-493.

Ronsky, J. L., Herzog, W., Brown, T. D., Pedersen, D. R., Grood, E. S., & Butler, D. L. (1995). In vivo quantification of the cat patellofemoral joint contact stresses and areas. *Journal of Biomechanics,* 28(8), 977-983.

Scherrer, P. K., & Hillberry, B. M. (1979). Piecewise mathematical representation of articular surfaces. *Journal of Biomechanics,* 12(4), 301-311.

Seering, W. P., Piziali, R. L., Nagel, D. A., & Schurman, D. J. (1980). The function of the primary ligaments of the knee in varus-valgus and axial rotation. *Journal of Biomechanics,* 13(9), 785-794.

Shelburne, K. B., Pandy, M. G., Anderson, F. C., & Torry, M. R. (2004). Pattern of anterior cruciate ligament force in normal walking. *Journal of Biomechanics,* 37(6), 797-805.

Shirazi-Adl, A., & Moglo, K. E. (2005). Effect of changes in cruciate ligaments pretensions on knee joint laxity and ligament forces. *Computer methods in biomechanics and biomedical engineering,* 8(1), 17-24.

Smith, B. A., Livesay, G. A., & Woo, S. L. (1993). Biology and biomechanics of the anterior cruciate ligament. *Clinics in sports medicine,* 12(4), 637-670.

Steele, J. R., & Brown, J. M. (1999). Effects of chronic anterior cruciate ligament deficiency on muscle activation patterns during an abrupt deceleration task. *Clinical biomechanics (Bristol, Avon),* 14(4), 247-257.

Thelen, D. G., & Anderson, F. C. (2006). Using computed muscle control to generate forward dynamic simulations of human walking from experimental data. *Journal of Biomechanics,* 39(6), 1107-1115.

Uhorchak, J. M., Scoville, C. R., Williams, G. N., Arciero, R. A., St Pierre, P., & Taylor, D. C. (2003). Risk factors associated with noncontact injury of the anterior cruciate ligament: a prospective four-year evaluation of 859 West Point cadets. *The American Journal of Sports Medicine,* 31(6), 831-842.

Un, B. S., Beynnon, B. D., Churchill, D. L., Haugh, L. D., Risberg, M. A., & Fleming, B. C. (2001). A new device to measure knee laxity during weightbearing and non-weightbearing conditions. *Journal of orthopaedic research : official publication of the Orthopaedic Research Society,* 19(6), 1185-1191.

Vahey, J. W., & Draganich, L. F. (1991). Tensions in the anterior and posterior cruciate ligaments of the knee during passive loading: predicting ligament loads from in situ measurements. *Journal of orthopaedic research : official publication of the Orthopaedic Research Society,* 9(4), 529-538.

van den Bogert, A. J. (1994). Analysis and simulation of mechanical loads on the human musculoskeletal system: a methodological overview. *Exercise and sport sciences reviews,* 22, 23-51.

van den Bogert, A. J., & McLean, S. G. (2007). ACL injuries: do we know the mechanisms? *The Journal of orthopaedic and sports physical therapy,* 37(2), A8-9.

Winter, D. A. (2005). *Biomechanics and Motor Control of Human Movement.* (Fourth Edition ed.)John Wiley and Sons, New York, NY.

Wismans, J., Veldpaus, F., Janssen, J., Huson, A., & Struben, P. (1980). A three-dimensional mathematical model of the knee-joint. *Journal of Biomechanics,* 13(8), 677-685.

Withrow, T. J., Huston, L. J., Wojtys, E. M., & Ashton-Miller, J. A. (2006a). The effect of an impulsive knee valgus moment on in vitro relative ACL strain during a simulated jump landing. *Clinical biomechanics (Bristol, Avon),* 21(9), 977-983.

Withrow, T. J., Huston, L. J., Wojtys, E. M., & Ashton-Miller, J. A. (2006b). The relationship between quadriceps muscle force, knee flexion, and anterior cruciate ligament strain in an in vitro simulated jump landing. *The American Journal of Sports Medicine,* 34(2), 269-274.

Woo, S. L., Debski, R. E., Withrow, J. D., & Janaushek, M. A. (1999). Biomechanics of knee ligaments. *The American Journal of Sports Medicine,* 27(4), 533-543.

Woo, S. L., Gomez, M. A., Seguchi, Y., Endo, C. M., & Akeson, W. H. (1983). Measurement of mechanical properties of ligament substance from a bone-ligament-bone preparation. *Journal of orthopaedic research : official publication of the Orthopaedic Research Society,* 1(1), 22-29.

Woo, S. L., Hollis, J. M., Adams, D. J., Lyon, R. M., & Takai, S. (1991). Tensile properties of the human femur-anterior cruciate ligament-tibia complex. The effects of specimen age and orientation. *The American Journal of Sports Medicine,* 19(3), 217-225.

Woo, S. L., Johnson, G. A., & Smith, B. A. (1993). Mathematical modeling of ligaments and tendons. *Journal of Biomechanical Engineering,* 115(4B), 468-473.

Woo, S. L., Orlando, C. A., Camp, J. F., & Akeson, W. H. (1986). Effects of postmortem storage by freezing on ligament tensile behavior. *Journal of Biomechanics,* 19(5), 399-404.

Woo, S. L. -., Fox, R. J., Sakane, M., Livesay, G. A., Rudy, T. W., & Fu, F. H. (1998). Biomechanics of the ACL: Measurements of in situ force in the ACL and knee kinematics. *Knee,* 5(4), 267-288.

Wroble, R. R., Grood, E. S., Cummings, J. S., Henderson, J. M., & Noyes, F. R. (1993). The role of the lateral extraarticular restraints in the anterior cruciate ligament-deficient knee. *The American Journal of Sports Medicine,* 21(2), 257-62; discussion 263.

APPENDIX

APPENDIX A

A1: Rotopod R2000, MicroScribe G2L digitizer and UFS SI-1500-240 specifications

Rotopod R2000 specifications

Feature	Value	Feature	Value
Platform Size (diameter)	780 mm	**Repeatability**	25 μm
Load capacity	2,000 N	**X-axis range of motion**	$\pm$110 mm
Torque capacity	1,000 N-m	**Y-axis range of motion**	$\pm$110 mm
Payload capacity	227 kg	**Z-axis range of motion**	$\pm$93 mm
Translational velocity	100 mm/s	**Roll range of motion**	$\pm 13^0$
Angular velocity	120^0/s	**Pitch range of motion**	$+12^0$, -19^0
Static accuracy	$\pm$50 μm	**Yaw range of motion**	$\pm 720^0$

MicroScribe specifications

Feature	Value
Workspace	168 cm sphere
Resolution	0.13 mm
Accuracy (110 point ANSI sphere)	0.43 mm

SI-1500-240 UFS performance characteristics

Feature	Value					
	F_x	F_y	F_z	M_x	M_y	M_z
Load rating (N, N-m)	1,500	1,500	3,750	240	240	240
Resolution (N, N-m)	0.5	0.5	1.1	0.07	0.07	0.07
Accuracy (% FS)	1.50	1.25	0.75	1.25	1.00	1.50

A2: IRB Exemption letter

Cleveland Clinic

Institutional Review Board

July 2, 2008

A.J. (Ton) van den Bogert, Ph.D. / ND20

RE: IRB 08-460: EXEMPT: Validation of computational models of the Kneww Joint used to Predict ACL injury mechanisms

Dear Dr. van den Bogert:

Your new study application received June 23, 2008 was reviewed and **Approved** under the IRB expedited review process on July 1, 2008. This research qualifies as exempt research under the following Exempt Research Category:#4: Research involving the collection or study of existing data, documents, records, pathological specimens, or diagnostic specimens, is exempt if these sources are publicly available or if the information is recorded by the Investigator in such a manner that subjects cannot be identified, directly or through identifiers linked to the subjects. This action will be reported to the full committee of the IRB.

Please note that Mr. R. Colbrunn needs to complete the CITI Course by going to www.citiprogram.org.

Exempt Research does not require continuing renewal reporting unless there is a change that makes this study ineligible under this exempt category.

Sincerely,

Daniel Beyer

Daniel Beyer, M.S., MHA, CIP

Executive Director, Institutional Review Board

DB:cmf

The Cleveland Clinic Foundation

9500 Euclid Avenue / Wb2
Cleveland, Ohio 44195

Tel 216 444-2924
Fax 216 445-4094
IRB@ccf.org

A3: Lifelegacy medical history and serology testing data for specimen # 2 & 3

DONOR INFORMATION LOG EXTERNAL VERSION

LIFELEGACY FOUNDATION®

DONOR INFORMATION

Donor Number	08-09034	Age	58
Sex	Male	Race	Caucasian
Primary COD	Lung CA with Mets to the Brain and Liver		
Cardiac Death Date	9/9/2008	Time	16:47

RECOVERY AND PROCESSING INFORMATION

Recovery Date	9/9/2008	Time	20:02

PHYSICAL EXAMINATION INFORMATION

Actual Height in Inches	70.00	Actual Weight in Pounds	154.00
Actual BMI	22		

Physical Exam Findings:

M1- ID Band L ankle, S1- 1" Sx scar upper R chest consistent with medport, S2- 4" Sx scar posterior lower back over lumbar, L1- multiple wounds over L ankle about .25 in, L2- small wound on top of head about .25 in

SUMMARY OF MEDICAL HISTORY

Liver Disorders:

Small Cell Lung Cancer with metastasis to the Liver (03/2008)

Neuro Disorders:

Small Cell Lung Cancer with metastasis to the Brain (03/2008) and Epilepsy (1967)

Lung Disorders:

Small Cell Lung Cancer with metastasis (03/2008) and Emphysema (03/2008).

Surgical Procedure:

Back Surgery x 2 (1992 & 1994) and Pancreas Stint Placement (05/2008).

Other History:

Small Cell Lung Cancer with metastasis (03/2008) with the last radiation treatment in 07/2008 and the last chemotherapy in in 06/2008.
Smoked 1 ppd x 40 yrs. Quit in 2008.
Moderate ETOH Use.
No additional comments at this time...RDL...09/09/2008.

MEDICATION INFORMATION

Lorazepam, OxyCodone, MS, OxyContin, Pericolace, Dulcolax, Albuterol, Spiriva, Cenna, and Tylenol.

SEROLOGY RESULTS

Serology Drawn	Post-Mortem	HBsAg	Non-Reactive
Source	Subclavian	HCV	Non-Reactive
Date Drawn	9/9/2008	HIV12	Non-Reactive
Time Drawn	20:12	HLTV	Not Applicable
Person Recording Result	Monroe Burgess	RPR	Not Applicable
Received Date	9/12/2008	Other	Not Applicable
Time	10:04		

PROGRESS NOTES

A4: Lifelegacy medical history and serology testing data for specimen # 4 & 5

DONOR INFORMATION LOG EXTERNAL VERSION

LIFELEGACY FOUNDATION

DONOR INFORMATION

Donor Number	08-09036	Age	58
Sex	Male	Race	Caucasian
Primary COD	Laryngeal Cancer		
Cardiac Death Date	9/9/2008	Time	15:43

RECOVERY AND PROCESSING INFORMATION

Recovery Date	9/10/2008	Time	17:49

PHYSICAL EXAMINATION INFORMATION

Actual Height in Inches	71.00	Actual Weight in Pounds	201.50
Actual BMI	28		

Physical Exam Findings:

M1, ID band Left wrist. M2, ID band Right wrist. S1, 1" SX scar upper right chest consistant with Med port. T1, 4"x3.5" tattoo upper left arm. T2, 4"x5" tattoo upper left chest. T3, 4.5"x2.5" tattoo upper right chest. T4, 2"x3" tattoo upper right arm. T5, 6"x3.5" tattoo right forearm. L1, 3"x3" wound at coccys. S2, 5 .25" SX Scars, 3 on right side of T spine and 2 on left side of T spine.

SUMMARY OF MEDICAL HISTORY

Heart Disorders:

HTN (2004) and Angina (2004).

Liver Disorders:

Laryngeal Cancer with metastasis to the Liver (08/2008)

Digestive Disorders:

Reflux Disease (2005)

Bone Disorders:

Arthritis in hands (2002), Degenerative Disc Disease (2002), and Laryngeal Cancer with metastasis to the spine/sternum/pelvis (08/2008)

Lung Disorders:

COPD (2006) and Laringeal Cancer with metastasis to the Lungs (08/2008).

Surgical Procedure:

Tonsillectomy (age 6) and Back Surgery (09/2008).

Other History:

Laryngeal Cancer with metastasis to the Liver (08/2008) with the last radiation treatment in 08/2008.
Smoked 1-2 ppd x 44 yrs.
Moderate-Heavy ETOH Use.
No additional comments at this time...RDL...09/09/2008.

MEDICATION INFORMATION

Lasix, MS, Atenolol, Pericolace, Dulcolax, and Tylenol.

SEROLOGY RESULTS

Serology Drawn	Post-Mortem	HBsAg	Non-Reactive
Source	Subclavian	HCV	Non-Reactive
Date Drawn	9/10/2008	HIV12	Non-Reactive
Time Drawn	18:05	HLTV	Not Applicable
Person Recording Result	Monroe Burgess	RPR	Not Applicable
Received Date	9/15/2008	Other	Not Applicable
Time	15:32		

PROGRESS NOTES

A5: DVRT product overview sheet from MicroStrain.

Technical Product Overview

Micro Gauging DVRT®

Differential Variable Reluctance Transducer

Introduction

Designed to get into tight spaces, the micro-miniature gauging DVRT® delivers high performance in a tiny package. A sapphire bearing and ruby ball guide the spring-loaded tip, providing an exceptionally smooth static & dynamic response.

Features of micro-gauging DVRTs include: micron to sub-micron resolution, linear analog output, flat dynamic response to kHz levels, and very low temperature coefficients. Extremely lightweight, captive cores are tiny yet rugged. Superelastic, corrosion-resistant alloys provide resistance to kinking & permanent deformation, and allow complete submersion of the instrument.

Micro-gauging DVRTs are ideal for applications requiring closely spaced sensing arrays. Sensor arrays of only 5 mm center-to-center spacing can be readily implemented with our clamping collar mounting system. This system also protects the sensor and test items from excess applied force or over-range displacement.

Miniature "plug and play" signal conditioners provide linear DC output when supplied with unregulated DC power. Multi-channel, OEM and digital display systems are also available.

Features & Benefits

- available with sub-micron resolution and long stroke range
- operating temperature to 175 °C
- frequency response up to 20 kHz
- lightweight core will not influence frequency response
- stainless steel and high-performance polymer design suitable for extremely harsh environments
- waterproof, suitable for submersion in corrosive media such as brake fluid and hot saline
- low-friction design suitable for high duty-cycle applications
- easily customized to suit specific application

Applications

- miniature control elements for automotive and robotic systems
- process control for production-line monitoring
- dimensional gauging for quality control applications
- measuring strain and deflection in materials science and civil structures
- linear/angular positioning of optical components
- miniature force, torque, acceleration sensors

BEST OF SENSORS EXPO SPRING 2002 GOLD

MicroStrain® Micro Sensors. Big Ideas.™ www.microstrain.com

How it works

Core position is detected by measuring the coils' differential reluctance, using a sinewave excitation and synchronous demodulator. This differential detection method provides a very sensitive measure of core position while cancelling out temperature effects.

The transducer's coils & multistranded leads are sealed in vacuum-pumped epoxy within the stainless-steel case. This provides outstanding environmental resistance. The DVRT® has been successfully employed in harsh applications, including immersion in saline and pressurized oil.

Differential
Variable
Reluctance
Transducer

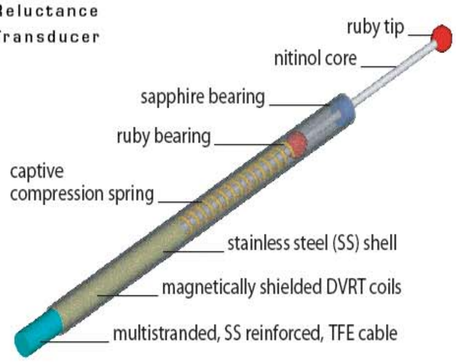

U.S. Patent No. 4,813,435 and Patents Pending

Electrical Specifications

(with MicroStrain DEMOD-DVRT®)

Linear Stroke Lengths	3, 6 & 9 mm (standard version) 1.5 mm (high resolution version)
Accuracy*	± 1.0% using straight line ± 0.1% using polynomial
Sensitivity	2 volts/mm typical
Signal to noise	2000 to 1 (with filter 3 dB down at 800 Hz, standard); 600 to 1 (unfiltered) noise measured peak to peak
Resolution (0.05% of full scale for standard version)	1.5 µm for 3 mm stroke 3.0 µm for 6 mm stroke 4.5 µm for 9 mm stroke 300 nm for high resolution version
Frequency response	7 KHz (unfiltered)
Temperature coefficient	offset 0.0029%/ °C (typical) span 0.030%/ °C (typical)
Hysteresis*	±1 micron
Repeatability*	± 1 micron
Cycle life	fully operational after >20 million cycles to full scale displacement

* at constant temperature

Mechanical Specifications

Overall length	24 mm for 3 mm stroke 40 mm for 6 mm stroke 50 mm for 9 mm stroke 24 mm for high res version
Outside diameter	1.8 mm (smooth body)
Spring stiffness	0.2 Newtons/mm (1 lb/inch)
Bearing materials	sapphire and ruby on stainless steel
Standard core tips	1.5 mm ruby ball, 1.5 mm sapphire cup, sapphire stylus with 60 micron tip radius
Housing material	stainless steel, smooth body, or 8-32/10-32 400 series stainless steel threaded body
Mounting system	clamping collar or threaded body
Sensor spacing	5.0 mm minimum center-to-center with smooth body & clamping collar mounting system
Leadouts	45 cm multistranded, shielded, stainless steel reinforced, teflon insulated
Connector	keyed Lemo 4-pin, polyolefin relief
Operating temperature	-55 to 175 °C
Core weight	30 milligrams, with ruby tip and bearing
Core material	superelastic NiTi alloy

MicroStrain®

MicroStrain Inc.
310 Hurricane Lane, Unit 4
Williston, VT 05495 USA
www.microstrain.com
ph: 800-449-3878
fax : 802-863-4093
sales@microstrain.com

Patent Pending

APPENDIX B

B1: MRI Scan Parameters

MRI Scan Details				
		Scan #		
		Sagittal	Axial	Coronal
Protocol Name				
Sequence Name (From ONI)				
Scan Parameters	**Pulse Sequence**	GE3D	GE3D	GE3D
	TR	30	30	30
	TE	8.9	8.9	8.9
	Frequency	260	260	260
	Phase	192	192	192
	FOV	150	150	150
	BW	20	20	20
	Echo Train	1	1	1
	NEX	1	1	1
	Flip Angle	35	35	35
	Time	5.03	3.19	3.30
Scan Options	**Graphics SL**	✓	✓	✓
	RF spoiling	✓	✓	✓
	Fat Suppression	×	×	×
	Minimum TE	✓	✓	✓
	Inversion Recovery	×	×	×
	Partial Data	×	×	×
	No Phase Wrap	✓	✓	✓
	Spatial Saturation	×	×	×
	Flow comp	×	×	×
	Magnetic Transfer	×	×	×
Prescan Parameters	**Prescan**	Auto	Auto	Auto
	Center Freq.	Peak	Peak	Peak
Slice Parameters	**Number of slices**	70	45	60
	Slice Thickness	1.5	1.5	1.5
	Gap	0	0	0
	Range	105	67.5	90
Comment				

B2: Surface Fitting Algorithm for Femoral Articular Cartilage

```
% This is a program to fit a TPS surface to a cloud of femoral points.
% The flow of events is as described below. Some key values like target
% RMS are taken as user input. Pl. see the script notes before deciding
% on target RMS value.

% First this script finds the best fitting cylinder axis orientation
% and position. We assume here that the cylinder axis is not parallel
% to XY plane so we can
% (1) parameterise the axis position as X,Y of the intersection of the
% axis with Z = 0 and
% (2) parameterize the axis orientation as a vector (Ax, Ay, 1.0)
% Thus we get the initial guess for five cylinder parameters using the
% cyl function. The five parameters are (X, Y, Ax, Ay, Radius).
% These parameters are displayed as best fitting parameters.
% After getting these parameters, we shift the origin of the data to
% this new location using the rotation matrix.
% Now we transform the data to cylindrical coordinates and plot X and Y
% points. As the X-axis pass through the data points, we will observe a
% gap on the plot that splits the data points splitting the cartilage
% surface.
% This gap needs to be eliminated.
% After getting the unsplitted X-Y plot, we do smoothing and gridding
% of these points using Thin Plate Splines. The smoothing is done by
% tpssurf function and gridding or resampling is done by script.
% After smoothing, the resampled points are converted back to
% the cartesian coordinate system.
% The unwanted points are discarded and a .3d file is created.
% end of program.
%


global xyzdata;
global neval;
neval = 0.0;

[filename,pathname]=uigetfile('*.txt',...
                            'txt-input file of surface data points');
path(path, pathname);
a = load (filename);

x = a(:,1);
y = a(:,2);
z = a(:,3);
xyzdata = [x y z]; % create xyzdata matrix

p0 = input('Enter initial guess matrix : '); % get initial guess from
                                                  user
p = lsqnonlin('cyl1',p0); % optimize the parameters using initial guess
display('Best fitting cylinder parameters : ');
p

% translation to new origin
[n,ncol] = size(xyzdata); % find size of point cloud
```

```matlab
for i = 1:n
    xyzdata(i,1) = xyzdata(i,1) - p(1,1); % translation of X-coordinate
    xyzdata(i,2) = xyzdata(i,2) - p(1,2); % translation of Y-coordinate
end

zaxisorient = [p(1,3) p(1,4) 1.0]';  % orientation of optimized z-axis
zaxisorient = zaxisorient/norm(zaxisorient);    % normalize the vector

% finding the rotation angles of X and Y-axis
beta = atan2(zaxisorient(1), sqrt((zaxisorient(2))^2 + ...
                            (zaxisorient(3))^2)); % y-axis rotation
alpha = atan2(-zaxisorient(2), zaxisorient(3)); % x-axis rotation

% rotation (transformation) matrix is
rotationmat = [cos(beta) sin(beta)*sin(alpha) -sin(beta)*cos(alpha);...
               0 cos(alpha) sin(alpha);...
               sin(beta) -sin(alpha)*cos(beta) cos(alpha)*cos(beta)];

% applying rotation to point translated data points
xyzdata2 = zeros(3,n);
xyzdata = xyzdata';
for i = 1:n
    xyzdata2(:,i) = rotationmat * xyzdata(:,i); % data transformations
end
xyzdata = xyzdata';
xyzdata2 = xyzdata2';

% data conversion from cartesian to cylindrical coordinate system
r = zeros(n,1);
theta = zeros(n,1);
zee = zeros(n,1);

r = sqrt(xyzdata2(:,1).^2 + xyzdata2(:,2).^2); % finding radius
theta = atan2(xyzdata2(:,2),xyzdata2(:,1)); % finding theta
zee = xyzdata2(:,3); % zee equals z of original data

% view the data
figure(1)
plot(theta(:,1),r(:,1),'.')

% After the z-axis rotation is performed, the negative x-axis
% is placed in a gap which avoids splitting of the cartilage surface.

gap = input('Look at figure 1. If small bunch of points is on right,
enter 1, else enter 2 : ');

for i = 1:n
    if gap == 1
        if theta (i,1) > 1.00
            theta (i,1) = theta(i,1) - (2*pi);
        end
    elseif gap == 2
        if theta (i,1) < -1.00
            theta(i,1) = theta(i,1) + (2*pi);
        end
```

```
    end
end

% view this data now
figure(2)
plot(theta(:,1),r(:,1),'.')

%%%%%%%%%%%%%%%%%%%%%%%%%%%%%%% test22.m %%%%%%%%%%%%%%%%%%%%%%%%%%%%%%%

% to create the TPS functions
% use the point cloud data set converted to cylindrical co-ordinates

xyzdata3 = [theta zee r];
thetamax = max(xyzdata3(:,1));
zeemax = max(xyzdata3(:,2));
thetamin = min(xyzdata3(:,1));
zeemin = min(xyzdata3(:,2));
rmin = min(xyzdata3(:,3))
rmax = max(xyzdata3(:,3))

% we will scale the theta and zee data from 0 to 1

xyzcyldata = zeros(n,3);

for i = 1:n
    xyzcyldata(i,1) = (theta(i,1)-thetamin)/(thetamax-thetamin);
    xyzcyldata(i,2) = (zee(i,1)-zeemin)/(zeemax-zeemin);
    xyzcyldata(i,3) = (r(i,1)-rmin)/(rmax-rmin);
end

% visualize the raw data in 3D
figure(3)
plot3(xyzcyldata(:,1),xyzcyldata(:,2),xyzcyldata(:,3),'.');
drawnow;
axis equal;
hold on

% determine the optimal smoothing factor for this dataset, using
% 1.0 mm as the target RMS fit error
disp('Finding optimal lambda...');

% Since the z-data is scaled down, target RMS should also be scaled
% down. For eg. the scaled down value for target RMS = 0.1mm is
% 0.1/(rmax-rmin). If z-data is not scaled down (as in case of patellar
% and tibial surface generation code) then we can use actual target RMS
% values.

targetrms = input('Enter the TargetRMS value = (required
targetRMS)/(rmax-rmin) (see notes in script): ');
lambda = optlam(xyzcyldata, targetrms);
fprintf('Optimal lambda for this dataset: %10.6f\n', lambda)

% create a square XY grid for resampling
disp('Resampling TPS...')
```

```
nx = input('Enter the number of grid points in a square XY grid: ');
ny = nx;
nresamp = 0;
disx = 1/nx; % increment on x-axis
disy = 1/ny; % increment on y-axis
for i = 1:(nx+1)
  for j = 1:(ny+1)
    nresamp = nresamp + 1;
    xyresamp(nresamp,1) = (i-1)*disx;
    xyresamp(nresamp,2) = (j-1)*disy;
  end
end

% now do the smoothing with this optimal lambda and resample to
% get the smooth surface
w = ones(n,1);
[outsurf] = tpssurf ( xyzcyldata, xyresamp, lambda, w);

% reshape outsurf into 3 matrices with ny rows and nx columns
xsurf = reshape(outsurf(:,1), ny+1, nx+1);
ysurf = reshape(outsurf(:,2), ny+1, nx+1);
zsurf = reshape(outsurf(:,3), ny+1, nx+1);

% draw lines in one direction
figure(4);
hold on
for i = 1:(nx+1)
  plot3(xsurf(:,i),ysurf(:,i),zsurf(:,i),'g');
end
% draw cross lines
for j = 1:(ny+1)
  plot3(xsurf(j,:),ysurf(j,:),zsurf(j,:),'g');
end

% get the co-ordinates of the resampled surface and view data
xs = outsurf(:,1);
ys = outsurf(:,2);
zs = outsurf(:,3);
figure(5)
surfl(xsurf,ysurf,zsurf)
display('hit any key to continue')
pause

%%%%%%%%%%%%%%%%%%%%%%%%% convertagain22.m %%%%%%%%%%%%%%%%%%%%%%%%%%%%

% now we will convert the cylindrical co-ordinates back to
% cartesian co-ordinate system

fprintf('Converting the coordinates back to cartesian coordinate
system')

for i = 1:((nx+1)*(ny+1))
    xs(i,1) = (xs(i,1)*(thetamax-thetamin)) + thetamin;
    ys(i,1) = (ys(i,1)*(zeemax-zeemin))+ zeemin;
    zs(i,1) = (zs(i,1)*(rmax-rmin))+ rmin;
```

```
end


backtonormal = zeros((nx+1)*(ny+1),3);
for i = 1:((nx+1)*(ny+1))
    backtonormal(i,1) = zs(i,1)*cos(xs(i,1));
    backtonormal(i,2) = zs(i,1)*sin(xs(i,1));
    backtonormal(i,3) = ys(i,1);
end

normal = zeros(3,(nx+1)*(ny+1));
backtonormal = backtonormal';

% rotation (transformation) matrix is
backrotation = inv([cos(beta) sin(beta)*sin(alpha) -
sin(beta)*cos(alpha);...
        0 cos(alpha) sin(alpha);...
        sin(beta) -sin(alpha)*cos(beta) cos(alpha)*cos(beta)]);

for i = 1:((nx+1)*(ny+1))
    normal(:,i) = backrotation * backtonormal(:,i);
end
backtonormal = backtonormal';
normal = normal';

for i = 1:n
    xyzdata(i,1) = xyzdata(i,1) + p(1,1); % translation of X-coordinate
    xyzdata(i,2) = xyzdata(i,2) + p(1,2); % translation of Y-coordinate
end

for i = 1: ((nx+1)*(ny+1))
    normal(i,1) = normal(i,1) + p(1,1); % trans^n of resampled X-coord
    normal(i,2) = normal(i,2) + p(1,2); % trans^n of resampled Y-coord
end

% reshape outsurf into 3 matrices with ny rows and nx columns
xsurf1 = reshape(normal(:,1), ny+1, nx+1);
ysurf1 = reshape(normal(:,2), ny+1, nx+1);
zsurf1 = reshape(normal(:,3), ny+1, nx+1);

% compare the fitted surface with original data set
figure(6)
surfl(xsurf1,ysurf1,zsurf1)
hold on
plot3(xyzdata(:,1), xyzdata(:,2), xyzdata(:,3),'o');
axis equal
%display('hit any key to continue')
%pause

%%%%%%%%%%%%%%%%%%%%%%%%%%%%%% discard22.m %%%%%%%%%%%%%%%%%%%%%%%%%%%%%%

% Time to discard unwanted resampled points
```

```matlab
fprintf('Now discarding unwanted resampled points...this may take some
time...Plz wait and be patient')

[norig, norigcol] = size(xyzdata);
[nresamp, nresampcol] = size(normal);

for i = 1: norig
    for j = 1: nresamp
    distance(i,j) = norm(normal(j,:) - xyzdata(i,:));
end
end

for i = 1: nresamp
    sdist(:,i) = sort(distance(:,i));
    eachpointavg(i,1) = mean(sdist(1,i));
end

% to find mean distance between entire set of points
% after we do sorting, just select first value as the min distance
% calculate all the minimum distances
% take average of all these distances
% this is mean distance

allaverage = mean(eachpointavg);

% discarding the resampled point
% if the average of three distances is greater than mean distance
% between entire dataset, then discard the resampled point

for i = 1: nresamp
    if eachpointavg(i,1) > allaverage
        normal(i,:) = NaN;
    end
end

% draw surface
xsurf2 = reshape(normal(:,1), ny+1, nx+1);
ysurf2 = reshape(normal(:,2), ny+1, nx+1);
zsurf2 = reshape(normal(:,3), ny+1, nx+1);

% compare the fitted surface with original data set
figure(7);
surfl(xsurf2,ysurf2,zsurf2);
hold on
plot3(xyzdata(:,1), xyzdata(:,2), xyzdata(:,3),'.');
axis equal
%display('hit any key to continue')
%pause

%%%%%%%%%%%%%%%%%%%%%%%%%%%% anatomical22.m %%%%%%%%%%%%%%%%%%%%%%%%%%%

% script to transform the origin from MRI axes to Anatomical axes of
the
% knee and then write the .3d file.
% Inputs are the medial and lateral epicondylar points on femur
```

```
% (Pm and Pl) and a point lying on the femoral axis (Pfaxis).

Pl = input('Enter lateral epicondylar point (in [x y z] format) : ');
Pm = input('Enter medial epicondylar point (in [x y z] format) : ');
Pfaxis = input('Enter point lying on femoral axis (in [x y z] format) :
');

% We will find out the unit vectors in each anatomical axis direction.

% Uy = -(Pl - Pm)/norm(Pl-Pm);
% Origin = (Pl+Pm)/2;
% Uz = -(Origin - Pfaxis)/norm(Origin - Pfaxis);
% Ux = cross(Uy,Uz);

% following changes are made to make my model coordinate system match
with
% robot coordinate system (reference JCS12.doc) and as per discussion
with
% Ton on 5/18/07


% Uy = -(Pl - Pm)/norm(Pl-Pm);
Origin = (Pl+Pm)/2;
Uz = (Pfaxis-Origin)/norm(Pfaxis-Origin);
% Uz = -(Origin - Pfaxis)/norm(Origin - Pfaxis);
Uy = cross(Uz,(Pm-Pl));
Uy = Uy/norm(Uy);
Ux = cross(Uy,Uz);
Ux = Ux/norm(Ux);

% Now we will find out the rotation matrix

R = [Ux; Uy; Uz]';

Panat = zeros(3,n);
Nanat = zeros(3,nresamp);

% Apply rotation matrix to MRI points

for i = 1:n
    Panat(:,i) = R * (xyzdata(i,:) - Origin)';
end

% Apply rotation matrix to resampled points

for i = 1:nresamp
    Nanat(:,i) = R * (normal(i,:) - Origin)';
end
Panat = Panat'/1000; % unit conversion to meter
Nanat = Nanat'/1000; % unit conversion to meter

% compare the fitted surface with original data set
xsurf3 = reshape(Nanat(:,1), ny+1, nx+1);
ysurf3 = reshape(Nanat(:,2), ny+1, nx+1);
```

```
zsurf3 = reshape(Nanat(:,3), ny+1, nx+1);
figure(8);
surfl(xsurf3,ysurf3,zsurf3);
hold on
plot3(Panat(:,1), Panat(:,2), Panat(:,3),'o');
axis equal
%display('hit any key to continue')
%pause

%%%%%%%%%%%%%%%%%%%%%%%%%%%%%% writer22.m %%%%%%%%%%%%%%%%%%%%%%%%%%%%%%

% simultaneously write the .3d file
% the script finds the rows and column numbers where data is present
% and writes it in .3D format.

% we reshape the data in the stacks of slices

fprintf('writing a .3D file...')

data(:,1,:) = reshape(Nanat(:,1),(nx+1),1,(ny+1));
data(:,2,:) = reshape(Nanat(:,2),(nx+1),1,(ny+1));
data(:,3,:) = reshape(Nanat(:,3),(nx+1),1,(ny+1));
p = 1;

% then we find out the rows and colums where data is present
% and discard the other points
% can we use this code instead??
% [notanumber] = find (isnan(tibia(:,1)));
%
% for ii = notanumber
%     tibia(ii,:) = [];
% end

m = 0;
for i = 1:(ny+1)
    while p < (nx+1)
        for k = p:(nx+1)
            if isnan(data(k,1,i)) == 0
                counter1 = k;
                counter2 = 1;
                break
            end
            counter1 = NaN;
        end
        for p =(k+1):(nx+1)
            if isnan(data(p,1,i)) == 1
                break
            end
            counter2 = counter2 + 1;
        end
        if isnan(counter1) == 0
            m = m+1;
            PM(m,:) = [counter1 counter2 i];
        end
        counter1 = NaN;
```

```
    end
    p = 1;
end

% Now we will create the .3d file.

[row, column] = size(PM);

filename = input('Save 3d file as (for e.g. femur_surf_1) : ','s');
fn3d = [filename '.3d'];
fid = fopen(fn3d,'w');
fprintf(fid,'%8.0f %8.0f\n', sum(PM(1:row,2)), row);
fprintf(fid,'%6.15f %6.15f %6.15f\n',...
                    max(Nanat(:,1)), min(Nanat(:,1)), max(Nanat(:,2)));
fprintf(fid,'%6.15f %6.15f %6.15f\n',...
                    min(Nanat(:,2)), max(Nanat(:,3)), min(Nanat(:,3)));
for i = 1:row
    fprintf(fid,'%3.0f %3.0f %3.0f\n', PM(i,1),PM(i,2),PM(i,3));
end
for i = 1:row
    fprintf(fid,'%4.15f %4.15f %4.15f\n',...
                    data((PM(i,1):(PM(i,1)+PM(i,2)-1)),:,PM(i,3))');
end
fclose(fid);
```

B3: Model input file

```
TITLE: 12 DOF simple model of knee joint
Convergence Criteria          !
     100,1.d-7,1.d-5          !* Max. iterations, Abs. error, Rel. error
     0.005,5.0                ! Max allowable change in A(m) and THETA(deg)
Description of Articular Surface Data   !
     5                        ! No. of articular surfaces
     0                        ! Body no. of surface 1
1135_tibsurf_med_S.3d         ! Tibia, medial surface
     0                        ! Body no. of surface 2
1135_tibsurf_lat_S.3d         ! Tibia, lateral surface
     1                        ! Body no. of surface 3
1135_femsurf.3d               ! Femur
       1                      ! Body no. of surface 4
1135_femsurf.3d               ! Femur
     0                        ! Body No. of surface 5
1135_mededge_38.3d            ! Tibia, medial bone edge
Description of Simplicial (Bone) surface data
     0                        ! No. of simplicial surfaces
Description of Body data      !
     7                        ! No. of bodies (other than ground)
Data for body 0 (ground)      ! Tibia
     20                       ! No. of entities
     1                        ! Entity 1 type 1= ligament insertion
  -0.084107468,  0.006898762, -0.003611592,      ! MCL1
     1                        ! Entity 2 type 1= ligament insertion
  -0.084221743,  0.005097154,  0.006111003,      ! MCL2
     1                        ! Entity 3 type 1= ligament insertion
  -0.081596239,  0.005364035,  0.015220040,      ! MCL3
     1                        ! Entity 4 type 1= ligament insertion
  -0.035748534, -0.005919792,  0.023141747,      ! PCL1 ALB
     1                         ! Entity 5 type 1= ligament insertion
  -0.039089490, -0.005093304,  0.025507161,      ! PCL2 MB
     1                        ! Entity 6 type 1= ligament insertion
  -0.042456414, -0.002788693,  0.029596357,      ! PCL3 PMB
     1                        ! Entity 7 type 1= ligament insertion
  -0.026808128, -0.003453381, -0.005947506,      ! ACL1 AMB
     1                        ! Entity 8 type 1= ligament insertion
  -0.030511268, -0.007214590, -0.006089709,      ! ACL2 MB
       1                      ! Entity 9 type 1= ligament insertion
  -0.031636648, -0.009033025, -0.003191889,      ! ACL3 PLB
       1                      ! Entity 10 type 1= ligament insertion
  -0.067284813, -0.056580661,  0.035283621,      ! LCL1
       1                      ! Entity 11 type 1= ligament insertion
  -0.064872294, -0.056186694,  0.037914134,      ! LCL2
```

```
      1                        ! Entity 12 type 1= ligament insertion
  -0.063378682,  -0.056036854,   0.043172759,      ! LCL3
    6                          ! Entity 13 type 6=bilinear patch surf
      1                        ! Surface no., contact with medial femur
      6                        ! Entity 14 type 6=bilinear patch surf
      2                        ! Surface no., contact with lateral femur
      6                        ! Entity 15 type 6=bilinear patch surf
      5                        ! Surface no., tibia medial bone contact mcl1_1
      6                        ! Entity 16 type=6bilinear patch surf
      5                        ! Surface no., tibia medial bone contact mcl1_2
      6                        ! Entity 17 type 6=bilinear patch surf
      5                        ! Surface no., tibia medial bone contact mcl2_1
      6                        ! Entity 18 type=6bilinear patch surf
      5                        ! Surface no., tibia medial bone contact mcl2_2
      6                        ! Entity 19 type 6=bilinear patch surf
      5                        ! Surface no., tibia medial bone contact mcl3_1
      6                        ! Entity 20 type=6bilinear patch surf
      5                        ! Surface no., tibia medial bone contact mcl3_2
Data for body 1                ! Femur
    F                          ! Particle status
    18                         ! No. of entities
    1                          ! Entity 1 type 1= ligament insertion
  -0.004769228,   0.046473667,  -0.001021253,      ! MCL1
    1                          ! Entity 2 type 1= ligament insertion
  -0.000100669,   0.045752990,   0.002343805,      ! MCL2
    1                          ! Entity 3 type 1= ligament insertion
   0.001061398,   0.044364227,   0.005569776,      ! MCL3
    1                          ! Entity 4 type 1= ligament insertion
  -0.009582339,   0.002739062,   0.000334912,      ! PCL1 ALB
    1                          ! Entity 5 type 1= ligament insertion
  -0.012838385,   0.005018050,   0.006232490,      ! PCL2 MB
    1                          ! Entity 6 type 1= ligament insertion
  -0.010961029,   0.006736792,   0.012740366,      ! PCL3 PMB
    1                          ! Entity 7 type 1= ligament insertion
   0.001207368,  -0.004671456,   0.012326747,      ! ACL1 AMB
    1                          ! Entity 8 type 1= ligament insertion
  -0.001464639,  -0.003616814,   0.010832752,      ! ACL2 MB
      1                        ! Entity 9 type 1= ligament insertion
  -0.006752469,  -0.006101877,   0.008686296,      ! ACL3 PLB
    1                          ! Entity 10 type 1= ligament insertion
   0.002579244,  -0.043989647,   0.006887139,      ! LCL1
    1                          ! Entity 11 type 1= ligament insertion
   0.002638733,  -0.044033192,   0.009007282,      ! LCL2
    1                          ! Entity 12 type 1= ligament insertion
   0.003428594,  -0.043927280,   0.010758874,      ! LCL3
    6                          ! Entity 13 type, 6=bilinear patch surf
```

```
       3                              ! Surface no., contact with medial tibia
       6                              ! Entity 14 type, 6=bilinear patch surf
       4                              ! Surface no., contact with lateral tibia
       2                              ! Entity 15 type, body fixed external force
 0.00E-0     0.00E-0     0.00E-0                      ! External force
 0.00E0      0.00E0      0.00E0                       ! Application and magnitude
       3                              ! Entity 16 type, body fixed external moment
 0.00E0      0.00E0      0.00E0  ! External moment
       4                              ! Entity 17 type, global external force
 0.00E0      0.00E0      0.00E0                       ! External force (global)
 0.00E0      0.00E0      0.00E0                       ! Application and magnitude
       5                              ! Entity 18 type, global external moment
 0.00E0      0.00E0      0.00E0                       ! External moment (global)
   0.00,  0.000,  -0.00               ! Initial guess for translation dof's
       F,F,F                          ! Constraint status on translation dof's
 0.000000E+00 0.000000E+00 0.000000E+00               ! Initial guess for rotation dof's
       F,T,F                          ! Constraint status on rotation dof's
Data for body 2                       ! MCL1_1 particle
          T                           ! Particle status
          3                           ! No. of entities
          1                           ! Entity 1 type 1= ligament insertion
   .000000,   .000000,   .000000,                     ! MCL1_1
          1                           ! Entity 2 type 1= ligament insertion
   .000000,   .000000,   .000000,                     ! MCL1_1
          1                           ! Entity 3 type 1= insertion
   .000000,   .000000,   .000000,                     ! MCL1_1 contact
  -0.042067370   0.027868888  -0.002239012            ! Initial guess for translation dof's
          F,F,F                       ! Constraint status on translation dof's
Data for body 3                       ! MCL1_2 particle
          T                           ! Particle status
          3                           ! No. of entities
          1                           ! Entity 1 type 1= ligament insertion
   .000000,  .000000,  .000000,                       ! MCL1_2
          1                           ! Entity 2 type 1= ligament insertion
   .000000,  .000000,  .000000,                       ! MCL1_2
          1                           ! Entity 3 type 1= insertion
   .000000,  .000000,  .000000,                       ! MCL1_2 contact
  -0.046539721   0.025638023  -0.002385031            ! Initial guess for translation dof's
          F,F,F                       ! Constraint status on translation dof's
Data for body 4                       ! MCL2_1 particle
          T                           ! Particle status
          3                           ! No. of entities
          1                           ! Entity 1 type 1= ligament insertion
   .000000,  .000000,  .000000,                       ! MCL2_1
          1                           ! Entity 2 type 1= ligament insertion
   .000000,  .000000,  .000000,                       ! MCL2_1
```

```
        1                          ! Entity 3 type 1= insertion
  .000000,  .000000,  .000000,                         ! MCL2_1 contact
 -0.041939171   0.025532382   0.004217461          ! Initial guess for translation dof's
        F,F,F                      ! Constraint status on translation dof's
Data for body 5                    ! MCL2_2 particle
        T                          ! Particle status
        3                          ! No. of entities
        1                          ! Entity 1 type 1= ligament insertion
  .000000,  .000000,  .000000,                         ! MCL2_2
        1                          ! Entity 2 type 1= ligament insertion
  .000000,  .000000,  .000000,                         ! MCL2_2
        1                          ! Entity 3 type 1= insertion
  .000000,  .000000,  .000000,                         ! MCL2_2 contact
  -0.047336946   0.022923630   0.004459190          ! Initial guess for translation dof's
        F,F,F                      ! Constraint status on translation dof's
Data for body 6                    ! MCL3_1 particle
        T                          ! Particle status
        3                          ! No. of entities
        1                          ! Entity 1 type 1= ligament insertion
  .000000,  .000000,  .000000,                         ! MCL3_1
        1                          ! Entity 2 type 1= ligament insertion
  .000000,  .000000,  .000000,                         ! MCL3_1
        1                          ! Entity 3 type 1= insertion
  .000000,  .000000,  .000000,                         ! MCL3_1 contact
 -0.040224451   0.024884405   0.010389891          ! Initial guess for translation dof's
        F,F,F                      ! Constraint status on translation dof's
Data for body 7                    ! MCL3_2 particle
        T                          ! Particle status
        3                          ! No. of entities
        1                          ! Entity 1 type 1= ligament insertion
  .000000,  .000000,  .000000,                         ! MCL3_2
        1                          ! Entity 2 type 1= ligament insertion
  .000000,  .000000,  .000000,                         ! MCL3_2
        1                          ! Entity 3 type 1= insertion
  .000000,  .000000,  .000000,                         ! MCL3_2 contact
  -0.044721384   0.022762626   0.010914907          ! Initial guess for translation dof's
        F,F,F                      ! Constraint status on translation dof's
Description of Link data           !
        26                         ! No. of links
Data for Link 1                    ! Fem to MCL1_1
        1                          ! Link type (ligament)
        1                          ! Body of first insertion
        2                          ! Body of second insertion
        1                          ! Entity number of first insertion
        1                          ! Entity number of second insertion
        8                          ! Lig type (non-lin, tension, F=ke**2/4e1)
```

```
     0.041281600        ! Resting length
     90000.0            ! Stiffness
   0.03                 ! e1 value
     0.1                ! linear stiffness term
Data for Link 2         ! MCL1_1 to MCL1_2
     1                  ! Link type (ligament)
     2                  ! Body of first insertion
     3                  ! Body of second insertion
     2                  ! Entity number of first insertion
     1                  ! Entity number of second insertion
     8                  ! Lig type (non-lin, tension, F=ke**2/4e1)
     .005               ! Resting length
     90000.0            !* Stiffness
   0.03                 ! e1 value
     0.1                ! linear stiffness term
Data for Link 3         ! MCL1_2 to Tib
     1                  ! Link type (ligament)
     3                  ! Body of first insertion
     0                  ! Body of second insertion
     2                  ! Entity number of first insertion
     1                  ! Entity number of second insertion
     8                  ! Lig type (non-lin, tension, F=ke**2/4e1)
     0.041580000        ! Resting length
     90000.0            !* Stiffness
   0.03                 ! e1 value
     0.1                ! linear stiffness term
Data for Link 4         ! Fem to MCL2_1
     1                  ! Link type (ligament)
     1                  ! Body of first insertion
     4                  ! Body of second insertion
     2                  ! Entity number of first insertion
     1                  ! Entity number of second insertion
     8                  ! Lig type (non-lin, tension, F=ke**2/4e1)
     0.046041320        ! Resting length
     90000.0            ! Stiffness
   0.03                 ! e1 value
     0.1                ! linear stiffness term
Data for Link 5         ! MCL2_1 to MCL2_2
     1                  ! Link type (ligament)
     4                  ! Body of first insertion
     5                  ! Body of second insertion
     2                  ! Entity number of first insertion
     1                  ! Entity number of second insertion
     8                  ! Lig type (non-lin, tension, F=ke**2/4e1)
     .006               ! Resting length
     90000.0            !* Stiffness
```

```
        0.03                    ! e1 value
          0.1                   ! linear stiffness term
Data for Link 6                 ! MCL2_2 to Tib
          1                     ! Link type (ligament)
          5                     ! Body of first insertion
          0                     ! Body of second insertion
          2                     ! Entity number of first insertion
          2                     ! Entity number of second insertion
          8                     ! Lig type (non-lin, tension, F=ke**2/4e1)
          0.040590000           ! Resting length
          90000.0               !* Stiffness
        0.03                    ! e1 value
          0.1                   ! linear stiffness term
Data for Link 7                 ! Fem to MCL3_1
          1                     ! Link type (ligament)
          1                     ! Body of first insertion
          6                     ! Body of second insertion
          3                     ! Entity number of first insertion
          1                     ! Entity number of second insertion
          8                     ! Lig type (non-lin, tension, F=ke**2/4e1)
          0.045445404           ! Resting length
          90000.0               ! Stiffness
        0.03                    ! e1 value
          0.1                   ! linear stiffness term
Data for Link 8                 ! MCL3_1 to MCL3_2
          1                     ! Link type (ligament)
          6                     ! Body of first insertion
          7                     ! Body of second insertion
          2                     ! Entity number of first insertion
          1                     ! Entity number of second insertion
          8                     ! Lig type (non-lin, tension, F=ke**2/4e1)
          .005                  ! Resting length
          90000.0               !* Stiffness
        0.03                    ! e1 value
          0.1                   ! linear stiffness term
Data for Link 9                 ! MCL3_2 to Tib
          1                     ! Link type (ligament)
          7                     ! Body of first insertion
          0                     ! Body of second insertion
          2                     ! Entity number of first insertion
          3                     ! Entity number of second insertion
          8                     ! Lig type (non-lin, tension, F=ke**2/4e1)
          0.040590000           ! Resting length
          90000.0               !* Stiffness
        0.03                    ! e1 value
          0.1                   ! linear stiffness term
```

Data for Link 10	! PCL1 ALB
1	! Link type (ligament)
1	! Body of first insertion
0	! Body of second insertion
4	! Entity number of first insertion
4	! Entity number of second insertion
8	! Lig type (non-lin, tension, F=ke**2/4e1)
0.041820102	! Resting length
56666.67	! Stiffness
0.03	! e1 value
0.1	! linear stiffness term
Data for Link 11	! PCL2 MB
1	! Link type (ligament)
1	! Body of first insertion
0	! Body of second insertion
5	! Entity number of first insertion
5	! Entity number of second insertion
8	! Lig type (non-lin, tension, F=ke**2/4e1)
0.036385685	! Resting length
56666.67	!* Stiffness
0.03	! e1 value
0.1	! linear stiffness term
Data for Link 12	! PCL3 PMB
1	! Link type (ligament)
1	! Body of first insertion
0	! Body of second insertion
6	! Entity number of first insertion
6	! Entity number of second insertion
8	! Lig type (non-lin, tension, F=ke**2/4e1)
0.036970510	! Resting length
56666.67	!* Stiffness
0.03	! e1 value
0.1	! linear stiffness term
Data for Link 13	! ACL1 AMB
1	! Link type (ligament)
1	! Body of first insertion
0	! Body of second insertion
7	! Entity number of first insertion
7	! Entity number of second insertion
8	! Lig type (non-lin, tension, F=ke**2/4e1)
0.034809720	! Resting length
50050.0	! Stiffness
0.03	! e1 value
0.1	! linear stiffness term
Data for Link 14	! ACL2 MB
1	! Link type (ligament)

```
            1                        ! Body of first insertion
            0                        ! Body of second insertion
            8                        ! Entity number of first insertion
            8                        ! Entity number of second insertion
            8                        ! Lig type (non-lin, tension, F=ke**2/4e1)
            0.032997177              ! Resting length
            50050.0                  !* Stiffness
          0.03                       ! e1 value
            0.1                      ! linear stiffness term
Data for Link 15                     ! ACL3 PLB
            1                        ! Link type (ligament)
            1                        ! Body of first insertion
            0                        ! Body of second insertion
            9                        ! Entity number of first insertion
            9                        ! Entity number of second insertion
            8                        ! Lig type (non-lin, tension, F=ke**2/4e1)
            0.027729141              ! Resting length
            50050.0                  !* Stiffness
          0.03                       ! e1 value
            0.1                      ! linear stiffness term
Data for Link 16                     ! LCL1
            1                        ! Link type (ligament)
            1                        ! Body of first insertion
            0                        ! Body of second insertion
            10                       ! Entity number of first insertion
            10                       ! Entity number of second insertion
            8                        ! Lig type (non-lin, tension, F=ke**2/4e1)
            0.074929190              ! Resting length
            32533.33                 ! Stiffness
          0.03                       ! e1 value
            0.1                      ! linear stiffness term
Data for Link 17                     ! LCL2
            1                        ! Link type (ligament)
            1                        ! Body of first insertion
            0                        ! Body of second insertion
            11                       ! Entity number of first insertion
            11                       ! Entity number of second insertion
            8                        ! Lig type (non-lin, tension, F=ke**2/4e1)
            0.072949482              ! Resting length
            32533.33                 !* Stiffness
          0.03                       ! e1 value
            0.1                      ! linear stiffness term
Data for Link 18                     ! LCL3
            1                        ! Link type (ligament)
            1                        ! Body of first insertion
            0                        ! Body of second insertion
```

12	! Entity number of first insertion
12	! Entity number of second insertion
8	! Lig type (non-lin, tension, F=ke**2/4e1)
0.073731659	! Resting length
32533.33	!* Stiffness
0.03	! e1 value
0.1	! linear stiffness term
Data for Link 19	! Medial tibio-femoral contact
2	! Link type (bilinear contact)
1	! Body of first insertion
0	! Body of second insertion
13	! Entity number of first insertion
13	! Entity number of second insertion
-.01	! Maximum overlap (1cm)
3	! Contact type
18.97d6	! Modulus
5.d-3	! Thickness of cartilage (5 mm)
Data for Link 20	! Lateral tibio-femoral contact
2	! Link type (bilinear contact)
1	! Body of first insertion
0	! Body of second insertion
14	! Entity number of first insertion
14	! Entity number of second insertion
-.01	! Maximum overlap (1cm)
3	! Contact type
18.97d6	! Modulus
5.d-3	! Thickness of cartilage (5 mm)
Data for Link 21	! MCL1_1 - tibia contact
5	! Link type (particle to surface)
2	! Body of first insertion
0	! Body of second insertion
3	! Entity number of first insertion
15	! Entity number of second insertion
-.005	! Maximum overlap (5mm)
1	! Contact type
1.d6	! Stiffness
Data for Link 22	! MCL1_2 - tibia contact
5	! Link type (particle to surface)
3	! Body of first insertion
0	! Body of second insertion
3	! Entity number of first insertion
16	! Entity number of second insertion
-.005	! Maximum overlap (5mm)
1	! Contact type
1.d6	! Stiffness
Data for Link 23	! MCL2_1 - tibia contact

```
         5                        ! Link type (particle to surface)
         4                        ! Body of first insertion
         0                        ! Body of second insertion
         3                        ! Entity number of first insertion
         17                       ! Entity number of second insertion
         -.005                    ! Maximum overlap (5mm)
         1                        ! Contact type
         1.d6                     ! Stiffness
Data for Link 24                  ! MCL2_2 - tibia contact
         5                        ! Link type (particle to surface)
         5                        ! Body of first insertion
         0                        ! Body of second insertion
         3                        ! Entity number of first insertion
         18                       ! Entity number of second insertion
         -.005                    ! Maximum overlap (5mm)
         1                        ! Contact type
         1.d6                     ! Stiffness
Data for Link 25                  ! MCL3_1 - tibia contact
         5                        ! Link type (particle to surface)
         6                        ! Body of first insertion
         0                        ! Body of second insertion
         3                        ! Entity number of first insertion
         19                       ! Entity number of second insertion
         -.005                    ! Maximum overlap (5mm)
         1                        ! Contact type
         1.d6                     ! Stiffness
Data for Link 26                  ! MCL3_2 - tibia contact
         5                        ! Link type (particle to surface)
         7                        ! Body of first insertion
         0                        ! Body of second insertion
         3                        ! Entity number of first insertion
         20                       ! Entity number of second insertion
         -.005                    ! Maximum overlap (5mm)
         1                        ! Contact type
         1.d6                     ! Stiffness
```

B4: MATLAB MEX function

The Mex-function interface is given by,

```
function [GF JAC TIB_F F_THETA] =
                  joint_model(fname,dof,ext_f,reslen,flex,ins,stiff);

% MEX function joint_model.mexw32
% This is the interface between MATLAB and fortran to access joint
% model software developed by Kwak et. al., 2000.
%
% Input:
%   fname   filename of .inp file
%   dof     Vector of degrees of freedom (1 x 23). Rotations are in
%           radians and translations are in meters
%                 Femur(X-tran, Y-tran, Z-tran, X-rot, Z-rot),
%                 Particle 1 to6 (X-tran, Y-tran, Z-tran)
%   ext_f   global external force and moment vector applied on femur
%           (1 x 5)
%                 distraction, medial force, posterior drawer, internal
%                 rotation moment, varus moment
%   reslen  resting length of each of 12 ligaments in the model
%           (1 x 12)
%                 MCL1,   MCL2,   MCL3,   PCL-ALB,   PCL-MB,   PCL-PMB,
%                 ACL-AMB,   ACL-MB,   ACL-PLB,   LCL1,   LCL2,   LCL3
%   flex    joint flexion in radians
%   ins     insertion coordinates of one bundle from each ligament
%           (3 x 8)
%                 TIBIA-MCL1(x,y,z),PCL1(x,y,z),ACL1(x,y,z),LCL1(x,y,z)
%                 FEMUR-MCL1(x,y,z),PCL1(x,y,z),ACL1(x,y,z),LCL1(x,y,z)
%   stiff       stiffness value of each ligament (1 x 4)
%
%
% Output:
%   GF      Generalized force vector giving force imbalance in the
%                 model (MAXDOF)
%   JAC     Global Jacobian Matrix (MAXDOF x MAXDOF)
%   TIB_F   Vector of forces acting on tibia body due to each entity
%                 attached to it (3 x MAXENT)
%   F_THETA femur rotation vector (3 x MAXNB)
%
%   The last three outputs are optional.
%   Jacobian matrix is needed while running optimiziations and TIB_F is
%   required to calculate the forces in ACL bundles after an
%   equilibrium is reached.
```

The MEX-function code is:

```
#include <C:/Program Files/MATLAB/R2007a/extern/include/fintrf.h>
c#include <C:/Program Files/MATLAB71/extern/include/fintrf.h>
c#include <C:/Program Files/MATLAB71/extern/include/mex.h>

    SUBROUTINE MEXFUNCTION(NLHS, PLHS, NRHS, PRHS)
    IMPLICIT     NONE
    INCLUDE          'model.inc'
    INCLUDE          'model_main.inc'
    INCLUDE          'model_data.inc'
    INCLUDE          'model_surf.inc'
    INCLUDE          'model_text.inc'
    INCLUDE          'iounit.inc'

c        Declare appropriate pointer type for platform
c        Any variable that ends up with _PR is used as a pointer
    MWPOINTER PLHS(*), PRHS(*)
    INTEGER MXGETM, MXGETN, MXISCHAR, MXISNUMERIC
    MWPOINTER MXCREATEDOUBLEMATRIX, MXGETPR
    MWPOINTER MXCREATESTRING, MXGETSTRING
    INTEGER NLHS, NRHS
c        Decalre pointers for input and output variables
    MWPOINTER Qinput_PR, EXTFORCES_PR, FLEXION_PR
    MWPOINTER RESTLENGTH_PR, INSERTION_PR, STIFF_PR
    MWPOINTER A_OUT_PR, THETA_OUT_PR
    MWPOINTER GF_OUT_PR, JAC_OUT_PR
    CHARACTER*255 INP_FNAME
c        Declare other variables needed
c        FNAME_STATS and STRLEN are needed for checking the correct INP_FNAME
         input
c        trulen in integer function needed to cut the extra space after INP_FNAME
    INTEGER FNAME_STATS, STRLEN, trulen
    INTEGER DOFM, DOFN, EXTFM, EXTFN, RLM, RLN, FLEXM, FLEXN
    INTEGER INSM, INSN, STIM, STIN, J, K
    INTEGER SIZE2, SIZE3, SIZE4, SIZE5, SIZE6, SIZE7
c        Declare input and output variables that will be used to call joint model program
    REAL*8 Qinput(23,1), EXTFORCES(5), FLEXION(1)
    REAL*8 RESTLENGTH(12), INSERTION(8,3), STIFF(4)
    REAL*8 RATIO1,RATIO2,RATIO3,INSDIFF(8,3)
    REAL*8 MCLTIB(3,3), MCLFEM(3,3), PCLTIB(3,3), PCLFEM(3,3)
    REAL*8 ACLTIB(3,3), ACLFEM(3,3), LCLTIB(3,3), LCLFEM(3,3)
c     REAL*8 JAC_OUT(MAXDOF,MAXDOF), GF_OUT(MAXDOF)
c        Qinput is the femur translation and rotation matrix. if we have patella as well,
         then Qinput
c        will become 4*3 matrix instead of 2*3.
c        EXTFORCES is the matrix that defines "global" external forces and moments
```

```
        acting on the
c       femur body. if you want to change these to local forces, then see the notes in
        notebook # 8
c       or # 9 for using correct variable names.

      INTEGER MODEL_LOADED
      CHARACTER*80          FLIS
      COMMON /MODELINIT/RATIO1,RATIO2,RATIO3
      COMMON /MODELINIT/MCLTIB,MCLFEM,PCLTIB,PCLFEM
      COMMON /MODELINIT/ACLTIB,ACLFEM,LCLTIB,LCLFEM
      COMMON /MODELINIT/MODEL_LOADED
c       MODEL_LOADED = 100     ! no need to initialize the model_loaded value
c       End of model parameter declarations


c       check for proper number of arguments
      IF (NRHS.NE.7) THEN
        CALL MEXERRMSGTXT ('SEVEN INPUT ARGUMENTS REQUIRED')
      ELSEIF (NLHS.LT.1) THEN
        CALL MEXERRMSGTXT('AT LEAST ONE OUTPUT IS REQUIRED')
      ELSEIF (NLHS.GT.4) THEN
        CALL MEXERRMSGTXT('AT MOST FOUR OUTPUTS ARE ALLOWED')

c       first input must be a string
      ELSEIF (MXISCHAR(PRHS(1)).NE.1) THEN
        CALL MEXERRMSGTXT ('FIRST INPUT MUST BE A FILENAME')
      END IF

c       get the length of the input filename
      STRLEN = MXGETM(PRHS(1))*MXGETN(PRHS(1))
c       get the string contents (dereference the input integer)
      FNAME_STATS = MXGETSTRING(PRHS(1), INP_FNAME, 80)
c       check if mxgetstring is successful
      IF (FNAME_STATS.NE.0) THEN
        CALL MEXERRMSGTXT('STRING LENGTH MUST BE LESS THAN 80')
      END IF


c       get the size of the SECOND input array
      DOFM = MXGETM (PRHS(2))
      DOFN = MXGETN (PRHS(2))
      SIZE2 = DOFM*DOFN
c       get the size of the THIRD input array
      EXTFM = MXGETM (PRHS(3))
      EXTFN = MXGETN (PRHS(3))
      SIZE3 = EXTFM*EXTFN
```

```
c        get the size of the FOURTH input array
      RLM = MXGETM (PRHS(4))
      RLN = MXGETN (PRHS(4))
      SIZE4 = RLM*RLN

c        get the size of the FIFTH input array
      FLEXM = MXGETM (PRHS(5))
      FLEXN = MXGETN (PRHS(5))
      SIZE5 = FLEXM*FLEXN

c        get the size of the FIFTH input array
      INSM = MXGETM (PRHS(6))
      INSN = MXGETN (PRHS(6))
      SIZE6 = INSM*INSN

c        get the size of the FIFTH input array
      STIM = MXGETM (PRHS(7))
      STIN = MXGETN (PRHS(7))
      SIZE7 = STIM*STIN

c        check to ensure the input is a number
      IF (MXISNUMERIC(PRHS(2)).EQ.0) THEN
        CALL MEXERRMSGTXT('INPUT # 2 IS A 23*1 INITIAL DOF ARRAY')
      ELSEIF (MXISNUMERIC(PRHS(3)).EQ.0) THEN
        CALL MEXERRMSGTXT('INPUT # 3 IS A 5*1 EXT. FORCES ARRAY')
      ELSEIF (MXISNUMERIC(PRHS(4)).EQ.0) THEN
        CALL MEXERRMSGTXT ('INPUT # 4 IS A 12*1 RES_LENGTH ARRAY')
      ELSEIF (MXISNUMERIC(PRHS(5)).EQ.0) THEN
        CALL MEXERRMSGTXT ('INPUT # 5 IS A 1*1 FLEXION ANGLE')
      ELSEIF (MXISNUMERIC(PRHS(6)).EQ.0) THEN
        CALL MEXERRMSGTXT ('INPUT # 6 IS A 8*3 INSERTIONS ARRAY')
      ELSEIF (MXISNUMERIC(PRHS(7)).EQ.0) THEN
        CALL MEXERRMSGTXT ('INPUT # 7 IS A 4*1 STIFFNESS ARRAY')
      END IF

c        create matrix for return argument
c        if input vector q is  mm*1  column vector then maxdof = mm and jac becomes
         mm*mm matrix
      Qinput_PR = MXGETPR (PRHS(2))
      EXTFORCES_PR = MXGETPR (PRHS(3))
      RESTLENGTH_PR = MXGETPR (PRHS(4))
      FLEXION_PR = MXGETPR (PRHS(5))
      INSERTION_PR = MXGETPR(PRHS(6))
      STIFF_PR = MXGETPR(PRHS(7))

c        load the data in fortran arrays
```

```
      CALL MXCOPYPTRTOREAL8 (Qinput_PR, Qinput, SIZE2)
      CALL MXCOPYPTRTOREAL8 (EXTFORCES_PR, EXTFORCES, SIZE3)
      CALL MXCOPYPTRTOREAL8 (RESTLENGTH_PR, RESTLENGTH, SIZE4)
      CALL MXCOPYPTRTOREAL8 (FLEXION_PR, FLEXION, SIZE5)
      CALL MXCOPYPTRTOREAL8 (INSERTION_PR, INSERTION, SIZE6)
      CALL MXCOPYPTRTOREAL8 (STIFF_PR, STIFF, SIZE7)

      FNAME = INP_FNAME(:trulen(INP_FNAME))//'.INP'
      FLIS = INP_FNAME(:trulen(INP_FNAME))//'.LIS'

c         here first action is to load the input file if not already loaded
      IF (MODEL_LOADED.NE.2008) THEN
c         now call the subroutine to load the input file
      CALL MODEL_INIT
      CALL IO_OPEN(FLIS)
      MODEL_LOADED = 2008
c         now call the subroutine to read the input parameters
      CALL INPUT_MODEL
c         store the fixed ratios MCL_TIBIA/MCL_FEMUR for 3 MCLs
      RATIO1 = ATTRIB(7,3)/ATTRIB(7,1)
      RATIO2 = ATTRIB(7,6)/ATTRIB(7,4)
      RATIO3 = ATTRIB(7,9)/ATTRIB(7,7)
C         store the original insertion points
        DO J = 1,3
          DO K = 1,3
            MCLTIB(J,K) = PI(K,J,1)
            PCLTIB(J,K) = PI(K,J+3,1)
            ACLTIB(J,K) = PI(K,J+6,1)
            LCLTIB(J,K) = PI(K,J+9,1)
            MCLFEM(J,K) = PI(K,J,2)
            PCLFEM(J,K) = PI(K,J+3,2)
            ACLFEM(J,K) = PI(K,J+6,2)
            LCLFEM(J,K) = PI(K,J+9,2)
          END DO
        END DO
      END IF

cccccccccccccccccccccccccccccccccccccccccccccccccccccccccccccccccccccccc
cccccccccccccccccccccccccccccccccccccccccccccccccccccccccccccccccccccccc
c         create matrix for return argument
      IF (NLHS.EQ.1) THEN
          PLHS(1) = MXCREATEDOUBLEMATRIX(MAXDOF, 1, 0) ! this is for GF
          GF_OUT_PR = MXGETPR (PLHS(1))
      ELSEIF (NLHS.EQ.2) THEN
          PLHS(1) = MXCREATEDOUBLEMATRIX(MAXDOF, 1, 0) ! this is for GF
          PLHS(2) = MXCREATEDOUBLEMATRIX(MAXDOF, MAXDOF, 0) ! this is
```

```
                                                             for JACOBIAN
          GF_OUT_PR = MXGETPR (PLHS(1))
          JAC_OUT_PR = MXGETPR (PLHS(2))
      ELSEIF (NLHS.EQ.3) THEN
          PLHS(1) = MXCREATEDOUBLEMATRIX(MAXDOF, 1, 0) ! this is for GF
          PLHS(2) = MXCREATEDOUBLEMATRIX(MAXDOF, MAXDOF, 0) ! this is
                                                             for JACOBIAN
          PLHS(3) = MXCREATEDOUBLEMATRIX(3, NBODY, 0)        ! for
                                                              translations
          GF_OUT_PR = MXGETPR (PLHS(1))
          JAC_OUT_PR = MXGETPR (PLHS(2))
          A_OUT_PR = MXGETPR (PLHS(3))
      ELSEIF (NLHS.EQ.4) THEN
          PLHS(1) = MXCREATEDOUBLEMATRIX(MAXDOF, 1, 0) ! this is for GF
          PLHS(2) = MXCREATEDOUBLEMATRIX(MAXDOF, MAXDOF, 0) ! this is
                                                             for JACOBIAN
          PLHS(3) = MXCREATEDOUBLEMATRIX(3, NBODY, 0)        ! for
                                                              translations
          PLHS(4) = MXCREATEDOUBLEMATRIX(3, NBODY, 0)        ! for rotations
          GF_OUT_PR = MXGETPR (PLHS(1))
          JAC_OUT_PR = MXGETPR (PLHS(2))
          A_OUT_PR = MXGETPR (PLHS(3))
          THETA_OUT_PR = MXGETPR (PLHS(4))
      END IF

C         COPY TRANSLATIONS - body 2 - femur
      A(1,2) = Qinput(1,1)
      A(2,2) = Qinput(2,1)
      A(3,2) = Qinput(3,1)
C         COPY ROTATIONS - body 2 - femur
      THETA(1,2)=Qinput(4,1)
      THETA(2,2)=FLEXION(1)        ! This is femur flexion set externally.
      THETA(3,2)=Qinput(5,1)
C         COPY TRANSLATIONS - body 3 - particle1
      A(1,3) = Qinput(6,1)
      A(2,3) = Qinput(7,1)
      A(3,3) = Qinput(8,1)
C         COPY TRANSLATIONS - body 4 - particle2
      A(1,4) = Qinput(9,1)
      A(2,4) = Qinput(10,1)
      A(3,4) = Qinput(11,1)
C         COPY TRANSLATIONS - body 5 - particle3
      A(1,5) = Qinput(12,1)
      A(2,5) = Qinput(13,1)
      A(3,5) = Qinput(14,1)
C         COPY TRANSLATIONS - body 6 - particle4
```

```
      A(1,6) = Qinput(15,1)
      A(2,6) = Qinput(16,1)
      A(3,6) = Qinput(17,1)
C       COPY TRANSLATIONS - body 7 - particle5
      A(1,7) = Qinput(18,1)
      A(2,7) = Qinput(19,1)
      A(3,7) = Qinput(20,1)
C       COPY TRANSLATIONS - body 8 - particle6
      A(1,8) = Qinput(21,1)
      A(2,8) = Qinput(22,1)
      A(3,8) = Qinput(23,1)
C       COPY FORCES
      F(1,17,2)=EXTFORCES(1)
      F(2,17,2)=EXTFORCES(2)
      F(3,17,2)=EXTFORCES(3)
C       COPY MOMENTS
      M(1,18,2)=EXTFORCES(4)
C     M(2,18,2)=EXTFORCES(5)
      M(3,18,2)=EXTFORCES(5)

c       change the ligament resting lengths here
      ATTRIB (7,1) = RESTLENGTH(1)        ! MCL1 - FEM TO PARTICLE 1
      ATTRIB (7,4) = RESTLENGTH(2)        ! MCL2 - FEM TO PARTICLE 3
      ATTRIB (7,7) = RESTLENGTH(3)        ! MCL3 - FEM TO PARTICLE 5
      ATTRIB (7,3) = RESTLENGTH(1)*RATIO1     ! MCL1 - TIB TO PARTICLE 2
      ATTRIB (7,6) = RESTLENGTH(2)*RATIO2     ! MCL2 - TIB TO PARTICLE 4
      ATTRIB (7,9) = RESTLENGTH(3)*RATIO3     ! MCL3 - TIB TO PARTICLE 6
      ATTRIB (7,10) = RESTLENGTH(4)       ! PCL1
      ATTRIB (7,11) = RESTLENGTH(5)       ! PCL2
      ATTRIB (7,12) = RESTLENGTH(6)       ! PCL3
      ATTRIB (7,13) = RESTLENGTH(7)       ! ACL1 - AMB
      ATTRIB (7,14) = RESTLENGTH(8)       ! ACL2 - MB
      ATTRIB (7,15) = RESTLENGTH(9)       ! ACL3 - PLB
      ATTRIB (7,16) = RESTLENGTH(10)      ! LCL1
      ATTRIB (7,17) = RESTLENGTH(11)      ! LCL2
      ATTRIB (7,18) = RESTLENGTH(12)      ! LCL3

cccccccccccccccccccccccccccccccccccccccccccccccccccccccccccccccccccccccc

C       CHANGE THE LIGAMENT INSERTIONS HERE
c       GET THE DIFFERENCE FROM ORIGINAL INSERTION POINT
       DO K = 1,3
        INSDIFF(1,K) = MCLTIB(1,K) - INSERTION(1,K)
        INSDIFF(2,K) = PCLTIB(1,K) - INSERTION(2,K)
        INSDIFF(3,K) = ACLTIB(1,K) - INSERTION(3,K)
        INSDIFF(4,K) = LCLTIB(1,K) - INSERTION(4,K)
```

```
     INSDIFF(5,K) = MCLFEM(1,K) - INSERTION(5,K)
     INSDIFF(6,K) = PCLFEM(1,K) - INSERTION(6,K)
     INSDIFF(7,K) = ACLFEM(1,K) - INSERTION(7,K)
     INSDIFF(8,K) = LCLFEM(1,K) - INSERTION(8,K)
    END DO
C       TIBIA INSERTIONS FIRST
    DO K = 1,3
      PI (K,1,1) = INSERTION(1,K) !  MCL1 - TIB INSERTION
      PI (K,4,1) = INSERTION(2,K) !  PCL1 - TIB INSERTION
      PI (K,7,1) = INSERTION(3,K) !  ACL1 - TIB INSERTION
      PI (K,10,1) = INSERTION(4,K)         !  LCL1 - TIB INSERTION
      PI (K,1,2) = INSERTION(5,K) !  MCL1 - FEM INSERTION
      PI (K,4,2) = INSERTION(6,K) !  PCL1 - FEM INSERTION
      PI (K,7,2) = INSERTION(7,K) !  ACL1 - FEM INSERTION
      PI (K,10,2) = INSERTION(8,K)         !  LCL1 - FEM INSERTION
              PI (K,2,1) = MCLTIB(2,K)+INSDIFF(1,K) !  MCL2 - TIB INSERTION
      PI (K,3,1) = MCLTIB(3,K)+INSDIFF(1,K)     !  MCL3 - TIB INSERTION
      PI (K,5,1) = PCLTIB(2,K)+INSDIFF(2,K)     !  PCL2 - TIB INSERTION
      PI (K,6,1) = PCLTIB(3,K)+INSDIFF(2,K)     !  PCL3 - TIB INSERTION
      PI (K,8,1) = ACLTIB(2,K)+INSDIFF(3,K)     !  ACL2 - TIB INSERTION
      PI (K,9,1) = ACLTIB(3,K)+INSDIFF(3,K)     !  ACL3 - TIB INSERTION
      PI (K,11,1) = LCLTIB(2,K)+INSDIFF(4,K)    !  LCL2 - TIB INSERTION
      PI (K,12,1) = LCLTIB(3,K)+INSDIFF(4,K)    !  LCL3 - TIB INSERTION
              PI (K,2,2) = MCLFEM(2,K)+INSDIFF(5,K)         !  MCL2 - TIB
INSERTION
      PI (K,3,2) = MCLFEM(3,K)+INSDIFF(5,K)     !  MCL3 - TIB INSERTION
      PI (K,5,2) = PCLFEM(2,K)+INSDIFF(6,K)     !  PCL2 - TIB INSERTION
      PI (K,6,2) = PCLFEM(3,K)+INSDIFF(6,K)     !  PCL3 - TIB INSERTION
      PI (K,8,2) = ACLFEM(2,K)+INSDIFF(7,K)     !  ACL2 - TIB INSERTION
      PI (K,9,2) = ACLFEM(3,K)+INSDIFF(7,K)     !  ACL3 - TIB INSERTION
      PI (K,11,2) = LCLFEM(2,K)+INSDIFF(8,K)    !  LCL2 - TIB INSERTION
      PI (K,12,2) = LCLFEM(3,K)+INSDIFF(8,K)    !  LCL3 - TIB INSERTION
    END DO

ccccccccccccccccccccccccccccccccccccccccccccccccccccccccccccccccccccccccc

c       change the ligament stiffness lengths here
   ATTRIB (8,1) = STIFF(1)         ! MCL1 - FEM TO PARTICLE 1
   ATTRIB (8,4) = STIFF(1)         ! MCL2 - FEM TO PARTICLE 3
   ATTRIB (8,7) = STIFF(1)         ! MCL3 - FEM TO PARTICLE 5
   ATTRIB (8,3) = STIFF(1)         ! MCL1 - TIB TO PARTICLE 2
   ATTRIB (8,6) = STIFF(1)         ! MCL2 - TIB TO PARTICLE 4
   ATTRIB (8,9) = STIFF(1)         ! MCL3 - TIB TO PARTICLE 6
   ATTRIB (8,2) = STIFF(1)         ! MCL1 - MCL1 TO PARTICLE 2
   ATTRIB (8,5) = STIFF(1)         ! MCL2 - MCL2 TO PARTICLE 4
   ATTRIB (8,8) = STIFF(1)         ! MCL3 - MCL3 TO PARTICLE 6
```

```
      ATTRIB (8,10) = STIFF(2)        ! PCL1
      ATTRIB (8,11) = STIFF(2)        ! PCL2
      ATTRIB (8,12) = STIFF(2)        ! PCL3
      ATTRIB (8,13) = STIFF(3)        ! ACL1 - AMB
      ATTRIB (8,14) = STIFF(3)        ! ACL2 - MB
      ATTRIB (8,15) = STIFF(3)        ! ACL3 - PLB
      ATTRIB (8,16) = STIFF(4)        ! LCL1
      ATTRIB (8,17) = STIFF(4)        ! LCL2
      ATTRIB (8,18) = STIFF(4)        ! LCL3

cccccccccccccccccccccccccccccccccccccccccccccccccccccccccccccccccccccccccccc
cccccccccccccccccccccccccccccccccccccccccccccccccccccccccccccccccccccccccccc
c     Now call the GF and Jacobian calculation algorithm
      CALL CALC_MODEL
cccccccccccccccccccccccccccccccccccccccccccccccccccccccccccccccccccccccccccc
c     get the GF and Jacobian matrix out to MATLAB
      IF (NLHS.EQ.1) THEN
         CALL MXCOPYREAL8TOPTR (GF, GF_OUT_PR, MAXDOF*1)
      ELSEIF (NLHS.EQ.2) THEN
         CALL MXCOPYREAL8TOPTR (GF, GF_OUT_PR, MAXDOF*1)
         CALL MXCOPYREAL8TOPTR (JAC, JAC_OUT_PR, MAXDOF*MAXDOF)
      ELSEIF (NLHS.EQ.3) THEN
         CALL MXCOPYREAL8TOPTR (GF, GF_OUT_PR, MAXDOF*1)
         CALL MXCOPYREAL8TOPTR (JAC, JAC_OUT_PR, MAXDOF*MAXDOF)
         CALL MXCOPYREAL8TOPTR (A, A_OUT_PR, 3*NBODY)
      ELSEIF (NLHS.EQ.4) THEN
         CALL MXCOPYREAL8TOPTR (GF, GF_OUT_PR, MAXDOF*1)
         CALL MXCOPYREAL8TOPTR (JAC, JAC_OUT_PR, MAXDOF*MAXDOF)
         CALL MXCOPYREAL8TOPTR (A, A_OUT_PR, 3*NBODY)
         CALL MXCOPYREAL8TOPTR (THETA, THETA_OUT_PR, 3*NBODY)

      END IF

      RETURN
      END
```

B5: Algorithm to convert JCS to attitude vector and attitude vector to JCS

```
%======================================================================

function [T] = attitude2matrix(angles, trans);

% equations are from
% http://www.euclideanspace.com/maths/geometry/rotations/
% conversions/angleToMatrix/

% angles are XYZ components of attitude vector

      eps = 1e-6;
      if(numel(angles) ~= 3 || numel(trans) ~= 3)
            error('attitude2matrix: incorrect inputs');
      end

      % amount of rotation
      ang = norm(angles);

      % unit vector along axis of rotation
      x = angles(1)/ang;
      y = angles(2)/ang;
      z = angles(3)/ang;

      % generate the transformation matrix
      s = sin(ang);
      c = cos(ang);
      t = 1-c;
      T = [ t*x*x+c     t*x*y-z*s   t*x*z+y*s   trans(1); ...
            t*x*y+z*s   t*y*y+c     t*y*z-x*s   trans(2); ...
            t*x*z-y*s   t*y*z+x*s   t*z*z+c     trans(3); ...
            0           0           0                 1];

end

%======================================================================

function [T] = JCS2matrix(angles, trans);

% convert from Robot lab JCS variables to transformation matrix for
% joint model

% angles are: flexion, valgus, internal rotation of tibia relative to
% femur
% translations are: medial, posterior, superior translation of tibia
% relative to femur (on JCS axes)

% the following equations come from JCS13.doc from robot lab: FEM_TIB
% transformation function
% These represent tibia motion relative to femur, in the coordinate
% system
% X is medial, Y is posterior, Z is superior

      eps = 1e-6;
      if(numel(angles) ~= 3 || numel(trans) ~= 3)
```

```
		error('JCS2matrix: incorrect inputs');
	end

	c = cos(angles);
	s = sin(angles);

	% rotation and translation on flexion axis
	T1 = [1     0     0     trans(1)    ; ...
	      0     c(1)  -s(1) 0           ; ...
	      0     s(1)  c(1)  0           ; ...
	      0     0     0     1           ];

	% rotation and translation on valgus axis
	T2 = [c(2)  0     s(2)  0           ; ...
	      0     1     0     trans(2)    ; ...
	      -s(2) 0     c(2)  0           ; ...
	      0     0     0     1           ];

	% rotation and translation on tibia (internal rotation) axis
	T3 = [c(3)  -s(3) 0     0           ; ...
	      s(3)  c(3)  0     0           ; ...
	      0     0     1     trans(3)    ; ...
	      0     0     0     1           ];

	% T is the matrix that describes tibia motion relative to femur
using JCS variables
	T = T1*T2*T3;

% in knee model, X is superior, Y is medial, Z is posterior
% so we need to rearrange the T matrix to get the T matrix for knee
model coordinate system
% we also need to invert it, to describe femur motion relative to tibia
	order = [3 1 2 4];
	T = inv(T(order,order));

end

%=======================================================================

function [angles, trans] = matrix2attitude(T);

% code for rotation adapted from PRP.FORTRAN by H.J. Woltring
% (www.biomch-l.org/files)

	sqrtol = 1e-6;

	phi(1) = 0.5 * ( T(3,2) - T(2,3) );
	phi(2) = 0.5 * ( T(1,3) - T(3,1) );
	phi(3) = 0.5 * ( T(2,1) - T(1,2) );
	si = norm(phi);
	ci = max(-1, 0.5*(T(1,1)+T(2,2)+T(3,3)-1) );
	sk = atan2(si,ci);                  % theta

	if (si+ci > 0.0)              % 0 <= theta < 3*PI/4
		if (si > sqrtol)
			ck = sk / si;           % theta / sin(theta)
		end
```

```
      else                                % 3*PI/4 <= theta <= PI
            k = 0;
            ck = 0.0;
            for i=1:3
                  if (abs(phi(i)) >= abs(ck))
                        k = i;
                        ck = phi(i);
                  end
            end
            for i=1:3
                  if (i == k)
                        phi(i) = T(i,k) - ci;
                  else
                        phi(i) = 0.5 * ( T(i,k) + T(k,i) );
                  end
            end
            ck = sign(ck)*sk/norm(phi)
      end
      angles = ck*phi;

% for translation, simply take them out of column 4 of T

      trans = T(1:3,4);

end

%======================================================================

function [angles, trans] = matrix2JCS(T);

% first we need to reorder the matrix from knee model coordinate system
% to robot lab coordinate system
% knee model:     X is superior     Y is medial       Z is posterior
% robot lab:      Z is superior     X is medial       Y is posterior
% we also need to invert matrix because knee model describes femur
% motion relative to tibia

      order = [2 3 1 4];
      T = inv(T(order,order));

% see JCS13 document from robot lab, equations are in KNEE_RobotToJCS
% MATLAB atan2 function needs sin,cos as inputs (not cos,sin as in
% Labview!)

      angles(1) = -atan2( T(2,3) , T(3,3) );
      angles(2) = atan2( T(1,3) , sqrt( T(2,3)^2 + T(3,3)^2 ) );
      angles(3) = -atan2( T(1,2) , T(1,1) );
      trans(2) = T(2,4)*cos(angles(1)) + T(3,4)*sin(angles(1));
      trans(3) = -(T(2,4)*sin(angles(1)) -
      T(3,4)*cos(angles(1)))/cos(angles(2));
      trans(1) = T(1,4) - trans(3)*sin(angles(2));

end
```

APPENDIX C

C1: Optimization fit for models using objective function of 'AP-IE-VV combined' set

Optimization fit for Model # 1 using objective function of 'AP-IE-VV combined' set

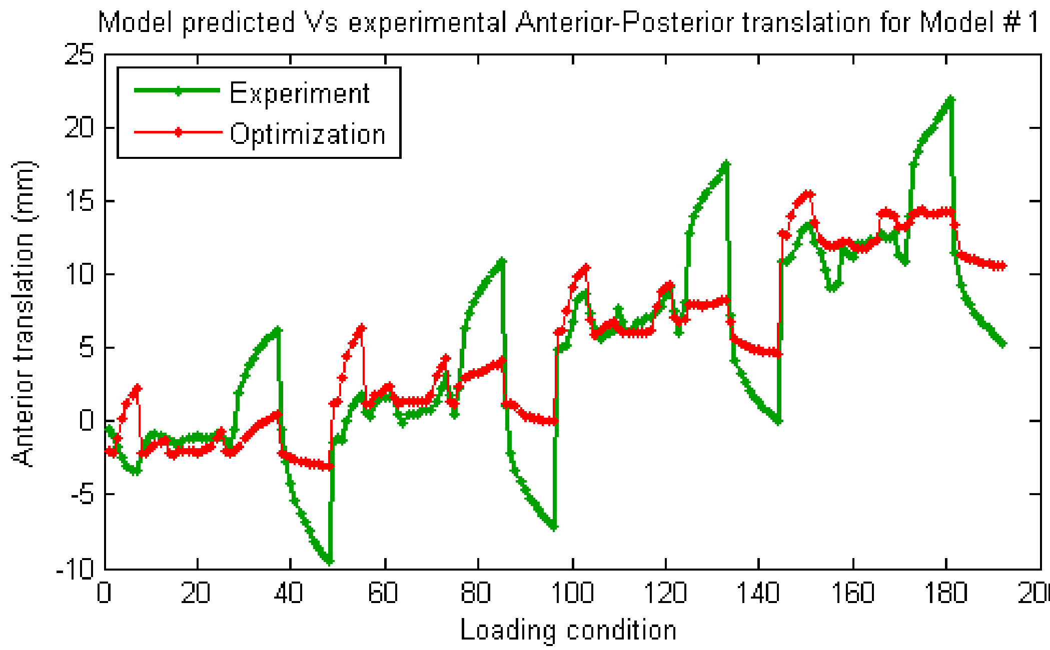

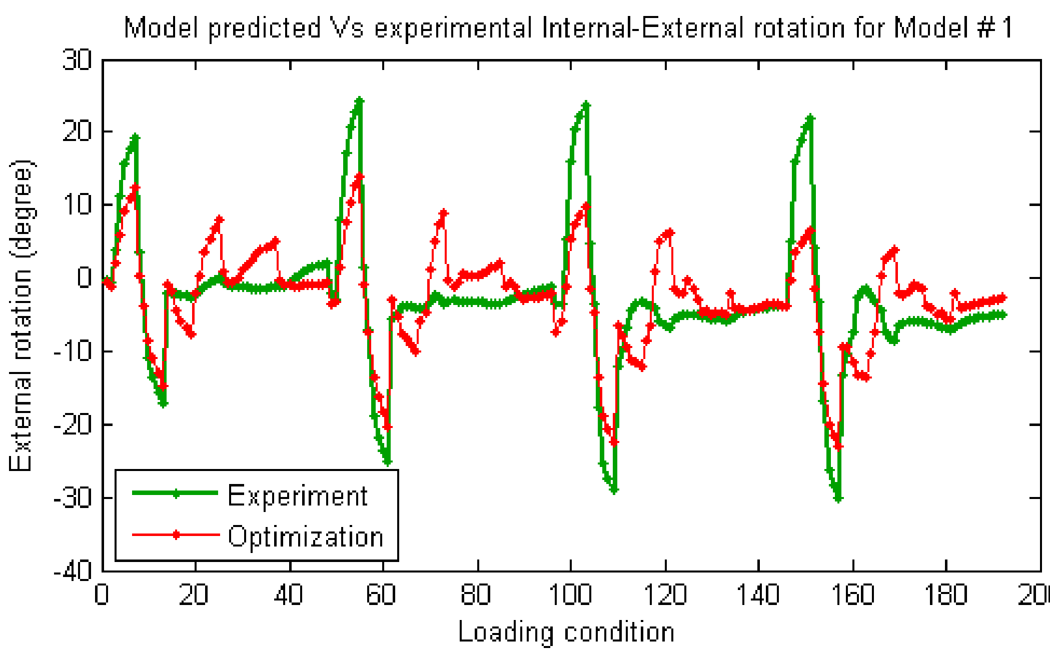

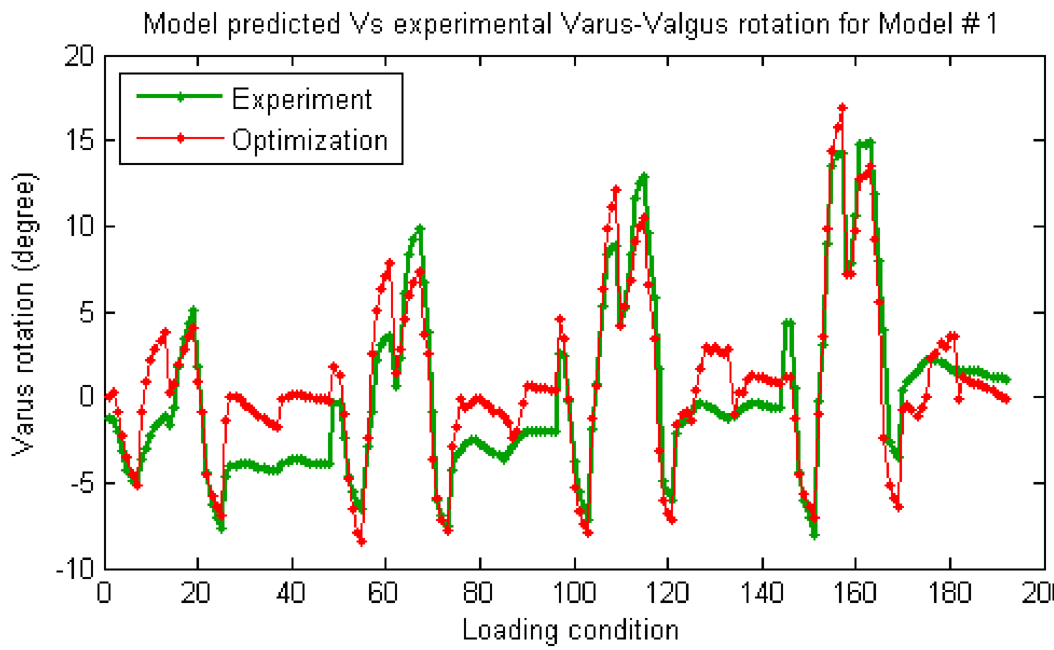

Optimization fit for Model # 2 using objective function of 'AP-IE-VV combined' set

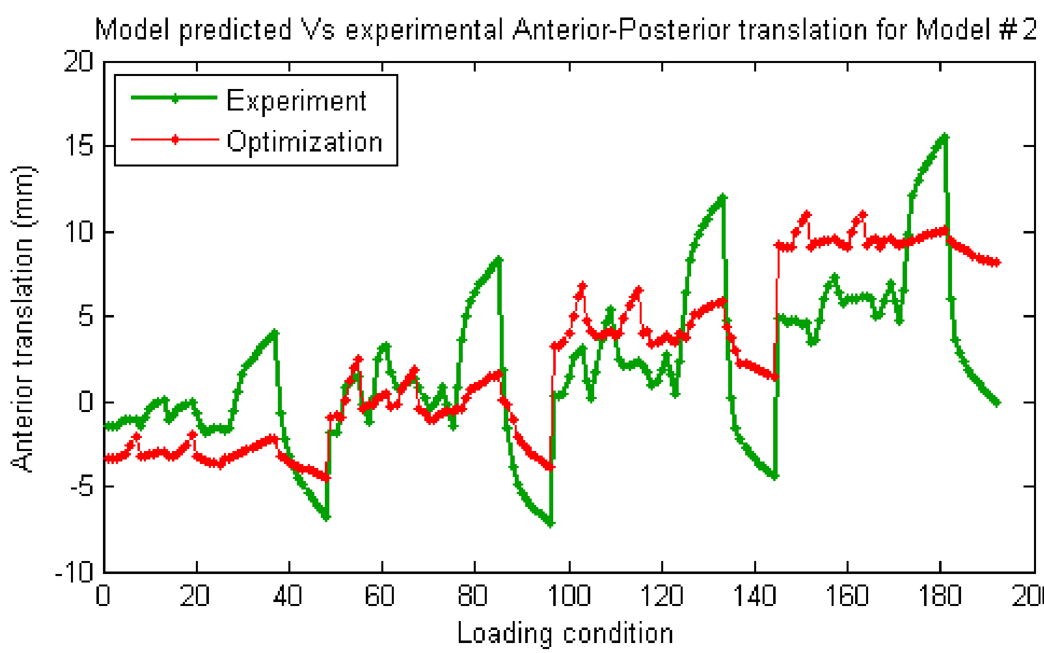

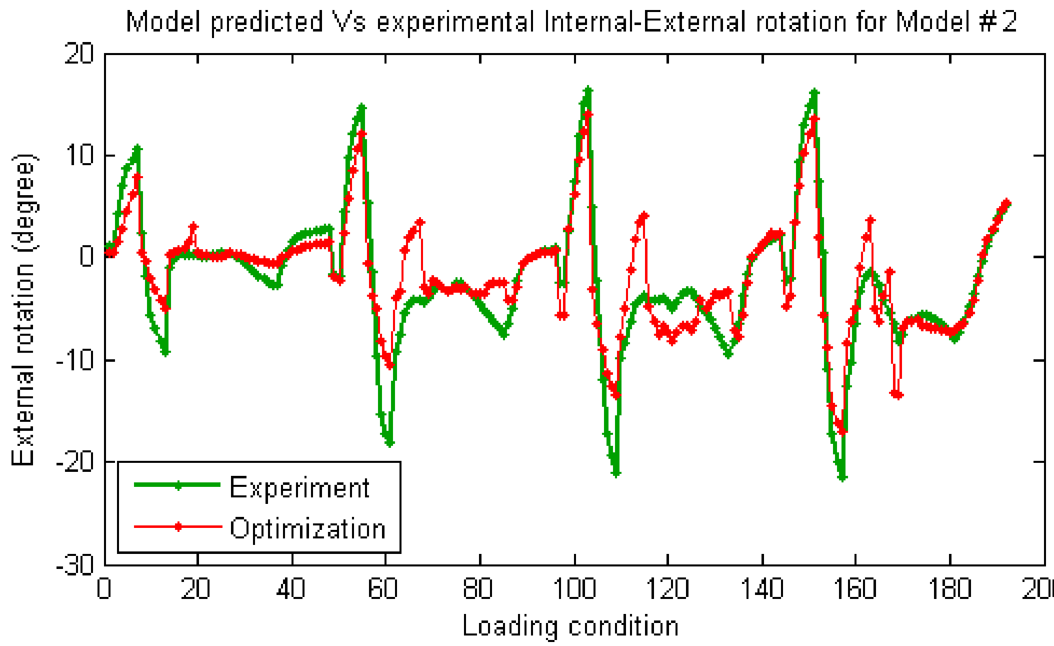
Model predicted Vs experimental Internal-External rotation for Model #2
External rotation (degree)
Loading condition
Experiment
Optimization
20
10
0
-10
-20
-30
0
20
40
60
80
100
120
140
160
180
200

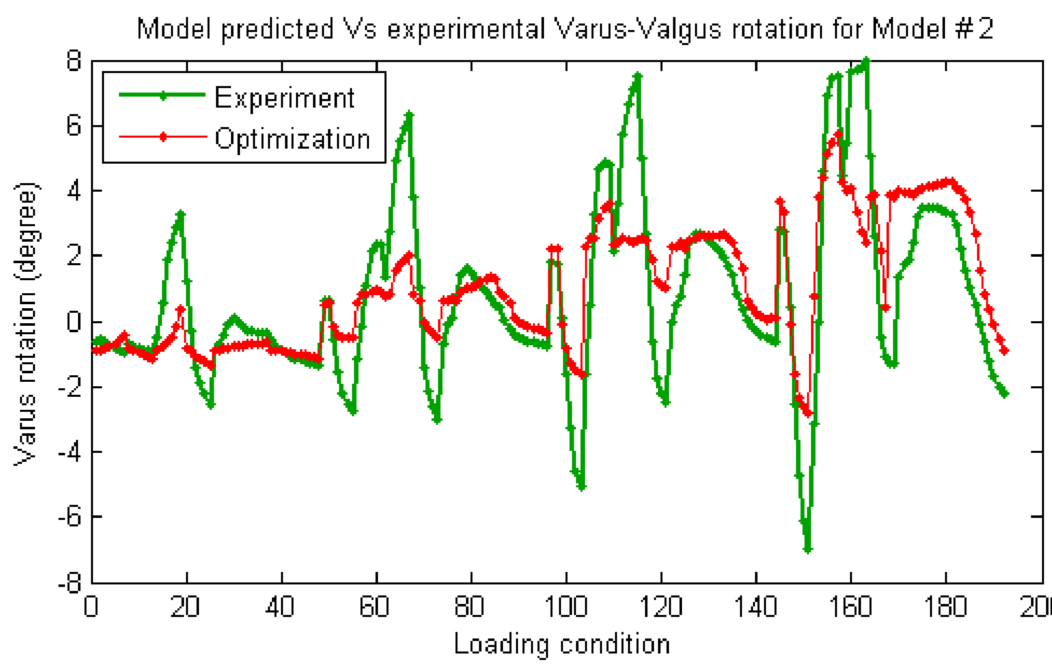
Model predicted Vs experimental Varus-Valgus rotation for Model #2
Varus rotation (degree)
Loading condition
Experiment
Optimization
8
6
4
2
0
-2
-4
-6
-8
0
20
40
60
80
100
120
140
160
180
200

Optimization fit for Model # 4 using objective function of 'AP-IE-VV combined' set

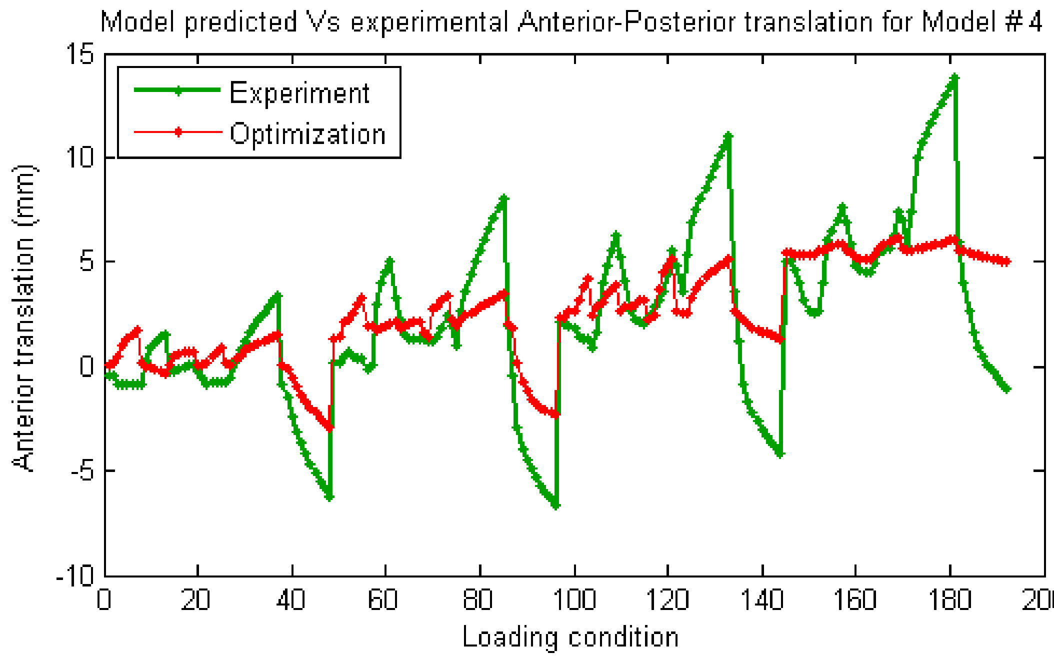

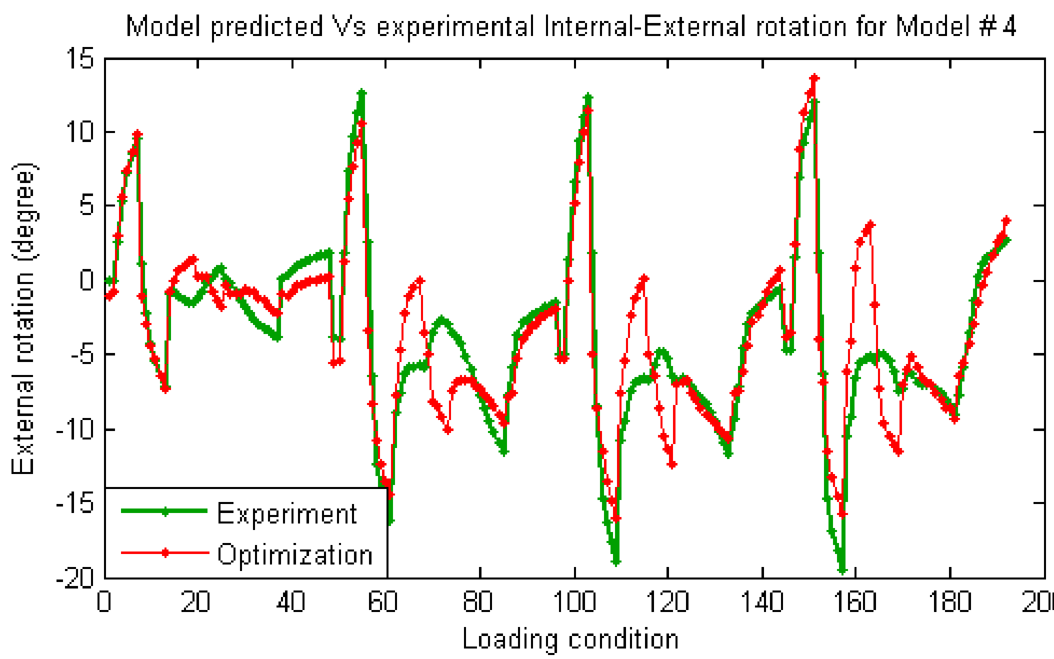

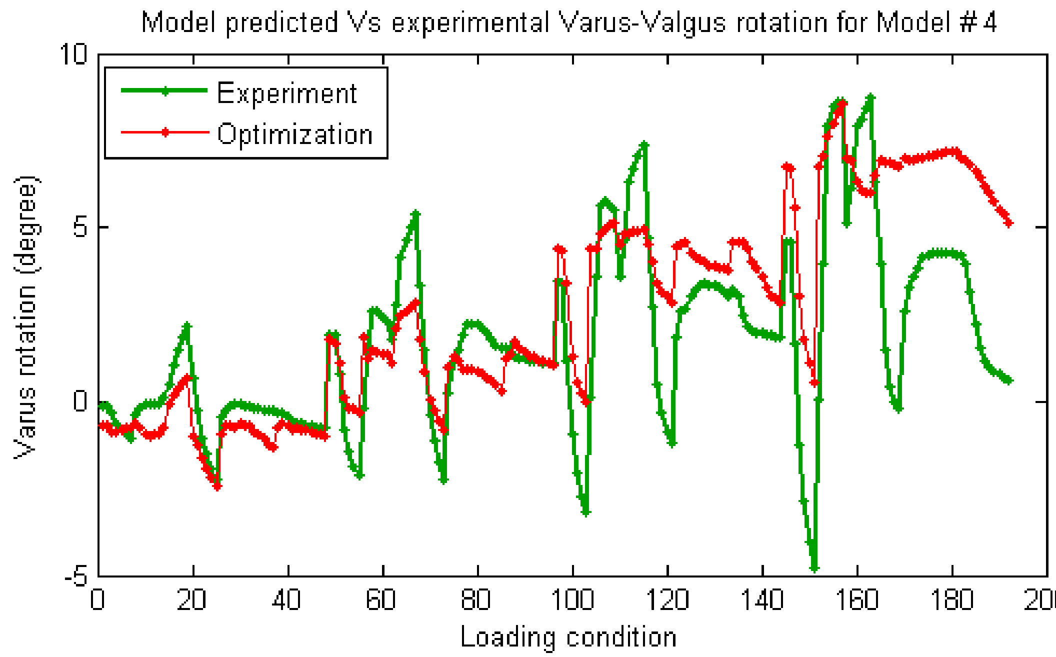

Optimization fit for Model # 5 using objective function of 'AP-IE-VV combined' set

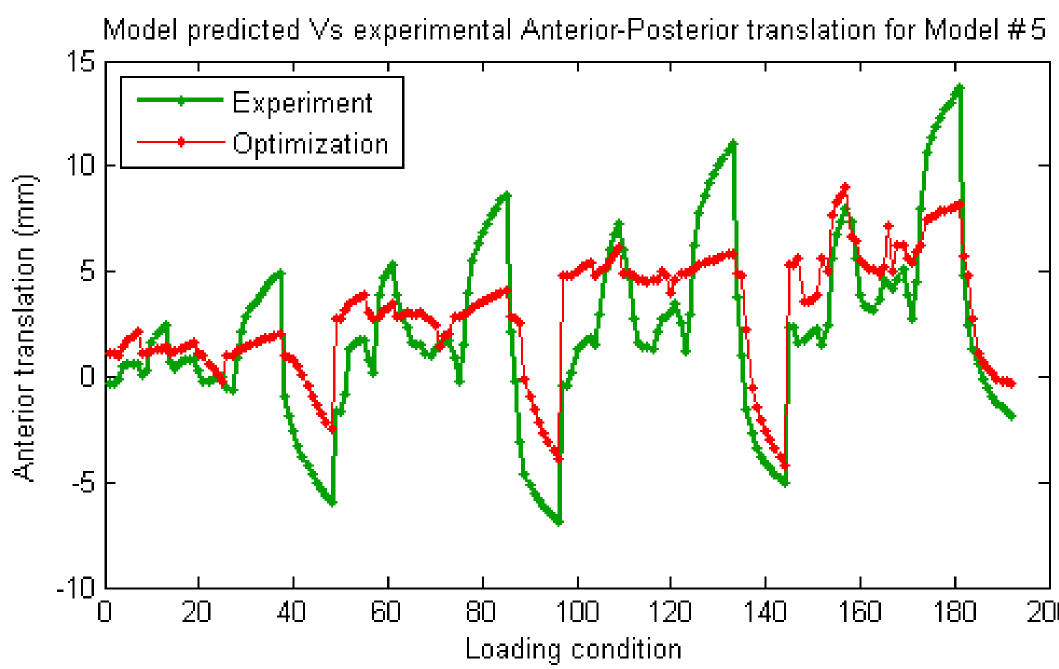

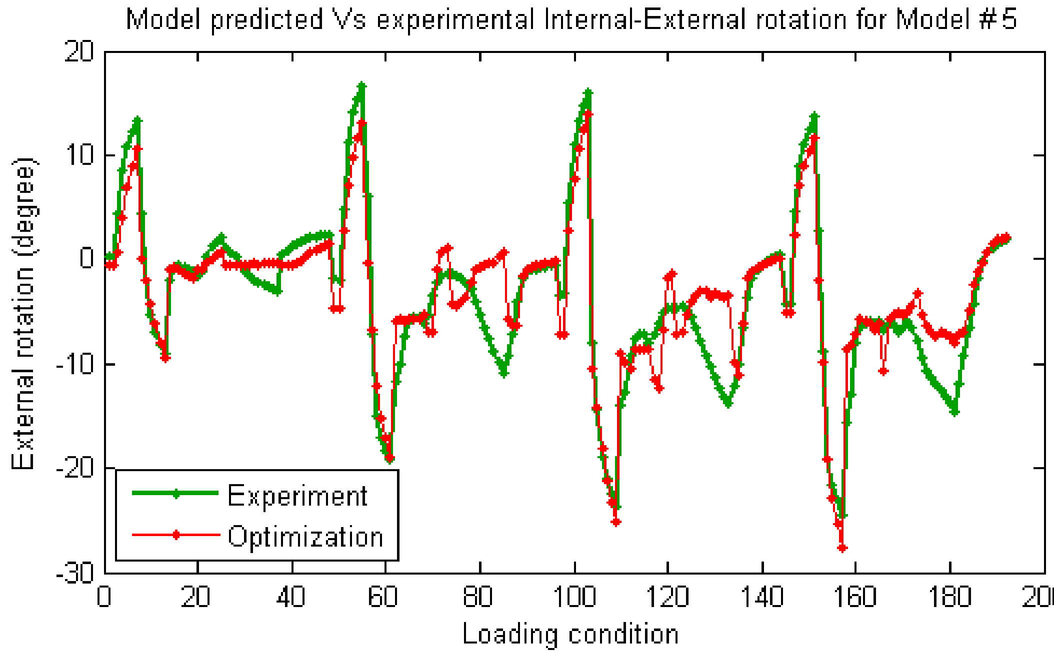

Model predicted Vs experimental Internal-External rotation for Model #5
External rotation (degree)
Loading condition
Experiment
Optimization

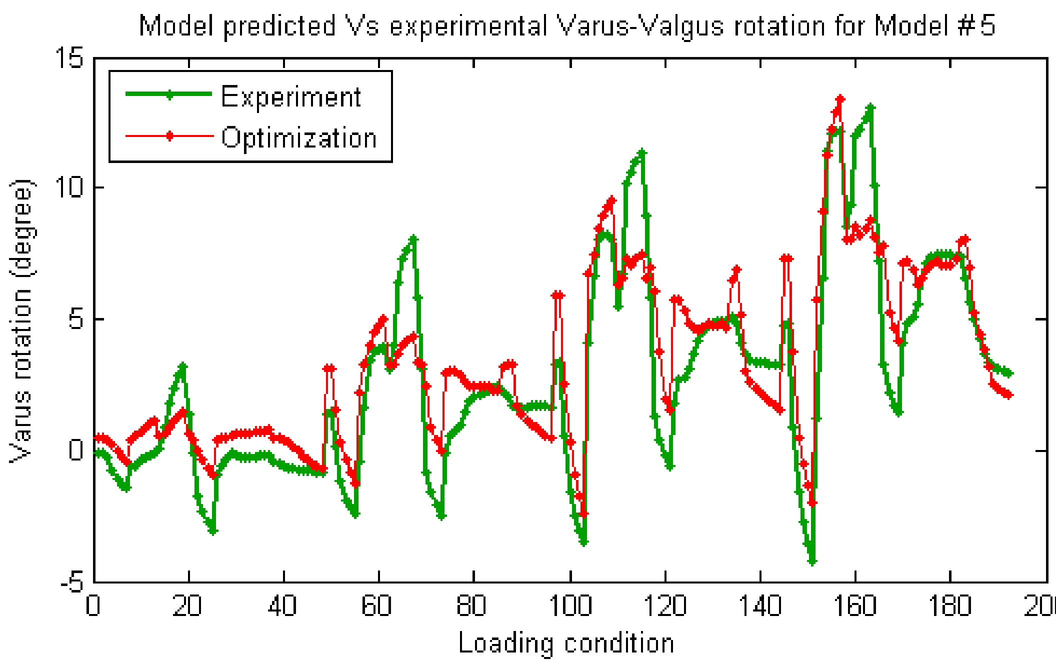

Model predicted Vs experimental Varus-Valgus rotation for Model #5
Varus rotation (degree)
Loading condition
Experiment
Optimization